



Technische Universität München

Fakultät für Physik

Lehrstuhl für Biophysik E22

In vitro analysis of the regulation of
Kinesin-2 motors from *C. elegans* and
X. laevis

Georg K. Merck

Vollständiger Abdruck der von der Fakultät für Physik der Technischen Universität München zur Erlangung des akademischen Grades eines Doktors der Naturwissenschaften (Dr. rer. nat.) genehmigten Dissertation.

Vorsitzender: Prof. Dr. Ulrich Gerland

Prüfer der Disseration: 1. TUM Junior Fellow Dr. Zeynep Ökten

2. Prof. Dr. Manfred Schliwa

Die Dissertation wurde am 23.10.2020 bei der Technischen Universität München eingereicht und durch die Fakultät für Physik am 14.01.2021 angenommen.

Table of contents

1.	Summary	1
2.	Zusammenfassung	2
3.	Introduction	5
3.1.	Cytoskeleton and cellular transport	5
3.2.	Kinesin-2	8
3.3.	Model systems to investigate Kinesin-2 motors	14
3.4.	Aims of this thesis	24
4.	Materials	27
4.1.	Enzymes, chemicals, Kits and media	27
4.2.	Buffers and solutions	27
4.3.	Oligonucleotides, Plasmids, Vectors, and functionalized dsDNA	28
4.4.	Organisms	29
4.5.	Software	29
5.	Methods	30
5.1.	Molecular biological methods	30
5.2.	Protein biochemical methods	38
6.	Results on the regulation of the Kinesin-2 motor KIF3A/B/KAP from <i>X. laevis</i>	56
6.1.	Experimental Concept	57
6.2.	Protein expression, purification, and experimental set-up	58
6.3.	KIF3A/B/KAP and KIF3A/B are both highly processive	60
6.4.	The tail domain of the KIF3A motor protein is responsible for KAP binding	61
6.5.	The tail domain of the KIF3B motor protein is necessary to achieve full runlength	63
6.6.	The KIF3A and the KAP subunits are targets of phosphorylation by protein kinase A (PKA)	67
7.	Results on coupling between KIF3A/B/KAP and other players of the melanosome transport system	76
7.1.	Experimental Concept	77
7.2.	The dynactin subunit p150 ^{glued} does not bind to the KIF3A/B/KAP motor	77
7.3.	Linking KIF3A/B/KAP and Myosin-Va/Melanophilin/Rab27a using a dsDNA handle	81
7.4.	The photoisomeric inhibitor AzoMyoVin-1 both specifically and reversibly inhibits the Myosin-Va motor	85

8.	Results on the regulation of the homodimeric Kinesin-2 motor OSM-3 from <i>C. elegans</i>	89
8.1.	Experimental approach	90
8.2.	The tail domains of OSM-3 bind to their head domains	92
8.3.	The tail domains are responsible for inhibition of the OSM-3 motor through binding to the head domains	94
8.4.	The OSM-3 ^{G444E} construct is inherently active due to the charge and size of the introduced glutamic acid	96
8.5.	Autoinhibition of OSM-3 is released through binding of the IFT subunits DYF-1/OSM-6 to the OSM-3 tail domains	97
9.	Discussion	99
9.1.	The KIF3A/B/KAP motor is deactivated by dephosphorylation <i>in vitro</i> and has two distinct, synergetic functions for its respective tail domains	100
9.2.	Linking KIF3A/B/KAP to other players of the melanosome transport system	106
9.3.	The OSM-3 motor is autoinhibited by its random tail domains and activated through binding of DYF-1/OSM-6 to its tail domains	110
9.4.	Summary and Outlook	115
10.	Supplementary Information	120
10.1.	SI Movies	120
10.2.	Supplementary Figures	123
10.3.	Abbreviations	127
10.4.	Sequences	128
11.	Literature	138
12.	Acknowledgements	149

1. Summary

Nearly all eukaryotic cells employ motor proteins that walk either on the f-actin or microtubule cytoskeleton, respectively. While kinesins and dyneins utilize the microtubule, myosin motors are specialized to walk on the f-actin network. The proper functioning of this intracellular transport system is essential for many cellular processes during interphase as well as mitosis and cell division. It is therefore unsurprising that defective motor proteins give rise to vastly different human disorders, e.g. blindness, infertility, or neurodegenerative diseases.

This thesis deals with kinesin-2 motors that have been co-evolved with the ciliary machinery to specifically participate in the Intraflagellar Transport (IFT) and have later been adapted to cytoplasmic transport processes. In particular, the cilia-specific kinesin-2 motor from *C. elegans* and the kinesin-2 motor from *X. laevis* that is involved in cytoplasmic transport are dissected in functional reconstitution assays to unmask their mechanistic adaptations to distinct transport processes. Moreover, we describe preliminary experimental approaches towards understanding the functional interplay between the kinesin and the myosin motors during cargo transport and means to specifically regulate the activity of the myosin motor in reconstitution assays.

When observed from outside, numerous intracellular organelles on microtubules instantaneously change direction of transport. In vast majority of cases, the oppositely directed kinesin and dynein motors give rise to such observations. In the most convoluted scenario, myosin joins the kinesin and dynein motors on the same cargo, as seen, for example, in the melanosome transport in *X. laevis*. The latter provokes the question of how the cell orchestrates the action of these three different motors to ensure the timely arrival or departure of cargo. It is well-established that spatial and temporal regulation of the cargo transport starts at the motor protein level. Namely, motors that are involved in long-range transport are auto-inhibited, i.e. they can switch themselves off when not bound to their designated cargo.

Here we show that the heterotrimeric KIF3A/B/KAP motor from *X. laevis* has evolved its two distinct tail domains to serve two synergetic functions. These

2 Zusammenfassung

functions are the binding of the cargo-binding KAP subunit to the motor subunits and the significant increase of the motors runlength, respectively. Curiously, we also found that this motor does not exhibit the commonly observed autoinhibition mechanism, in which the C-terminal tail domains are thought to suppress the catalytic function of the N-terminal head domains. Instead, dephosphorylation of the head domains diminished the motor's processivity in a regulatable manner. These findings fit perfectly with previously postulated models for the melanosome transport, in which the KIF3A/B/KAP motor is constantly bound to the surface of the melanosome vesicle and in which its processivity is suppressed via decreased intracellular PKA activity.

In stark contrast to the heteromeric KIF3A/B motor, however, the cilia-specific OSM-3 homodimer was shown to be clearly autoinhibited. Here, we describe that the OSM-3 motor's tail domains bind directly to the catalytic head domains and thereby suppress the motor's activity as proposed previously. Furthermore, we showed that the IFT-B cargo subunits OSM-6/DYF-1 bind to the same tail domains of the OSM-3 motor, indicating the mechanism for the release of the autoinhibition. These findings again fit perfectly into the postulated function of the OSM-3 motor. Its only regulatory function is proposed to be switched on upon cargo binding at the base of the cilium, and subsequently to be switched off at the tip of the cilium, upon release of the cargo.

Taken together, we present here mechanistic clues to explain how two distantly related kinesin-2 motors have evolved their diverse protein domains in order to adapt to their specific tasks, despite their otherwise similar overall features and structure.

2. Zusammenfassung

Nahezu alle eukaryotischen Zellen verwenden Motorproteine, die entweder auf dem f-Aktin- oder dem Mikrotubuli-Zytoskelett laufen. Während Kinesine und Dyneine die Mikrotubuli nutzen, sind die Myosin-Motoren darauf spezialisiert, auf dem f-Aktin-Netzwerk zu laufen. Das einwandfreie Funktionieren dieses intrazellulären

2 Zusammenfassung

Transportsystems ist für viele zelluläre Prozesse während der Interphase sowie der Mitose und Zellteilung von wesentlicher Bedeutung. Es ist daher nicht überraschend, dass defekte Motorproteine zu ganz unterschiedlichen Störungen beim Menschen führen, z.B. zu Blindheit, Unfruchtbarkeit oder neurodegenerativen Erkrankungen.

Diese Arbeit befasst sich mit Kinesin-2-Motoren, die zusammen mit der Ziliarmaschinerie entstanden sind, um spezifisch am Intraflagellaren Transport (IFT) teilzunehmen, und die später an zytoplasmatische Transportprozesse angepasst wurden. Im Detail werden der Zilien-spezifische Kinesin-2-Motor von *C. elegans* und der am zytoplasmatischen Transport beteiligte Kinesin-2-Motor von *X. laevis* in funktionellen Rekonstitutionsassays seziert, um ihre mechanistischen Anpassungen an bestimmte Transportprozesse zu entlarven. Darüber hinaus beschreiben wir vorläufige experimentelle Ansätze zum Verständnis des funktionellen Zusammenspiels zwischen dem Kinesin- und dem Myosin-Motor während des Frachttransports und Mittel zur spezifischen Regulierung der Aktivität des Myosin-Motors in Rekonstitutionsassays.

Bei der Beobachtung von außen ändern zahlreiche intrazelluläre Organellen auf Mikrotubuli augenblicklich die Transportrichtung, wofür in den allermeisten Fällen die entgegengesetzt gerichteten Kinesin- und Dynein-Motoren Anlass zu solchen Beobachtungen geben. Im kompliziertesten Szenario bindet auch noch Myosin zusätzlich zu den Kinesin- und Dynein-Motoren an dieselbe Fracht, wie es z.B. beim Melanosomentransport in *X. laevis* beobachtet werden kann. Vor allem Letzteres provoziert die Frage, wie die Zelle die Aktivität dieser drei verschiedenen Motoren orchestriert, um die rechtzeitige Ankunft oder Abfahrt der Fracht zu gewährleisten. Es ist erwiesen, dass die räumliche und zeitliche Regulation des Frachttransports auf der Ebene der Motorproteine beginnt, da Motoren, die an diesem Langstreckentransport beteiligt sind, nämlich auto-inhibiert sind, d.h. sie können sich selbst abschalten, wenn sie nicht an ihre vorgesehene Fracht gebunden sind.

Wir zeigen hier, dass sich der heterotrimere KIF3A/B/KAP-Motor von *X. laevis* mit seinen zwei unterschiedlichen Schwanzdomänen so entwickelt hat, dass er zwei synergetische Funktionen erfüllen kann. Diese Funktionen sind die Bindung der

2 Zusammenfassung

Fracht-bindenden KAP-Untereinheit an die Motor-Untereinheiten bzw. die signifikante Erhöhung der Lauflänge des Motors. Merkwürdigerweise fanden wir auch heraus, dass dieser Motor nicht den allgemein beobachteten Autoinhibitionsmechanismus aufweist, bei dem angenommen wird, dass die C-terminalen Schwanzdomänen die katalytische Funktion der N-terminalen Kopfdomänen unterdrückt. Stattdessen verringerte Dephosphorylierung der Kopfdomänen die Prozessivität des Motors auf regulierbare Weise. Diese Ergebnisse passen perfekt zu den zuvor postulierten Modellen für den Melanosomentransport, in denen der KIF3A/B/KAP-Motor ständig an die Oberfläche des Melanosomenvesikels gebunden ist und in denen seine Prozessivität durch verminderte intrazelluläre PKA-Aktivität unterdrückt wird.

Im krassen Gegensatz zum heteromeren KIF3A/B-Motor zeigte sich jedoch, dass der zilien-spezifische OSM-3-Homodimer autoinhibiert ist. In dieser Arbeit zeigen wir, dass die Schwanzdomänen des OSM-3-Motors direkt an die katalytischen Kopfdomänen binden und dadurch die Aktivität des Motors, wie zuvor postuliert, unterdrücken. Darüber hinaus zeigen wir, dass die IFT-B-Cargo-Untereinheiten OSM-6/DYF-1 an die gleichen Schwanzdomänen des OSM-3-Motors binden, was auf den Mechanismus zur Freisetzung der Autoinhibition hindeutet. Diese Ergebnisse passen wiederum perfekt in die postulierte Funktion des OSM-3-Motors. Seine einzige Funktion soll es sein bei der Bindung an die Fracht an der Basis des Ziliums eingeschaltet zu werden und anschließend bei der Freigabe der Fracht an der Spitze des Ziliums wieder ausgeschaltet zu werden.

Zusammengefasst präsentieren wir hier mechanistische Hinweise, um zu erklären, wie zwei entfernt verwandte Kinesin-2-Motoren, trotz ihrer ansonsten ähnlichen Gesamteigenschaften und Struktur, ihre verschiedenen Proteindomänen entwickelt haben, um sich an ihre spezifischen Aufgaben anzupassen.

3. Introduction

3.1. Cytoskeleton and cellular transport

The cytoskeleton, which is a highly dynamic system of microtubule, intermediate filaments and actin filaments, is an essential part of every eukaryotic cell, providing not only structural integrity and spatial organization for stable cell formation and motility, but also the basis for intracellular transport by motor proteins. The two filaments – f-actin and microtubule – act as tracks for three distinct families of molecular motors, namely the actin-based myosins, and the two microtubule-based motors kinesin, and dynein. These motor proteins are able to convert chemical energy in the form of adenosine triphosphate (ATP) into mechanical work [3-7]. Apart from crucial functions like, e.g. cell division [8, 9], these filament-based motor proteins provide an efficient and directed way to transport organelles and cargos bidirectionally within the cell [10-12]. These transport processes are a requirement for the complex and well-organized system of any eukaryotic cell. The vast range of unrelated diseases caused by faulty transport within all kinds of cell types and organisms demonstrates the importance of a well-functioning system of filaments and molecular motors. Blindness and infertility and other so-called ciliopathies are caused by defects in the intraflagellar transport driven by molecular motors [13-17] or neurodegenerative diseases, like Alzheimer's, Huntington's, Amyotrophic Lateral Sclerosis (ALS) and Parkinson's [18-22] - prompted by impaired axonal transport - are only a few examples.

3.1.1. The filaments of the cytoskeleton

The cytoskeleton itself consists of a large network of microtubule and f-actin filaments, as well as intermediate filaments and countless associated proteins [23], the latter being responsible for e.g. the stability or regulation of these filaments [24].

3 Introduction

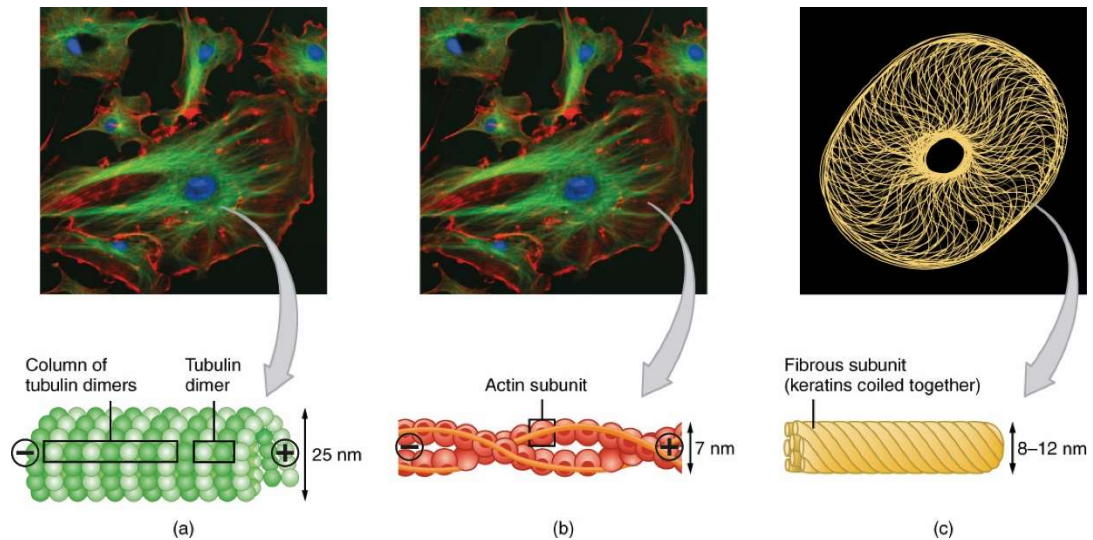


Figure 1: **Structure and location of the three filaments of the cytoskeleton.** (top row) Widefield fluorescent images reveal filaments present in cells (green = microtubule, red = f-actin, yellow = intermediate filaments, blue = nucleus). (lower row) Simplified schematic diagrams showing the structure of (a, green) microtubule, (b, red) f-actin and (c, yellow) intermediate filaments [25].

Actin and microtubule filaments are highly dynamic structures, with a fast growing plus and a slow growing minus end, that can undergo, but not always do, so-called treadmilling, a process, by which the plus end of a filament grows constantly in length, whereas the minus end depolymerizes faster than it polymerizes, giving the filament the appearance of moving through the cell [26]. These plus and minus ends also provide the necessary polarization for directed movement of motor proteins.

Microtubules form a cylindrical polymer with a diameter of 23 - 27 nm with an inner diameter of 11 – 15 nm that can grow to up to 50 μm in length [27]. The microtubule filaments are formed by two distinct, globular protofilament proteins – alpha and beta tubulin - upon binding to guanosine triphosphate (GTP), usually consisting of 13 protofilaments in one tubular arrangement [28] (Figure 1 a). Microtubules are most commonly found radiating from the cell center to the cell periphery, in the cell cytoplasm or as a backbone structure that forms the so-called cilia – projections from the cell body (3.3.2) [29-31]. Microtubules with their morphologically and chemically distinct plus and minus ends build the basis for two classes of motor proteins – the anterograde kinesin (towards the plus-end), and the retrograde dynein (towards the minus-end), as well as a vast number of microtubule associated proteins (MAPs) responsible for maintaining and regulating the microtubule growth and interactions [32].

3 Introduction

Actin filaments (f-actin), on the other hand, are built up through polymerization of 42 kDa globular actin monomers (g-actin) upon binding to ATP. These building blocks form two stranded helical polymers that repeat every 37 nm and provide the tracks for the myosin motor (Figure 1 b). F- actin has a diameter of around 7 nm and – with the help of various actin binding proteins – forms a dense network of filaments usually concentrated at the cell periphery [33-35].

Intermediate filaments are short filaments with a diameter of around 10 nm, mainly responsible for the mechanical integrity of the cell without any enzymatic function [36] (Figure 1 c). They are highly dynamic structures that are known to move within the cell, and are associated with their assembly, disassembly, and subcellular organization. This movement is either intrinsic to the intermediate filaments or driven by motor proteins bound to microtubule/actin filaments during crosstalk with these filaments [37]. However, unlike the microtubule and actin filaments, they do not undergo treadmilling. More importantly, these intermediate filaments do not have a defined orientation (plus/minus end), and thus are not apt to serve as tracks for the directional motility of molecular motors [37, 38].

3.1.2. The molecular motors

Molecular motors are defined both by their filament interaction and by the direction in which they “walk”, i.e. to the plus or the minus end of their filaments. To this day, eighteen myosin classes [39], fourteen kinesin families [40, 41] and fifteen types of axonemal (responsible for transport in cilia) as well as two cytoplasmic types of dynein are known [42].

However, only a small number of so-called toolbox motors fulfil distinct transport processes, moving along their respective filaments within their cell (Figure 2). This small number of motors is however found in all organisms ranging from single cells to humans [30]. These toolbox motors are the microtubule-based Kinesin-1, hetero- and homodimeric Kinesin-2 and the Kinesin-3 motor Unc104, which all travel towards the plus end, as well as dynein, moving towards the minus end of the microtubule, and lastly the actin-based Myosin-V (Figure 2).

3 Introduction

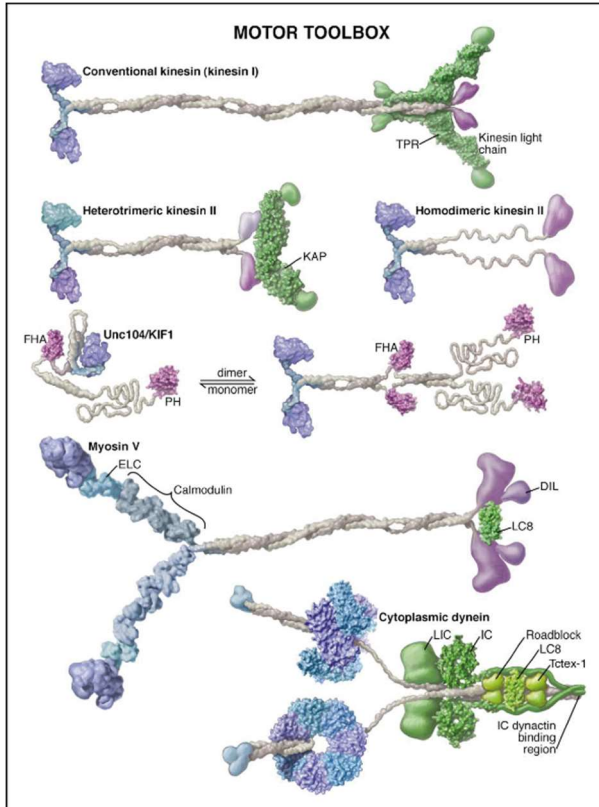


Figure 2: The “Toolbox” of molecular motor proteins. The motor toolbox includes (top row) the homodimeric Kinesin-1, (second row) the heterotrimeric and homodimeric Kinesin-2, (third row) the Kinesin-3 motor Unc104, in its monomeric and dimeric, active form, (fourth row) the actin-based Myosin-V, and (bottom row) the cytoplasmic dynein. Catalytic domains and mechanical amplifiers are displayed blue and tail domains in purple. Structural stalk domains are depicted in grey and tightly associated motor subunits (e.g. KAP) in green. Surface features are rendered based upon atomic resolution structures available at <http://www.cell.com/cgi/content/full/112/4/467/DC1>. Image adapted from [30].

Despite their distinct function and structure, all kinesins and the myosins share a conserved three part structure (Figure 2): an enzymatic head domain that binds reversibly to the filaments, a stalk domain that dimerizes the motor, and the C-terminal tail domain.

While the head domain is highly conserved throughout the motor classes, the divergent tail domain allows for unrelated functions, like specific binding to various cargos, activators, the filaments, or to the motor itself (Figure S 1) [30, 43, 44].

The dimeric structure of dynein is made up of several light and intermediate chains, responsible for e.g. cargo binding; two heavy chains containing the enzymatic AAA+ ATPase head domain, and two C- and N-terminal tail domains binding to the microtubule and the remaining subunits, with mostly unknown functions, respectively (Figure 2) [42, 43].

Amongst those motors, the Kinesin family, as the most extensively studied motor protein, can serve as a classical example for the description of motor-driven transport and is therefore the focus of this thesis.

3.2. Kinesin-2

3.2.1. General structure

Kinesin-2, one of the kinesin toolbox motors, is particularly noteworthy, as it has two distinct forms. This motor exists either as a homodimer, formed by dimerization of

3 Introduction

two identical motor polypeptides, or as a heterotrimer, from dimerization of two different motor polypeptides, which C-terminally bind to a third non-motor subunit, the Kinesin-associated protein (KAP) (Figure 2) [45]. This heterotrimeric structure is remarkably unique among motor proteins. It has been shown that homodimeric Kinesin-2 moves considerably faster and, when under load, is less likely to detach from the filament than the heterotrimer; two of the most basic functions of every motor [45-51]. Still, later studies have shown that the heterotrimeric complex has evolved independently numerous times in the course of evolution [52-55], which is an indication for a functional or structural advantage over the homodimeric motors. An increasing number of publications have highlighted the advantages of this heterotrimerization, and why it is necessary, e.g. giving the motor the ability to side-step and in turn to elude roadblocks on their filaments [56, 57] This interesting preference for heterotrimerization is further underpinned by the fact that the two distinct monomers, which build the heterodimeric motor can no longer form stable homodimers between themselves [46, 58].

Since their first discovery and purification from sea urchin eggs in 1992 [59], Kinesin-2 orthologues have been discovered in many different organisms, from green algae to mammals, which, despite their structural similarities, are deployed very distinctively to fulfill specific unrelated functions within their respective cell [30].

As Kinesin-1 and most other kinesins, the motor subunits of both the homo- and heterodimeric Kinesin-2 motor in detail consist of three parts [30, 60] (Figure 3):

The first part are the N-terminal head domains that convert the chemical energy of ATP into mechanical work [61]. These highly conserved domains bind to the microtubule β -protofilaments and - through hydrolysis of ATP and resulting conformational changes within the head and neck linker domain - displace the motor complex along the microtubule filament by taking consecutive steps [5, 57, 62-65].

The second part are the stalk domains. These α -helical structures dimerize [66, 67], resulting in a coiled-coil structure which, throughout all Kinesin-2 sequences, is interrupted by a conserved and flexible helix breaker region that is believed to allow the stalk to bend down to the head domain and to thereby inhibit its function (Figure 3, Figure 4) [44, 46, 64, 68-72].

3 Introduction

The C-terminal random-coiled tail domain is separated from the stalk by a similarly conserved position, again a helix breaker, which separates the coiled-coil from the random-coil conformation (Figure 3). The ensuing tail domain, however, varies greatly even within kinesin families, providing for specific functions like regulation of the motor, the binding to the cargo/KAP subunit, or the binding to microtubule filaments [2, 43].

The kinesin associated protein KAP, as part of the heterotrimeric Kinesin-2, has no known filament or nucleotide binding site, nor any enzymatic capability whatsoever. However, it is rich in so-called α -helical armadillo repeats which are well-known protein interaction sites [73-75]. Therefore, its main task is proposed to be the link

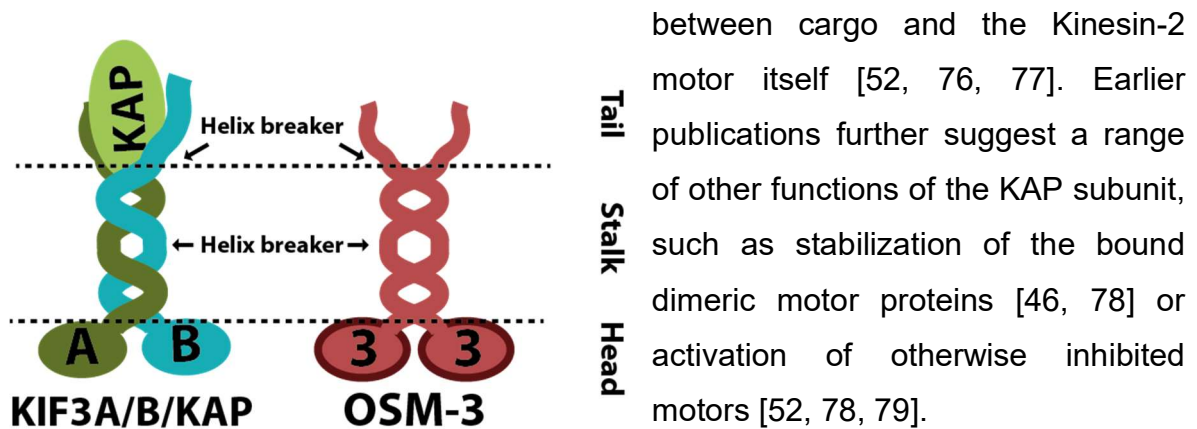


Figure 3: Graphic depiction of the heterotrimeric KIF3A/B/KAP from *X. laevis* (left, KIF3A dark green, KIF3B, teal, KAP light green) and homodimeric OSM-3 from *C. elegans* (right, red). The dashed lines separate the three different domains of each motor: head domains (lowest), coiled-coiled stalk with helix breaker position (middle) and random coil tail domain (upper) separated from the coiled-coil by another conserved helix breaker position.

3.2.2. Regulation of the molecular motors

In addition to the basic kinetic property of transporting cargo across the cell via hand-over-hand movement, the second common feature of every toolbox motor is the regulatable activity. The most common example of this regulation is autoinhibition, by which the motor switches from an active to an inactive form via conformational changes within the motor. This mechanism is best studied with the Kinesin-1 motor. In the case of Kinesin-1, the coiled-coil stalk domain folds at its helix breaker position and in this manner allows the random coil tails to bend down to inhibit ATPase activity of the motor (Figure 4A) [2, 30, 68-70, 80, 81]. Analysis of crystal structures of Kinesin-1 have clarified this process in detail, revealing that the

3 Introduction

tails are binding to the head domains and thereby inhibit any conformational change and any movement of the head and neck linker domains. As a consequence, the tail domains inhibit ADP release, i.e. significantly reduce the frequency of ATP hydrolysis, but they do not interfere with the binding of the head domains to the microtubule [82-84]. This same inhibitory effect of the tails could be verified by addition of tail domains to active motor domains *in trans* [82, 85]. A similar autoinhibition mechanism has furthermore been suggested for Kinesin-2 through deletion or mutation of the helix breaker position. In both of these experiments, the motor was prevented from folding and thus from inhibiting its activity [44, 46, 72]. Since this only suggests the same mechanism of autoinhibition, as seen in Kinesin-1, but does not prove it, detailed experimental evidence, and structural insight into the molecular mechanism of the regulation of all Kinesin-2 motors are still missing. It has often been found that conclusions by analogy between one motor class and another remain speculative and should not be drawn without experimental proof.

a Autoinhibited kinesins

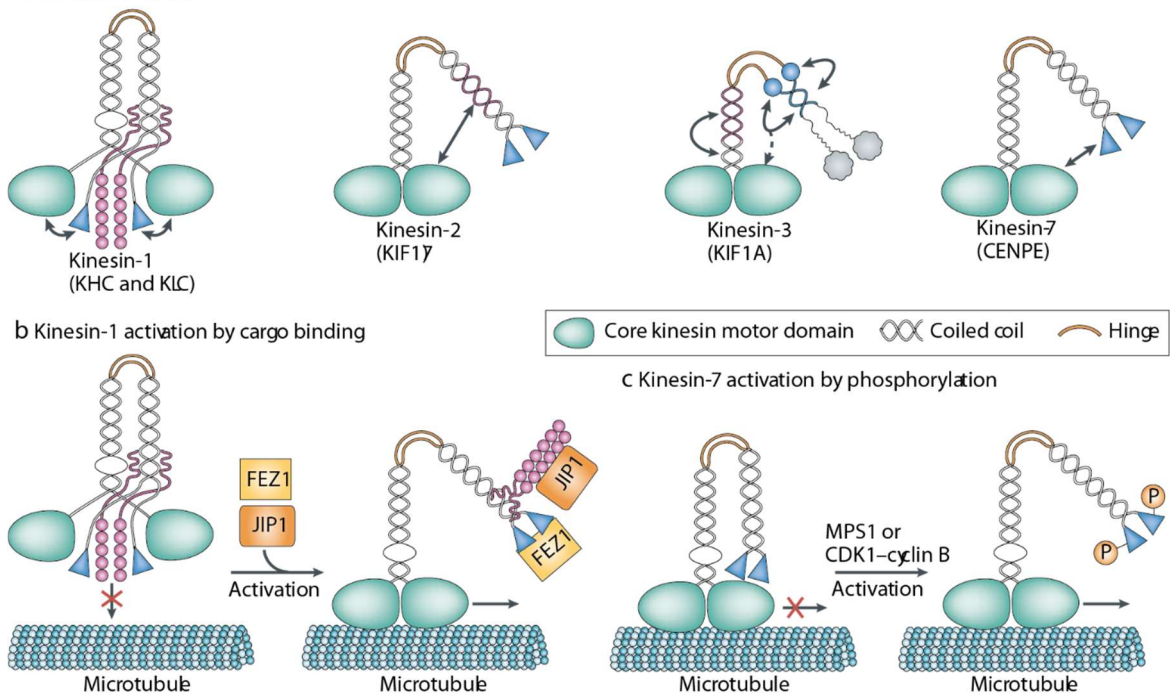


Figure 4: **Autoinhibition mechanisms used in the Kinesin family.** (a) Inactive Kinesin motors assume a folded conformation that enables the inhibiting tail to head domain binding. Double arrows indicate binding. Kinesin-1 has both, a microtubule binding suppression mechanism by its light chains (purple) and a processive motility inhibition by its heavy chain tail domains (blue). (b) These inhibition mechanisms can be released by interaction with two different cargo units (FEZ1 and JIP1) that release both chains from their binding sites. (c) Autoinhibition of Kinesin-7 can be released by phosphorylation of the tail domain. Image and text adapted from [2]

3 Introduction

This is all the more true considering how strongly the sequences of the respective tail domains differ between motor classes [30].

Concurrent with the evolutionary adaptation of the motor domains to the different functions and requirements of the motor, the mechanism behind the regulation of different motors can vary from plain autoinhibition by the tail domain to e.g. a combination of more subtle ways of regulation. For example, Kinesin-3 has been shown to possess more than only one regulatory mechanism, namely the already discussed autoinhibition by tail to head binding, but also the ability to only dimerize upon activation [86-89]. It is therefore possible that several other motor families and their homologs have also evolved multiple or different inhibitory mechanisms for the purpose of finer adjustment to diverse motor functions. In addition to ATP hydrolysis, these functions could include microtubule binding or cargo association [2, 86].

One purpose of the regulation of the motors is to prevent needless activity during absence of cargo. And the simplest model of release of the autoinhibition is based on prevention of the binding between the tail and head domains. (i.e. autoinhibition of motor movement) by binding cargo to the tail domains of the motor [2, 90, 91]. This has been shown to be true for Kinesin-1 and Kinesin-2 by simply mimicking cargo binding through attachment of micron-sized beads to the tail domains [69, 72]. Activating the motors *in vitro* with their physiological relevant binding partners, however, is more complicated than such artificial activation with e.g. beads. Motors tend to have either multiple regulation mechanisms – like Kinesin-1, which is activated through simultaneous binding to two proteins (Figure 4B) [90]; or the inhibited motor can only be activated by through a complex mechanism, e.g. a scaffold of effector/cargo proteins – as shown for the Kinesin-2 homodimer OSM-3, which is only fully activated through binding to two cargo proteins at the same time [92, 93]. Another complex example is the Myosin-Va motor, which can be recruited by a whole range of proteins, which all have different current functions and locations in the cell. The recruitment is therefore very specific and depend on as yet unknown environmental conditions [94-96]. Yet another example are the cytoplasmic dynein and heterotrimeric Kinesin-2. Both supposedly compete in binding to

3 Introduction

dynactin/p150^{glued} subunits, which are non-motor domains of the dynein motor complex [76, 97, 98].

It is still debated to this day, whether the KAP subunit of the heterotrimeric Kinesin-2 motor is one of these factors affecting a regulation of the motor subunits or solely a cargo binder. Many publications have shown in *in vivo* experiments that, knockout of the KAP subunit leads to severe dysfunctions in respective transport processes [52, 99], highlighting its purpose as a cargo binder or linker between organelles and the kinesin motor. However, among the few *in vitro* publications concentrating on the KAP subunit and the motor's processivity, some have suggested the KAP subunit to have no influence on the processivity, while others did suggest it would indeed have some influence [79, 100].

Another way how, in cells, motor proteins regulation is governed are post-translational modifications (PTMs), e.g. phosphorylation by protein kinases. For example, the affinity of mammalian Kinesin-1 towards its cargo is changed upon phosphorylation of the Kinesin-1 light chain, as is the velocity under load changed when the motor domains of the Kinesin-1 heavy chains are phosphorylated [101]. Also, microtubule binding, velocity, as well as even the directionality of Kinesin-5 from *S. cerevisiae* are influenced by phosphorylation [102] and Kinesin-7, upon phosphorylation, unfolds from its inhibited state [103]. Liang *et al.* showed in 2014 that the heterotrimeric Kinesin-2 FLA8/10/KAP from *C. reinhardtii* is released from its designated cargo after phosphorylation of the tail domain of the FLA8 motor subunit, which is an indication that binding to the cargo/KAP subunit is regulated in this way [104].

A recent publication by Oberhofer *et al.* revealed yet another novel mechanism of motor regulation. Melanophilin, an adaptor protein of Myosin-Va, has a preferred affinity towards microtubule or towards f-actin depending on its state of phosphorylation, which in turn is a control mechanism for the overall track selection of Myosin-Va [105, 106].

Modifying the microtubule and f-actin tracks themselves, and, as a consequence altering e.g. the connection of the head domains with their tracks is yet another mechanism of regulation. Kinesin-1 shares a lot of conserved sequences in its head

3 Introduction

domains with Kinesin-2 and Kinesin-3; still only Kinesin-1 shows an enhanced preference towards microtubule filaments when these are acetylated and deetyrosinated, suggesting that other very specific mechanisms do exist to govern the affinity of certain filaments to certain groups of motors [107].

In vitro bottom-up reconstitutions of the molecular mechanisms behind transport parameters and structures of individual motors have uncovered, and will uncover, many details. However, these bottom-up reconstitutions are difficult to accomplish, as the molecule is observed in a completely artificial environment and only reveals one feature of one transport participant at a time. Consequently, there remains a significant gap between those direct, single molecule *in vitro* bottom-up findings and the more indirect and more common top-down findings of cargo transport *in vivo*. In the latter, in addition to multiple motors from different families, an unknown number of accessory non-motor proteins get involved in the observed cargo transport, resulting in an obscuring of any deductions about direct causality between e.g. motor activity and overall transport. As a consequence, the mechanics behind the intracellular transport, through bidirectional interplay of two or three motor groups (from kinesin, myosin, and dynein) has become the target of extensive work, both *in vivo* and - with growing complexity - *in vitro*, in an increasing number of model systems [55, 108-116].

3.3. Model systems to investigate Kinesin-2 motors

In this thesis, we will follow up this research and will discuss two of the a.m. model systems. First, the melanosome system, that transports melanosome pigment vesicles across the cell of the amphibian *X. laevis*, and secondly, the intraflagellar transport (IFT) in *C. elegans* that maintains and builds cilia. Both systems were chosen, because there is extensive knowledge about them from top—down *in vivo* observations, and some basic, though scarce information about their molecular mechanisms from *in vitro* observations.

3.3.1. The melanosome transport system

The first interesting model system is the melanosome transport machinery from the amphibian organism *Xenopus laevis*, which we have used to study the heterotrimeric Kinesin-2 motor KIF3A/B/KAP. In this model system, a well-coordinated system of heterotrimeric Kinesin-2, homodimeric Myosin-Va, and dynein transports melanosomes (vesicles that synthesize and store melanin pigments) along microtubule and f-actin filaments [117]. One particularly interesting hallmark of this transport is that instead of unidirectional movement, as seen e.g. in the intraflagellar transport system (3.3.2), this machinery shows constant directional switching interspersed by pauses. This seemingly ineffective motion has been hypothesized to give the motors the ability to maneuver around roadblocks on the filaments, disperse the vesicles more evenly throughout the cell, or to provide a type of “proofreading” mechanism, where the destination can still be changed during a run [108, 109, 113].

One conclusion from these constant changes in direction is that at all times more than one type of motor is active, and that the “net total” directional transport of the cargo results from these interactions between the motors [118]. In detail, the ability to transport melanosomes within pigment cells enables organisms to change the color of their skin, which in turn serves for many biological functions like camouflage or sexual display [119]. Transporting the melanosomes to the cell periphery (dispersion) spreads the melanosomes more evenly across the cytoplasm and makes the organism appear darker (Figure 5A); and the organism appears lighter when the melanosomes are moved to the cell center (aggregation) (Figure 5B). Aggregation and dispersion of melanosomes are induced by up- and down regulation of cAMP levels triggered by melanocyte stimulating hormones (MSH) and melatonin, respectively. cAMP in turn regulates the activity of the protein kinase A or cAMP-dependent kinase (PKA), which in turn influence the transport in a yet mostly unknown manner [120, 121].

The backbone of this transport system is the cytoplasmic cytoskeleton and its microtubule and f-actin filaments (Figure 5). Like most other cell types, melanophore microtubules radiate from the cell nucleus to the plasma membrane, with the minus

3 Introduction

ends towards the cell center and the plus ends towards the cell periphery [122, 123]. Additionally, f-actin forms a random meshwork of filaments in between the microtubules [124]. In this way, melanosome dispersion is achieved by plus-end movement on microtubule and subsequent further dispersion on f-actin. Aggregation is achieved by minus-end directed movement on microtubule towards the cell center. These two different transport modes are driven by the interplay of the three motors Kinesin-2, Myosin-Va, and dynein and their specificity for filament selection and direction of movement. How the up-regulation of protein kinase or phosphatase activities influences the melanosome transport in detail and whether this is achieved through direct influence on these motors remains largely unknown [117, 122]. Interestingly, the PKA enzyme has been shown to be bound to both the melanosome surface as well as to each of the three motors involved in the melanosome transport, pointing towards a direct effect of the PKA enzyme on the motors [125, 126]. Recently, Oberhofer *et al.* were indeed able to reconstitute the Myosin-Va motor complex *in vitro* and show for the first time how the regulation of the activity of the protein kinase A directly regulates the behavior of this motor [105, 106].

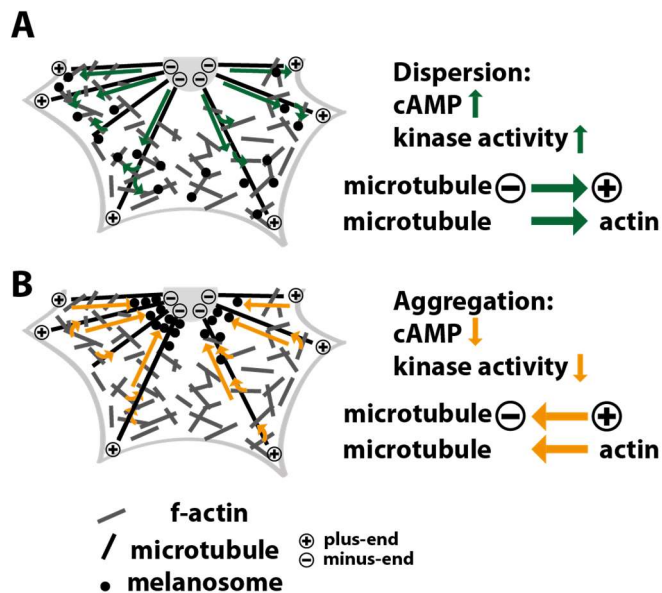


Figure 5: **Graphical depiction of the regulation of the melanosome transport model.** (A) Upon increased cAMP levels, the activity of the protein kinase A is increased and the melanosomes are dispersed throughout the cell by plus-end directed microtubule transport of the KIF3A/B/KAP and consecutive actin-based transport by Myosin-Va. (B) Decreasing the activity of the protein kinase, induced by decreased cAMP levels, leads to aggregation of the melanosomes in the cell center. This is achieved by minus-end directed transport by the cytoplasmic dynein. Image is adapted from Oberhofer *et al.* [127]

3.3.1.1. The KIF3A/B/KAP motor

The heterotrimeric KIF3A/B/KAP Kinesin-2 motor is one of the motors involved in the melanosome transport. Not much is known specifically about the molecular structure and mechanism of this amphibian motor. However, it is generally assumed that this motor behaves similar to other heterotrimeric Kinesin-2 motors, since amphibian KIF3A/B/KAP and for example KLP11/20/KAP from *C. elegans* or KIF3A/B/KAP from *M. musculus* share an identical overall structure, as in consisting of head, stalk and tail domains or the helix breaker positions both within the stalk or between the stalk and the tail domain (Figure 3) (3.2 Kinesin-2).

Prior to this work, it could be shown in a microtubule stimulated ATPase enzyme activity assay that the KIF3A/B motor is indeed autoinhibited and that the truncation of the C-terminal tail domain of the KIF3A subunit restores the activity of the motor (unpublished data) [128]. The same restoration is achieved by addition of the KAP subunit to the full-length motor. This suggests that, like Kinesin-1, KIF3A/B is autoinhibited by binding of the KIF3A tail domain to the head domain and that binding of the non-motor KAP domain suppresses this autoinhibition. Furthermore, it could be shown that the KAP subunit is bound by the C-terminal tail domains of both the KIF3A and KIF3B subunit (unpublished data) [128].

3.3.1.2. The Myosin-Va motor

Myosin-Va, the unconventional class V of the myosin family is responsible for the actin-based transport. It is found in many organisms as one of the so-called toolbox motors (Figure 2). This homodimeric motor is structured like the Kinesin motor, i.e. with an enzymatic head domain, a coiled-coil stalk domain and C-terminal random coil tail domain, mediating cargo binding [129] (Figure 2, Figure 6). For the melanosome transport in *X. laevis*, Myosin-Va is linked with the melanosome vesicle surface via Melanophilin and the GTPase Rab27a. In detail, GTP-bound Rab27a binds to the melanosome and in turn to the N-terminal domain of Melanophilin [130]. Finally, the Melanophilin/Rab27a complex recruits the Myosin-Va motor by binding to the tail domains of this motor [131].

3 Introduction

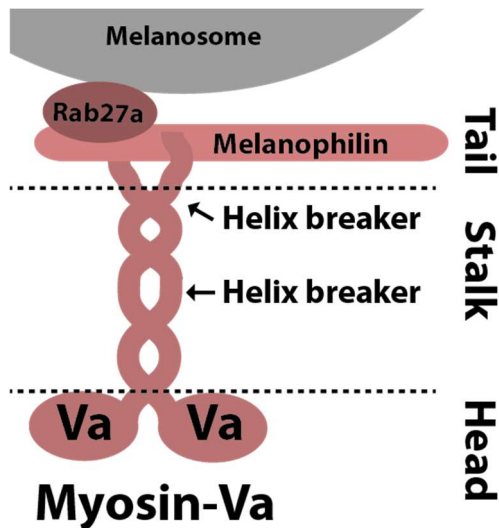


Figure 6: **Graphical depiction of the structure of the Myosin-Va/Melanophilin/Rab27a complex.** Like Kinesin-2, Myosin-Va consists of two N-terminal enzymatic head domains. The coiled-coiled stalk domains possess a helix breaker and are followed C-terminally by the random coil tail domains that are separated from the stalk domains by a helix breaker position. The GTPase Rab27a links the motor complex to the melanosome vesicle via the Melanophilin subunit.

Oberhofer *et al.* were able to reconstitute this tripartite complex of Myosin-Va, Melanophilin and Rab27a *in vitro* and show that this complex has a regulatable preference towards either f-actin or microtubules, depending on

the state of phosphorylation of the complex [105]. Curiously however, the target of the phosphorylation is not the motor Myosin-Va itself, but rather Melanophilin or more specifically the C-terminal end of it, which is known to be the filament binding domain. These findings have shown for the very first time one mechanism from the previously discussed melanosome dispersion triggered by increased activity of the protein kinase A on a molecular level. Namely, they showed that the actin-based Myosin-Va/Melanophilin/Rab27a transport is up-regulated by the protein kinase A and in turn distributes the melanosomes across the actin mesh across the cytoplasm.

3.3.1.3. The dynein motor

The structure of cytoplasmic dynein is distinctly different from that of the Kinesin and myosin motors (Figure 2). Similar to the other motors it forms a dimer. However, it consists not only of two heavy chains containing the motor domains, but also features various intermediate, light intermediate, and light chains [132] (Figure 2). Although it has two motor subunits, like Kinesin-2, dynein cannot properly move the melanosome by itself, but only with the help of a large complex of proteins that link the melanosome vesicle and dynein directly to the microtubule tracks and help it maneuver the filaments [43, 132, 133].

3 Introduction

One of the most distinct subunits of this microtubule binding complex of the dynein motor is the dynactin complex, consisting of 23 distinct subunits, including the p150^{glued} protein [1, 134]. The importance of the p150^{glued} subunit derives from the

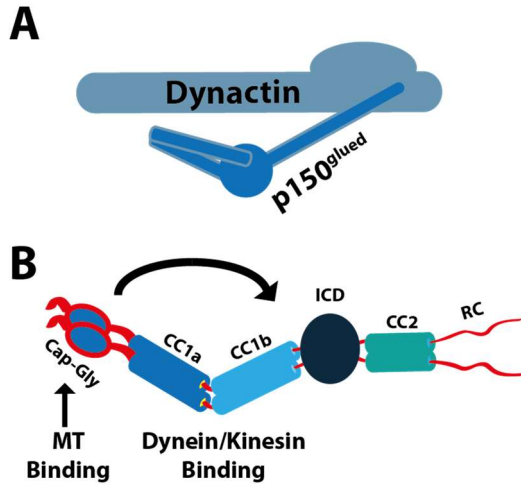


Figure 7: **The schematic structure of the p150^{glued} subunit of the dynactin complex.** (A) Schematic illustration of the p150^{glued} subunit within the dynactin. (B) Schematic illustration of the structure of the p150^{glued} subunit: (Cap-Gly) The N-terminal Cap-Gly domain that supposedly binds to the microtubule filaments, (CC1A and CC1B) the two coiled-coil domains that bind to the dynein or kinesin motor and supposedly can fold onto each other, (ICD) the intercoiled domain, (CC2) coiled-coil domain 2 and (RC) the random coil that links the p150^{glued} with the remaining dynactin complex. Adapted from [1].

fact that it is the actual linker protein between the dynein motor and the rest of the dynactin complex, as well as the microtubule filaments [1, 135, 136]. In 2002, it was also shown *in vivo* that there is a correlation between the state of phosphorylation, and binding to the plus-end of microtubule filaments [135]. However, this has so far been the only indication for such a correlation between microtubule binding behavior and state of phosphorylation, or that the p150^{glued} subunit is the direct target for phosphorylation altogether. Curiously, other studies have also shown that the p150^{glued} subunit interacts with the KAP subunit of the heterotrimeric Kinesin-2 as well, and that it might, therefore, function as a receptor for the plus-end directed transport [76].

p150^{glued} consists of six domains (Figure 7B): the N-terminal Cap-Gly domain, responsible for the binding to microtubule and the two adjacent coiled-coil domains (CC1A and CC1B) that can fold onto each other to the following Intercoiled domain (ICD), burying the Cap-Gly domain in the process. On the C-terminal end of the intercoiled domain follows another coiled-coil (CC2) followed by the random coil (RC) domain that binds the p150^{glued} subunit to the remaining dynactin complex (Figure 7A) [1].

3.3.1.4. Cooperation and interaction between molecular motors

In vitro bottom-up reconstitutions of the different individual motor proteins in combination with top-down isolation and consequent manipulation of entire

3 Introduction

melanosomes and their bound transport complexes have uncovered more and more of the molecular mechanisms behind the structure and regulation of the single motors. Still, very little is known about the direct coordination and interaction of multiple motors at the molecular level.

From numerous top-down observations of the melanosome transport, it is known that the motors involved in this transport move in an either coordinated manner between the Kinesin-2 and dynein motor or a so-called tug-of-war motion between the microtubule-based (Kinesin-2 and dynein) and actin-based (Myosin-Va) transport, where opposing motors interact directly by force transduction through the cargo [76, 109, 110, 113, 118, 137]. That these motors work together and not simply against each other is highlighted in the described paradox of the “co-dependency among antagonistic motors” [113]. This paradox describes the observation that the processivity of one motor indeed decreases and not increases, when the opposing motor is switched off. This has previously been attributed to a.o. a processivity increasing load force provided by the opposing motor [113]. All in all, the result of the melanosome transport is thus a bidirectional and only overall unidirectional net movement, which depends on the degree of activity of each motor or simply on the number of motors bound to the cargo in a finely tuned, interconnected manner [109, 110, 138-141].

Gross *et al.* postulated a model of the melanosome transport by these three previously discussed motors based on *in vivo* data published prior to his work and own *in vivo* data obtained by tracking individual melanosomes with wild-type or dominant inactive Kinesin-2 and Myosin-Va motors, respectively (Figure 8) [118].

During dispersion or increased protein kinase A activity, the processivity of the microtubule-based dynein is down regulated resulting in a reduced runlength of the minus-end movement and an overall dominance of the plus-end driven Kinesin-2 movement, even though the processivity of the opposing Kinesin-2 remains unchanged (Figure 8 A+B). Additionally to the down regulation of the dynein motor, the binding preference of Myosin-Va towards actin is increased, which enables the Myosin-Va to pull the melanosome vesicle from the microtubule filaments onto the actin filaments at intersections during dynein driven movement (Figure 8 B to C).

3 Introduction

This dominant tug-of-war behavior from Myosin-Va further favors the overall dispersion of the melanosome vesicles throughout the cell and has since been shown *in vitro* by Oberhofer *et al.*, even though she showed that it is the binding behavior of the cargo protein Melanophilin and of not the motor itself that is altered by phosphorylation [105]. Curiously, the Myosin-Va seems to be unable to pull the melanosomes off the microtubule during Kinesin-2 driven transport, suggesting a strong affinity of the Kinesin-2 towards the microtubule filaments (Figure 8 C to A).

During aggregation, all melanosome vesicles are pulled from the actin onto the microtubule filaments, as the activity of Myosin-Va is downregulated, seemingly by reduction of the number of bound motors to the vesicle surface (Figure 8 F to D or E). Also, the minus-end directed movement by dynein dominates the melanosome transport, induced by an up regulated mean runlength of the dynein motor, while the plus-end directed transport of Kinesin-2 seemingly remains again unchanged (Figure 8 D+F), a mechanism confirmed a few years later by Zaliapin *et al.* [142].

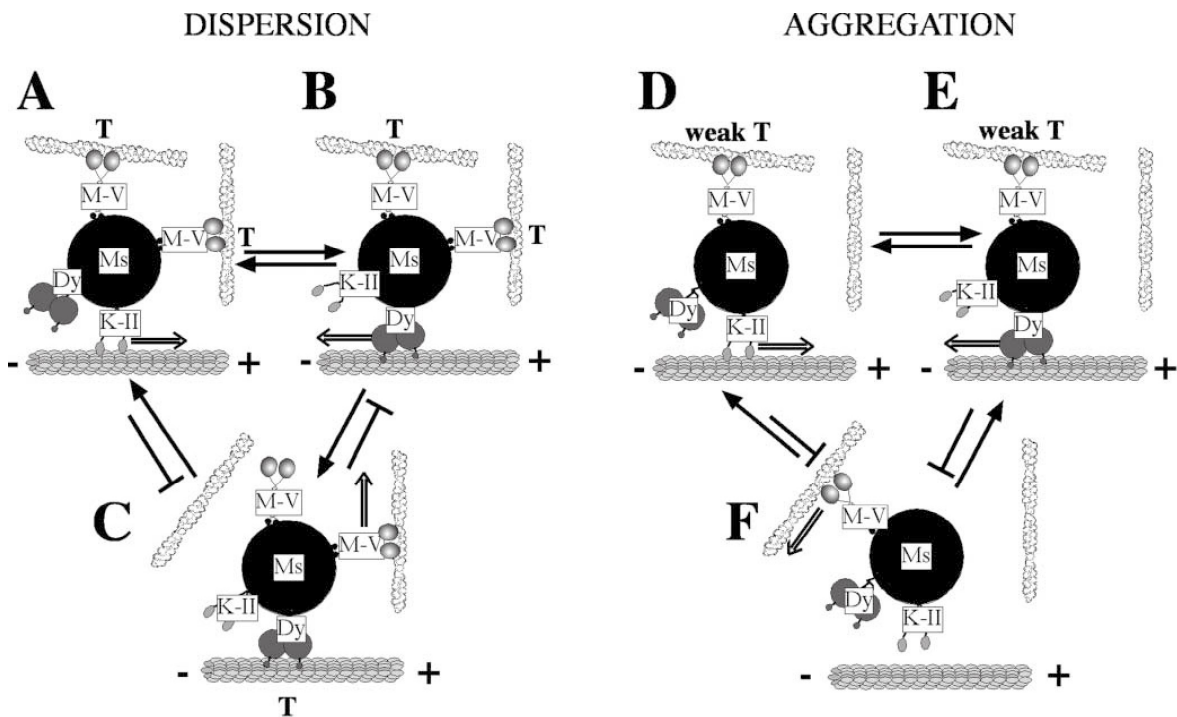


Figure 8: **Theoretical model for the melanosome transport in *X. laevis* by the f-actin- and microtubule-based motors.** The melanosome (Ms) is transported by either the microtubule-based Kinesin-2 (K-II, A + D), dynein (Dy, B + E) or actin-based Myosin-Va (M-V, C + F). Direction of movement is indicated by double arrows. Single arrows show switching between transport systems. Transient interaction is indicated by (T). Figure adapted from [118]

3 Introduction

Since actual molecular work in the amphibian melanosome transport system from the bottom up has scarcely been done in the past, little is known about the molecular regulation and mechanism behind the Kinesin-2, dynein and Myosin-Va interplay. Only Oberhofer *et al.* were able to reconstitute for the first time the Myosin-Va motor complex and show its regulation by the Melanophilin subunit. However nothing is known about its effect on the entire three-motor transport complex or the other two motors at the molecular level [105, 106].

3.3.2. The intraflagellar transport system

The second model system we were investigating was the intraflagellar transport (IFT) machinery. This transport system builds and maintains cilia and flagella (Figure 9A). Cilia and flagella are highly conserved protrusions that are found in most eukaryotic organisms, from protozoa to humans, and which have a multitude of functions, like cell motility or sensory signal transduction [55]. The elaborate “axoneme”, a ring-shaped assembly of nine peripherally arranged microtubule doublets, interconnected, amongst others, by densely packed nexin and dynein arms, is the backbone of these cilia, and serve as a track for the IFT-trains; the IFT-trains being the motor proteins plus a. o. the cargo-binding protein complexes IFT-A and IFT-B (Figure 9B) [143]. IFT-A consists of six proteins, while the IFT-B complex consists of sixteen proteins including nine core complex proteins, all with mostly unknown functions [144-146]. The IFT-B protein complex - bound to homodimeric OSM-3 - and the IFT-A protein complex - bound to the heterotrimeric KLP11/20/KAP - work in coordination to assure the anterograde transport towards the tip of the cilium, while dynein is responsible for the retrograde transport back to the base of the cilium (Figure 9 B) [55, 147, 148]. In this system, knock-out studies have shown that KLP11/20/KAP and OSM-3 assemble the middle segment together, while OSM-3 alone builds the cilium all the way to the distal segment (Figure 9B) [149, 150].

3 Introduction

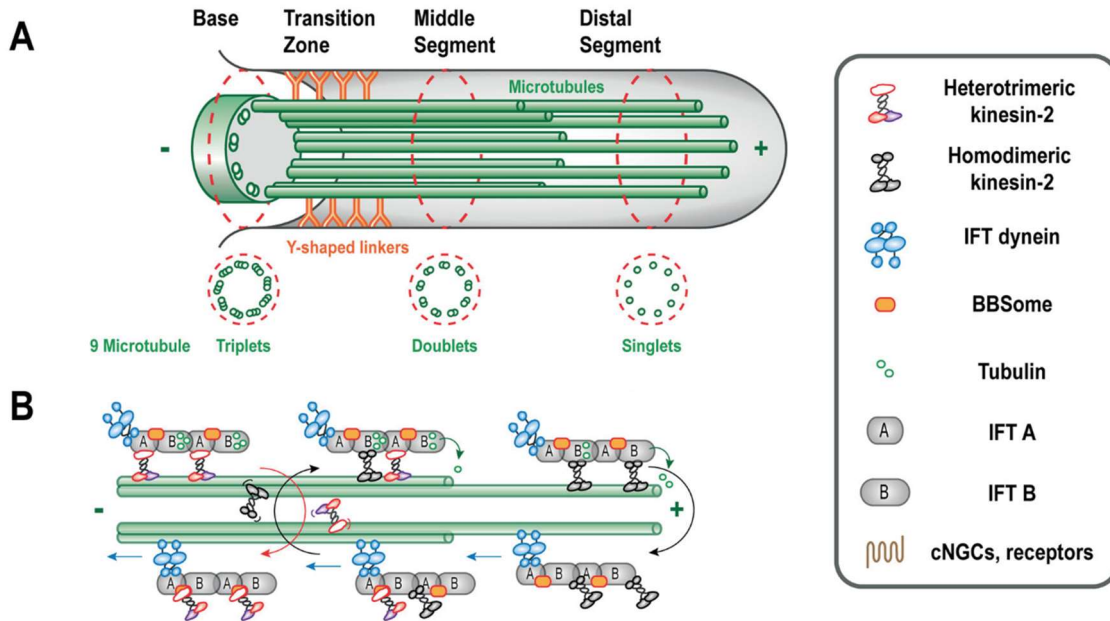


Figure 9: **Intraflagellar transport within the chemosensory cilium of *C. elegans*.** (A) The axoneme is the backbone of the cilium, consisting of 9 microtubule filaments. (B) IFT is driven by the homodimeric OSM-3 and heterotrimeric KLP11/20/KAP, delivering the cargo train (IFT-A, IFT-B, BBSome, Tubulin, etc., simplified) to the tip of the axoneme. Ciliary dynein provides transport back to the base. Text and image adapted from [147].

In vivo, KLP11/20/KAP in isolation moves at a velocity of approximately 0.5 $\mu\text{m/s}$, OSM-3 at a velocity of 1.3 $\mu\text{m/s}$, and the IFT trains, with both motors attached, at an intermediate speed of 0.7 $\mu\text{m/s}$. This intermediate speed most likely results from the coordinated simultaneous action of both motors up to the middle segment [151]. Such a mechanism with intermediate velocity has recently been shown for the artificially linked motors FLA8/10/KAP and KLP11/20/KAP [79].

The homodimeric motor OSM-3 has been shown to be auto-regulated *in vitro*. This autoregulation is most likely achieved through the binding of the previously discussed tail domains to the head domains, by bending of the stalk domains (Figure 4). This is underpinned by the finding that converting a glycine to a glutamic acid at the hinge region in the stalk domain (G444E) resulted in an extended conformation and considerably stimulated processivity in single molecule assays [72]. Cleetus *et al.* recently reconstituted the connection of the OSM-3 motor with its physiologically relevant IFT-B cargo units in an *in vitro* bottom-up approach and showed its activation by the binding of two of the IFT-B core complex proteins to the OSM-3 motor: DYF-1 and OSM-6 [93]. However, detailed information about the

molecular mechanism behind the regulation of this motor and about the exact connection between the core complex proteins and the motor are still missing.

3.4. Aims of this thesis

The intracellular transport and its motor proteins can and have been studied extensively in the past with either a top-down or bottom-up approach. In the more common top-down approach, single, known players, e.g. motors or adaptor proteins, of a given transport system are mutated and consequently any effect of this alteration observed on the whole system either *in vivo* or, e.g. after purification of an entire cargo complex. This has been the case in the extraction of entire melanosomes and the subsequent observation on surface fixed microtubule [152]. This approach is taken to attempt a more physiologically relevant picture, and due to its almost intact, natural state, a more stable state of the observed system. However, if most participating proteins and their distinct functions are unknown, as it is e.g. the case with all intracellular transport systems, direct causality between alterations of one player and the observed effect on the whole system can only be deduced. The bottom-up approach, which we are taking here, on the other hand is done to observe single players, e.g. said motor proteins, separately in an artificial environment and consequently mutate them to observe a direct effect. Subsequently, they are extended with proposed binding partners to gradually fill the gap between the bottom-up and the top-down approaches. This gradual reconstitution avoids ancillary effects of unknown binding partners, but is at the same time, due to its artificial state and environment, considerably more complicated to accomplish.

In this thesis, we shed some light on the molecular mechanics behind two distinct Kinesin-2 motors by observing them in the a.m. bottom-up *in vitro* approach.

To this end, we focused on the molecular mechanism behind the function of the different tail domains of two distinct Kinesin-2 motors. While the structure and in turn the function of the enzymatic head domains are quite conserved throughout organisms and cell types, the tail domains vary considerably depending on specific cargoes and functions which the motors carry. Therefore, we investigated two

3 Introduction

Kinesin-2 motors and their distinct molecular mechanisms and functions from two different organisms and model systems: the homodimeric OSM-3 motor involved in the Intraflagellar Transport (IFT) of protein cargoes in *C. elegans* and the heterotrimeric KIF3A/B/KAP involved in the cytoplasmic transport of melanosome vesicles in *X. laevis*.

Little is known about the amphibian heterotrimeric KIF3A/B/KAP motor from the melanosome vesicle transport. Based on previous findings of the structurally similar KLP11/20/KAP from *C. elegans* (and Intraflagellar transport) [46], a series of experiments were conducted on the KIF3A/B/KAP motor in the past and it was shown that the tail domain of the KIF3A subunit is indeed responsible for the autoinhibition and that this autoinhibition is released upon binding of the KAP subunit to both, the tail domains of the KIF3A and KIF3B subunit. In order to continue and verify these first findings, we designed fluorescently labeled full-length constructs of the KIF3A/B and KIF3A/B/KAP motor to investigate this autoinhibition in - amongst others - a processivity assay on fixed microtubules in a TIRF microscope. Additionally, we designed constructs missing one or both of the tails to determine any specific function of these domains. Finally, since the melanosome transport in *X. laevis* is heavily regulated by the activity of the protein kinase A [117, 122], we tested all features of the KIF3A/B/KAP that had been found during the course of this thesis for regulation by its state of phosphorylation.

Next, we attempted to provide some insight into the interplay of the different motors of the amphibian melanosome transport and determine their influence on each other, as the understanding of the coordination and regulation of the entire melanosome transport system appears to be equally important and complex as that of each individual motor.

To this end, we designed constructs of the p150^{glued} subunit of the dynactin complex and tested these for a number of their proposed functions, namely binding to the microtubule or f-actin filaments or to the KIF3A/B/KAP motor and in turn influencing the motor's processivity positively [1, 76].

Additionally, we attempted to couple the Myosin-Va/Melanophilin/Rab27a complex, with its well-studied regulation [105, 106], with the KIF3A/B/KAP via an artificial

3 Introduction

linker, since the only known connection *in vivo* are the melanosome vesicles themselves. After successful coupling of the KIF3A/B/KAP and the p150^{glued} or Myosin-Va/Melanophilin/Rab27a complexes, our intention was to check their direct interaction on a mixed f-actin/microtubule network, and their possible regulation by external factors like phosphorylation.

The finishing chapter of this thesis deals with the OSM-3 homodimer from *C. elegans*, as another comparative example of the toolbox motor Kinesin-2 with their shared overall structure, but very distinct deployment and functions. The OSM-3 motor, as a homodimer, has a simpler composition as e.g. the heterotrimeric motor KIF3A/B/KAP and a lot is already known about this specific protein. Previous work has shown that the regulation by autoinhibition can be released by binding of the physiologically relevant IFT-B subunits DYF-1/OSM-6 to the motor [72, 92, 93]. This gives us the unique opportunity to determine, for the first time, the exact molecular mechanism behind the regulation of a motor with their naturally found cargo units. The most plausible deduction from these previous findings would be that DYF-1/OSM-6 bind to the tail domains of the OSM-3 motor and release its autoinhibition [72, 92]. In order to clarify this, we designed several, distinct constructs of the different domains of the motor, namely the head, stalk, and tail, as well as of the DYF-1/OSM-6 IFT-cargos. Subsequently, we tested their interaction and effect on each other with co-precipitation, micro-scale thermophoresis, as well as ATPase assays.

4. Materials

4.1. Enzymes, chemicals, Kits and media

Name	Company
Platinum® Pfx Polymerase (Kit)	Life Technologies, Darmstadt
EZ-Vision™ 6x DNA-Dye as loading buffer	New England Biolabs, Frankfurt a. Main
1kb DNA Ladder	New England Biolabs, Frankfurt a. Main
Quiaquick® Gel extraction Kit	Qiagen, Hilden
Quiaquick® PCR purification Kit	Qiagen, Hilden
Var. restriction enzymes	New England Biolabs, Frankfurt a. Main
Antarctic Phosphatase (Kit)	New England Biolabs, Frankfurt a. Main
T4 DNA Ligase (Kit)	New England Biolabs, Frankfurt a. Main
QIAprep Spin Miniprep Kit	Qiagen, Hilden
Bac-to-Bac® Baculovirus Expression Sys.	Life Technologies, Darmstadt
SF900 II SFM medium	Life Technologies, Darmstadt
Cellfectin™ II Reagent	Thermo Fisher Scientific, Darmstadt
Fetal Bovine Serum (FBS)	Sigma-Aldrich, Taufkirchen
Gentamicin (50 mg/ml)	Bio&Sell, Feucht bei Nürnberg
FLAG® resin	Sigma-Aldrich, Taufkirchen
FLAG® peptides	Sigma-Aldrich, Taufkirchen
Ni-NTA agarose beads	Qiagen, Hilden
SNAP-Surface® Alexa Fluor® 488/555/647	New England Biolabs, Frankfurt a. Main
HaloTag® Alexa Fluor® 488/660	Promega, Walldorf
Glucose Oxidase Type VII	Sigma-Aldrich, Taufkirchen
Catalase from bovine liver	Sigma-Aldrich, Taufkirchen

4.2. Buffers and solutions

All buffers and solutions were prepared using reagents from Sigma-Aldrich (Taufkirchen) and Carl Roth (Karlsruhe).

Detailed protocols are listed in the appropriate chapter described in the methods section.

4.3. Oligonucleotides, Plasmids, Vectors, and functionalized dsDNA

4.3.1. PCR-Primers

Primer name	Sequence	Restr.site
S/B/X_Snap_Fw	AAGACTAGTGGATCCCTCGAGATGGATAAGGACTGT GAAATGAAAAGG	SpeI, Bam, XhoI
Kin2a_FIP_Flag_ K/H/N_Rev	ATTGCGGCCGCAAGCTTGGTACCTTACTTGTCATCG TCGTCTTTGTAGTCACCACCGGGATGAAAGAGTC GATGATGTTTCATCTGC	KpnI, HindIII, NotI
XL_Kin2A_Fw	AGGACTAGTATGCCGATCAACAGAGC	SpeI
Kin2a-GCN- 4_AscI_Rev	TGGCGCGCCAATTTCTTTTTGAAACTCTCG	AscI
Kin2B_FIP Fwd	AGGGGGCCCATGTTTATTCCGCTGGAAGAAAAA	Apal
Kif3B_FIP_Rev	TATGCGGCCGCTCACTTGTTCGTCATCGTCCTTGTA TCGCCGCCGGAATAAAGTTTTCTATAATAAGATGC	NotI
FIP +52AA FLAG Rev NotI	TTATGCGGCCGCTCACTTGTTCGTCATCGTCCTTGTA GTCGCCGCCCTTTTCGCATGCTGGCACAGCGGGCGGT T	NotI
FIP +109AA FLAG Rev NotI	TTATGCGGCCGCTCACTTGTTCGTCATCGTCCTTGTA GTCGCCGCCATCCACCTGAATATCATCTTCATCCTG	NotI
FIP +131AA FLAG Rev NotI	TTATGCGGCCGCTCACTTGTTCGTCATCGTCCTTGTA GTCGCCGCCCGGCTGGCGGCTGCTTTTCGGGCGG GT	NotI
Spe_Kin2b_AscI	AGGACTAGTATGAGCAAAGCAAAGCAGCG	SpeI
Kin2b_GCN- 4_AscI_Rev	TGGCGCGCCAATTTCTTCCTGAAATTCGCG	AscI

4.3.2. Sequencing Primers

Primer name	Sequence 5' - 3'
-------------	------------------

4 Materials

PH	cctataaatattccggattattcataccg
SNAP_Kin2A_FLAG-GenScript_Seq_01	atgccaatcaaccgtgccgac
SNAP_Kin2A_FLAG-GenScript_Seq_02	tggcgctactaacaatgaacg
SNAP_Kin2A_FLAG-GenScript_Seq_03	agaagaagaagaagcgccgcg
XI_Kinesin2B_WT_01	gatctgagcagctttgtgacc
XI_Kinesin2B_WT_02	cagctggataaacgcgtggggcg
XI_Kinesin2B_WT_03	gaacgccaggaactgg

4.3.3. Vectors

The pFastBac™1 Vector from LifeTechnologies (Darmstadt) was used for all plasmids in this study

4.3.4. ssDNA for motor coupling

Name	Sequence
Atto633-ssDNA	5'-ATTO633-CCGAGGACTGTCCTCCCGAGTGCGGCT ACGACGTTACCC GGGTGAGCA-3'
Thiol-ssDNA	5'-Thiol-C6-TGCTCACCCGGGTAACGTCGTA GCCGCACTCGGGAGGACAGTCCT CCG-Thiol-C6-3'

4.4. Organisms

XL1-Blue Subcloning-Grade Competent Cell <i>E. coli</i>	Stratagene, La Jolla (U.S.A.)
MAX Efficiency® DH10Bac™ Competent <i>E. coli</i>	Life Technologies, Darmstadt
SF9 <i>S. frugiperda</i>	Life Technologies, Darmstadt

4.5. Software

Microsoft Office 2013	Microsoft, Redmond, WA, U.S.A.
-----------------------	--------------------------------

ImageJ 1.52n	NIH, U.S.A.
MatLab R2016b	The MathWorks, Natick, U.S.A.
Adobe Design Standard CS5	Adobe Systems Inc., San José, USA
Origin Pro 9.1G 64-bit	OriginLab, Northampton, USA
NanoTemper Analysis Software	NanoTemper Tech., Munich

5. Methods

5.1. Molecular biological methods

If not described otherwise, all standard molecular biological methods were executed following instructions as described in [153].

Most of the proteins used in this study are motor proteins, which functionality is highly dependent on the quality of the expression, proper folding and post-translational modifications like phosphorylation. Therefore, the baculovirus expression system hosted by a SF9 cell line (a cell line from ovaries of *S. frugiperda*) was chosen, since it ensures these conditions by also having high expression levels and low safety requirements.

5.1.1. Constructs synthesized with PCR or restriction enzyme-based cut-and-paste cloning

The constructs from Table I were cloned inside the desired vector with the help of restriction and ligation enzymes.

Table I: Constructs synthesized with PCR and restriction enzyme-based cloning into pfastBac1 vector

Construct name	5' restriction site	3' restriction site
N-SNAP_KIF3A_1-597_C-FLAG (KIF3A^{FIP})	SpeI	NotI
KIF3A¹⁻³⁶⁷GCN-4_C-FLAG_C-sfGFP	SpeI	AscI
KIF3B¹⁻⁵⁹²C-6xHis (KIF3B^{FIP})	Apal	NotI
KIF3B¹⁻⁶⁴⁴C-6xHis	Apal	NotI
KIF3B¹⁻⁷⁰¹C-6xHis	Apal	NotI

5 Methods

KIF3B¹⁻⁷²³C-6xHis	Apal	NotI
KIF3B¹⁻³⁶¹GCN-4_C-FLAG_C-sfGFP	SpeI	Ascl
KAP_WT_C-SNAP_C-6xHis	SpeI	Ascl
Rab27a_Q78L_C-6xHis_C-Halo	XhoI	Kpn

All Primers used are listed in 4.3.2. If not mentioned otherwise, all PCR products were introduced into a **pFastBacTM1** vector via the specified restriction sites.

N-SNAP_KIF3A_1-597_C-FLAG (KIF3^{FIP}) was generated by PCR with N-SNAP_KIF3A_WT_FL_C-FLAG as template and S/B/X_Snap_Fw and Kin2a_FIP_Flag_K/H/N_Rev as primers.

KIF3A¹⁻³⁶⁷GCN-4_C-FLAG_C-sfGFP was generated by PCR with N-SNAP_KIF3A_WT_FL_C-FLAG (Genscript) as template and XL_Kin2A_Fw and Kin2a-GCN-4_AscI_Rev as primers. The PCR product was cloned into a pFastBacTM1 vector containing a C-terminal GCN-4_sfGFP_FLAG sequence after the AscI site.

The KIF3B truncations KIF3B¹⁻⁵⁹²C-6xHis (KIF3B^{FIP}), KIF3B¹⁻⁶⁴⁴C-6xHis, KIF3B¹⁻⁷⁰¹C-6xHis, and KIF3B¹⁻⁷²³C-6xHis were generated by PCR with KIF3B_WT_FL_C-6xHis (Genscript) as template and Kin2B_FIP Apal Fwd as the forward primer. The reverse primers were Kif3B_FIP_Rev, FIP +52AA FLAG Rev NotI, FIP +109AA FLAG Rev NotI, and FIP +131AA FLAG Rev NotI, respectively.

KIF3B¹⁻³⁶¹GCN-4_C-FLAG_C-sfGFP was generated by PCR with KIF3B_WT_FL_C-6xHis (Genscript) as template and Spe_Kin2b_AscI and Kin2b_GCIN-4_AscI_Rev as primers. The PCR product was cloned into a pFastBacTM1 vector containing a C-terminal GCN-4_sfGFP_FLAG sequence after the AscI site.

KAP_WT_C-SNAP_C-6xHis was generated by enzyme-mediated cut-and-paste of XI_KAP_C-6His (Genscript) at the specified restriction sites into a pFastBacTM1 vector containing a C-terminal SNAP_FLAG sequence after the AscI site.

Rab27a_Q78L_C-6xHis_C-Halo was generated by enzyme-mediated introduction of a C-terminal Halo-tag into the Rab27a_Q78L_C-6xHis (Genscript) plasmid using the restriction sites AscI and Kpn.

5.1.2. Polymerase chain reaction (PCR)

PCR was conducted using specifically designed forward and reverse primers (4.3.2) and the following reaction-mixture (Table II).

Table II: Reaction mixture for PCR

Components (conc.)	Final concentration	Applied volume
Reaction buffer (10x)	1x	10 μ l
Template DNA	200-300 ng	
dNTP-Mix (10 mM)	0,4 mM	2 μ l
Forward primer (10 μ M)	0,5 μ M	2,5 μ l
Reverse primer (10 μ M)	0,5 μ M	2,5 μ l
Taq Polymerase (5000U/ml)	2,5 U	0,5 μ l
ddH ₂ O		Δ 50 μ l

The mixture was subjected to a predefined thermal cycle to amplify the desired DNA sequence. The PCR cycle included an initial heat-denaturation of the double-stranded DNA, a hybridization of the then one-stranded DNA with the primers, and subsequent synthesis of the desired DNA strand by the polymerase. This thermal cycle was repeated 35 times. The duration of the elongation step was relative to the desired DNA strand's length (1min per 1000 bp). The applied PCR thermal cycle is shown in Table III.

Table III: Thermal cycle protocol for PCR.

	Temperature [°C]	Cycle time [s]	Repetitions
Denaturation	94°C	300 s	
Denaturation	94°C	30 s	35x
Annealing	57°C	30 s	35x
Elongation	68°C	60 s per 1000 bp	35x
Elongation	68°C	420 s	
Storage	22°C	-	

5.1.3. Analysis of PCR product by agarose gel electrophoresis

The amplified PCR product was checked for the right size by agarose gel electrophoresis (1% agarose in 1x TAE buffer). A sample of PCR product was mixed with 6xDNA-Dye and run at approx. 50 to 90 Volts for 20-30 mins and compared to 1 kb DNA ladder. DNA bands were detected by UV light.

50xTAE-Buffer (pH=7.0): TRIS-Base (24.2 % w/v), Glacial acetic acid (5.7 % (v/v), EDTA pH=7.0 (50 mM)

5.1.4. Purification of DNA segment

After confirmation of successful PCR, the rest of the PCR product is run through 1% agarose gel as described before and the band of the desired DNA fragment is cut out of the gel with a clean scalpel. Subsequently, the DNA was purified using the Qiaquick® Gel extraction kit (Qiagen) and eluted in 30 µl Elution buffer (Qiagen).

5.1.5. Restriction digestion of DNA segment

The purified DNA segments were digested for 60 min at 37°C with the desired restriction enzymes after adding 1µl of each enzyme and 3.5µl of 10x CutSmart buffer to the 30 µl DNA solution according to the manufacturer's guidelines in order to create the desired restrictions sites at the 5' and 3' ends. Finally, the DNA was purified again using the Qiaquick PCR purification kit (Qiagen) and eluted in 30 µl Elution buffer (Qiagen).

5.1.6. Preparation of target vector

5µg DNA of the target vector were linearized by restriction digestion and purified as described before. In order to prevent spontaneous relegation, the linearized vector was dephosphorylated at the 5' end by incubating the DNA with Antarctic Phosphatase for 60 min at 37°C. After Dephosphorylation, the enzyme was inactivated by incubating the mixture for 5 min at 70°C.

5.1.7. Ligation of DNA segment into vector plasmid

Ligation of the DNA Insert into the vector was accomplished by mixing 7,5 µl of the Insert DNA with 0,5 µl of the Vector DNA, 1 µl T4 DNA ligase as well as 1 µl T4 DNA ligase buffer and incubating the mix over night or up to 72 h at 16°C.

5.1.8. Transformation of plasmid vector into chemically competent *E. coli*

XL1-Blue cells

100µl *E. coli* XL1-Blue were slowly thawed on Ice, mixed with 10 µl ligated Vector plasmid and incubated on Ice for at least 5 min. The cell-plasmid mix was heat shocked for 70 s at 42°C and subsequently put back and incubated for 2 min on Ice. 200 µl S.O.C. medium was added to the cells and incubated in a thermo mixer at 900 rpm and 37°C. After 60 min, 100 µl of the cell mix was plated into LB-agar/ampicillin plates and incubated over-night in an incubator at 37°C.

S.O.C. medium: Tryptone (2 % w/v), Yeast extract (0.5 % w/v), NaCl (10 mM), KCl (2.5 mM), MgCl₂ (10 mM), MgSO₄ (10 mM), Glucose (2 % v/v with 1M)

LB-agar/ampicillin plates: Agar (1.5 % w/v), Tryptone (1 % w/v), Yeast extract (0.5 % w/v), NaCl (1 % w/v), Ampicillin solution (100mg/ml) (0.1 % v/v)

5.1.9. Amplification of transformed *E. coli* cells

The addition of ampicillin to the LB-agar plates ensures that only ampicillin resistant cells are growing over-night. Since there is an ampicillin resistance cassette encoded in the pFastBac1 plasmid vector, successfully transformed cells can be easily distinguished from “untransformed”/non-resistant cells. After incubation, four 6 ml tubes with 3 ml LB-Ampicillin medium were inoculated with a single colony from the agar plates. The LB-Ampicillin-tubes were incubated over-night at 37°C and 150 rpm in a shaking incubator.

LB-ampicillin medium: Tryptone (1 % w/v), Yeast extract (0.5 % w/v), NaCl (2.5 M) (1 % w/v), Ampicillin solution (100mg/ml) (0.1 % v/v)

5.1.10. Plasmid-DNA extraction from amplified *E. coli* cells

2 ml of the culture medium were transferred into a 2 ml reaction tube. The 2 ml reaction tube was centrifuged at 14 krpm for 1 min. The supernatant was discarded, and the DNA extracted from the cell pellet using the QIAprep Spin Miniprep Kit (Qiagen) following the manufacturer's instructions for DNA precipitation purification. The purified DNA was eluted in 30µl EB buffer.

5.1.11. Determination of DNA concentration

The concentration of the purified DNA was determined using a NanoDrop System following instructions of the manufacturer's instructions.

5.1.12. Test-restriction of purified DNA

In order to test for a successful ligation, transformation and purification of the plasmid DNA containing the desired DNA sequence, a 3 µl sample of the purified DNA was digested with the appropriate restriction enzymes and run through a 1% agarose gel as described before. Two bands (Insert DNA and linearized vector) on the agarose gel at the right sizes confirm a successful test restriction.

5.1.13. DNA sequencing

In order to check for unwanted point-mutations within the PCR product, the remaining 1 ml culture medium from "Plasmid-DNA extraction from amplified *E. coli* cells" were supplemented with 2 ml fresh LB-ampicillin medium and incubated overnight. Subsequently, the DNA was extracted as described before (Plasmid-DNA extraction from amplified *E. coli* cells).

50 – 100 ng/µl DNA were mixed with 15 pmol of the respective sequencing primer (4.3.2) to a total volume of 17 µl and send to MWG Eurofins (Ebersberg) for "Single Read" sequencing. Resulting sequences were aligned with the desired sequences and checked for mutations.

5.1.14. Synthesis of vector for baculovirus expression system

The pFastBacTM1 donor plasmid DNA in this study was provided either by GenScript (Piscataway, U.S.A.) or by self-employed synthesis via PCR, as described above.

5 Methods

The amplified pFastBacTM1 vector was transformed into *E. coli* MAX Efficiency®DH10BacTM cells to transpose the baculovirus shuttle vector. The MAX Efficiency®DH10BacTM bacmid contains a kanamycin marker and a mini attTn7 cassette, which is embedded in the LacZ α peptide. Recombinant bacmid generation is achieved by site-specific transposition between the mini-Tn7 sequence of the pFastBacTM1 vector and the mini-attTn7 site on the bacmid, resulting into the severance of the LacZ α gene on the vector [154]. This disruption inhibits the synthesis of functional β -galactosidase, which enables for the necessary blue/white screening for successful insertion of the gene of interest.

In detail, *Escherichia coli* MAX Efficiency®DH10BacTM cells were thawed on Ice, mixed with approximately 300 ng of the donor DNA, and incubated on Ice for at least 30 min. Subsequently, the cell-DNA mix was heat shocked for 70 s at 42°C and put back on Ice. 800 μ l of S.O.C. medium was added, the cell suspension transferred into 13 ml reaction tubes and incubated for 4 h at 150 rpm and 37 °C in a shaking incubator.

10 and 50 μ l of the grown cell suspension were plated onto blue-white plated and incubated for three days at 37°C. White colonies were re-striking onto fresh blue-white plates to exclude false-positives and incubated for another day.

White colonies were picked, transferred into 6 ml blue-white medium and incubated over-night.

The next day, the cells were centrifuged, and the DNA was purified from the cell pellet with the QIAprep Spin Miniprep Kit (Qiagen) for DNA purification by sedimentation, following the manufacturer's instructions. The isolated DNA was dissolved in 100 μ l ddH₂O.

S.O.C. medium: Trypton (2 % w/v), Yeast extract (0.5 % w/v), NaCl (10 mM), KCl (2.5 mM), MgCl₂ (10 mM), MgSO₄ (10 mM), Glucose (2 % v/v with 1M)

Blue-white plates: Agar (1.5% w/v), Tryptone (1% w/v), Yeast extract (0.5% w/v), NaCl (2.5 M) (1% w/v), Blue-gal (0.1 mg/ml), IPTG (0.04 mg/ml), Kanamycin (0.05 mg/ml), Gentamicin (7 μ g/ml), Tetracycline (0.02 mg/ml)

Blue-white medium: Tryptone (1% w/v), Yeast extract (0.5% w/v), NaCl (2.5 M) (1% w/v), Blue-gal (0.1 mg/ml), IPTG (0.04 mg/ml), Kanamycin (0.05 mg/ml), Gentamicin (7 µg/ml), Tetracycline (0.02 mg/ml)

5.1.15. Purification and activation of fluorescent thiol-dsDNA

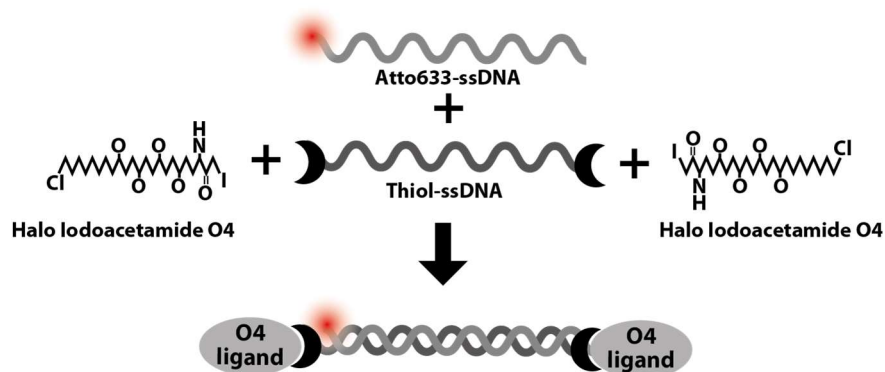


Figure 10: Dimerization and functionalization of the fluorescent, iodoacetamide-bi-functionalized dsDNA. Atto633-ssDNA and Thiol-ssDNA (4.3.4) were mixed in equimolar concentration and incubated for 30 min at room temperature to dimerize. The sulfhydryl-groups (-SH) of Thiol-ssDNA were regenerated by the addition of 10% (final v/v) TCEP (100 mM) and incubation of 30 min at room temperature. 10% (final v/v) of NaAc (3 M, pH=5.2) and 2.5x volume of ice-cold ethanol were added, incubated for 60 min at -20°C and finally centrifuged for 30 min at 4°C at 14 krpm. The DNA pellet was subsequently washed three times with 70% (v/v) ethanol and resolubilized in bicarbonate buffer. The dissolved DNA was immediately reacted with 5-fold excess of Halo Iodoacetamide O4-ligand (in 100 mM DMSO) and incubated for 45 min on a rotor at room temperature. Unbound O4-ligand was removed via HPLC and the functionalized dsDNA stored at -20°C for later use.

Bicarbonate buffer: Ammonium bicarbonate (200 mM, pH=8.0), TCEP (1 mM)

5.2. Protein biochemical methods

5.2.1. Protein expression

5.2.1.1. Transfection of SF9-cells with BacMid plasmid

2 ml SF9-cells with a concentration of 0.5×10^6 cells/ml were put into a 6-well plate (35-mm each) and incubated for at least 30 min (four copies of the desired construct and one control). For each of the four wells, 200 μ l of SF900 serum/gentamicin free Medium, 10 μ l Cellfectin and 10-15 μ l BacMid DNA (at least 30 μ g) were mixed and incubated for at least 30 min. Finally, 800 μ l of SF900 serum/gentamicin free Medium were added.

Next in the 6-well plates, cells that did not bind to the surface were washed off by removing and replacing the serum/gentamicin free medium twice before adding the Cellfectin/DNA mix and incubating for 5 h at 28°C. Finally, the SF900 serum free Medium was replaced with SF900 Medium supplemented with FBS and gentamicin, the 6-well plate were sealed and the cells incubated for 3 - 4 days at 28°C. The thus generated virus generation (P_0) in the supernatant was transferred via syringe through a 0.2 μ m pore size filter into a 2 ml reaction tube and stored at 4°C for future use.

5.2.1.2. Amplification of the baculovirus

To generate the next, amplified generation (P_1), 30 ml of SF9 cells at a concentration of 0.5×10^6 cells/ml were placed in a 26-cm tissue-culture dish and infected with ~500 μ l of the P_0 virus generation. The infected cells were incubated at 28°C for 7-10 days. Afterwards, the cell suspension was centrifuged for 15 min at 3500 rpm to pellet the cell fragments and the supernatant stored in a 50 ml reaction tube at 4°C.

The steps described above were repeated to amplify a P_2 generation from the P_1 generation and so on.

5.2.1.3. Protein expression

The desired amount of SF9 cells at a concentration of 2.0×10^6 cells/ml were infected with 2 – 8 % (v/v) of virus and incubated in a sterile Erlenmeyer flask in an incubation shaker for 48 to 60 hours at 28°C and 110 rpm.

After the incubation time, the cell suspension was centrifuged at 2500 rpm for 15 min and the cell pellet either stored at -20°C or directly used for protein purification.

5.2.2. Protein purification and functionalization

5.2.2.1. Protein purification via FLAG-tag

The cell pellet was resuspended in 4 % (v/v Cell suspension) FLAG-Lysis buffer, homogenized by pipetting up and down and centrifuged at 30 krpm and 4°C for 10 min to clear of the cell suspension from cell debris. The supernatant was transferred into 15 ml reaction tube and incubated for 90 min at 4°C with 2.5 % (v/v Lysis Buffer) FLAG® Resin (Sigma-Aldrich) on a rotor.

After the incubation, the cell suspension was centrifuged at 1000 rpm and 4°C for 15 mins. The supernatant was discarded and the pelleted FLAG® Resin with the bound proteins were transferred into a fresh 1,5 ml reaction tube with 1 ml FLAG-Wash-Buffer I. The solution was centrifuged at 14000 rpm for 1 min at 4°C and the supernatant replaced with fresh 1 ml of FLAG-Wash-Buffer I. This was repeated once more with FLAG-Wash-Buffer I and another three times with FLAG-Wash-buffer II. Finally, the washed proteins were eluted with a desired amount of FLAG-Elution-Buffer (FLAG-Wash-Buffer II Buffer + 10 % (v/v) FLAG® peptides) and either used directly or shock-frozen in liquid nitrogen and stored at -80 °C.

FLAG-Lysis-Buffer: Pipes (50 mM), KAc (300 mM), $MgCl_2$ (1 mM), DTT (1 mM), ATP (0.1 mM), Triton (0.5 % v/v), Protease inhibitor cocktail, Glycerine (10 % v/v)

FLAG-Wash-buffer I: Pipes (50 mM), KAc (500 mM), $MgCl_2$ (1 mM), DTT (1 mM), ATP (0.1 mM), EGTA (1 mM), Tween20 (0.1 % v/v), Glycerine (10 % v/v)

FLAG-Wash-buffer II: Pipes (50 mM), KAc (200 mM), $MgCl_2$ (1 mM), DTT (1 mM), ATP (0.1 mM), EGTA (1 mM), Tween20 (0.1 % v/v), Glycerine (10 % v/v)

5.2.2.2. Protein purification via 6xHis-tag

The cell pellet was resuspended in 4 % (v/v Cell suspension) His-Lysis buffer, homogenized by pipetting up and down and centrifuged at 30 krpm and 4°C for 10 min to clear of the cell suspension from cell debris. The supernatant was transferred into 15 ml reaction tube and incubated for 90 min at 4°C with 2.5 % (v/v Lysis Buffer) Ni-NTA beads (Qiagen) on a rotor.

After the incubation, the cell suspension was centrifuged at 500 rpm and 4°C for 15 mins. The supernatant was discarded and the pelleted Ni-NTA beads with the bound proteins were transferred into a fresh 1,5 ml reaction tube with 1 ml His-Wash-Buffer. The solution was centrifuged at 14000 rpm for 1 min at 4°C and the supernatant replaced with fresh 1 ml of His-Wash-Buffer. This was repeated twice more with His-Wash-Buffer. Finally, the washed proteins were eluted with a desired amount of Elution-Buffer and either used directly or shock-frozen in liquid nitrogen and stored at -80 °C.

His-Lysis-Buffer (pH=8.0): Pipes (50 mM), KAc (300 mM), MgCl₂ (1 mM), DTT (1 mM), ATP (0.1 mM), Triton (0.5 % v/v), Protease inhibitor cocktail, Glycerine (10 % v/v), Imidazole (10 mM)

His-Wash-buffer (pH=8.0): Pipes (50 mM), KAc (500 mM), MgCl₂ (1 mM), DTT (1 mM), ATP (0.1 mM), EGTA (1 mM), Tween20 (0.1 % v/v), Glycerine (10 % v/v), Imidazole (40 mM)

His-Elution-buffer (pH=7.0): Pipes (50 mM), KAc (100 mM), MgCl₂ (1 mM), DTT (1 mM), ATP (0.1 mM), EGTA (1 mM), Tween20 (0.1 % v/v), Glycerine (10 % v/v), Imidazole (500 mM)

5.2.2.3. Tandem protein purification via FLAG- and 6xHis-tag

For the tandem purification, the proteins were purified following the instructions for 5.2.2.1. The purified product was consequently incubated with Ni-NTA beads and washed as well as eluted as described in 5.2.2.2 Protein purification via 6xHis-tag.

5.2.2.4. Protein purification of analytical co-expression via FLAG- and 6xHis-tag rescue

For this analytical rescue purification, the proteins were purified following the instructions for 5.2.2.1. with the exception that, after the incubation with the FLAG® Resin, the cell lysate was not discarded. Instead, the cell lysate was incubated once more, but with Ni-NTA beads and consequently washed as well as eluted as described in 5.2.2.2.

5.2.2.5. Binding assay by incubation on beads

For this analytical purification, two potential binding partners – one of which has a FLAG tag and the other a 6xHis-tag and no FLAG-tag - were purified as described before via FLAG-tag purification 5.2.2.1 and 6xHis tag purification 5.2.2.2, respectively. The protein batch purified via the FLAG-tag was not eluted and left on the beads after the washing steps. The finished eluate from the 6xHis-tag purification was mixed with the FLAG-beads to incubate over night at 4°C on a rotor. The next day, the FLAG beads were washed three times with FLAG-Wash-Buffer II and finally eluted.

5.2.2.6. Fluorescent labeling of proteins

N- or C-terminally functionalized Proteins with an either Halo- or SNAP-tag were purified as described above. However, before elution, the proteins were incubated for 40 min at 4°C on a rotor in the dark with 10µM Halo- or SNAP-tag dye dissolved in FLAG-Wash-Buffer II or His-Wash-Buffer. The proteins were consequently washed again with FLAG-Wash-Buffer II or His-Wash-Buffer for three times and eluted as described above.

5.2.2.7. Dephosphorylation and phosphorylation of proteins

In order to phosphorylate or dephosphorylate, a batch of proteins were purified as described above. However, before elution – and, if combined with fluorescent labeling, after labeling – the proteins were incubated at room temperature for 30 min on a rotor with either 200µl of phosphorylation or dephosphorylation mix. For the dephosphorylation Mix, the Antarctic phosphatase buffer containing ZnCl₂ was

5 Methods

replaced by a self-developed Pipes-Zinc-Acetate buffer, because the $ZnCl_2$ inadvertently inhibits the motors' processivity.

The proteins were consequently washed again with FLAG-Wash-Buffer II or His-Wash-Buffer for three times and eluted as described above.

Phosphorylation Mix: fresh PKA (400 nM/26.2 UN), DTT (10 mM), Pipes (50 mM), $MgCl_2$ (2 mM), Phosphatase inhibitor cocktail PhosSTOP, ATP (0.25 mM)

Dephosphorylation Mix: Antarctic phosphatase (30 UN), DTT (10 mM), Pipes (50 mM), $MgCl_2$ (2 mM), ZnAc (0.1 mM)

PKA preparation

The delivered vial of 400 UN of PKA was centrifuged for 3 mins at 2000 rpm and 4 °C, and 1 ml of 6 mg/ml DTT was added. The mix was vortexed and incubated for 10 mins at room temperature. The ready-to-use PKA solution was consequently stored on Ice for not more than 7 days.

5.2.2.8. Optimized FLAG-tag purification for Myosin-Va

Purification of FLAG-tagged Myosin-Va was based on [155] with minor changes. Virus-infected cells were harvested after a desired time of incubation by centrifuging and discarding the supernatant. The cell pellet was subsequently flash-frozen with liquid nitrogen and stored at -80°C. The pellets were thawed gently, resuspended in M5-lysis buffer, and homogenized in a glass homogenizer in ice for approx. five mins. The homogenate was transferred into a fresh falcon tube and incubated for 20 mins at 4°C on a rolling device. The cell-suspension was centrifuged for 15 mins at 4°C and 30 krpm and the supernatant incubated with FLAG-resin for 90 – 120 mins. The Resin was subsequently washed on a PolyPrep column (BioRad) with 2 ml of M5-I and M5-II. The Myosin-Va was fluorescently labeled by adding 10µM SNAP-tag dye dissolved in M5-I and incubated for 40 mins, by gently stirring every 5 min with a glass rod to prevent sedimentation of the beads. Subsequently, the proteins were washed further with 2ml of M5-I, M5-III, M5-IV, M5-III and M5-I. The purified Myosin-Va was finally eluted with M5 elution buffer and stored on Ice for further use. PMSF was added to the buffers right before use.

5 Methods

M5 lysis buffer: MOPS (10 mM, pH=7.0), KAc (200 mM), MgCl₂ (10 mM), EGTA (1 mM), ATP (2 mM), PMSF (0.1 mM), DTT (1 mM), protease inhibitor cocktail

M5-I: MOPS (10 mM, pH=7.0), KAc (500 mM), EGTA (0.1 mM), DTT (1 mM)

M5-II: MOPS (10 mM, pH=7.0), KAc (500 mM), MgCl₂ (5 mM), EGTA (0.1 mM), ATP (1 mM), PMSF (0.1 mM), DTT (1 mM)

M5-III: MOPS (10 mM, pH=7.0), EGTA (0.1 mM), PMSF (0.1 mM), DTT (1 mM), EDTA (1 mM)

M5-IV: MOPS (10 mM, pH=7.0), KAc (500 mM), EGTA (0.1 mM), PMSF (0.1 mM), DTT (1 mM), EDTA (1 mM)

M5 elution buffer: MOPS (10 mM, pH=7.0), KAc (200 mM), EGTA (0.1 mM), PMSF (0.1 mM), DTT (1 mM), 0.3 mg/ml FLAG[®]-peptides

5.2.2.9. G-actin purification from rabbit muscle tissue

Actin from rabbit skeletal muscle was extracted from an acetone powder as described [156]. The back and upper thigh muscles of a rabbit were chilled, grounded twice and, to remove myosins and extracted with high-salt extraction buffer for 10-15 mins on a stirrer. The mixture was centrifuged at 4k x g, 4°C for 10 mins and re-extracted. The pellet was then stirred in cold distilled water for 10 mins and subsequently centrifuged as before with repeats until swelling of the sediment was observed. The pellet was incubated with cold acetone for about 30 mins, filtered, and dried overnight. The acetone powder was stored at -20 °C for subsequent actin preparations.

Usually, 10 g acetone powder were extracted with 200 ml G-buffer plus 0.2 mM ATP at 4 °C for 30 mins, filtered through nylon nets, and re-extracted for 15 mins. The filtrate was centrifuged at 30k x g for 30 mins at 4 °C. Actin polymerization was promoted by the addition of 50 mM KCl, 2 mM MgCl₂, and 1 mM ATP dissolved in 100 mM NaOH and the mixture was incubated at 4 °C for two hours or overnight. To remove tropomyosin, solid KCl was slowly added until a final concentration of 0.8 M was reached. Filamentous actin was subsequently pelleted by centrifugation (150 000X g, 3 hours, 4 °C), the supernatant was discarded, and the pellet was

5 Methods

homogenized in G-buffer with a douncer. For actin depolymerization, the homogenized F-actin pellet was dialyzed against G-buffer for 2-3 days with a total of about 6 buffer changes.

The solution was centrifuged at 150 000X g and 4 °C for 3 hours, and about 65% from the top supernatant were further purified using a Sephacryl S300 gel filtration column (2.5 x 45 cm, Pharmacia). Fractions were collected and the actin concentrations determined by measuring the optical density at 280 nm (1 mg/ml pure actin: OD_{290nm}=0.65) (93) and their quality tested in a falling ball viscometry assay. The prepared G-Actin could be stored on ice for up to 3 weeks for most applications and was dialyzed against fresh G-buffer before usage.

High-salt extraction buffer: KCl (0.5 M), K₂HPO₄ (0.1 M)

G-buffer: Tris HCl (2 mM, pH 8.0), CaCl₂ (0.2 mM), DTT (0.5 mM), NaN₃ (0.01%)

5.2.2.10. F-actin polymerization

For the polymerization of labeled and biotinylated F-actin, 0.25 µM biotin-G-actin, 4.75 µM G-actin, 5 µM Phalloidin dye of the desired wavelengths, as well as Pipes (50 mM), MgCl₂ (2 mM), EGTA (1 mM) were mixed together and incubated for 40 min at room temperature in the dark. The polymerized F-actin was subsequently stored on Ice.

5.2.2.11. Tubulin purification from porcine brain tissue

Porcine tubulin was purified as described before [157]. Brains were provided by the "Bayer. Landesanstalt für Landwirtschaft, Institut für Tierzucht, Versuchsstation Grub, Poing".

In a cold room on Ice, approximately 24 brain halves were quickly cleaned from connective tissue and veins. 700g of the brain matter were mixed with 1:1 (w/w) buffer A and homogenized in a mixer. The resulting mixture was centrifuged at 10 krpm and 4°C for 70 min. The supernatant was transferred into a fresh Erlenmeyer flask and 25 % (v/v) glycerine as well as 2 mM ATP were added. The solution was incubated for at least 30 min at 35°C in a rotating water bath to let the tubulin polymerize. Afterwards, the solution was centrifuged at 45 krpm at 32°C for 50 min

5 Methods

to separate the polymerized microtubule. The pelleted microtubule were dissolved in about 50 ml Buffer C, transferred into a cooled glass homogenizer and homogenized for at least 30 min on Ice. The homogenized tubule were centrifuge for 30 min at 36 krpm and 4°C and the supernatant was transferred yet again in a fresh Erlenmeyer falcon. 2 mM fresh ATP were added and the tubule polymerize for 30 min at 35°C in a rotating water bath. The polymerized microtubule were centrifuged at 35 krpm and 35°C for 40 min and the resulting pellet was transferred into a pre-cooled homogenizer with about 30 ml of Buffer B. The microtubules were homogenized and at least 30 min and centrifuged again for 30 min at 4°C and 36 krpm. In order to polymerize the tubule yet again for 30 min at 35°C, the supernatant was transferred into a fresh Erlenmeyer flask and 10% (v/v) DMSO as well as 2 mM ATP were added. The microtubules were yet again centrifuged at 33 krpm and 35°C for 40 min, transferred into a homogenizer with 10 ml Buffer D, homogenized for at least 30 min, and centrifuged again for 15 min at 50 krpm and 4°C. The supernatant was transferred onto an equilibrated phosphocellulose (P-11) column to purify the tubulin from microtubule-associated proteins (MAPs). The fractions containing tubulin were gathered, aliquoted, shock frozen in liquid nitrogen, and stored at -80°C.

Buffer A: Pipes (100 mM, pH 6.8), EGTA (2 mM), MgSO₄ (1 mM), DTT (1 mM), ATP (0.1 mM)

Buffer B: Pipes (500 mM, pH 6.8), EGTA (2 mM), MgSO₄ (1 mM), DTT (1 mM), ATP (1 mM)

Buffer C: Pipes (100 mM, pH 6.8), EGTA (1 mM), MgSO₄ (1 mM), DTT (1 mM), ATP (1 mM)

Buffer D: Pipes (100 mM, pH 6.8), EGTA (1 mM), MgSO₄ (1 mM), ATP (0.05 mM), GTP (0.022 mM), DTT (1 mM)

5.2.2.12. Tubulin Polymerization

Various amounts of purified tubulin with a concentration between 50 and 200 mM were subjected to a clear spin at 80 krpm and 4 °C for 10 min to clear off aggregated tubulin. 1 mM of GTP was added to the supernatant, mixed, and incubated for 60

5 Methods

min at 35 °C in a heat block to allow polymerization. Finally, 20 µM of Paclitaxol were added, the microtubule mixed gently mixed, and incubated over night at 35°C.

For filament-based assays in the TIRF microscope, around 10 mM biotinylated tubulin and 5 mM fluorescently labelled tubulin were added to the initial mix before clear spin.

For the tubulin-stimulated ATPase assay, the polymerized tubulin was centrifuged one more time for 10 min at 80 krpm and 4°C through a sucrose cushion (BRB50Tax + 40% (v/v) sucrose) to separate unpolymerized tubulin. The resulting pellet of polymerized microtubule was washed 4 times with BRB50Tax and finally resuspended in BRB50Tax.

Sucrose cushion: Pipes (50 mM), EGTA (1 mM), MgCl₂ (2 mM), Sucrose (40% w/v)

BRB50Tax: Pipes (50 mM), EGTA (1 mM), MgCl₂ (2 mM), Paclitaxel (5 µM)

Calculation of microtubule concentration

The concentration of the microtubules for the ATPase assay was determined by denaturing the polymerized microtubule and measuring its absorbance at 280nm using a NanoDrop Spectralphotometer system. 10 µl of a 1:5 and 1:10 dilution of the microtubule in BRB50Tax were added to 90µl of 6.6 M guanidium·HCl, mixed very well and its absorbance at 280nm measured. Assuming a molecular weight of 100000 g/mol for a tubulin dimer, the microtubule concentration was determined with the following formula:

$$\left(\frac{E_{280}}{1.03}\right) \times (\text{final dilution of MT mix}) = x \mu\text{M MT}$$

BRB50Tax: Pipes (50 mM), EGTA (1 mM), MgCl₂ (2 mM), Paclitaxel (5 µM)

5.2.2.13. Protein analysis by SDS-polyacrylamid gel electrophoresis (SDS-PAGE)

After protein purification, the purity, size and - in the case of heteromeric proteins – stoichiometry were verified by SDS-polyacrylamid gel electrophoresis as described in [153]. 7%, 10% or 12% acrylamide separating gels were used in this study,

5 Methods

depending on the range of sizes of the analysed proteins, with an 4% acrylamide stacking gel on top. 1 to 15 μ l protein sample were added to water up to a total volume of 15 μ l and consequently mixed with 10 μ l SDS loading buffer (6X). The samples were mixed well and cooked for 5 min at 95°C before being loaded into the gel. Finally, an electric current of 20 to 80 mA was applied for at least 40 mins to separate the proteins. The gel was consequently stained for at least 60 min with Coomassie Brilliant Blue in a shaker, as well as destained twice afterwards with destaining buffer, and finally documented and stored in water.

SDS-polyacrylamide separating buffer (10x): TRIS-Base (0.5 M, pH=6.8), SDS (0.4 % w/v)

SDS-polyacrylamide stacking buffer (10x): TRIS-Base (1.5 M, pH=8.8), SDS (0.4 % w/v)

SDS-polyacrylamide separating Gel (10%): Rotiophorese Gel 30 (3.3 ml), Separating buffer (10x) (2.5 ml), ddH₂O (4.2 ml), TEMED (10 μ l), APS (100x) (100 μ l)

SDS-polyacrylamide stacking Gel: Rotiophorese Gel 30 (1.3 ml), Stacking buffer (10x) (2.5 ml), ddH₂O (6.2 ml), TEMED (10 μ l), APS (100x) (100 μ l)

SDS-PAGE running buffer: TRIS-Base (3 % w/v, pH=8.8), SDS (1 % w/v), Glycine (14 % w/v)

SDS protein sample buffer (6X): TRIS-Base (200 mM, pH=6.8), EDTA (15 mM), SDS (12 % w/v), Glycerol (30 % (v/v), Bromphenol Blue (0.06 % v/v), β -mercaptoethanol (15 % v/v)

Commassie brilliant blue Staining solution: Brilliant Blue R-250 (0.25 % w/v), Methanol (50 % v/v), Glacial acetic acid (10 % v/v)

Destaining solution: Glacial acetic acid (10 % v/v), Isopropanol (25 % v/v)

5.2.2.14. Determination of protein concentration by SDS-polyacrylamid gel electrophoresis (SDS-PAGE)

In this study, the concentration of all proteins was determined by comparison to Bovine Serum Albumin (BSA) standards. To this end, 4 samples of BSA

(0,1/0,2/0,3/0,4 mg/ml) were run with the unknown proteins. Using the ImageJ software plugin “Analyze Gels”, the band intensities of the sample proteins were compared with a calibrated trend line of the BSA standard band intensities.

5.2.3. *In vitro* phosphorylation assay with isotope-labeled ATP

This assay was used to detect phosphorylation of given proteins by the protein kinase A (PKA) enzyme. The desired proteins were purified as described before, with the distinct difference that there is no ATP in the elution buffer and the buffer for the last two washing steps. PKA was prepared as described before.

200 nM PKA and a desired amount of substrate motor complex were mixed in Phosphatase buffer without ATP to a constant total volume of 26.9 μ l. To start the reaction 3.1 μ l of 1 μ M isotope-labeled ATP (diluted in 1:30 “cold” ATP) were added to the PKA-substrate mix and incubated for 20 min at 30 °C. The reaction was quenched by adding 10 μ l of 6x SDS-sample buffer and cooked for 5 mins at 95 °C. 15 μ l of the cooked solution were applied onto a 10% SDS gel and separated by electrophoresis. The Gel was subsequently wrapped in cling foil and placed in a phosphor storage screen overnight. The screen was scanned using a phosphorimager (Typhoon 9200, Molecular Dynamics) and acquired images were analyzed with ImageJ.

Phosphatase buffer: fresh PKA (400 nM/26.2 UN), DTT (10 mM), Pipes (50 mM), $MgCl_2$ (2 mM), Phosphatase inhibitor cocktail PhosSTOP

SDS protein sample buffer (6X): TRIS-Base (200 mM, pH=6.8), EDTA (15 mM), SDS (12 % w/v), Glycerol (30 % (v/v), Bromphenol Blue (0.06 % v/v), β -mercaptoethanol (15 % v/v)

5.2.4. *In vitro* colocalization assay

This assay was used to detect binding between two distinct proteins. To this end, both binding partners were functionalized with two different dyes, as described in 5.2.2.6, mixed in appropriate ratios, and incubated over night at 4°C on a rotor. The next day, a sample of the mixture was diluted with BRB50, 4 μ l were pipetted onto a glass slide and covered with a cover slip. Images of the fluorescently labelled

5 Methods

proteins were taken with a commercially available TIRF microscope (DMI8, Leica (Germany)) equipped with a plan objective lens (100x, N.A. 1.47 oil) and a back-illuminated Andor U897 EMCCD camera (Andor, UK) controlled by the “AF 6000” software (Leica, Germany). Images were processed using ImageJ and colocalization spots were detected using MatLab software. The software selected spots in the acquired image automatically by comparing their brightness to the mean brightness of each frame. Spots of each channel were saved and colocalization was determined if spots were superimposed within a 3x3 pixel window.

BRB50: Pipes (50 mM), MgCl₂ (2 mM), EGTA (1 mM), DTT (2.5 mM)

5.2.5. *In vitro* bleaching assay

This assay was used to verify that single molecules were measured in the microscopic assays, as described in [158]. To this end, proteins were diluted in BRB50, pipetted onto a glass slide, and covered with a glass slip. Fluorescence and consequent bleaching were observed with a commercially available TIRF microscope (DMI8, Leica (Germany)) equipped with a plan objective lens (100x, N.A. 1.47 oil) and a back-illuminated Andor U897 EMCCD camera (Andor, UK) controlled by the “AF 6000” software (Leica, Germany). The movies were processed using ImageJ and bleaching numbers were detected using MatLab software.

The software selected spots in the acquired video automatically by comparing their brightness to the mean brightness of each frame. The intensity values for a 3x3 pixel window were summarized. Performing a gliding *t-value* test with a corresponding threshold identified the bleaching steps [158].

BRB50: Pipes (50 mM), MgCl₂ (2 mM), EGTA (1 mM), DTT (2.5 mM)

5.2.6. Flow chambers

So-called Flow chambers were used for most assays in the TIRF microscope.

The Parafilm slip was cut in the right shape using a TEKA (Velen) GCC Lasercuter, placed between the glass slide and the coverslip and bonded by gently applying heat. The chamber volume is between 4 – 6 µl.

5.2.7. *In vitro* filament decoration assay

This assay was used to determine, if a protein is able to bind to fixed filaments, microtubule and/or actin.

First, 6 μ l of 0.5 mg/ml biotinylated BSA was flushed through a flow chamber, incubated for 2 min and the glass surface blocked with 20 μ l BRB-BSA. Next, 6 μ l of 0.5 mg/ml Streptavidin was added into the flow chamber, incubated for 2 min and the chamber washed with 20 μ l of BRB-BSA. Biotinylated and fluorescently labeled filaments diluted in BRB-Tax were gently pipetted into the flow chamber, incubated for 2 mins, and unbound filaments washed out with 20 μ l of BRB-BSA.

Lastly, fluorescently labeled protein diluted in BRB50, an oxygen scavenger enzyme system (0.4% Glucose, 0.18 mg/ml glucose-oxidase and 0.06 mg/ml catalase) and, if necessary, 2 mM Adenylyl-imidodiphosphate (AMPPNP) were flushed into the chamber. Pictures of the fluorescently labelled proteins and filaments were taken using a commercially available TIRF microscope (DMI8, Leica (Germany)) equipped with a plan objective lens (100x, N.A. 1.47 oil) and a back-illuminated Andor U897 EMCCD camera (Andor, UK) controlled by the "AF 6000" software (Leica, Germany).

BRB-BSA: Pipes (50 mM), MgCl₂ (2 mM), EGTA (1 mM), DTT (2.5 mM), BSA (10 mg/ml)

BRB50: Pipes (50 mM), MgCl₂ (2 mM), EGTA (1 mM), DTT (2.5 mM)

5.2.8. *In vitro* single molecule processivity assay

In this assay, single fluorescently labelled motor proteins were tested for their ability to show processivity on fluorescently labeled filaments.

To this end, fluorescently labeled filaments were fixed on the glass surface of a flow chamber as described before (5.2.7 *In vitro* filament decoration assay).

Next, the fluorescently labeled protein was diluted in the desired BRB-buffer, an oxygen scavenger enzyme system (0.4% Glucose, 0.18 mg/ml glucose-oxidase and 0.06 mg/ml catalase) and 2mM ATP were flushed into the chamber. Pictures and

movies were taken using a TIRF microscope, as described above, and processed using ImageJ and MatLab (Mathworks Inc.) software.

Runlength and velocity were analyzed with custom-written methods using MatLab software (Mathworks Inc.) The software selected spots in the acquired video automatically by comparing their brightness to the mean brightness of each frame. The exact position of the spot was calculated using the FIONA method, a radial center approach. Determined spots for each frame were saved and compared to the following frame. Runs were considered processive and smooth with a minimal run length of 1 μm . The run length data were fit to a truncated ($x_0 = 1 \mu\text{m}$) single-exponential distribution. Parts of the distance over time data were considered for speed calculation if a linear fit of at least six frames resulted in a r^2 -value of more than 95%.

Statistical significance between datasets was determined by a two-sample t-test performed in *R*: random resampling of the data by bootstrapping ($R=1000$) resulted in p -values for the comparison of the means. p -values of <0.01 were used to reject the null hypothesis [159].

BRB50: Pipes (50 mM), MgCl_2 (2 mM), EGTA (1 mM), DTT (2.5 mM)

HSBRB80: Pipes (50 mM), KAc (100 mM), MgCl_2 (2 mM), EGTA (1 mM), DTT (2.5 mM)

5.2.9. Microtubule-stimulated ATPase enzyme activity assay

In this assay, the enzymatic activity of the head domain of each motor was determined. The head domains of the motors used in this thesis are filament

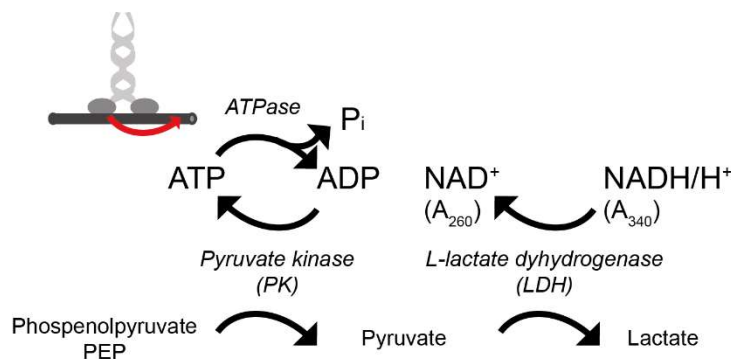


Figure 11: **Coupled enzymatic steady-state ATPase assay.** The motor domains hydrolyze ATP to ADP and inorganic Phosphate, if active. The Pyruvate kinase (PK) resynthesizes the ATP back from the generated ADP, providing a constant ATP level. The linked Lactate dehydrogenase (LDH) oxidizes one NADH to NAD^+ per resynthesized ATP. The concentration of NADH - and in turn the ATP consumption - can be monitored by measuring the absorption decrease at 340 nm.

stimulated ATPases, which hydrolyze ATP and thus turn the gained chemical

5 Methods

energy in kinetic energy in the presence of its respective filament. The degree of hydrolysis was measured with a coupled enzymatic assay, which upon hydrolysis of ATP to ADP oxidizes NADH/H⁺ to NAD⁺ to regenerate ATP. In detail (Figure 11), pyruvate kinase (PK) regenerates ATP by oxidizing phosphoenolpyruvate (PEP) to pyruvate, which in turn is reduced to lactate by L-lactate dehydrogenase (LDH) fueled by the oxidation of NADH/H⁺ to NAD⁺. This last oxidation step and in turn the consumption of ATP can be quantified, since NADH/H⁺, in contrast to NAD⁺, absorbs light at a wavelength of 340 nm.

In this thesis, eight 50 µl samples containing 7.7 µl of motor protein with desired concentration, 2,3 µl of the enzymatic regeneration system, a dilution series of eight steps from 1.25 to 80 mM microtubule, and 3,3 µl of 30 mM ATP-MgCl₂ and were mixed and pipetted into a 96-well plate. The decrease of light absorption at 340 nm was measured for 30 min at 25°C. Four blank measurements with twice no ATP-MgCl₂ or no microtubule respectively were also measured. The decrease of NADH/H⁺ concentration was calculated applying the Law of Lambert-Beer (Equation 1:):

Equation 1: [160]

$$\frac{\Delta E}{t} = \frac{\epsilon \times \Delta(NADH) \times d}{t}$$

$\Delta E/t$ Change of extinction over time

ϵ Extinction coefficient for NADH at 340 nm ($\epsilon_{(NADH,340)} = 6.22 \text{ Mol}^{-1} \text{ cm}^{-1}$)

d Diameter of a well in 96-well plate

k_{cat} was determined by plotting the change of absorption over time against microtubule concentration (1.25 – 80 mM) and fitting a hyperbolic curve based on Michaelis-Menten kinetics to the determined values. The maximum number of ATP hydrolyzed per head domain per minute (k_{cat}) was calculated using the Equation 2::

Equation 2:

$$k_{cat} = \frac{\frac{\Delta c_{ATP}}{\Delta t}}{c_{enzyme}}$$

BRB50: Pipes (50 mM), MgCl₂ (2 mM), EGTA (1 mM), DTT (2.5 mM)

ATPase regeneration system: NADH (1.5 mM), Hepes (100 mM), Phosphoenolpyruvate (PEP) (3 mM), Pyruvate kinase (PK) (1.6 U/m), Lactate dehydrogenase (LDH) (2.2 U/ml)

ATP-MgCl₂: ATP (30 mM), MgCl₂ (75 mM)

5.2.10. Micro-scale thermophoresis

In this study, we applied the micro-scale thermophoresis (MST) Monolith NT.115 (NanoTemper Technologies, Munich) to determine the binding affinity of two given proteins (Figure 12A) [161]. This assay is based on thermophoresis or the Ludwig-Soret effect, the directed movement of molecules in a temperature gradient, which strongly depends on a variety of molecular properties such as size, charge, hydration shell or conformation [162]. This biophysical feature has been reported and discussed many times before [163-165]: Generally, the movement or velocity of each molecule in an temperature gradient can be described with a linear drift response (Equation 3), which is linearly dependent on the temperature gradient (gradT) with the proportionality constant D_{Ti} (thermal diffusion coefficient):

Equation 3

$$v = -D_{Ti}gradT$$

The index “i” represents the different states and types of molecules. For low molecular concentrations (~ nM) and the addition of the diffusion coefficient D_i and the concentration of the molecule c_i , the equation for the molecule flow density becomes (Equation 4):

Equation 4

$$j_i = -c_i D_{Ti} gradT - D_i gradc_i$$

Assuming that the thermal diffusion coefficient D_{Ti} and diffusion coefficient D_i are temperature independent, Equation 4 can be integrated to a steady state concentration at the position of the temperature difference of (Equation 5)

5 Methods

Equation 5

$$c_{ti} = c_i \exp(-S_{Ti} dT)$$

The Ludwid-Soret coefficient S_{Ti} can thus be described as (Equation 6)

Equation 6

$$S_{Ti} = D_{Ti}/D_i$$

and is therefore highly dependent on the properties of the molecule which affect its overall diffusion coefficient, like the size, charge, or interaction with the solvent [164, 166]. Binding of a given ligand to this molecule changes at least one if not all these properties and - as a result - can be detected by the MST.

During an MST measurement, a capillary - containing the ligand protein in degressive concentration and the fluorescently labelled protein - is exposed to a temperature gradient of about 2-6 °C with a diameter of 50 µm induced by an infrared laser. Right before and during the exposure time, the fluorophore-labeled protein's movement is traced and quantified (Figure 12B-C). Any changes made to the size, charge, hydration shell or conformation of the given proteins, e.g. by binding to a prospect binding partner, influence the movement of the protein and thus allows the user to determine the given proteins' binding affinity. The K_d of this binding can be determined by applying a dilution series of ligand proteins to the fluorescently labeled binding partner (Figure 12D).

In detail, a dilution series of 16x 20 µl samples was created, containing the fluorescently labeled protein with a fixed concentration of about 10-fold below the expected K_d and the ligand protein as a non-linear dilution series, starting at a concentration around 10 fold higher than and at least half of the samples close to the expected K_d .

Prior to the sample testing, the capillaries as well as buffer and experimental conditions were tested to avoid unwanted effects such as aggregation/degradation of the proteins or unspecific binding to the wall of the capillaries, namely coating of the capillaries, buffer types and salt concentrations, as well as detection- and infrared laser power. Consequently, the assay was conducted using uncoated capillaries, the standard TRIS-MST buffer with 50 mM KAc and 100% LED power,

5 Methods

40% MST laser power, and a constant temperature of 23°C. The time settings (Figure 12C) were set to Fluorescent measurement start 5s before IF-laser on, MST IR-laser on for 20s, and Fluorescent measurement 5s after IF-laser off with a 25s delay time in between measurements.

Acquired results were analyzed using NT control and analysis software. F_{cold} was set to 1s before IF-laser on, and F_{hot} to 1s before 10s On time of the IR-laser (Figure 12D).

TRIS-MST buffer: TRIS (50 mM), KAc (50 mM), MgCl_2 (1 mM), DTT (1 mM), ATP (0.1 mM), Tween20 (0.05 % v/v), EGTA (1 mM), Glycerol (10% v/v)

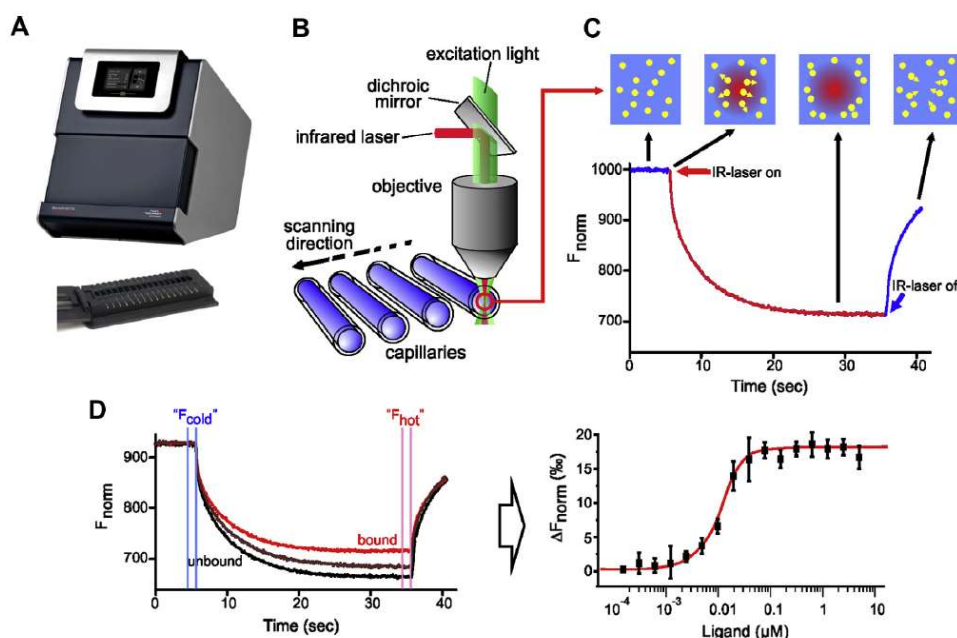


Figure 12: **MST setup and experiments.** (A) The Monolith NT.115 (NanoTemper Technologies GmbH) used in this thesis. (B) Schematic representation of MST optics. The fluorescence within the capillary is excited and detected through the same objective. A focused IR-Laser is used to create the local temperature gradient, resulting in detectable thermophoresis of the fluorophore-labeled molecules. (C) Typical signal of a MST measurement. First, the molecules are evenly distributed by diffusion and the base fluorescence is detected. Subsequently, the IR-laser is turned on for approx. 30 s and the thermophoretic movement of the molecule out of the heated sample volume can be detected. After deactivation of the IR-Laser the “back diffusion” of the molecules can be detected. (D) Typical results from a binding experiment. The thermophoretic movement of a fluorophore-labeled molecule (black trace, “unbound”, left graph) is measured and compared to traces with increasing amounts of unlabelled ligand (red trace, “bound”, left graph). Titration of the non-fluorescent ligand results in a gradual change in thermophoresis (right panel) which is normalized and plotted as [%] Fraction bound. To yield a binding curve, which can be fitted to derive binding constants (e.g. K_D). Image and Caption have been adopted from [161].

6. Results on the regulation of the Kinesin-2 motor KIF3A/B/KAP from *X. laevis*

The amphibious, heterotrimeric KIF3A/B/KAP is known for its role in the melanosome transport system in pigment cells [53, 167]. In this transport system, melanosomes – organelles that synthesize, store and transport pigments – are transported within the cell by a combination of three motors: the actin-based Myosin-Va and the two microtubule-based motors, the anterograde KIF3A/B/KAP and the retrograde dynein [129, 152]. These motors and the direction of the transport are said to be controlled by a so-called “coordinated tug-of-war”, where all motors are bound to the cargo at all times struggling to move the cargo in their direction [113]. This tug-of-war is coordinated by e.g. the adjustable activity of said motors by phosphorylation of the motors by protein-kinase A (PKA), or binding to effector proteins, or even by binding and unbinding of the motors to the cargo [109, 113, 138].

While the other motors of the melanosome transport (Myosin-Va and dynein) have become the target of many studies in the past, the exact molecular mechanisms behind the regulation of the heterotrimeric KIF3A/B/KAP and its role in the coordination of the melanosome transport system are still unknown. However, previous studies have shown that the eukaryotic, ciliary motor KLP11/20 from *C. elegans* is autoinhibited, most likely by folding down at a helix-breaker position and thereupon by binding its C-terminal tail domains to its head domains [168]. The same study has also shown that simultaneously, the tail domain of the KLP11 subunit binds the KAP subunit.

Based on these studies, first attempts to dissect the KIF3A/B/KAP motor have been made by v. Roman [128]. Her studies have shown that both KLP11/20/KAP and KIF3A/B/KAP share many of the highlighted domains and sequences, suggesting similar molecular mechanisms behind both autoinhibition and cargo/KAP binding. By applying co-immunoprecipitation and microtubule decoration experiments, she was able to show that the KAP subunit is bound to the C-terminal tail domain of both KIF3A and KIF3B independently. Additionally, she was able to show in an ATPase

activity assay, that the otherwise autoinhibited KIF3A/B can be activated through deletion of the tail domain of KIF3A.

Building on the previously shown results, the goals of this chapter were therefore:

1. Is the KIF3A/B motor inhibited by the C-terminal tail domain of its KIF3A subunit?
2. Is the KAP subunit bound by the tail domains of the KIF3A or KIF3B subunit and is the previously shown autoinhibition suppressed by the bound KAP?
3. Are any of the found features of the KIF3A/B, e.g. autoinhibition or KAP binding, regulated by its state of phosphorylation?

6.1. Experimental Concept

Previous studies on the functional properties of KLP11/20 from *C. elegans* were conducted in optical tweezer experiments. Micron-sized polystyrene beads were attached to the motor complexes via their C-terminal tail domains, thereby inhibiting any prior function of these domains [46]. In order to test whether the C-terminal tail domain of the KIF3A really inhibits the heterodimer, we needed to test the processivity of single molecule motors with free C-terminal tail domains in a TIRF microscope, rather than in optical tweezer assays. To this end, the motors also needed to be fluorescently labeled without being bound to Q-dots or other complexes. Thus, we designed SNAP-tagged heterodimeric and -trimeric constructs of the KIF3A/B/KAP motor (Figure 13) that were in this way fluorescently labeled: A heterodimeric wild-type construct to verify the autoinhibition (Figure 13 B 1) henceforth called “KIF3A/B” and a heterotrimeric wild-type (Figure 13 B 2) to test for possible activation by KAP binding – “KIF3A/B/KAP”. Additionally, we designed three constructs truncated at the conserved helix breaker (Figure 13 B 3-5) to test for the function of each C-terminal tail domains – e.g. binding of the KAP subunit or the autoinhibition of the motor complex: KIF3A¹⁻⁵⁹⁷/B, KIF3A/B¹⁻⁵⁹² and KIF3A¹⁻⁵⁹⁷/B¹⁻⁵⁹² (Detailed listing in SI).

6 Results on the regulation of the Kinesin-2 motor KIF3A/B/KAP from *X. laevis*

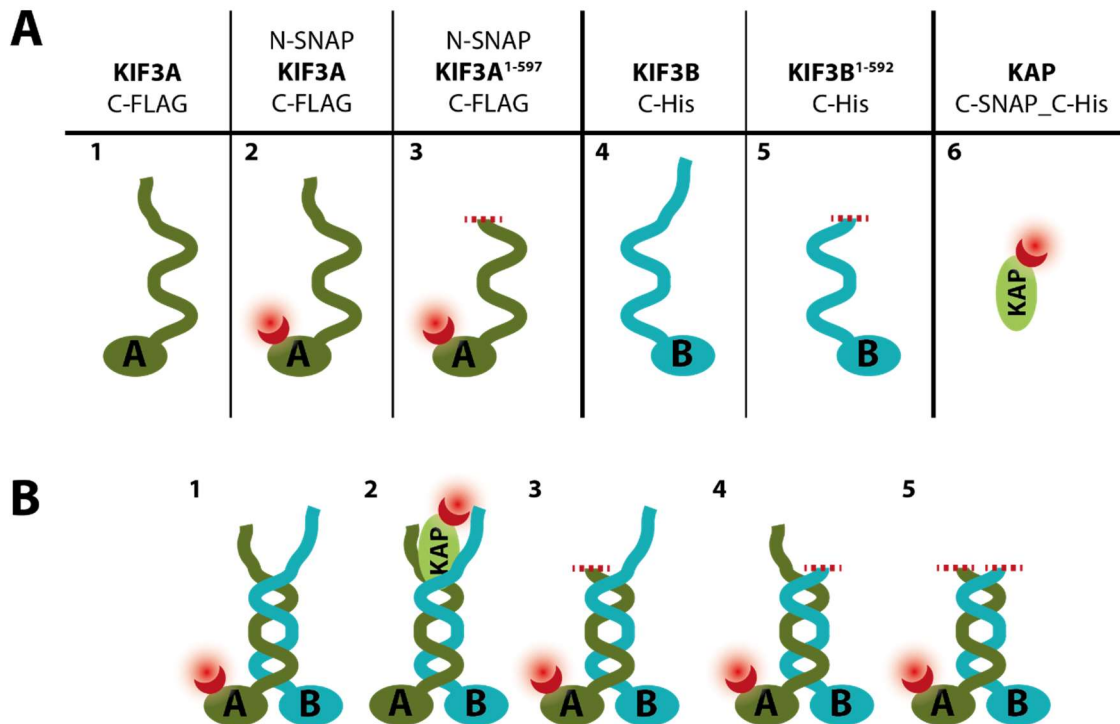


Figure 13: **Overview of generated constructs from *X. laevis***: (A) KIF3A from *X. laevis* was either (1) C-terminally tagged with FLAG or (2) N-terminally tagged with SNAP and C-terminally with FLAG or (3) N-terminally tagged with SNAP and C-terminally tagged with FLAG as well as truncated C-terminally at position 597. KIF3B from *X. laevis* was either (4) C-terminally tagged with 6x-His or (5) C-terminally tagged with 6x-His and truncated C-terminally at position 592. (6) The KAP subunit from *X. laevis* was C-terminally tagged with SNAP and 6x-His. (B) Co-expression of the various constructs resulted in: (1) KIF3A/B: Full-length KIF3A/B N-terminally tagged with SNAP on the KIF3A head-domain, (2) KIF3A/B/KAP: Full-length KIF3A/B/KAP C-terminally tagged with SNAP at the KAP subunit, (3) KIF3A¹⁻⁵⁹⁷/B: KIF3A/B N-terminally tagged with SNAP on the KIF3A head-domain and truncated at the KIF3A subunit (1-597), (4) KIF3A/B¹⁻⁵⁹²: KIF3A/B N-terminally tagged with SNAP on the KIF3A head-domain and truncated at the KIF3B subunit (1-592), (5) KIF3A¹⁻⁵⁹⁷/B¹⁻⁵⁹²: KIF3A/B N-terminally tagged with SNAP on the KIF3A head-domain and truncated at both the KIF3A (1-597) and KIF3B subunit (1-592).

After addressing the function of the different C-terminal tail domains and the KAP sub-unit, the possible phosphorylation of the motor complexes was tested. We conducted a phosphorylation assay with isotope-labeled ATP on all constructs. Subsequently, the full-length motor complexes were phosphorylated or dephosphorylated respectively to test for any regulation of any previously established functions by the protein kinase A.

6.2. Protein expression, purification, and experimental set-up

Prior to testing for processivity by determining the runlength and velocity of the different motor complexes, we needed to ensure that the fluorescently labeled motors were assayed as single motor complexes. Thus, we obtained confirmation

6 Results on the regulation of the Kinesin-2 motor KIF3A/B/KAP from *X. laevis*

of the successful co-expression of the motor complexes and specific fluorescent labeling (Figure 14 A) by FLAG-tag affinity purification, fluorescent labeling of the SNAP-tagged constructs and consequent bleaching assays (5.2.5).

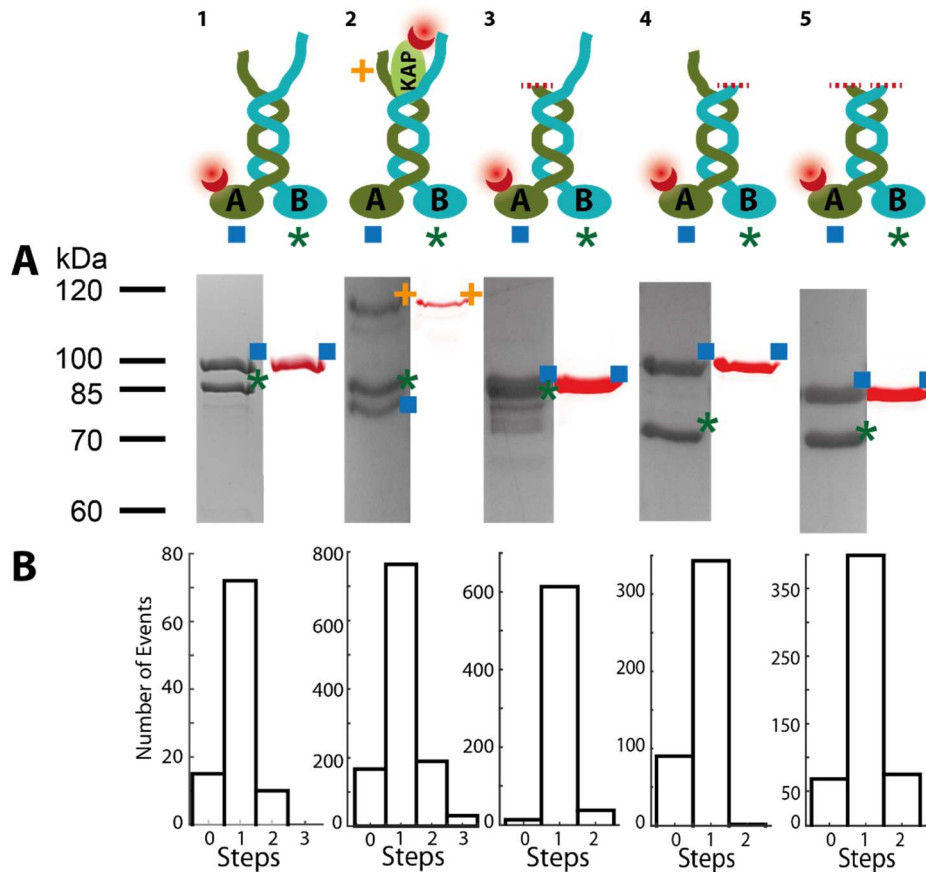


Figure 14: Protein expression, labeling and bleaching assays of the generated constructs: (A) FLAG-tag affinity purification of the constructs (1) – (5) via the KLP3A subunit. (1) SNAP-tagged KIF3A/B, (2) SNAP-tagged KIF3A/B/KAP, (3) SNAP-tagged KIF3A¹⁻⁵⁹⁷/B, (4) SNAP-tagged KIF3A/B¹⁻⁵⁹², (5) SNAP-tagged KIF3A¹⁻⁵⁹⁷/B¹⁻⁵⁹². All KIF3A constructs were also C-terminally FLAG-tagged. (KIF3A^{SNAP} = 103 kDa, KIF3A = 81 kDa, KIF3B = 86 kDa, KAP^{SNAP} = 112 kDa, KIF3A^{1-597,SNAP} = 90 kDa, KIF3B¹⁻⁵⁹² = 69 kDa). All proteins have been incubated with the fluorescently labeled peptide for labeling at the SNAP-tag. Scanning at 642 nm showed that the only labeled protein band is the SNAP-tagged protein – KIF3A or KAP respectively. (B) Photobleaching analysis of the fluorescently labeled constructs displayed single bleaching steps after adjusting of the buffer conditions to 80 mM Pipes and 100 mM KAc. (1) N=97, (2) N=1142, (3) N=654, (4) N=435, (5) N=543, repeated six times.

Initial bleaching assays showed aggregation of both the heterodimer and the heterotrimer. In order to obtain satisfying bleaching results, we increased the Pipes concentration from 50 mM to 80 mM and furthermore to add of 100 mM KAc to the BRB assay buffer (HS-BRB80) (Figure 14B).

6.3. KIF3A/B/KAP and KIF3A/B are both highly processive

Prior to this work, it had been suggested in ATPase assays on KIF3A/B full-length and truncated constructs, that the C-terminal tail domains of the KIF3A subunit is responsible for the motor's autoinhibition [128]. In order to conclusively show the inhibitory function of the tail domains, we conducted single-molecule assays with fluorescently labeled and freely moving KIF3A/B and KIF3A/B/KAP constructs under saturated ATP conditions in the a.m. HS-BRB80 buffer (5.2.8). Surprisingly, both motor complexes were highly processive, traveling approximately three microns with a velocity of around 0.3 $\mu\text{m/s}$ before dissociating from the microtubules (Figure 15). Kymographs, as shown in Figure 15 C, show that those high values for the runlength are indeed the result of uninterrupted runs.

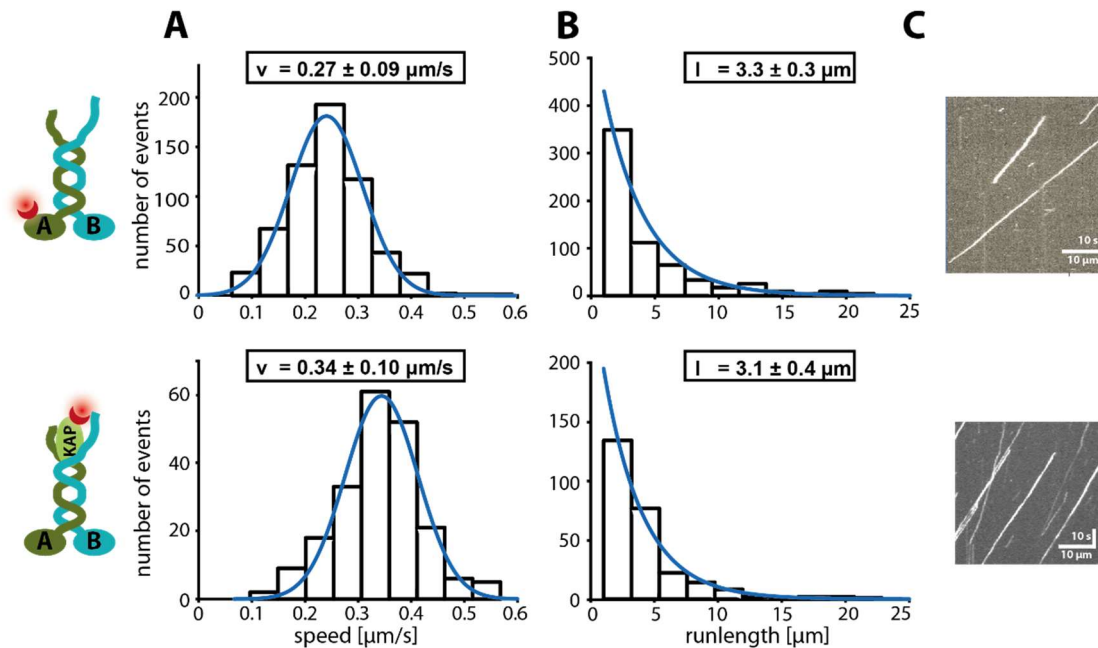


Figure 15: **Single-molecule processivity assay of the full-length KIF3A/B (upper row) and KIF3A/B/KAP (lower row) motors on fixed microtubule.** The movement of single, fluorescently labeled KIF3A/B and KIF3A/B/KAP motors were tracked on fixed microtubule in a TIRF microscope setting (5.2.8). The velocity (A) and run length data (B) were fit to a Gaussian (\pm width of distribution) and single-exponential distribution (\pm confidence interval), respectively. (N = 599 for KIF3A/B, N = 207 for KIF3A/B/KAP, repeated three times). (C) Representative kymographs of the KIF3A/B and KIF3A/B/KAP motors on fixed microtubule.

Repetition of the ATPase assay with the full-length KIF3A/B (Figure 16, blue) delivered the same contrasting results with those that had been observed before in the single molecule assay, namely suppression of the kinetic properties of the full-length motor in the ATPase assay [128]. Curiously, we could also observe that the

6 Results on the regulation of the Kinesin-2 motor KIF3A/B/KAP from *X. laevis*

activity of the motor could be restored by cutting off the tail domain of the KIF3A subunit (Figure 16, green). Increasing salt and buffer concentrations from the initial 50 mM Pipes and 0 mM KAc to 80 mM Pipes and 100 mM KAc, as done for the single molecule assay, and other adaptations, such as temperature, motor concentration or addition of 7,5 % (v/v) of PEG8K detergent could not rescue the activity of the full-length KIF3A/B in the ATPase assay (Figure 16, red). Thus, the false-negative depiction of the motor's autoinhibition in this bulk assay could unfortunately not be fixed and we consequently had to abandon further testing of the KIF3A/B/KAP motor in the ATPase assay.

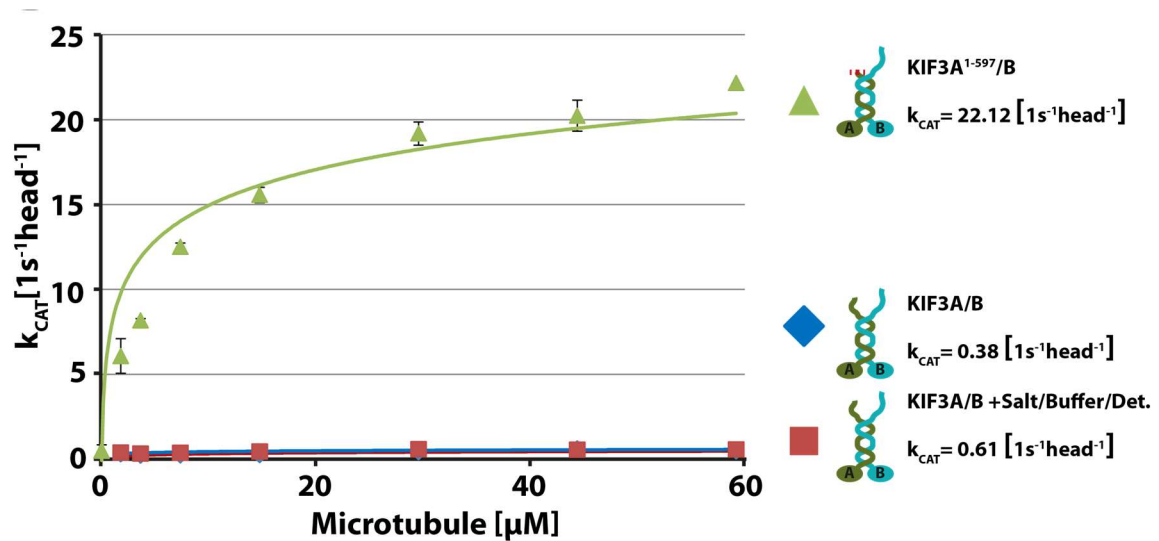


Figure 16: **The activity of the full-length KIF3A/B motor is autoinhibited in bulk ATPase assays.** Microtubule-based ATPase assay shows autoinhibited activity of the full-length KIF3A/B construct, with (red square) or without (blue diamond) increase in concentration of Pipes buffer and salt as well as addition of detergents. Green triangle depicts activity of KIF3A¹⁻⁵⁹⁷/B construct with missing KIF3A tail domain. Repeated two times.

6.4. The tail domain of the KIF3A motor protein is responsible for KAP binding

Since the full-length motors were not autoinhibited (Figure 15), it appeared that the tail domains do not have any influence on the regulation of the activity of the KIF3A/B motor. Therefore, it was now more probable that the tails might be solely responsible for the KAP binding. To test this theory, two distinct assays were utilized.

For the first assay, the full-length and truncated constructs of the KIF3A/B were co-

6 Results on the regulation of the Kinesin-2 motor KIF3A/B/KAP from *X. laevis*

expresses with the KAP subunit and purified by pull-down via the FLAG-tag of the KIF3A or KIF3A¹⁻⁵⁹⁷ subunit, respectively. The formed heterodimers KIF3A/B and KIF3A/B¹⁻⁵⁹² were able to pull-down the KAP subunit, whereas KIF3A¹⁻⁵⁹⁷/B and KIF3A¹⁻⁵⁹⁷/B¹⁻⁵⁹² were unable to do so (Figure 17 A).

In a second assay, the KAP subunit, the full-length and the truncated heterodimers of KIF3A/B were expressed separately and were fluorescently labeled with Alexa-SNAP-647 and Alexa-SNAP-488 dyes, respectively. The motor complexes were immobilized on fixed microtubule in a flow-chamber, using the non-hydrolysable analogue of ATP, AMP-PNP (5.2.7). Subsequently, the KAP subunit was flushed into the flow chamber and monitored for possible binding to the different motor complexes. These co-localization assays confirmed the results from the co-precipitation assay: the KAP subunit was linked to the microtubule by the KIF3A/B and KIF3A/B¹⁻⁵⁹² motor complexes, which was, however, not the case for the KIF3A¹⁻⁵⁹⁷/B complex, and not for the KIF3A¹⁻⁵⁹⁷/B¹⁻⁵⁹² complex neither (Figure 17 B). Together, these results suggest that the KIF3A tail domain is responsible for binding the KAP subunit to the KIF3A/B motor.

6 Results on the regulation of the Kinesin-2 motor KIF3A/B/KAP from *X. laevis*

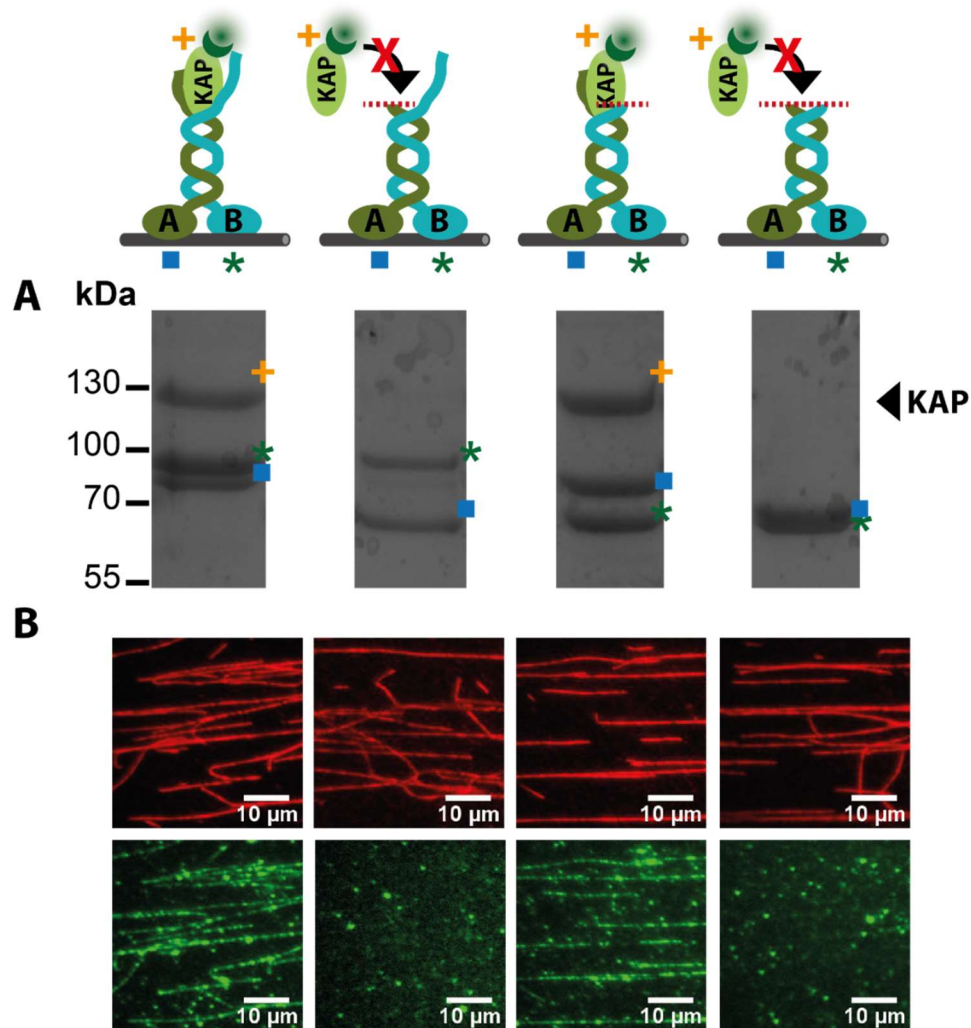


Figure 17: **The C-terminal tail domain of KIF3A is responsible for the binding of KAP.** (A) Co-expression of the KAP subunit with the full-length and truncated KIF3A/B constructs. Constructs were purified via the FLAG-tagged KIF3A subunits of each Co-expression. Only KIF3A/B and KIF3A/B¹⁻⁵⁹² were able to pull-down the KAP subunit. (KIF3A = 81 kDa, KIF3B = 86 kDa, KAP^{SNAP} = 112 kDa, KIF3A¹⁻⁵⁹⁷ = 69 kDa, KIF3B¹⁻⁵⁹² = 69 kDa) (B) (red) Fluorescently labeled full-length and truncated KIF3A/B constructs were bound to (unlabeled) surface-fixed microtubule with AMP-PNP. Subsequent addition of (green) fluorescently labeled KAP showed possible binding of KAP to the KIF3A/B constructs: Only the full-length KIF3A/B and truncated KIF3A/B¹⁻⁵⁹² constructs were able to bind the KAP subunit. Repeated three times.

6.5. The tail domain of the KIF3B motor protein is necessary to achieve full runlength

We were surprised not only by the general processivity and by the absence of autoinhibition of the KIF3A/B motor, but also by the average distance covered by the motors. Previous publications on KLP11/20 - conducted in optical tweezer assays, where the motors are bound to a micron-sized polystyrene bead via their C-terminal tail domains - or mammalian KIF3A/B - conducted with C-terminally

6 Results on the regulation of the Kinesin-2 motor KIF3A/B/KAP from *X. laevis*

truncated motors - had shown a far lower run length, namely between 1 - 2 μm [46]. In contrast to those set-ups, in our assays both tail domains of the KIF3A/B motor remained free. We, therefore, became interested in finding out whether one or both free tail domains would be responsible for full processivity.

To this end, we fluorescently labeled the full-length and truncated KIF3A/B constructs and carried out single molecule processivity assays on fixed microtubule under saturated ATP concentration and the previously established buffer conditions (HS-BRB80 = 80 mM Pipes, 100 mM KAc, 2 mM MgCl_2 , 1 mM EGTA, 2.5 mM DTT) (5.2.8). Strikingly, while the speed of the full-length and the truncated constructs did not differ much and were found to be around 0.3 $\mu\text{m}/\text{s}$, we obtained reliably different results for the runlength of the motor complexes missing the KIF3B tail domain. In detail, the runlength turned out to be significantly reduced by some 50% from $3.3 \pm 0.3 \mu\text{m}$ for the KIF3A/B full-length motor (Figure 15 A) and $2.8 \pm 0.2 \mu\text{m}$ for the KIF3A¹⁻⁵⁹⁷/B motor, down to $1.8 \pm 0.1 \mu\text{m}$ for the KIF3A/B¹⁻⁵⁹² and down to $1.8 \pm 0.3 \mu\text{m}$ for the KIF3A¹⁻⁵⁹⁷/B¹⁻⁵⁹² constructs. We obtained additional confirmation that the differences between those values were significant by conducting a two-sample t-test (5.2.8, Figure 18).

6 Results on the regulation of the Kinesin-2 motor KIF3A/B/KAP from *X. laevis*

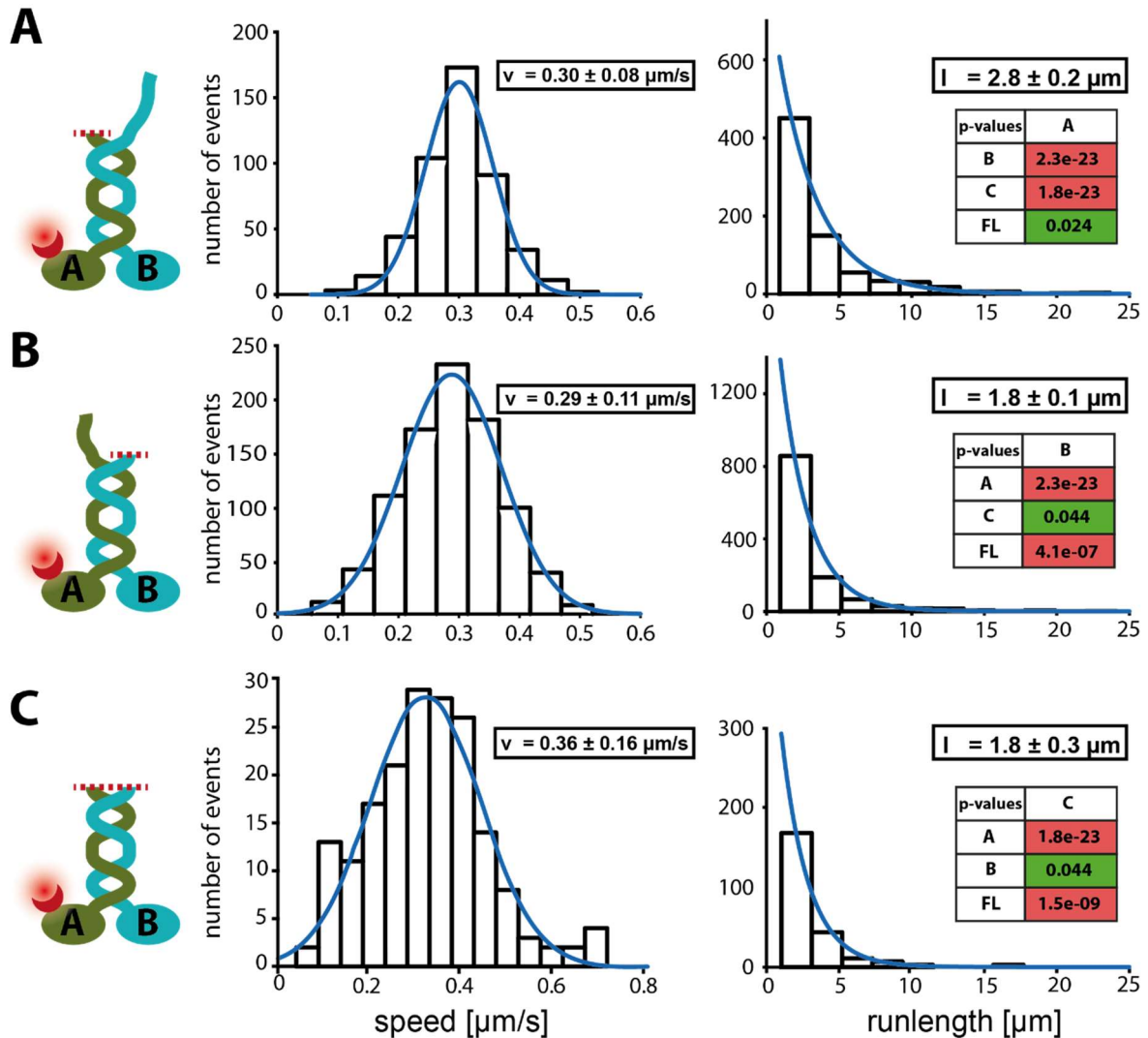


Figure 18: **The C-terminal tail domain of the KIF3B subunit is responsible for full runlength.** (A) Removal of the C-terminal tail domain of the KIF3A subunit resulted in no significant change of the transport parameters of the heterodimer (N = 752). (B) Deletion of the C-terminal tail domain of KIF3B (593-744) resulted in a significant reduction of the runlength of the heterodimer without substantially affecting the velocity (N = 1183). (C) Removal of both tail domains resulted in the same effect as the removal of the tail domain of the KIF3B subunit (B) (N = 173). All values were collected in a fixed microtubule single molecule processivity assay under saturated ATP concentration. The velocity and run length data points were fitted to a Gaussian (\pm width of distribution) and single-exponential distribution (\pm confidence interval), respectively. Repeated three times. The P-values for the statistical test were obtained from a two-sample t-test (A = KLP3A¹⁻⁵⁹⁷/B, B = KLP3A/B¹⁻⁵⁹², C = KLP3A¹⁻⁵⁹⁷/B¹⁻⁵⁹², FL = KIF3A/B (Figure 15))

The tail domain of the KIF3B subunit - seemingly responsible for the increased runlength - contains 152 amino acids (593-744). To narrow down the responsible sequence of the tail domain, we systematically elongated the previously tested truncated KIF3B¹⁻⁵⁹² construct by 131 amino acids (KIF3B¹⁻⁷²³, Figure 19, Sequence in SI)

6 Results on the regulation of the Kinesin-2 motor KIF3A/B/KAP from *X. laevis*

Analysis of the results from the single-molecule motility assay conducted with the new heterodimer revealed that this elongation - being merely 21 amino acids shorter than the full-length KIF3B subunit – could not rescue the increased runlength observed for the KLP3B full-length subunit (compare Figure 19 and Figure 18). This suggests that it is the tail domain of the KIF3B subunit, more precisely the last 21 amino acids, that are necessary to achieve the full runlength, observed with the full-length KIF3A/B motor.

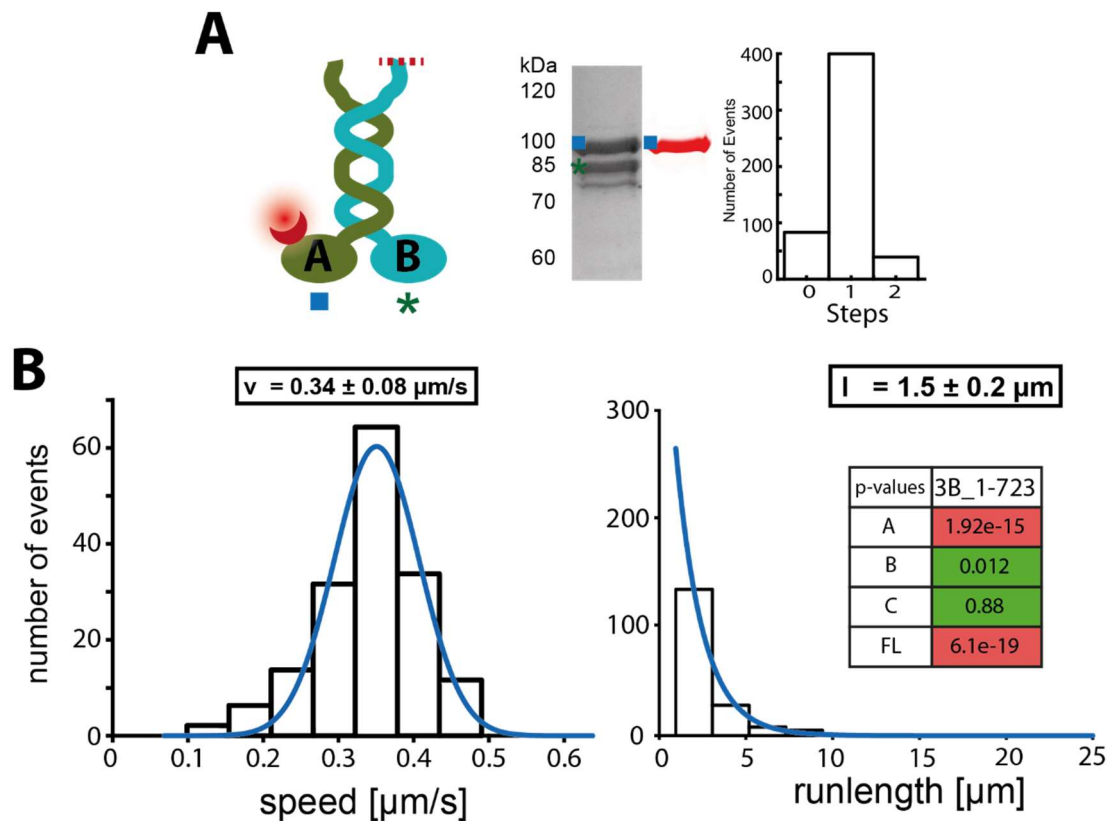


Figure 19: **The last 21 amino acids of the KIF3B C-terminal tail domain are responsible for the increased runlength.** (A) Schematic depiction of the heterodimer with the full-length KIF3A and the elongated construct of the former truncated KIF3B subunit KIF3B¹⁻⁷²³. Successful co-expression, specific fluorescent labeling and non-existent aggregation were confirmed by SDS-PAGE, scanning at 642 nm and subsequent photobleaching assay (N = 521), as described before (Figure 14). (KIF3A^{SNAP} = 103 kDa, KIF3B¹⁻⁷²³ = 80 kDa) (B) Elongation of the KIF3A/B¹⁻⁵⁹² subunit by another 131 amino acids could not rescue the increased runlength achieved by the full-length heterodimer. Values were collected in a fixed microtubule single molecule processivity assay under saturated ATP concentration. The velocity and run length data points were fitted to a Gaussian (\pm width of distribution) and single-exponential distribution (\pm confidence interval), respectively. N = 156, repeated three times. The P-values for the statistical test were obtained from a two-sample t-test (A = KLP3A¹⁻⁵⁹⁷/B, B = KLP3A/B¹⁻⁵⁹², C = KLP3A¹⁻⁵⁹⁷/B¹⁻⁵⁹² (Figure 18), FL = KIF3A/B (Figure 15)).

6.6. The KIF3A and the KAP subunits are targets of phosphorylation by protein kinase A (PKA)

Having established that the C-terminal tail domain of the KIF3A subunit is responsible for the binding of KAP and that the KIF3B tail domain is necessary for the full runlength, the question remained if any of these features would be regulatable by phosphorylation.

The influence of phosphorylation, especially by protein kinase A (PKA), on the properties of the melanosome transport system and hereby most probable on the motors and its subunits, has been shown in multiple publications in the past [105, 106, 117, 122]. The exploration of a governing influence of phosphorylation on the features of the KIF3A/B/KAP motor, therefore, appeared to be a reasonable objective for further study.

To this end, we conducted an *in vitro* phosphorylation assay with isotope-labeled ATP on the heterotrimer, - the dimer and the three separate monomers (5.2.3). Strikingly, the KIF3A monomer and KIF3A/B heterodimer were heavily phosphorylated, while this occurred only slightly with the KIF3B monomer. Even more surprising was that the KAP subunit was also a very strong target of the PKA enzyme, while the heterotrimer KIF3A/B/KAP, in contrast to expectations, appeared

to be a weak target for phosphorylation (Figure 20).

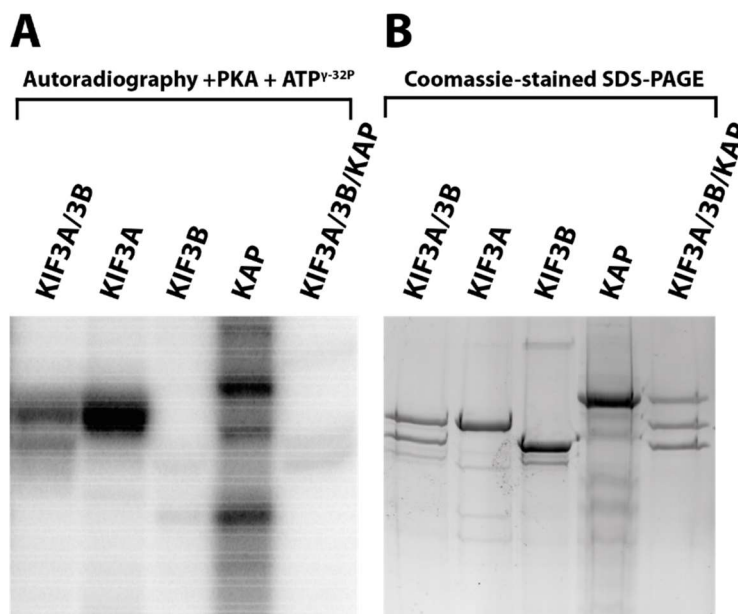


Figure 20: **The KIF3A and KAP subunit are target of phosphorylation by PKA.** (A) Autoradiography images show phosphorylation of KIF3A and KAP. Heterodimerization of KIF3A with KIF3B reduced the phosphorylation degree noticeably. KIF3B and KIF3A/B/KAP seem to be no target for phosphorylation at all. All listed proteins were treated with PKA and radiolabeled ATP^{γ-32P} (5.2.3). (B) Coomassie-stained SDS-PAGE images were used to ensure comparability of the results from the phosphorylation assay.

6 Results on the regulation of the Kinesin-2 motor KIF3A/B/KAP from *X. laevis*

Binding and recognition sites for kinases like the PKA are a continuous topic for debate, however, many publications agree that patches of arginine prior to a serine or threonine point towards a recognition site [169, 170]. After analyzing the sequence of the C-terminal tail domain of the KIF3A subunit, a number of distinct patches of arginine and serine/threonine stood out (Figure 21 A). Based on these findings, we designed a so-called Phos-Mutant (called KIF3A^{Phos-mutant} from here on, Sequence in SI), where prominent serine/threonine amino acids were replaced by glutamic acid to mimic phosphorylation of said amino acids (Figure 21 B).

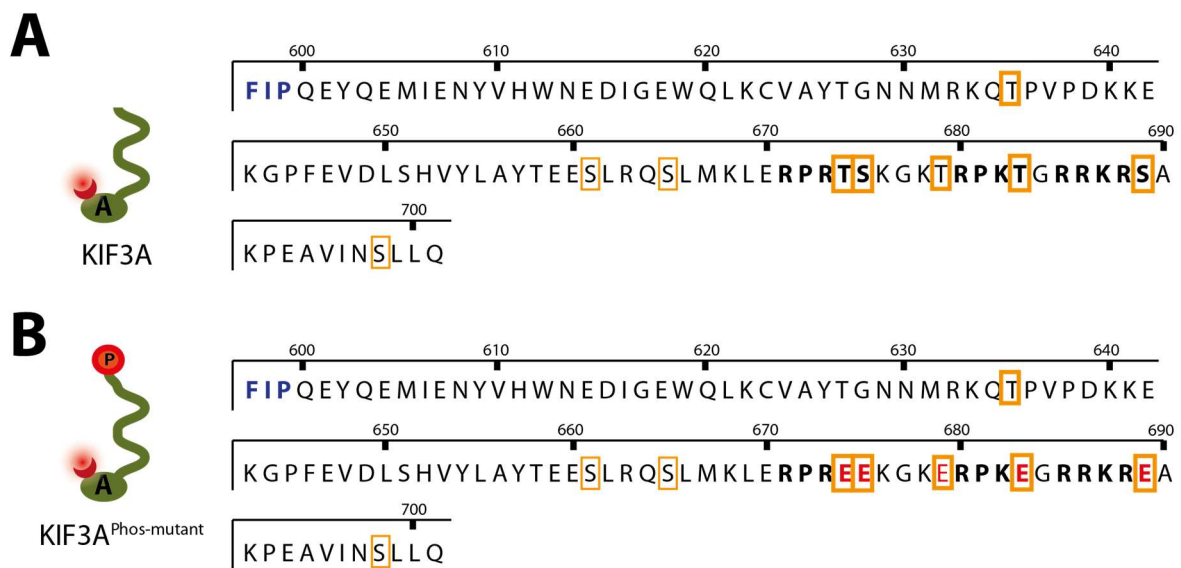
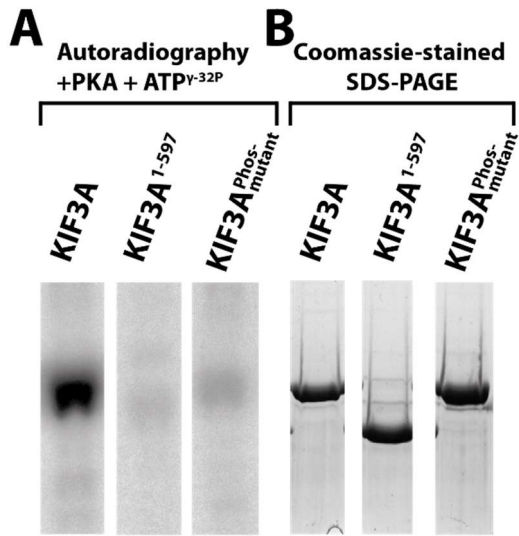


Figure 21: **Sequence of the KIF3A C-terminal tail domain with predicted phosphorylation sites and consequent point mutations mimicking phosphorylation.** (A) Sequence of the wild-type KIF3A C-terminal tail domain with the (blue) conserved FIP helix breaker sequence and predicted phosphorylation sites (orange boxes = Phosphorylation target, Bold text = likely PKA recognition site). Phosphorylation site predictions are taken from [171] (B) The most prominent possible phosphorylation targets were mutated (red) to mimic phosphorylation.

6 Results on the regulation of the Kinesin-2 motor KIF3A/B/KAP from *X. laevis*

In order to verify that mutation took place at the correct positions, we conducted another *in vitro* phosphorylation assay with isotope-labeled ATP with the full-length



KIF3A and truncated KIF3A¹⁻⁵⁹⁷ constructs, as well as with the KIF3A^{Phos-mutant} mutant (5.2.3). As expected, only the full-length wild-type KIF3A construct was indeed a target of phosphorylation (Figure 22).

Figure 22: **The Phos-mimic mutant is not phosphorylated by PKA.** (A) Autoradiography images show the phosphorylation of the KIF3A full-length wild-type construct, but not the truncated KIF3A¹⁻⁵⁹⁷ or mutated full-length KIF3A^{Phos-mutant} construct. All listed proteins were treated with PKA and radiolabeled ATP^{γ-32P} (5.2.3). (B) Coomassie-stained SDS-PAGE image of equivalent concentration as used in the phosphorylation assay ensure comparability.

6.6.1. The binding behavior of the KAP subunit is not influenced by phosphorylation

Following up on the results from the isotope assay showing that both binding partners – the KIF3A and the KAP subunit – are PKA substrates (Figure 20), we investigated whether the PKA enzyme would regulate their binding to one another. To this end, we expressed the KIF3A/B heterodimer and the KAP subunit separately, phosphorylated and dephosphorylated a batch from each protein and tested their binding behavior in a colocalization assay on surface-bound microtubule (5.2.7). The results from this assay suggest that the binding of KAP to the KIF3AB heterodimer is not regulated by phosphorylation at all (Figure 23), but instead seems to be a substantial feature of this motor.

6 Results on the regulation of the Kinesin-2 motor KIF3A/B/KAP from *X. laevis*

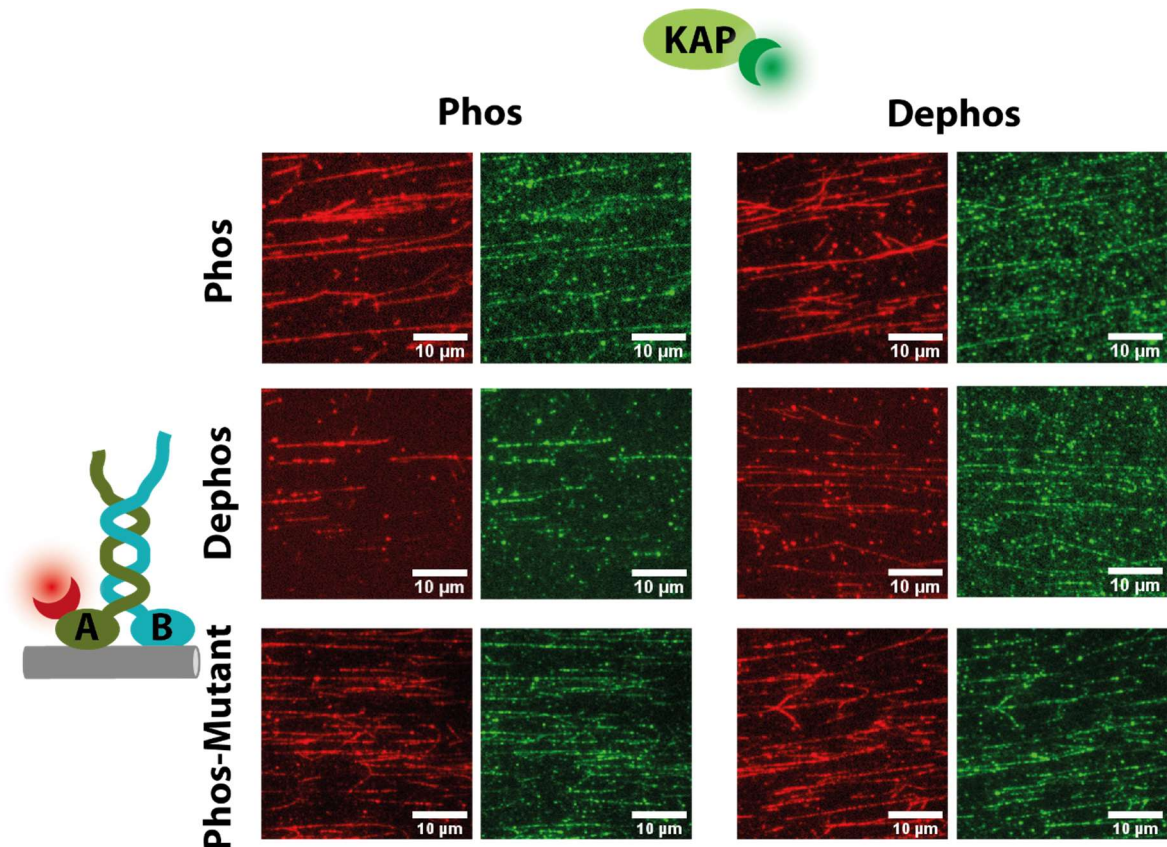


Figure 23: **KIF3A/B binds the KAP subunit, regardless of the phosphorylation state of either subunit.** (red) Fluorescently labeled full-length KIF3A/B wild-type motors were phosphorylated and dephosphorylated, respectively and bound to (unlabelled) surface-fixed microtubule with AMP-PNP. In a third assay, the Phos-mimic mutant KIF3A^{Phos-mutant}/B was bound in the same manner to the microtubule. Subsequent addition of (green) fluorescently labeled KAP (also either phosphorylated or dephosphorylated respectively) showed no regulation of the binding of KAP to the KIF3A/B constructs by their state of phosphorylation. Repeated two times.

In the case of the heterotetramer Myosin-Va/Melanophilin/Rab27a, the actin-based antagonist of KIF3A/B/KAP in the melanosome transport, it is not the motor subunit Myosin-Va itself that is regulated by the activity of the PKA enzyme. Rather, the non-motor subunit Melanophilin is influenced by its state of phosphorylation, as it can switch from f-actin affinity to microtubule affinity [105]. Therefore, we also investigated whether the affinity of KAP, the non-motor subunit of the KIF3A/B motor, towards microtubule or f-actin would be controllable. For this assay, we phosphorylated and dephosphorylated batches of purified and fluorescently labeled KAP and flushed them onto surface-fixed microtubule or f-actin filaments. However, regardless of its phosphorylation state, the KAP subunit would not bind to any filament type (Figure 24).

6 Results on the regulation of the Kinesin-2 motor KIF3A/B/KAP from *X. laevis*

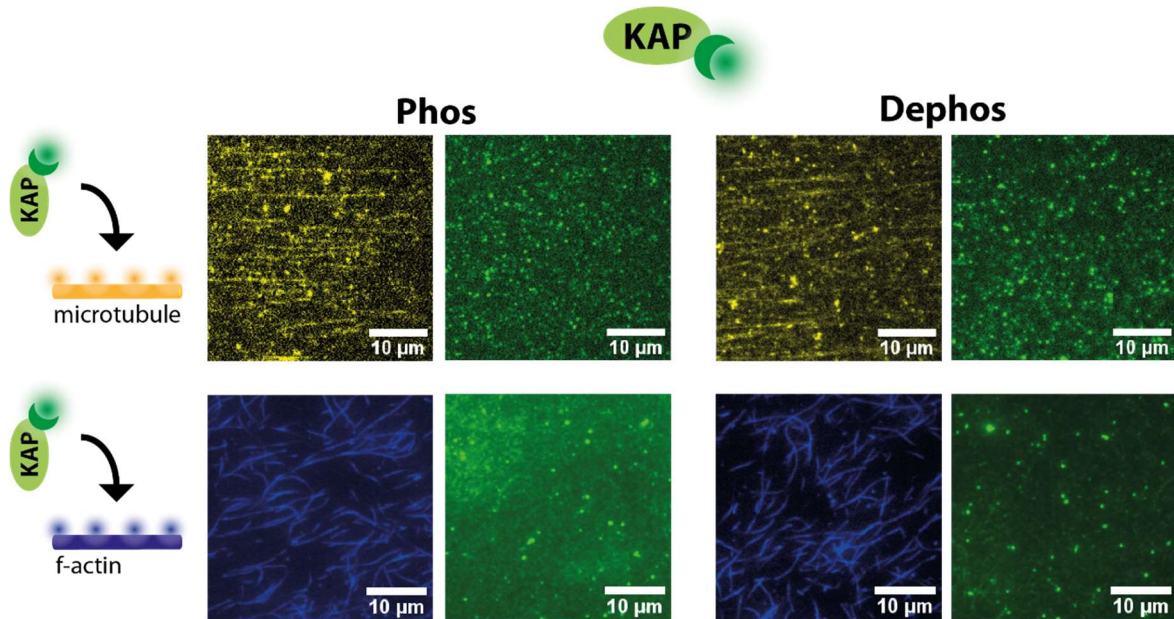


Figure 24: **The KAP subunit does not bind noticeably to either the microtubule or f-actin filaments, regardless of its phosphorylation state.** The (green) fluorescently labeled KAP protein was phosphorylated and dephosphorylated, respectively and flushed onto surface-fixed (yellow) microtubule or (blue) f-actin. Neither phosphorylated nor dephosphorylated KAP binds to either filament. Repeated two times.

6.6.2. Phosphorylation has no influence on the processivity of the KIF3A/B motor

So far, results on the KAP subunit and its phosphorylation state seem to be inconsequential regarding their impact on the processivity of the KIF3A/B motor complex. Nevertheless, one final question remained to be answered, namely whether direct phosphorylation of the heterodimer KIF3A/B would influence the processivity of the motor in any way. Therefore, we phosphorylated and dephosphorylated purified batches of the heterodimer and assessed their processivity in a single-molecule motility assay. With a runlength of $2.9 \pm 0.2 \mu\text{m}$ as well as a velocity of $0.34 \pm 0.08 \mu\text{m/s}$, the heterodimer showed no change in processivity after phosphorylation with PKA whatsoever (Figure 25 A vs. Figure 15). Repetition with the Phos-Mutant (KIF3A^{Phos-mutant}/B) confirmed these findings (runlength $l = 2.9 \pm 0.2 \mu\text{m}$, velocity $v = 0.33 \pm 0.10 \mu\text{m/s}$) (Figure 25 B).

6 Results on the regulation of the Kinesin-2 motor KIF3A/B/KAP from *X. laevis*

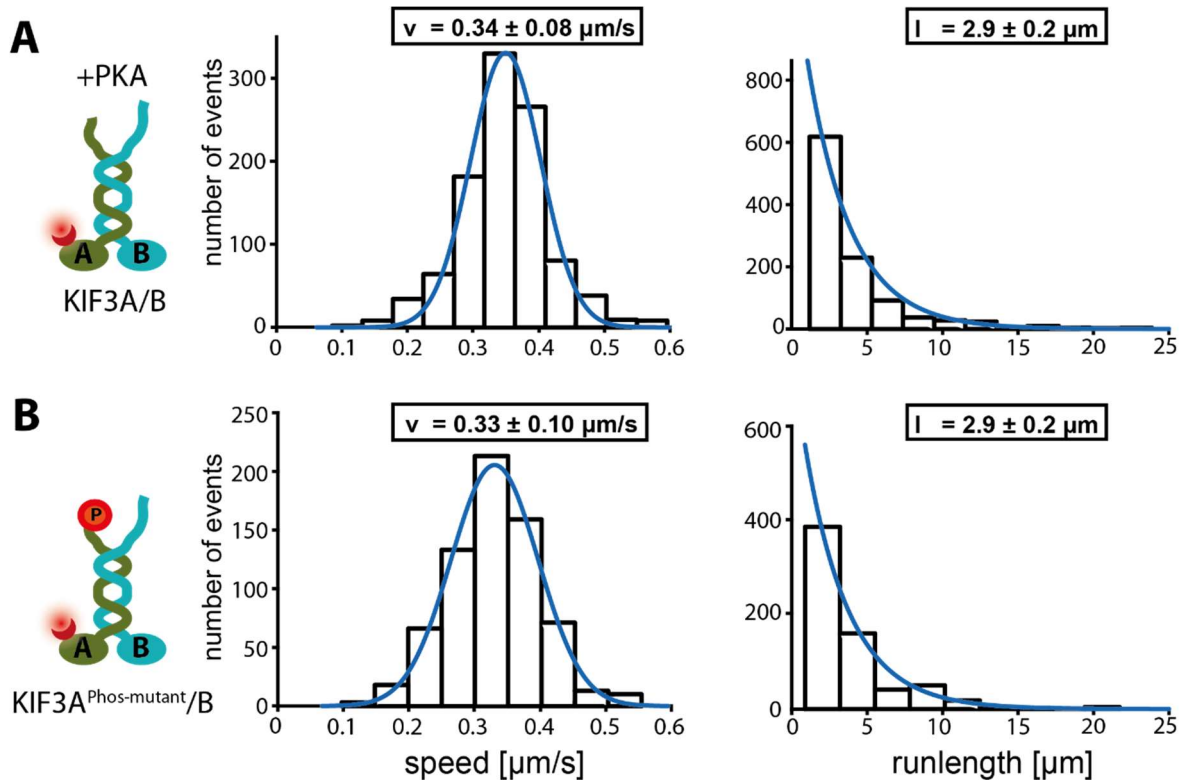


Figure 25: **Phosphorylation by PKA has no influence on the processivity of the KIF3A/B motors.** (A) Phosphorylation of the full-length wild-type KIF3A/B motor has no influence on its velocity, nor its runlength (N = 1018) (compare Figure 15). (B) single molecule processivity assays conducted on the Phos-mimic mutant confirm these findings (N = 686). All values were collected in a fixed microtubule single molecule processivity assay under saturated ATP concentration. The velocity and run length data points were fitted to a Gaussian (\pm width of distribution) and single-exponential distribution (\pm confidence interval), respectively. Repeated three times.

6.6.3. *In vitro* dephosphorylation of the KIF3A/B heterodimer and KIF3A/B/KAP heterotrimer inhibits their processivity

In stark contrast to the lacking effect of PKA treatment on the processivity of the heterodimer, both the KIF3A/B as well as the KIF3A/B/KAP motor complexes showed no processivity upon dephosphorylation (Figure 26, SI Movie 1, 2 left and right panel).

6 Results on the regulation of the Kinesin-2 motor KIF3A/B/KAP from *X. laevis*

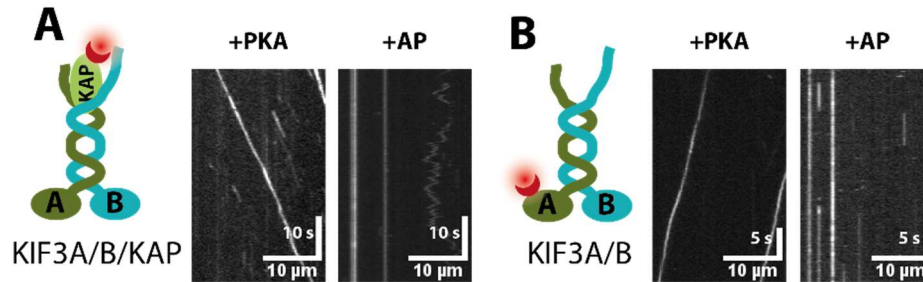


Figure 26: **Dephosphorylation inhibits processivity of the KIF3A/B/KAP and KIF3A/B motor protein.** Representative kymographs of the full-length (A) KIF3A/B/KAP and (B) KIF3A/B motors on fixed microtubule in a single molecule processivity assay after treatment with either (+PKA) Protein Kinase A or (+AP) Antarctic Phosphatase. Both motors are inhibited by the treatment of Antarctic Phosphatase. Repeated four times.

In order to verify that the absence of motor processivity was due to dephosphorylation and not to some other unwanted ancillary effect, we conducted a range of single molecule control assays. Especially, the 30 min of incubation at room temperature (RT) required by the dephosphorylation protocol, as well as the Zinc ions in the Antarctic phosphatase buffer were likely candidates for unwanted inhibition of the motor. However, control assays showed that neither the incubation of the motor for 30 mins at RT, nor the enzyme or buffer, respectively, could influence the activity of the motor significantly. Also, treating the motors with other phosphatases like PP2A did not have any effect on the KIF3A/B heterodimer (Figure 27, SI Movie 3).

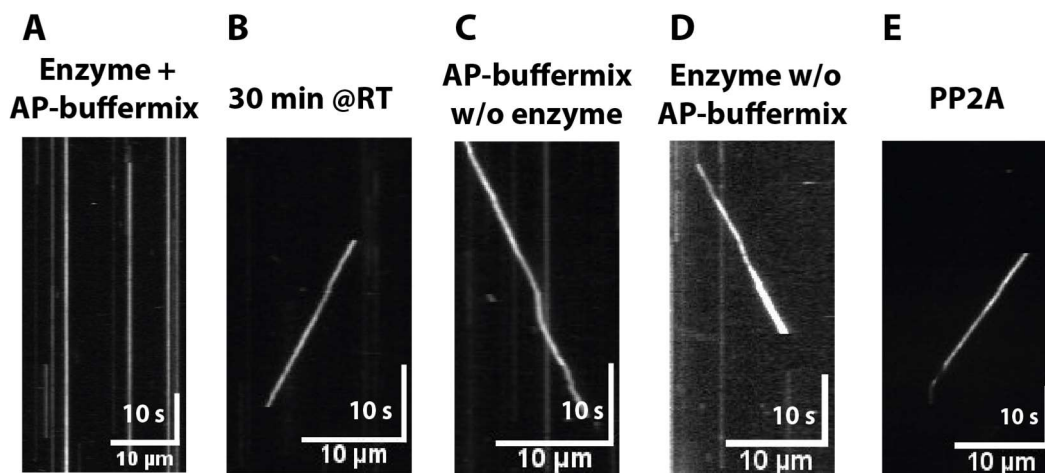


Figure 27: **Inhibition of the KIF3A/B motor is a direct effect of the treatment with the Antarctic Phosphatase enzyme.** Representative kymographs of the full-length wild-type KIF3A/B motor treated at room temperature for 30 min with either (A) the AP-enzyme and AP-buffer, (B) HS-BRB80, (C) the AP-buffer without the enzyme, (D) the AP-enzyme without the AP-buffer or (E) the PP2A phosphatase in its respective buffer. Apart from a general decrease of active motors, only the Antarctic phosphatase buffer with its buffer inhibits the motor successfully. Repeated three times.

6 Results on the regulation of the Kinesin-2 motor KIF3A/B/KAP from *X. laevis*

Earlier, we showed that the full-length and truncated constructs of the KIF3A/B complex, lacking the C-terminal tail domains, were not autoinhibited (Figure 15, Figure 18). Therefore, we suspected that solely the head domains might be the target of this dephosphorylation. To test this theory, we designed constructs with the head domains only which are dimerized by so-called GCN-4-coils (Figure 28, Sequence in SI).



Figure 28: Schematic illustration of the KIF3A and KIF3B head-domain-GCN-4 constructs. Either head domain from (dark green) KIF3A or (teal) KIF3B were substituted with a GCN-4 sequence to allow subsequent dimerization of the head domains. Addition of GFP sequences allowed tracking of the constructs.

Testing them in the same manner as the full-length motor resulted in an equal loss of processivity (Figure 29, SI Movie 4, Figure S 2). Since head domains are the most conserved domain between molecular motors (Figure S 1), we additionally tested the GCN-4-head domain constructs of the OSM-3 and Kinesin-1 homodimers, to check whether this feature would be specific to the KIF3A/B motor. Curiously, unlike the OSM3-head domain, the Kinesin-1 seemed to be unaffected by dephosphorylation (Figure 29, SI Movie 4, Sequence in SI). All in all, we were able to reveal the novel mechanism to regulate the processivity of the KIF3A/B/KAP motor by dephosphorylation of the head domains, which are both specific properties of the Kinesin-2 motor as well as of the phosphatase enzyme used.

6 Results on the regulation of the Kinesin-2 motor KIF3A/B/KAP from *X. laevis*

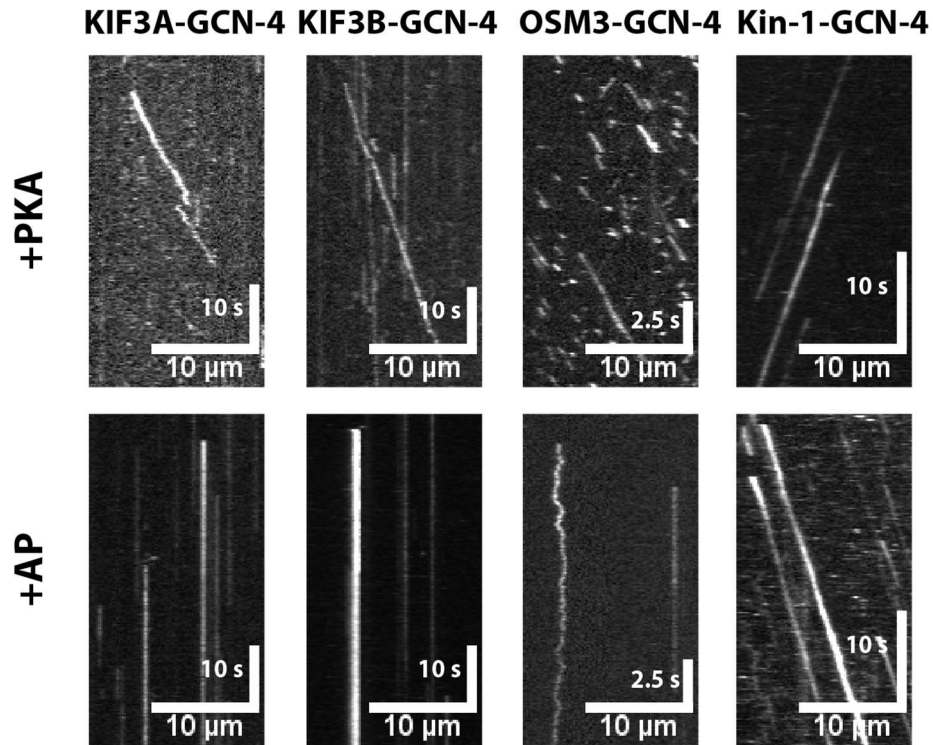


Figure 29: **The head-domains of KIF3A and KIF3B, as well as of OSM-3, but not of Kin-1 are affected by the Antarctic Phosphatase.** Representative kymographs of the head-domain-GCN-4 constructs of KIF3A, KIF3B, OSM-3 and Kin-1 after treatment with either (+PKA) Protein Kinase A or (+AP) Antarctic Phosphatase. Velocities of the processive motors are depicted in **Figure S 2**.

7. Results on coupling between KIF3A/B/KAP and other players of the melanosome transport system

The KIF3A/B/KAP kinesin motor is one of three different motors involved in the transport of melanosomes, with the opposing microtubule-based dynein motor and actin-based myosin motor being the other two [129, 152]. A combination of these motors plus several additional proteins with various functions, e.g. scaffolding to the melanosome or affinity to the filaments, drive and regulate the dispersion and aggregation of the melanosomes. However, details about the organization of this delicate transport system remain mostly unknown [98, 140, 141]. Publications from Oberhofer *et al.* shed a lot of light on the direct regulatory mechanism of the Myosin-Va/Melanophilin/Rab27a complex. Their work showed that the Melanophilin governs the complexes' affinity towards the f-actin or microtubule filaments dependent on its phosphorylation state, thereby demonstrating for the first time how the activity of protein kinase directly regulates the melanosome transport [105, 106].

Like Melanophilin, the protein complex dynactin and its subunit p150^{glued} are supposedly scaffolding dynein to the melanosome and binding to the microtubule filaments in a mechanism which depends on phosphorylation [135, 136]. Furthermore, the subunit p150^{glued} is believed to also bind to the KAP subunit of the KIF3A/B/KAP motor [76]. A phosphorylation dependent affinity of p150^{glued} towards the filaments could therefore also influence the behavior of the KIF3A/B/KAP complex, when bound to it.

Looking at our previous findings on the KIF3A/B/KAP subunit, together with those of Oberhofer *et al.* on the Myosin-Va/Melanophilin/Rab27a, and with publications on the p150^{glued} subunit, prompted us to attempt to answer the following questions:

1. Does the KIF3A/B/KAP motor complex bind to the p150^{glued} protein? Does the p150^{glued} subunit bind selectively to the microtubule or f-actin filaments? And if yes, does the p150^{glued} subunit influence the KIF3A/B/KAP complex's processivity on microtubule or affinity towards f-actin?

7 Results on coupling between KIF3A/B/KAP and other players of the melanosome transport system

2. Can we couple the KIF3A/B/KAP and Myosin-Va/Melanophilin/Rab27a complex? And if so, how does such a linked complex behave on a reconstituted microtubule/f-actin mixed filament network?

7.1. Experimental Concept

In order to identify the affinity of the dynactin subunit p150^{glued} towards the filaments and/or towards the KIF3A/B/KAP motor complex, we designed full-length and truncated constructs of the p150^{glued} subunit and conducted filament decoration as well as single molecule processivity assays in combination with the KIF3A/B/KAP motor complex in a phosphorylated and in a dephosphorylated state.

Also, we conceptualized a way to couple the melanosome transport motor complex Myosin-Va/Melanophilin/Rab27a with the KIF3A/B/KAP motor complex. For this motor coupling, we used a double-stranded DNA handle that binds to both a Halo-tagged Rab27a and to a Halo-tagged KAP subunit via bound thiol groups that were functionalized with anti-Halo Iodoacetamide O4-ligands, and attempted through this approach to link the two motor complexes. Subsequently, we tested the behavior of the resulting complex on a microtubule/f-actin mixed network in a single molecule processivity assay.

Additionally, we tried to establish a photo-switchable inhibitor of the Myosin-Va motor: AzoMyoVin-1. This photoisomer would allow us to readily switch the Myosin-Va motor off and on during runs with the KIF3A/B/KAP motor in order to observe the resulting processivity of the double motor complex. To this end, we established a protocol allowing us to carry out reproducible, single molecule processivity runs in a controlled photoexcitation environment.

7.2. The dynactin subunit p150^{glued} does not bind to the KIF3A/B/KAP motor

Much alike the Myosin-Va motor and its cargo proteins Melanophilin/Rab27a, the dynein, the third of the three motors involved in the melanosome transport, requires

7 Results on coupling between KIF3A/B/KAP and other players of the melanosome transport system

a complex of filament- and cargo-binding proteins that link the melanosome vesicle to the motor and the microtubule. In the case of dynein, this complex is the dynactin cluster which contains 23 subunits of a combined size of approx. 1.0 MDa [1]. One of these 23 subunits – the protein p150^{glued} – plays an important role in this complex. It functions not only as the direct binding partner between the dynactin and the dynein motor, but also as a link between dynein and to the microtubule, very much like the kinesin motor's KAP subunit [76]. The links of p150^{glued} to either KAP or to the dynein motor are assumed to compete with each other [76, 97]. These features make the p150^{glued} a candidate to find out more about the governing factors for the processivity and/or filament selection of the KIF3A/B motor.

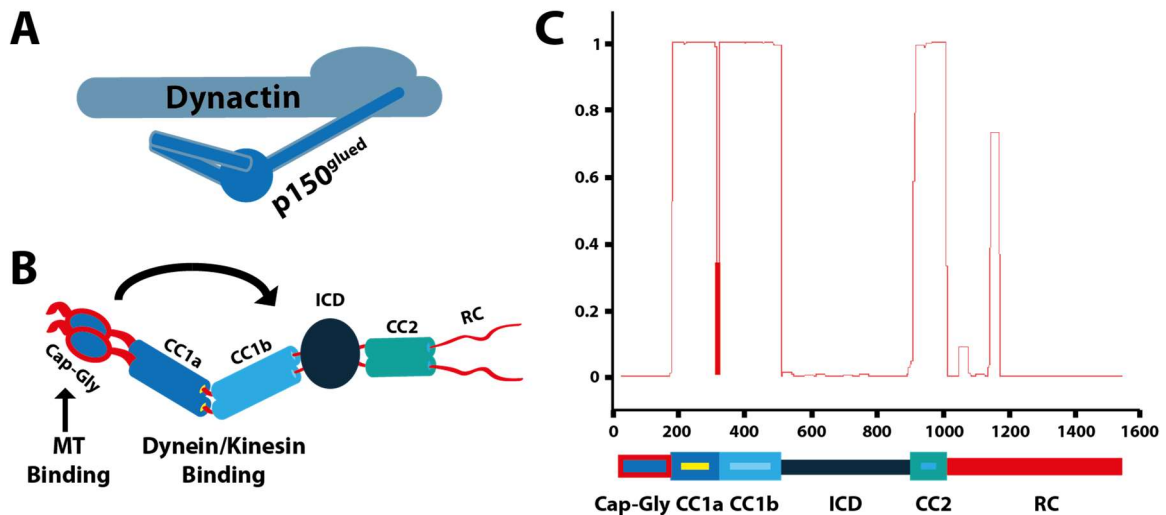
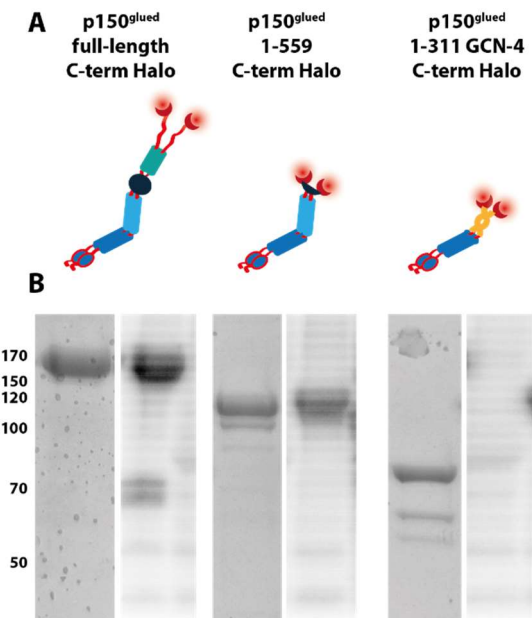


Figure 30: **The schematic structure of the p150^{glued} subunit of the dynactin complex.** (A,B) Schematic illustration of the p150^{glued} subunit within the dynactin as shown above (Figure 7). (C) Coil-prediction of the sequence of the p150^{glued}. Figures are adapted from [1]

7 Results on coupling between KIF3A/B/KAP and other players of the melanosome transport system

Based on previous work on the overall structure of p150^{glued}, our assumption for this series of experiments was that the C-terminal microtubule binding Cap-Gly domain folds onto the Intercoil domain (ICD), which would lead to autoinhibition of its



capability to bind to the microtubule (Figure 30B). This folding mechanism might then again depend on e.g. the phosphorylation state of the subunit, or on p150^{glued} being bound to a motor protein or not [1].

Figure 31: **The full-length and truncated constructs of p150^{glued} are successfully expressed, but only the p150^{glued,1-311} construct is not a target of phosphorylation.** (A) schematic depiction of the full-length (172 kDa) and truncated p150^{glued} constructs p150^{glued,1-559} (98 kDa) and p150^{glued,1-311} (66 kDa). (B) (Each left) Coomassie-stained SDS-PAGE images show successful expression of the constructs. (Each right) Autoradiography images from subsequent treatment with PKA and radio-labeled ATP^{γ-32P} reveal that p150^{glued,1-311} is no target for phosphorylation, but p150^{glued} and p150^{glued,1-559} are.

To find out more about this, we designed one full-length and two truncated constructs of the p150^{glued} subunit. The first truncated construct (p150^{glued,1-559}) contained the Cap-Gly, CC1a and CC1b, as well as a fraction of the ICD, to check whether the Cap-Gly domain would still fold back and be buried in the ICD fragment. The second construct, truncated p150^{glued,1-311}, was cut C-terminally behind the CC1a domain, and became augmented by a GCN-4 domain, to ensure dimerization and to guarantee an exposed Cap-Gly domain. A Halo-tag was also added to each of these three constructs to allow fluorescent labeling (Figure 31 A, Sequence in SI). An *in vitro* phosphorylation assay with isotope-labeled ATP^{γ-32P} was conducted on all of these to check for possible phosphorylation (5.2.3). The resulting autoradiography images clearly showed that the p150^{glued} in general, but in detail only the full-length protein and the p150^{glued,1-559} protein were phosphorylated, hinting towards the ICD or CC1b being the phosphorylation target (Figure 31 B).

From these findings, we attempted to answer whether the full-length and/or the truncated constructs bind to either the microtubule or f-actin filaments or to the

7 Results on coupling between KIF3A/B/KAP and other players of the melanosome transport system

KIF3A/B of KIF3A/B/KAP motor and subsequently to the filaments. Also, we wanted to determine, in the case binding to the motor or to the filaments would take place, whether these interactions can be controlled by the construct's state of phosphorylation.

To this end, we treated batches of fluorescently labeled p150^{glued} constructs, both full-length and the truncated, with either Protein Kinase A or with Antarctic Phosphatase. We then flushed these onto equally fluorescently labeled and surface fixed microtubule and f-actin filaments, respectively (5.2.7). What we found in these experiments confirmed our expectation that, regardless of its state of phosphorylation, the p150^{glued,1-311} construct with its exposed Cap-Gly domain binds to the microtubule, but not to the f-actin filaments (Figure 32 C). In contrast, full-length p150^{glued} and p150^{glued,1-559} showed no binding to any filaments, whether phosphorylated or dephosphorylated (Figure 32 A and B).

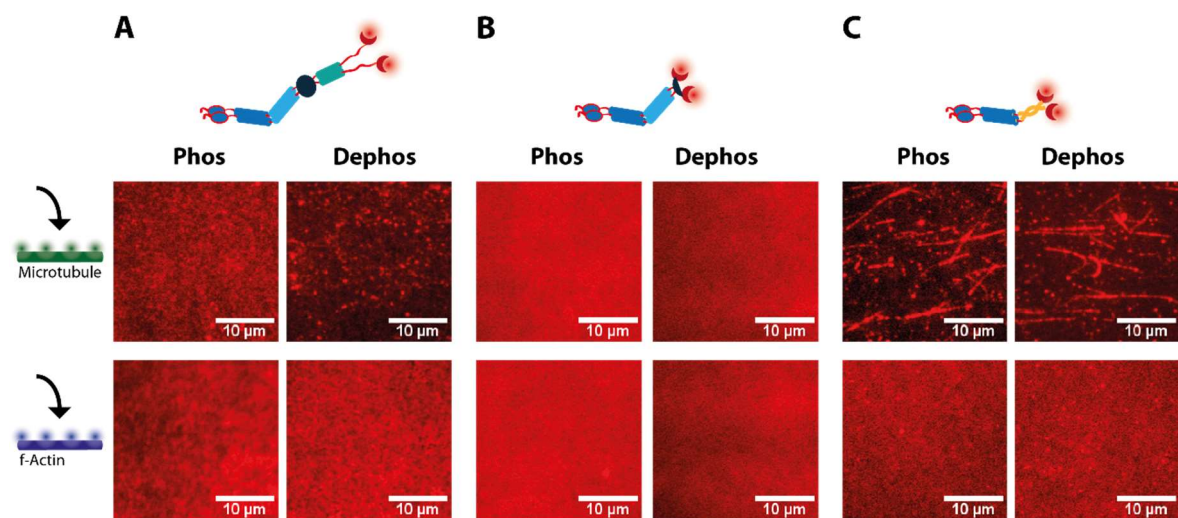


Figure 32: **Full-length p150^{glued} and p150^{glued, 1-559} do not bind to microtubule nor to f-actin filaments. Truncated p150^{glued, 1-311} binds to microtubule. All features are not influenced by the state of phosphorylation of the constructs.** The (red) fluorescently labeled p150^{glued} constructs were (+PKA) phosphorylated and (+AP) dephosphorylated, respectively and flushed onto surface-fixed (green, not shown) microtubule or (blue, not shown) f-actin. (A) full-length p150^{glued} does not bind to either filament regardless of its state of phosphorylation. (B) p150^{glued, 1-559} shows same behavior as the full-length construct. (C) p150^{glued, 1-311} binds to microtubule filaments, but not f-actin filaments, regardless of its state of phosphorylation. Repeated three times.

Next, we investigated whether the p150^{glued} subunits – full-length or p150^{glued, 1-311} – would bind to the KIF3A/B or to the KIF3A/B/KAP subunits. To this end, we conducted co-localization assays with the heterodimeric and heterotrimeric motors

7 Results on coupling between KIF3A/B/KAP and other players of the melanosome transport system

plus the full-length and truncated p150^{glued} (5.2.4). However, even after extensive buffer adjustments, we did not find any binding between the full-length and the truncated p150^{glued}, and the KIF3A/B or the KIF3A/B/KAP motors (Figure 33). We furthermore tested the KAP subunit alone against the p150^{glued} constructs, to check whether the KIF3A/B and p150^{glued} would compete for the same binding site. The results were negative here as well (Figure 33).

In summary, even though we could show with a truncated construct that the C-terminal Cap-Gly domain of the p150^{glued} does indeed bind to the microtubule, we could show that similar binding of the full-length p150^{glued} did not take place, regardless of its phosphorylation state. Additionally, the previously postulated binding of the KIF3A/B/KAP motor to the p150^{glued} could not be confirmed here, at least not with the *in vitro* assays used here [76].

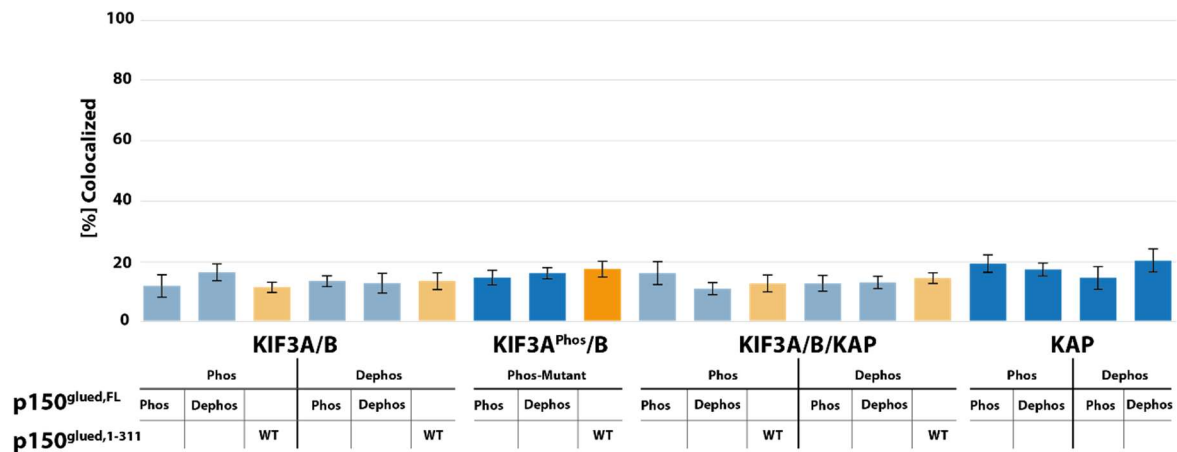


Figure 33: p150^{glued} (full-length and truncated 1-311) does not bind to KIF3A/B, KIF3A/B/KAP, nor KAP constructs, regardless of the state of phosphorylation of any of the players involved. Various fluorescently labeled subunits of the KIF3A/B/KAP motor and p150^{glued} constructs were incubated overnight and their binding tested in a colocalization assay. This assay clearly shows that there is no binding between p150^{glued} and KIF3A/B/KAP. (Phos) Treated with PKA, (Dephos) Treated with Antarctic Phosphatase, (WT) untreated. Error bars represent SD. N=10 for all assays, repeated three times.

7.3. Linking KIF3A/B/KAP and Myosin-Va/Melanophilin/Rab27a using a dsDNA handle

Since the binding of KIF3A/B/KAP to the p150^{glued} subunit of dynactin yielded no new insight into a possible regulation of the KIF3A/B/KAP motor, we turned to the Myosin-Va/Melanophilin/Rab27a complex. Prior work had shown that the affinity of

7 Results on coupling between KIF3A/B/KAP and other players of the melanosome transport system

Melanophilin towards the f-actin or microtubule filaments is strongly governed by its phosphorylation state [105]. By coupling these two motor complexes, we intended to establish, whether the filament affinity of the Melanophilin could also govern the behavior of the KIF3A/B/KAP motor, or vice versa. However, there is so far no evidence that the Myosin-Va and Kinesin-2 motor complexes share a direct connection to one another except indirectly via the melanosome membrane itself. Therefore, in order to link those two complexes, we needed to design an artificial connection.

We approached this task through the use of a double-stranded DNA scaffold. To this end, we designed two approximately 16 nm long 48 bp ssDNA strands (4.3.4), one functionalized on the 5' end with an Atto633 dye and the other functionalized with Thiol groups on both ends. We dimerized the ssDNA strands to obtain a fluorescently labelled dsDNA strand with a thiol group on each end. We then functionalized the thiol group with an "anti-Halo" Iodoacetamide O4-ligand to link to Halo-tagged proteins (5.1.15, Figure 34 A). Finally, we designed Halo-tagged Rab27a and KIF3B constructs and co-expressed them with Melanophilin and KIF3A respectively along with the Myosin-Va motor (Figure 34 B) to complete the list of necessary players for the coupling (Sequence in SI).

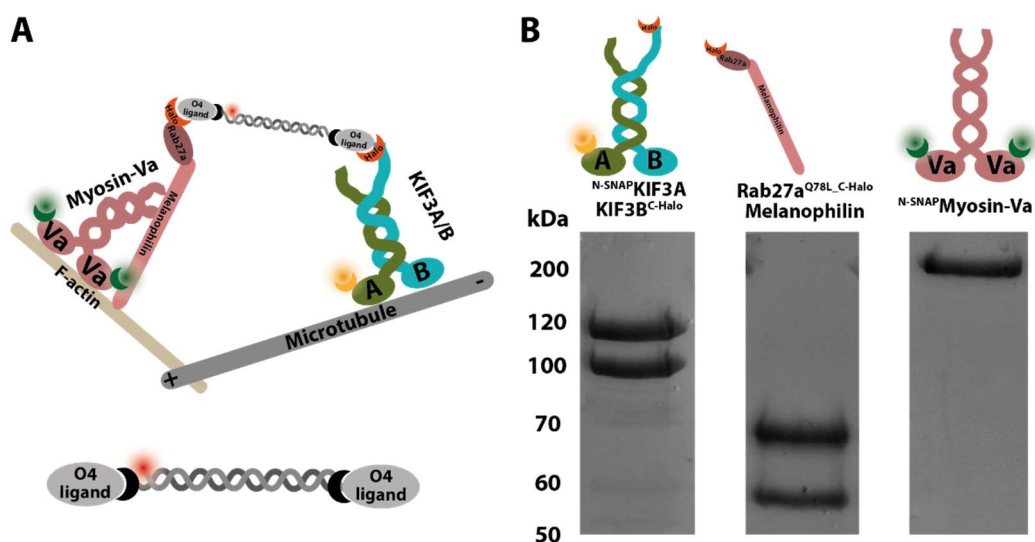


Figure 34: **Concept for dsDNA handle as linker between the Myosin-Va and KIF3A/B motor complexes.** (A) Schematic illustration of the dsDNA handle with an anti-Halo O4 ligand and an Atto633 on either end. (B) Halo-tagged Rab27a and KIF3B were designed to bind to the dsDNA handle. Successful dimerization of KIF3B^{C-Halo} (122 kDa) with KIF3A^{N-SNAP} (100 kDa) and Rab^{Q78L,C-Halo} (60 kDa) with Melanophilin (67 kDa) as well as expression of Myosin-Va^{N-SNAP} (235 kDa) is shown in a Coomassie stained SDS-PAGE Gel.

7 Results on coupling between KIF3A/B/KAP and other players of the melanosome transport system

We approached the assembly of the motor-scaffold complex gradually by starting with the KIF3A/B and dsDNA strand alone. On that point, we mixed fluorescently labeled KIF3A/B with the dsDNA and tested for binding first in a simple colocalization assay and thereafter in a colocalized single molecule processivity assay on fixed microtubule (5.2.4 and 5.2.8). After mixing the KIF3A/B motor and the dsDNA in equimolar concentrations, we could, as a result, show the successful linking of the motor complex to the dsDNA strand (Figure 35A) with 66.1 ± 4.3 % of the dsDNA colocalizing with the KIF3A/B motor. Next, we added two KIF3A/B constructs, with different fluorescent labelling, to the dsDNA to check whether two motors could simultaneously bind to the dsDNA. The result was that 44.5 ± 4.2 % of the motors colocalized with a differently labeled motor, showing clearly that the KIF3A/B motor can indeed be linked via the dsDNA handle (Figure 35B). The fact that only 16.4 ± 3.7 % of the motors colocalize when no dsDNA was present proved that the previously shown binding was accomplished by the dsDNA handle (Figure 35C). Subsequently conducted single molecule processivity assays on fixed microtubule confirmed this (Figure 35 III, SI Movie 5, 6, 7).

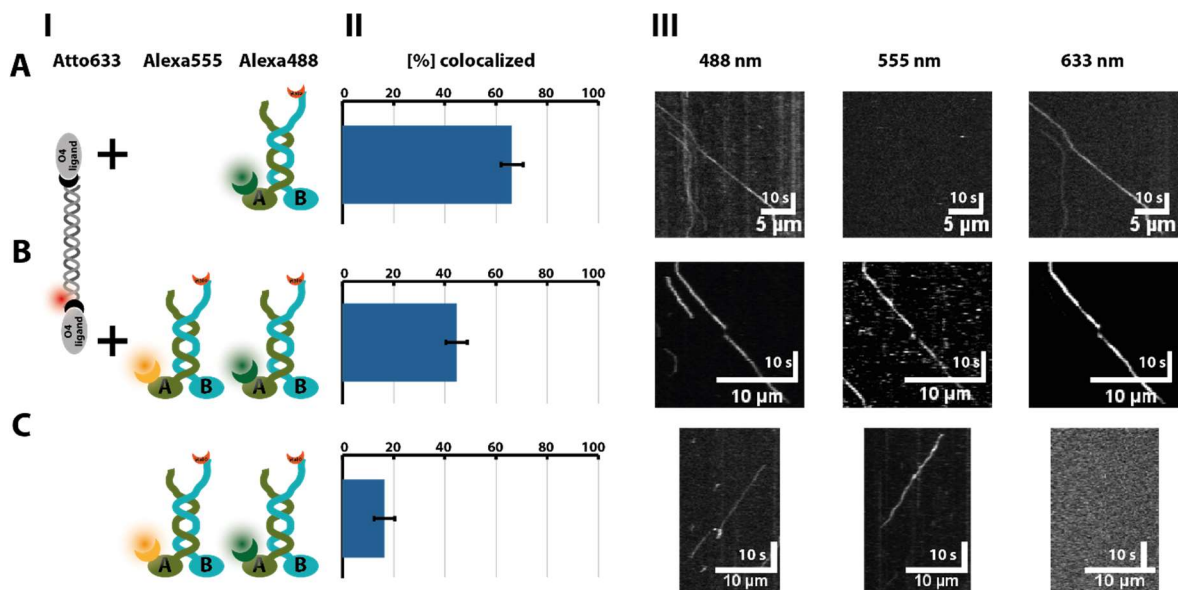


Figure 35: **KIF3A/B can be linked via the dsDNA handle.** (A) 66.1 ± 4.3 % of the dsDNA^{Atto633} colocalize with the KIF3A^{SNAP488}/B. Single molecule processivity assay show clear and numerous colocalized runs, verifying successful link between the dsDNA and the motor. (B) 44.5 ± 4.2 % of KIF3A^{SNAP488}/B colocalize with KIF3A^{SNAP555}/B and show colocalized runs between two distinct motors linked by the dsDNA. (C) Control assays with KIF3A^{SNAP488}/B and KIF3A^{SNAP555}/B without the addition of dsDNA^{Atto633} show that without the dsDNA^{Atto633} the motors do not colocalize (16.4 ± 3.7 %) and move independently. (I) Schematic illustration of the mixed components, (II) Quantitative results of the colocalization assay. Error bars represent SD. N=10 for all assays, repeated three times (III) Representative Kymographs of the colocalized single molecule assays on fixed microtubule. All three channels are shown: Laser excitation with 488 nm, 555 nm, and 633 nm Laser light.

7 Results on coupling between KIF3A/B/KAP and other players of the melanosome transport system

After establishing that the dsDNA and its O4 ligands work with the KIF3A/B motor and ensuring that the dsDNA would bind to the Myosin-Va/Melanophilin/Rab27a complex in a Colocalization assay, as well (Figure 36A = 63.9 ± 4.1 %), we tried to link the KIF3A/B with the Myosin-Va/Melanophilin/Rab27a complex. Unfortunately, we would not obtain colocalization numbers for KIF3A^{SNAP488}/B and for Myosin-Va^{SNAP555}/Melanophilin/Rab27a any higher than 28.4 ± 1.9 %. Control assays without addition of dsDNA to the two motor complexes yielded even higher numbers (Figure 36 C = 41.3 ± 6.6 %) and showed aggregation. This effect could not be reversed by the increase of e.g. the salt concentration in the buffer. Mixing Myosin-Va motors with (Figure 36 D = 44.6 ± 3.3 %) and without Melanophilin/Rab27a (Figure 36 E = 12.4 ± 3.1 %) suggested that it is indeed the Melanophilin/Rab27a adaptor units that would unspecifically bind to both the KIF3A/B motor as well as to itself. Therefore, we decided to discontinue this approach to our project until this obstacle could be surmounted.

7 Results on coupling between KIF3A/B/KAP and other players of the melanosome transport system

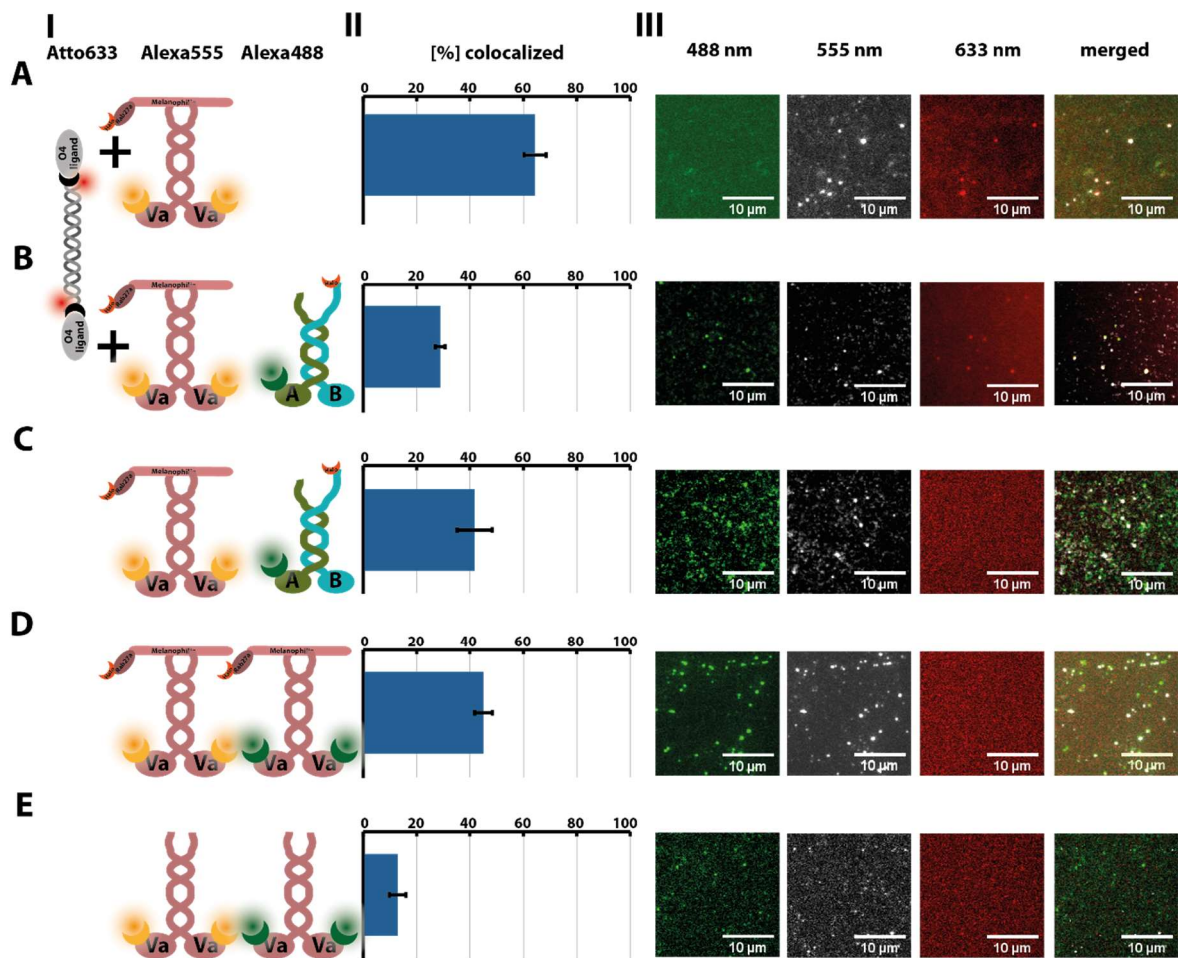


Figure 36: **Melanophilin/Rab27a bind unspecifically to other motor complexes.** (A) Colocalization rate of 63.9 ± 4.1 % of the $\text{dsDNA}^{\text{Atto633}}$ with the Myosin- $\text{Va}^{\text{SNAP555}}$ /Melanophilin/Rab27a complex confirm that the dsDNA can also bind this motor complex. (B) Binding both kinesin and myosin complexes via the $\text{dsDNA}^{\text{Atto633}}$ handle was not as successful, with only 28.4 ± 1.9 % of KIF3A $^{\text{SNAP488}}$ /B binding to the Myosin- $\text{Va}^{\text{SNAP555}}$ /Melanophilin/Rab27a complex. (C) Even more problematic than the low numbers from (B) is the fact that the two motor complexes seem to colocalize equally well without the addition of the $\text{dsDNA}^{\text{Atto633}}$ handle (41.3 ± 6.6 %). Control assays with two differently labeled myosin motors (Myosin- $\text{Va}^{\text{SNAP555}}$ and Myosin- $\text{Va}^{\text{SNAP488}}$) with Melanophilin/Rab27a (D) and without (E) point towards the Melanophilin/Rab27a complex as the source for the unspecific binding: D = 44.6 ± 3.3 %, E = 12.4 ± 3.1 %. (I) Schematic illustration of the mixed components, (II) Quantitative results of the colocalization assay. N=10 for all assays, repeated three times. Error bars represent SD. (III) Representative images of the colocalization assay: Laser excitation with 488 nm, 555 nm and 633 nm Laser light and a merged image of all three channels.

7.4. The photoisomeric inhibitor AzoMyoVin-1 both specifically and reversibly inhibits the Myosin-Va motor

Simultaneously to the DNA-linker project, we attempted to establish a protocol for the photoisomeric inhibitor of Myosin-Va: AzoMyoVin-1. This molecule was designed and synthesized by Katharina Huell (NYU, Department of Chemistry) and the Thorn-Seshold group (LMU, Faculty of chemistry) based on the commercially

7 Results on coupling between KIF3A/B/KAP and other players of the melanosome transport system

available and well-known Myosin-Va inhibitor Myovin-1 (Figure 37 B) and on prior experience with photoisomeric, inhibitory compounds [172]. However, nothing was known about the compound's functionality. The goal of this project was to find a way to readily switch the Myosin-Va off and on, in order to be able to show more precisely each players' influence on the processivity of the Myosin-Va-KIF3A/B complex at any given moment, once such a link between the two motors would have been successfully achieved (Figure 37 A).

The AzoMyoVin-1 has two isoforms: The trans-form, mimicking the original structure of the MyoVin-1, and the cis-form, which has no inhibiting capability. However, which isoform the molecule occupies when radiated with a wavelength of 360 nm or below was still unknown (Figure 37 C).

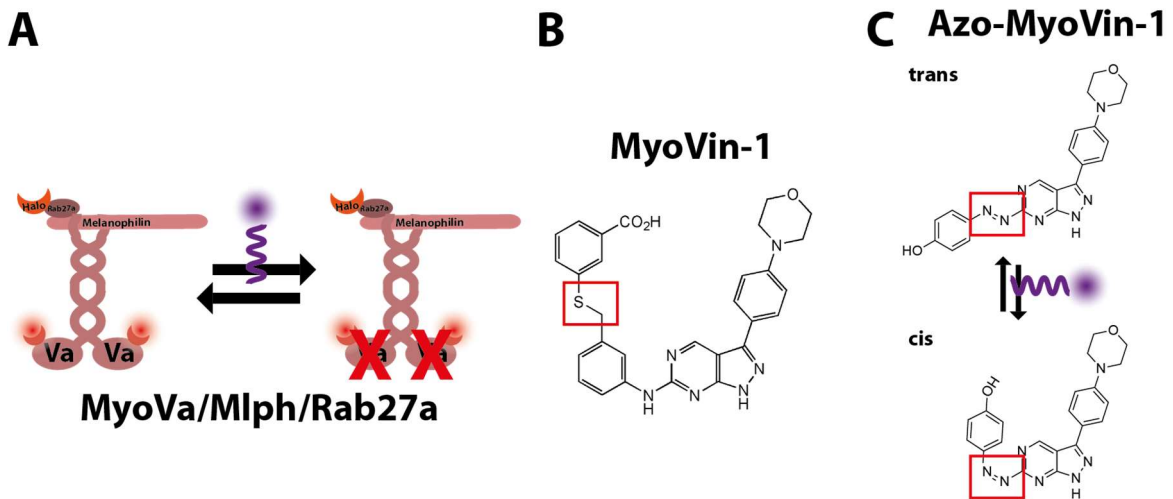


Figure 37: **Concept of the AzoMyoVin-1 project.** (A) The goal was to determine, whether the photoisomeric AzoMyoVin-1 compound can readily switch between inhibiting and non-inhibiting isoform by exposure to ultraviolet light. (B) The AzoMyoVin-1 compound was based on the commercially available MyoVin-1, a well-known inhibitor of the Myosin-Va motor protein. (C) The AzoMyoVin-1 has two isoforms: The trans-form, which resembles the inhibiting MyoVin-1, and the cis-form, which is proposed to be inert.

7 Results on coupling between KIF3A/B/KAP and other players of the melanosome transport system

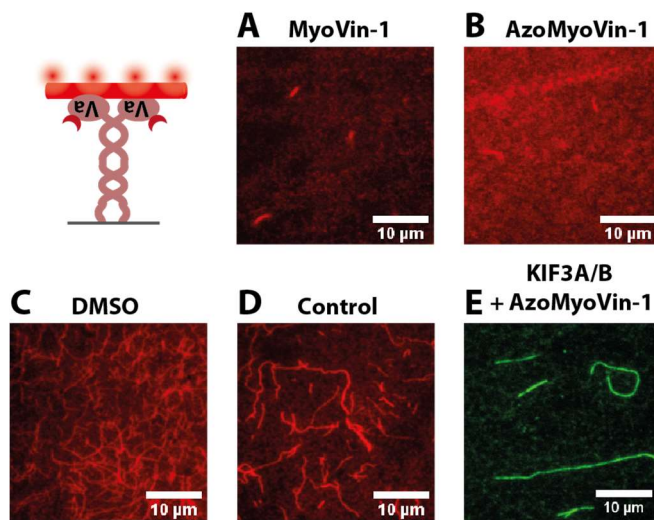


Figure 38: **AzoMyoVin-1 specifically inhibits the Myosin-Va motor, just as MyoVin-1 does.** Gliding assay with surface-fixed Myosin-Va motors and fluorescently labeled f-actin. Myosin-Va batches (approx. 100 nM) were mixed with (A) 140 µM MyoVin-1, (B) 140 µM AzoMyoVin-1, (C) 2% (v/v) DMSO, (D) and nothing, as a control. (E) surface-fixed KIF3A/B motors and fluorescently labeled microtubule + 140 µM AzoMyoVin-1 show specificity of compound for Myosin-Va.

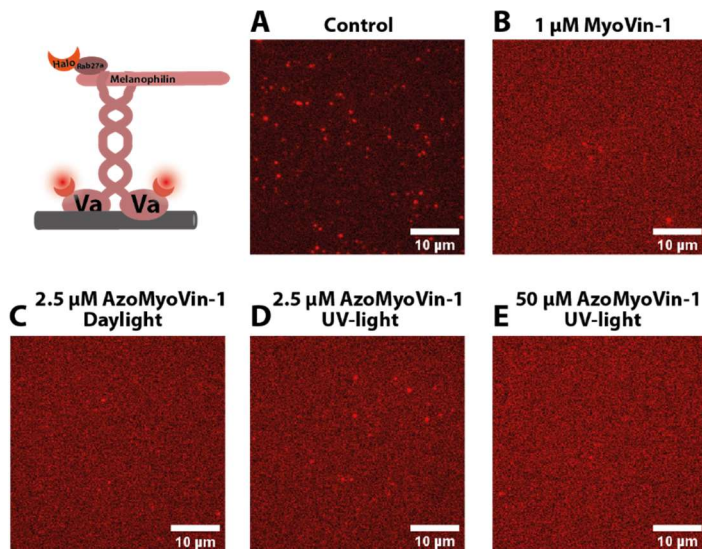
First, we had to establish that implementation of the photo-switch did not corrupt the inhibitory function of the molecule, and that inhibition of the Myosin-Va was both specific to the Myosin-Va as well as to the AzoMyoVin-1. To this end, we incubated approx. 100 nM Myosin-Va motor in a bulk assay with either 140 µM MyoVin-1, 140 µM AzoMyoVin-1 or 2% (v/v) DMSO (which the AzoMyoVin-1 is dissolved in) and approx. 100 nM KIF3A/B with 140 µM AzoMyoVin-1. Subsequently

conducted gliding assay showed that only the addition of AzoMyoVin-1 or MyoVin-1 would inhibit the function of only the Myosin-Va motor domain (Figure 38, SI Movie 8) and suggested that the AzoMyoVin-1 compound mainly occupies the inhibiting trans-form when exposed to natural light.

In order to verify and determine in more detail the compounds “photoswitchability”, we tested the effect on the Myosin-Va/Melanophilin/Rab27a under different light conditions. To this end, we covered the room with curtains, illuminating it with nothing but a dim, red light and designed a sealable icebox containing a 360 nm light source. Next, we mixed samples of the motor complex (approx. 1 nM) with 2,5 and 50 µM of AzoMyoVin-1 and irradiated the samples with either the 360 nm ultraviolet light source or the white ceiling lamp. In the single molecule motility assay, the motor complex mixed with 2.5 µM AzoMyoVin-1 and irradiated with natural light showed only very few processive motors as compared to the untreated control mix (Figure 39 C, SI Movie 9). However, when we irradiated a mix of the motor complex and an equal amount of 2.5 µM AzoMyoVin-1 with a 360 nm light source, an increased number of mobile motors would appear, in contrast to what

7 Results on coupling between KIF3A/B/KAP and other players of the melanosome transport system

happened with the mix exposed to natural light (Figure 39 D, SI Movie 9). Although, the number of mobile motors was clearly lower than those in the untreated control,



the results clearly suggest that irradiation with 360 nm light switches the compounds mainly occupied state from the inhibiting trans-form to the inert cis-form (Figure 39 A, SI Movie 9). Finally, motors mixed with 50 μM AzoMyoVin-1 showed no processivity whatsoever, regardless of prior light exposure (Figure 39 E, SI Movie 9).

Figure 39: **Exposure of UV-light to the AzoMyoVin-1 compound shows isomerization to the non-inhibiting form.** Single molecule processivity assay conducted on fixed f-actin filaments (not shown) with approx. 1 nM (red) Myosin-Va/Melanophilin/Rab27a complexes treated with (A) nothing, as a control, (B) 1 μM MyoVin-1, (C) 2.5 μM AzoMyoVin-1 and natural light, (D) 2.5 μM AzoMyoVin-1 and UV-light and (E) 50 μM AzoMyoVin-1 and UV-light. Whereas 2.5 μM of AzoMyoVin-1 are sufficient to inhibit most of the approx. 1 nM of Myosin-Va when exposed to natural light (C), the number of active motors bound to f-actin and moving is increased noticeably when exposed to UV-light prior (D).

In the end, first attempts to inhibit the Myosin-Va motor both specifically and reversibly were successful and showed the potential of the AzoMyoVin-1. However, further efforts will be necessary to turn this compound into a reliable tool for future investigation of the Myosin-Va motor.

8. Results on the regulation of the homodimeric Kinesin-2 motor OSM-3 from *C. elegans*

The Intraflagellar transport (IFT) machinery builds and maintains the cilia or flagella in most organisms [147, 173]. In this machinery from *C. elegans*, cargoes are carried by homodimeric OSM-3 and heterotrimeric KLP11/20/KAP to the tip and by dynein back to the base in an uninterrupted unidirectional manner [55, 147, 174]. Previous studies have shown that loss of the OSM-3 motor leads to loss of the distal segment of the cilia [149]. Despite the obvious importance of this motor for the IFT machinery, not much is known about the regulation and the mechanisms of the OSM-3 motor at the molecular level. Similarly to the overall structure of most homodimers, like Kinesin-1, it is assumed that the OSM-3 motor is inhibited through folding down of its stalk domain at the helix breaker position and through binding of the tail to the head domains. Indeed, previous work from Imanishi *et al. in vitro* could show that the OSM-3 motor is autoinhibited, and that inhibition can be suppressed by introduction of a point mutation at the predicted helix breaker position, or by deletion of said domain resulting in an unfolded conformation [72]. Mimicking cargo binding by binding the motor to beads in an optical trap led to activation of the motor as well [72]. Mohamed *et al.* furthermore showed in an *in vitro* bottom-up reconstitution of the IFT-B complex, that indeed four core subunits of this complex – OSM-5, OSM-6, DYF-1 and DYF-6 – were bound to the OSM-3 motor, with the DYF-1 subunit being the direct linker, and thereby activated the motor [92]. Additionally, Cleetus *et al.* could recently show that DYF-1 and OSM-6 are the subunits which activate the motor [93]. However, molecular insight into the exact mechanism behind this regulation is still missing.

Therefore, in this part of this thesis, we tried to find answers to the following questions:

1. Is the OSM-3 homodimer indeed inhibited through the binding of its C-terminal tail domain to its head domains?
2. Is this inhibition directly suppressed by the binding of the OSM-6/DYF-1 dimer to the tail domains, obstructing the a.m. autoinhibition mechanism?

8.1. Experimental approach

To gain a more detailed insight into the mechanism of the regulation of the OSM-3 motor and which domain would bind to which, we designed fragmented constructs to check for binding within the OSM-3 motor (Figure 40). Firstly, we synthesized the full-length, wild-type OSM-3 construct as an autoinhibited control, thereafter the monomeric head domain OSM-3¹⁻³⁴⁹ and then - with the help of introduced C-terminal GCN-4 domains - artificially dimerized head domains OSM-3¹⁻³⁴⁹GCN-4. Also, we designed two coiled-coil domains of the stalk OSM-3³⁵⁰⁻⁴⁴⁴ and OSM-3⁴⁴⁵⁻⁵⁵², as well as constructs of the C-terminal tail domain - also as single and artificially dimerized - OSM-3⁵⁵²⁻⁶⁹⁹ and OSM-3⁵⁵²⁻⁶⁹⁹GCN-4. Lastly, we took the DYF-1 and OSM-6 constructs described by Mohamed *et al.* to check where these cargo subunits would bind to exactly [92] (Figure 40, Detailed listing in SI).

In detail, we employed the binding assay by incubation on beads (5.2.2.5) to check for the exact binding partners within the OSM-3 motor. Subsequently, we carried out microtubule-based ATPase enzyme activity assays (5.2.9) to obtain confirmation that the full-length wild type OSM-3 motor is inhibited and that the OSM-3¹⁻³⁴⁹GCN-4 construct is inherently active. Thereafter, we incubated the OSM-3¹⁻³⁴⁹GCN-4 constructs with the two coiled-coil domains from the stalk and the C-terminal random coil from the tail domains (OSM-3³⁵⁰⁻⁴⁴⁴, OSM-3⁴⁴⁵⁻⁵⁵², OSM-3⁵⁵²⁻⁶⁹⁹ and OSM-3⁵⁵²⁻⁶⁹⁹GCN-4, respectively) in order to find out if any of these constructs would inhibit the motor domains.

Additionally, we designed a OSM-3^{G444Q} mutant, in addition to the previously described OSM-3^{G444E} mutant, which is known to be permanently active, to check whether the impairment of the helix breaker position and in turn the released autoinhibition of the motor would have to be attributed to the disruption of the whole helix breaker or steric and/or charge-based hindrance by the glutamic acid of the folding process. To this end, we wanted to verify whether this release of autoinhibition could be achieved by the merely steric hindrance of the equally long, but uncharged glutamine as well.

8 Results on the regulation of the homodimeric Kinesin-2 motor OSM-3 from *C. elegans*

The final step of investigation was to check how the OSM-6/DYF-1 dimer binds to the motor and in turn possibly suppresses the autoinhibition. We again employed the binding assay by incubation on beads (5.2.2.5), and subsequently determined the binding kinetics between the tail domains (OSM-3⁵⁵²⁻⁶⁹⁹GCN-4) and the head domains (OSM-3¹⁻³⁴⁹GCN-4), as well as the OSM-6/DYF-1 dimer, respectively. Applying a micro-scale thermophoresis assay (5.2.10), we verified the ability of the IFT subunit dimer to supersede the binding of the tail domains to the head domains.

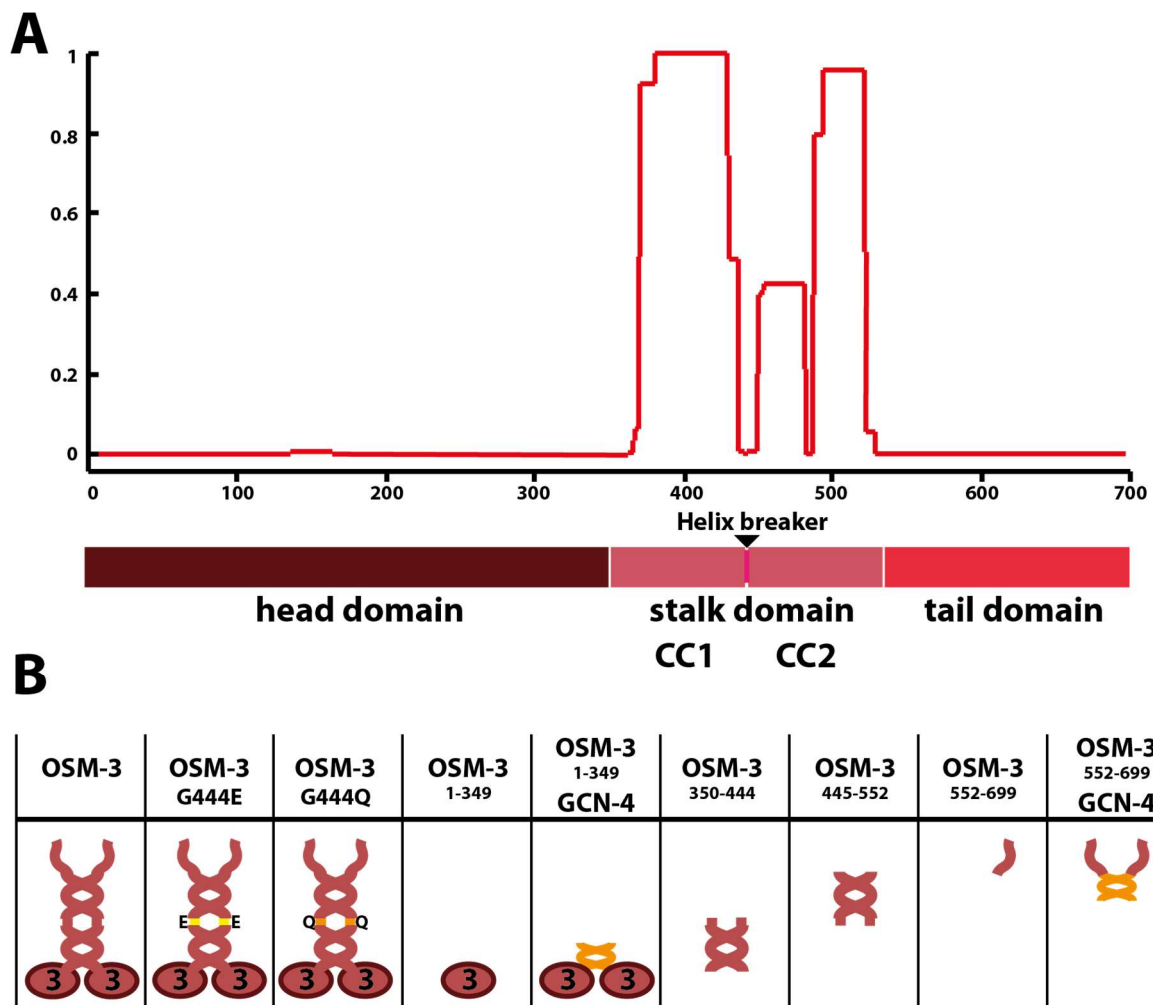


Figure 40: **Overview of the *C. elegans* OSM-3 motor and constructs.** (A) Prediction of coiled-coil regions of the wild-type, full-length OSM-3 motor [175]. The three major domains are depicted with the head domain (1-349), coiled-coil stalk domain (350-552) divided into coiled-coil 1 (CC1, 350-444) and coiled-coil 2 (CC2, 445-552), and the C-terminal random coil tail domain (552-699) (B) Listing and depiction of the used constructs in this chapter: the OSM-3 full-length wild-type constructs OSM-3 and the two point mutations in the helix breaker position OSM-3^{G444E} and OSM-3^{G444Q}, as well as the five segmentations of the OSM-3 motor, the single head domain OSM-3¹⁻³⁴⁹, the artificially dimerized head domains OSM-3¹⁻³⁴⁹GCN-4, the stalk domains CC1 (OSM-3³⁵⁰⁻⁴⁴⁴), and CC2 (OSM-3⁴⁴⁵⁻⁵⁵²), as well as the single tail domain OSM-3⁵⁵²⁻⁶⁹⁹, and the artificially dimerized tail domain OSM-3⁵⁵²⁻⁶⁹⁹GCN-4.

8.2. The tail domains of OSM-3 bind to their head domains

We obtained confirmation that the full-length, wild-type OSM-3 homodimer is indeed autoinhibited and that the OSM-3¹⁻³⁴⁹GCN-4 as well as the OSM-3^{G444E} construct are active in a microtubule based ATPase enzyme activity assay (Figure 43). In a next series of experiments, we tested the binding of the OSM-3 head domains to its own fragments, i.e. the different stalk and tail constructs, through carrying out binding assays by co-immunoprecipitation, to determine which missing domain is responsible for the autoinhibition observed with the full-length motor (5.2.2.5).

These experiments were FLAG resin based co-precipitation assays of the dimerized tail domains OSM-3⁵⁵²⁻⁶⁹⁹GCN-4^{6xHis} with both the dimerized head domains OSM-3¹⁻³⁴⁹GCN-4^{FLAG}, as well as the head domain monomers OSM-3^{1-349,FLAG}. They revealed that the tail domains indeed bind to the head domains, when both heads are present as dimers (Figure 41 A and B). Corresponding tests were carried out on binding between the two coiled-coil domains of the stalk domain (OSM-3^{350-444,FLAG}, OSM-3^{445-552,FLAG}) and the head domains (Figure 41 C and D). They revealed that these do not bind to each other, highlighting the fact that both head domains need to be present as dimers to successfully bind to the tail domains.

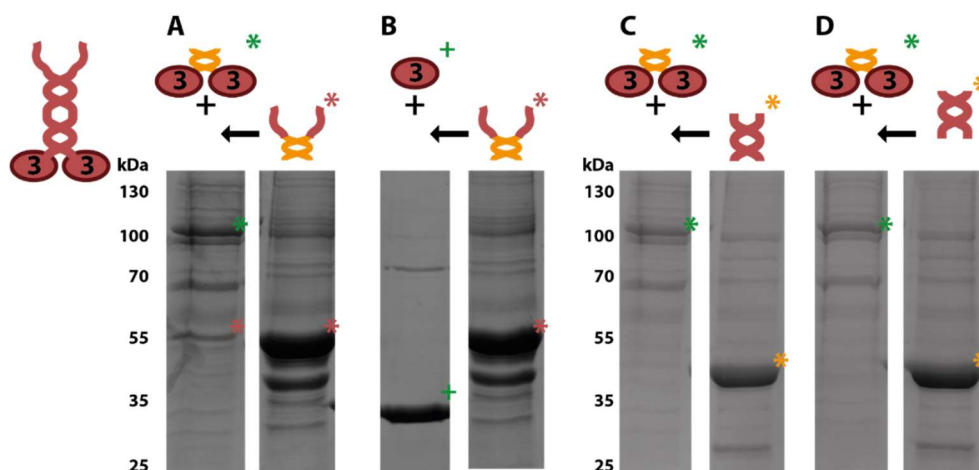


Figure 41: **The C-terminal tail domains bind to the dimerized head domains.** FLAG-tag purified dimerized motor domains (A, C, D left lanes, green asterisk, 96 kDa) and monomeric head domains (B left lane, green cross, 37 kDa) were left on the FLAG-resin beads and incubated with 6xHis purified dimerized tail domains (A, B, right lane, red asterisk, 52 kDa) and CC1 (C, right lane, yellow asterisk, 42 kDa) and CC2 domains (D, right lane, yellow asterisk, 42 kDa), respectively. (A) clearly shows dimerized tail domains (red Asterisks, A, left lane, 52 kDa) bound to the FLAG resin via the dimerized head domains. See 5.2.2.5 for assay protocol.

8 Results on the regulation of the homodimeric Kinesin-2 motor OSM-3 from *C. elegans*

To further characterize the found binding between the tail domains and the head domains, or rather the lack of it, in the case of the stalk domains and the head domains, we conducted a series of micro-scale thermophoresis assays (5.2.10). In these assays, we carried out series of titrations of a given ligand with a potential binding partner to verify any binding. More precisely, we titrated an increasing concentration of the OSM-3¹⁻³⁴⁹GCN-4 dimerized head domains to a constant concentration of the fluorophore-labeled OSM-3⁵⁵²⁻⁶⁹⁹GCN-4^{Halo660} tail domains (

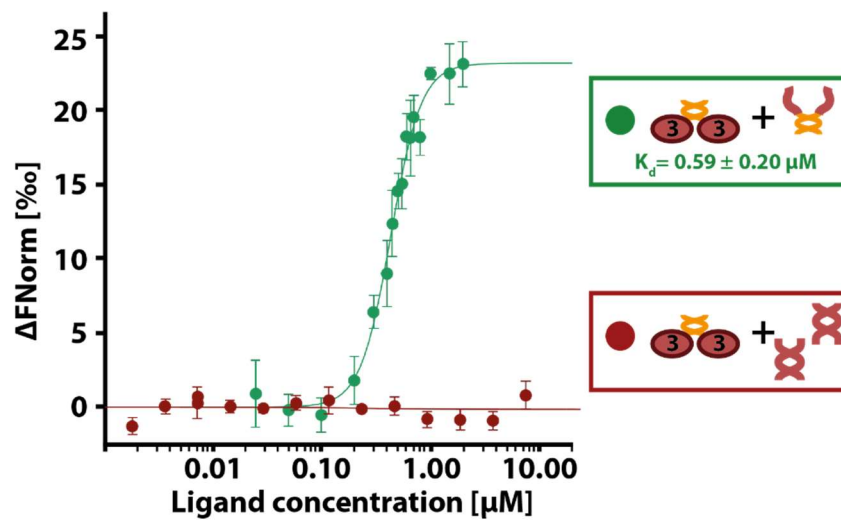
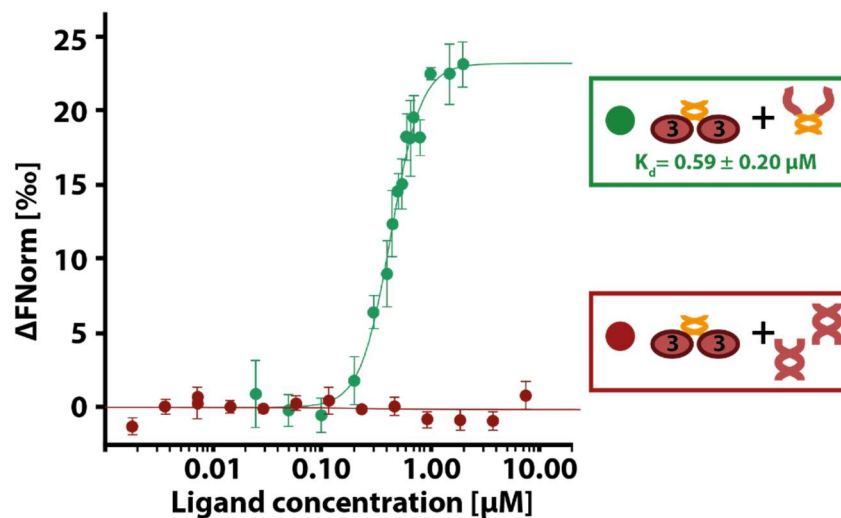


Figure 42, green) and an increasing concentration of the OSM-3³⁵⁰⁻⁴⁴⁴GCN-4^{Halo660}/OSM-3⁴⁴⁵⁻⁵⁵²GCN-4^{Halo660} stalk domains to a constant concentration of the fluorophore-labeled OSM-3¹⁻³⁴⁹GCN-4^{Halo660} head domains (



8 Results on the regulation of the homodimeric Kinesin-2 motor OSM-3 from *C. elegans*

Figure 42, red). The acquired binding curve clearly show binding between the tail domains and the head domains with a K_d value of $0.59 \pm 0.20 \mu\text{M}$, while the stalk domains do not seem to bind to the head domains whatsoever.

These results confirmed our expectations that only the OSM-3 tail domains bind to the OSM-3 head domains and suggest that the stalk domains are not involved in the direct regulation of the head domains at all.

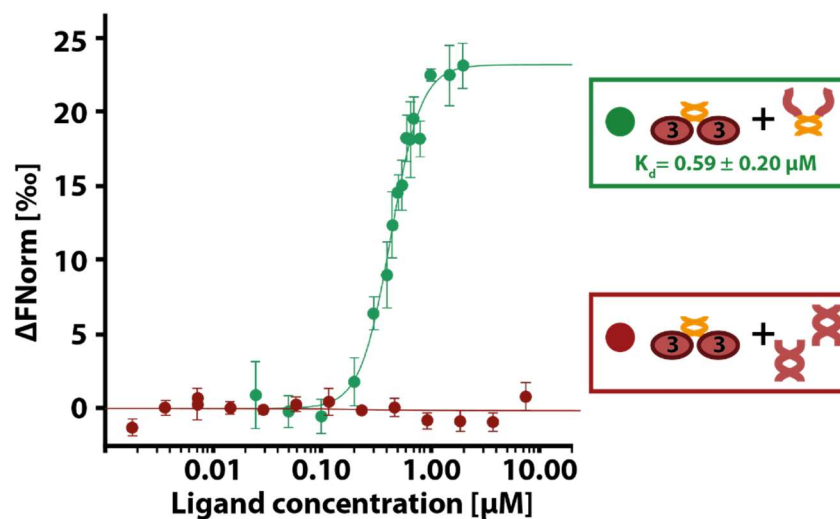


Figure 42: **The OSM-3 tail domains bind to the OSM-3 head domains.** (green) OSM-3¹⁻³⁴⁹GCN-4 dimerized head domains were titrated to fluorophore-labeled OSM-3⁵⁵²⁻⁶⁹⁹GCN-4 dimerized tail domains (constant concentration of 20 nM) in microscale thermophoresis assays (MST). The results show that the OSM-3 tail domains indeed bind to the OSM-3 head domains. Analyzing the data with the a.m. settings (5.2.10) yielded a K_d of $0.59 \pm 0.20 \mu\text{M}$. (red) As a control, OSM-3³⁵⁰⁻⁴⁴⁴GCN-4 and OSM-3⁴⁴⁵⁻⁵⁵²GCN-4 stalk domains were titrated to fluorophore-labeled OSM-3¹⁻³⁴⁹GCN-4 dimerized head domains (constant concentration of 20 nM), which show no binding. The binding curve between (green) OSM-3⁵⁵²⁻⁶⁹⁹GCN-4 and OSM-3¹⁻³⁴⁹GCN-4 was fitted using a Hill coefficient of 3,0. Error bars represent SD, repeated three times.

8.3. The tail domains are responsible for inhibition of the OSM-3 motor through binding to the head domains

Next, we tested whether the binding of the tail domains to the head domains had the assumed inhibitory effect on the motor. To this end, we incubated dimerized head domains OSM-3¹⁻³⁴⁹GCN-4 with the single and dimerized tails (OSM-3⁵⁵²⁻⁶⁹⁹ and OSM-3⁵⁵²⁻⁶⁹⁹GCN-4) as well as stalk domains (OSM-3^{350-444,FLAG} and OSM-3^{445-552,FLAG}) and subsequently assessed the activity of the motor constructs in a microtubule stimulated ATPase activity assay (5.2.9).

8 Results on the regulation of the homodimeric Kinesin-2 motor OSM-3 from *C. elegans*

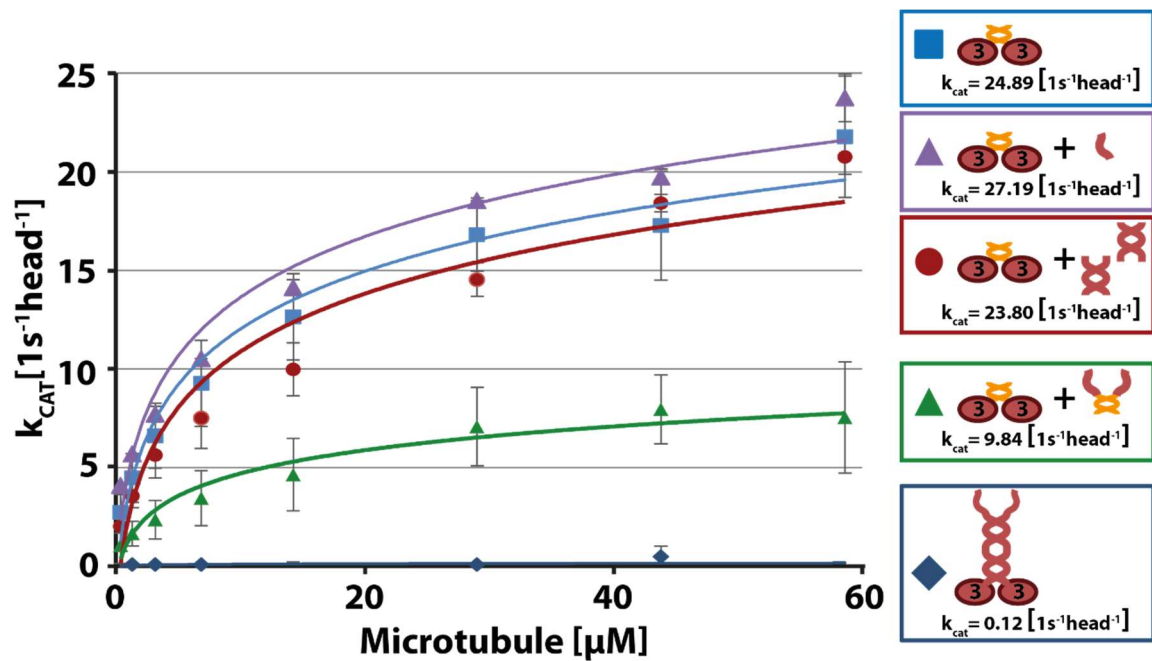


Figure 43: **The dimerized OSM-3 C-terminal tail domains inhibit the activity of the head domains.** Microtubule based ATPase activity assay of dimerized OSM-3 head domains (OSM-3¹⁻³⁴⁹GCN-4) that were incubated with both stalk domains (OSM-3^{350-444,FLAG} and OSM-3^{445-552,FLAG}, red circle), single tail domain (OSM-3⁵⁵²⁻⁶⁹⁹, purple triangle) or dimerized tail domains (OSM-3⁵⁵²⁻⁶⁹⁹GCN-4, green triangle) show that the tail domains inhibit the activity significantly only if dimerized. (blue square) shows activity of dimerized head domains, (blue diamond) shows inhibited activity of the full-length wild-type motor OSM-3 as controls. Error bars represent SD, repeated three times.

The results in Figure 43 clearly show that the dimerized motor domains of the OSM-3 motor protein are significantly inhibited through binding to dimerized tail domains. The full-length, wild-type OSM-3 is autoinhibited, with a k_{cat} of $0.12 \text{ s}^{-1}\text{head}^{-1}$, and the dimerized head domains OSM-3¹⁻³⁴⁹GCN-4 show activity with a k_{cat} of $24.89 \text{ s}^{-1}\text{head}^{-1}$. In contrast, the addition of the stalk domains OSM-3³⁵⁰⁻⁴⁴⁴ and OSM-3⁴⁴⁵⁻⁵⁵², as well as single tail domains (OSM-3⁵⁵²⁻⁶⁹⁹) had no impact on the enzymatic activity of the head domains (k_{cat} of $23.80 \text{ s}^{-1}\text{head}^{-1}$ and $27.19 \text{ s}^{-1}\text{head}^{-1}$, respectively). However, incubating the OSM-3¹⁻³⁴⁹GCN-4 head domains with the OSM-3⁵⁵²⁻⁶⁹⁹GCN-4 tails resulted in a significant decrease in enzymatic activity (Figure 43, green triangle).

8.4. The OSM-3^{G444E} construct is inherently active due to the charge and size of the introduced glutamic acid

Previous work by Imanishi *et al.* showed that the folded and thus autoinhibited conformation of the wild type was replaced by a more extended conformation upon point mutation of a glycine in the helix breaker position to a glutamic acid [72]. It nevertheless remains unknown, if this extended conformation was indeed permanent, or simply a shift in balance between the folded and the unfolded conformation, and if this was due to steric hindrance by the increased size of the mutated position or due to the highly negative charge of the glutamic acid. Therefore, we also designed - in addition to the previously discussed OSM-3^{G444E} - the OSM-3^{G444Q} mutant, in which the prominent glycine at the helix breaker position is replaced by a glutamine instead of a glutamic acid (Figure 44A) [72].

To our surprise, the OSM-3^{G444Q} mutant showed a reduced k_{cat} of 14.23 s⁻¹head⁻¹ when compared to the OSM-3^{G444E} mutant (k_{cat} of 24.82 s⁻¹head⁻¹). Still, this k_{cat} of 14.23 s⁻¹head⁻¹ is considerably higher than that of the previously measured wild type construct (Figure 44B), which suggests that both size and charge of the glutamic acid at the helix breaker position are responsible for the complete suppressed autoinhibition of the motor.

8 Results on the regulation of the homodimeric Kinesin-2 motor OSM-3 from *C. elegans*

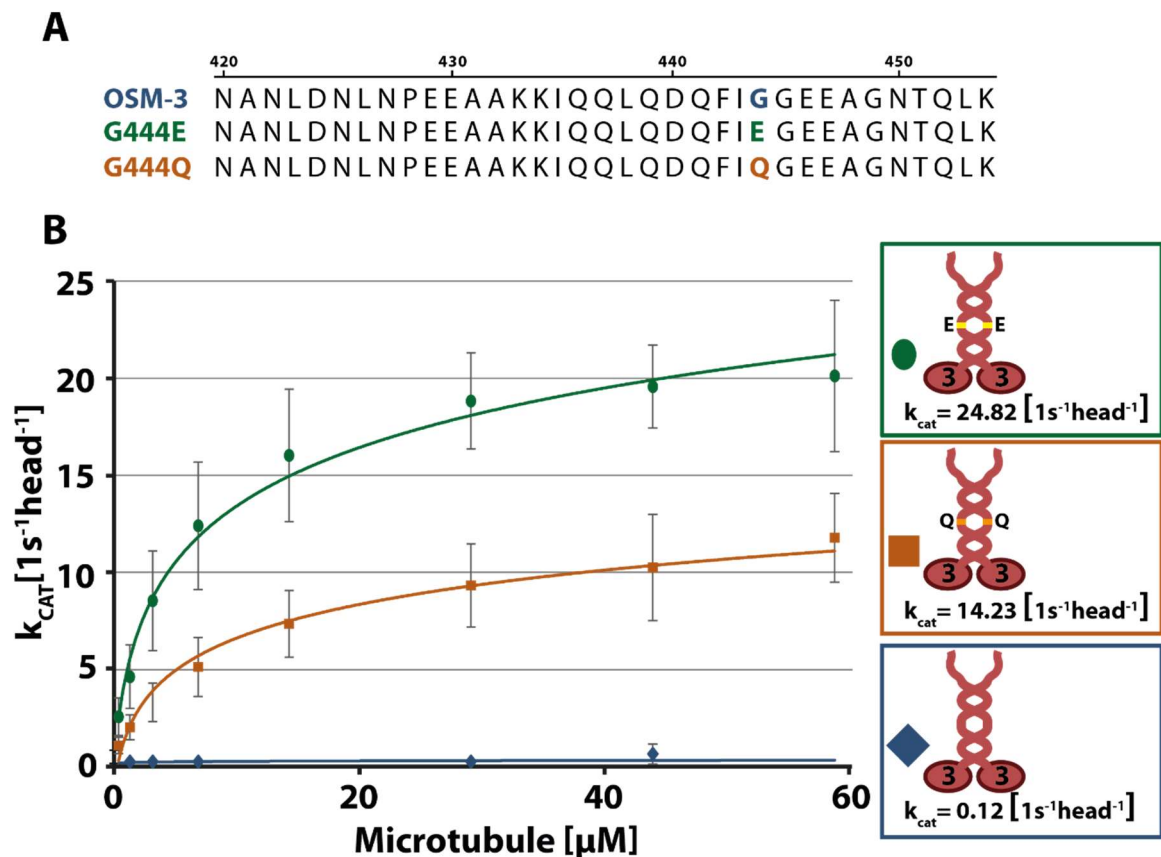


Figure 44: **Mutation at the helix breaker position with glutamine instead of glutamic acid results in reduced, but still existing activity of the head domains.** (A) Sequence alignments of the wild-type OSM-3, OSM-3^{G444E}, and OSM-3^{G444Q} mutants. (B) Microtubule based ATPase activity assay with full-length wild-type OSM-3 (blue diamond), OSM-3^{G444E} mutant (green circle) and OSM-3^{G444Q} mutant (orange square). Error bars represent SD, repeated three times.

8.5. Autoinhibition of OSM-3 is released through binding of the IFT subunits DYF-1/OSM-6 to the OSM-3 tail domains

Mohamed *et al.* [92] and Cleetus *et al.* [93] previously showed that the IFT-B subunit DYF-1 and OSM-6, through binding to OSM-3, are able to fully suppress the inhibition of OSM-3. However, the exact location and mechanism of said binding has remained unknown. To find out about this, we conducted a series of binding assays (5.2.2.5) between, on one side, the IFT subunits DYF-1/OSM-6^{FLAG} and on the other side, as potential binding partners, A) the head domain OSM-3¹⁻³⁴⁹GCN-4^{6xHis}, the stalk domains B) OSM-3³⁵⁰⁻⁴⁴⁴,6xHis and C) OSM-3⁴⁴⁵⁻⁵⁵²,6xHis, and the tail domains D) OSM-3⁵⁵²⁻⁶⁹⁹GCN-4^{6xHis} of the OSM-3 motor (Figure 45).

8 Results on the regulation of the homodimeric Kinesin-2 motor OSM-3 from *C. elegans*

Intriguingly, the OSM-6/DYF-1 dimer binds to the tail domains of the OSM-3 motor protein (Figure 45D), just as the OSM-3 head domains bind to the tail domains (Figure 41A). In contrast, the IFT-B subunit dimer OSM-6/DYF-1 did not bind to the OSM-3 stalk domain, nor to the head domains (Figure 45A - C). These findings suggest a regulatory mechanism based on two domains, namely the OSM-6/DYF-1 dimer and OSM-3 head domains, which competitively bind to the tail domains as a regulatory mechanism.

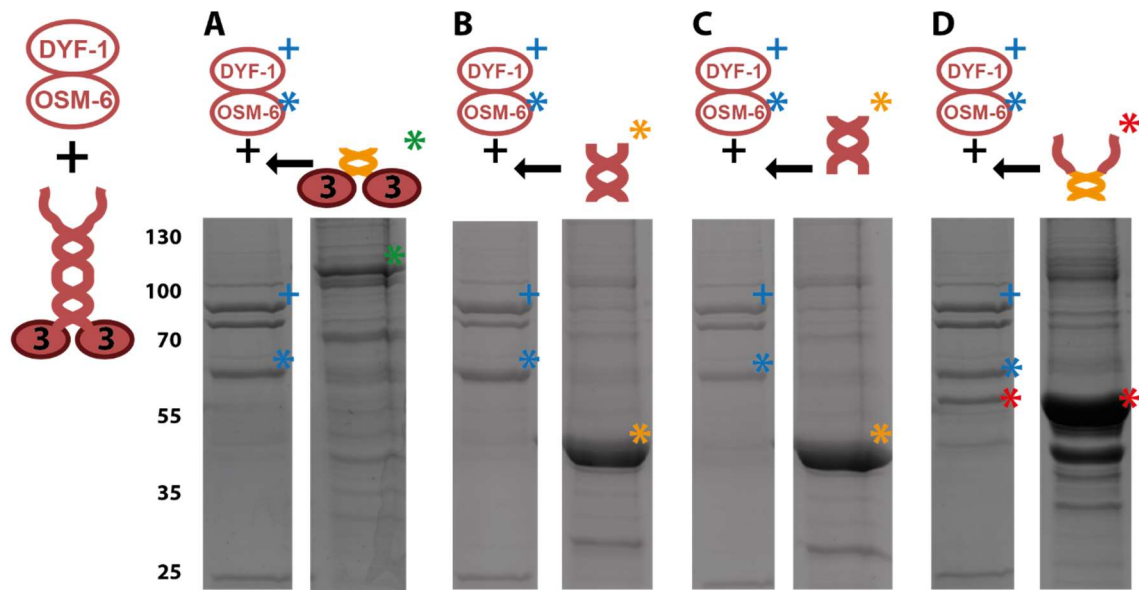


Figure 45: **The IFT-B subunit DYF-1/OSM-6 bind to the tail domains of OSM-3.** FLAG-tag purified OSM-6 (blue Asterisks, 53 kDa, runs higher) and DYF-1 (blue cross, 76 kDa) were left on FLAG-resin beads after purification and incubated with 6xHis purified dimerized head domains (OSM-3¹⁻³⁴⁹GCN-4^{6xHis}, A, right lane, green Asterisks, 52 kDa) and CC1 (OSM-3³⁵⁰⁻⁴⁴⁴,6xHis, B, right lane, orange Asterisks, 42 kDa) and CC2 (OSM-3⁴⁴⁵⁻⁵⁵²,6xHis, C, right lane, orange Asterisks, 42 kDa), as well as dimerized tail domains (OSM-3⁵⁵²⁻⁶⁹⁹,6xHisGCN-4 d, right lane, red Asterisks, 52 kDa), respectively. (D) clearly shows dimerized tail domain (red Asterisks) bound to the FLAG resin via the OSM-6/DYF-1 dimer. See 5.2.2.5 for assay protocol.

9. Discussion

Prerequisite for every eukaryotic cell and its complicated workings is the cytoskeleton and its molecular motors that are responsible for finely tuned, well-coordinated transport across the cell body. The importance of these motors is particularly obvious in the wide range of unrelated diseases linked to malfunctioning motors, like ciliopathies [13-17] or neurodegenerative diseases [18-22]. A detailed understanding of the molecular mechanism, structure and regulation of molecular motors is therefore crucial for finding cures and therapies for many diseases.

Next to the enzymatic head domains – the actual driving force of every motor protein - the tail domains are especially interesting, because their structure differs greatly between motor families and organisms, pointing towards a finely tuned role in adjusting the motor to its specific function within the cell (Figure 2, Figure S 1). The two most common specifications of every motor are therefore often linked to these domains: The specific binding to its target cargo and/or the precisely adjusted regulation of its activity [2, 30, 137].

However, even the total understanding of the molecular details behind functionality of an individual motor is only the basis to a complete understanding of the transport system the motor is involved in. Most transport systems are driven by a multitude of well-coordinated and competing motors, whose combined grade of activity results in the directionality of the whole transport system. Therefore, it is equally important to look at the functional cooperation between motors as it is to understand the individual motors themselves.

In this work, we studied two well-known Kinesin-2 motors, the heterotrimeric KIF3A/B/KAP from the cytoplasmic melanosome transport in *X. laevis* and the homodimeric OSM-3 from the Intraflagellar transport in *C. elegans*. Our main goal was to provide insight into the molecular mechanisms of the regulation and cargo binding of the two highly specialized kinesin-2 motors.

Also, we attempted to link the KIF3A/B/KAP motor with the p150^{glued} protein, a proposed binding partner that is known to recruit the cytoplasmic dynein [1]. As the native structure of the respective motor complexes remain unknown [126, 140], we

further explored means to artificially link the KIF3A/B/KAP to the Myosin-Va motor as both are activated during the melanosome transport upon increase of intracellular PKA activity.

9.1. The KIF3A/B/KAP motor is deactivated by dephosphorylation *in vitro* and has two distinct, synergetic functions for its respective tail domains

The first motor we analyzed was the KIF3A/B/KAP motor from the cytoplasmic melanosome transport in *X. laevis*. Most notably, this is a heterotrimeric motor with two distinct motor subunits and a third non-motor subunit (Figure 3). This diversity makes this motor especially interesting, since its two unique tail domains may allow for an even more precise regulation of inhibition, and/or cargo binding.

While considerable work has already been done on other motors like the Kinesin-1 motor prior to this thesis, little was known about the amphibian KIF3A/B/KAP motor, apart from the findings described in a previous doctoral dissertation [128]. Through use of an ATPase assay it was shown that it is a tail domain, namely that of the KIF3A subunit, which auto-inhibits the motor. It was further proposed that this inhibition was released when the KAP subunit was bound to the tails. Following up on these findings, we started investigations to get a more complete picture of the molecular mechanics behind the autoinhibition and cargo binding of this heterotrimeric motor.

We carried out fluorescent labeling of the heterodimeric KIF3A/B and heterotrimeric KIF3A/B/KAP motor and tested those constructs in a single molecule assay on surface-attached microtubules in a TIRF microscope. To our surprise both motors were equally processive (Figure 15). This appeared to refute not only the underlying theory regarding the autoinhibition, but also regarding the release of the autoinhibition by the KAP subunit, which seems to have no influence on the processivity whatsoever (Figure 15). Although these results were surprising, given the previously found, contradicting results and a recent publication showing how the KAP subunit in *C. reinhardtii* affects the motor's activity, this lack of influence of the KAP subunit on the motor's processivity had also been shown before e.g. for the

9 Discussion

mammalian homolog of this non-motor subunit [79, 100, 128]. In our single molecule experiments on surface-attached microtubules, we significantly increased the salt concentrations to prevent aggregation of the motors. Therefore, we suspected unwanted binding, especially with the unfixed microtubule filaments used in subsequently conducted ATPase bulk assays, to be a factor in these contrasting results. However, we were unable to verify our suspicion and could not suppress this autoinhibited behavior in the ATPase assays, by e.g. the increase in salt concentration in the used buffer. Regarding the reason why the construct truncated at the KIF3A subunit (KIF3A¹⁻⁵⁹⁷/B) nevertheless showed activity in the ATPase assay, we were later able to show that it is the tail of the KIF3A subunit that binds to the KAP subunit (6.4), making the protein binding capability the likely root for unwanted aggregation of the heterodimeric motor and in turn lack of activity as well. This inadvertent binding is naturally suppressed by deleting said tail domain of the KIF3A subunit.

Since the “classic” mechanism of full autoinhibition by tail-to-head domain binding [46, 72] was seemingly disproven, we explored two potential functions of the tail domains: The general binding of the motor to its cargo via its KAP subunit [43], as well as the up and down regulation of the general processivity of the motor [2, 79]. Additionally, since phosphorylation was already proven to somehow alter and regulate the different players of the melanosome transport like Myosin-Va and its adaptor Melanophilin [105], phosphorylation and dephosphorylation were the most obvious approaches to test for the regulation of any found feature of the KIF3A/B/KAP motor, as well. To this end, we conducted *in vitro* phosphorylation assays with isotope-labeled ATP, showing that indeed both the KIF3A and KAP subunits are target of phosphorylation (Figure 20). However, phosphorylation of the heterotrimeric KIF3A/B/KAP complex was considerably weaker, suggesting that both phosphorylation sites of KIF3A and KAP were buried by heterotrimerization.

Also, we showed that it is indeed solely the KIF3A tail that binds to the KAP subunit (Figure 17). However, phosphorylation or dephosphorylation did not impact binding between the KAP and the KIF3A tail domain (Figure 23), nor the binding of the KAP adaptor protein to cytoskeletal filaments (Figure 24) as seen previously with the adaptor protein Melanophilin of the Myosin-Va motor [105]. However, subtle

9 Discussion

changes in binding behavior towards the filaments or the KIF3A tail domain that we could not quantify here in our *in vitro* bulk assays could very well have a physiologically relevant impact *in vivo*. This has been shown e.g. for the binding behavior of Melanophilin to the f-actin and microtubule tracks, where slight, but in this case detectable changes in binding preference towards either filament have a tremendous effect on the overall direction of the melanosome transport [105, 106]. Additionally, the phosphorylation of the KAP subunit could alter the affinity of KAP to other cargo units instead, and not to the motor subunits. The Kinesin-1 light chains, for example, have been shown to change their binding behavior to their respective cargoes upon phosphorylation without having any other effect on its link to the Kinesin-1 heavy chains (Figure 2) [176-178].

While our previously mentioned measurements for velocity of the heterodimer and -trimer were in good agreement with previous publications on other heterotrimeric Kinesin-2 motors [46, 48] (Figure 15), the runlength of approx. 3 μm (Figure 15) was considerably higher than from studies conducted in optical tweezer assays where the motors are attached to micron-sized beads via their tail domains [46].

We therefore turned our attention yet again to the tail domains, as we suspected the occupation of the tail domains by the bound micron-sized beads to be the cause of the reduced runlength observed in the optical tweeter assays [46]. Having attributed the function of binding the KAP subunit to the KIF3A/B motor to the tail domain of the KIF3A, we showed that it is indeed the function of the KIF3B tail domain to increase the runlength significantly (Figure 18). This could be explained by the previously postulated theory, which states that electrostatic interactions of positively charged patches of the tail with the negatively charged E-hooks of the microtubule filaments could tether the motor to the tracks and thus increase its runlength. This same process has been shown in detail before for the dynein, for the Kinesin-1, for the mammalian Kinesin-2 KIF-17, and for Kinesin-3 [179-182]. The determined sequence of the responsible KIF3B tail is 21 amino acids long (Figure 19) and analysis of that sequence revealed that it is indeed slightly positively charged (Net charge at pH7 = +2, pepcalc.com). However, the last 21 amino acids of the KIF3A tail are even more positively charged (Net charge at pH7 = +5, pepcalc.com). Directly aligning the tail domains of KIF3A and KIF3B shows that the

most outstanding feature of the KIF3B tail, as opposed to the KIF3A tail, is its length (Figure S 4). The KIF3A tail is 102 amino acids long from the conserved helix breaker position, the KIF3B tail measures 152 amino acids. This may enhance binding of the KIF3B tail to microtubules when compared to the significantly shorter KIF3A tail. In turn, this would suggest that the truncation of the last 21 amino acids of the KIF3B tail does not lead to reduced runlength due to its specific sequence, but rather due to the simple reduction of the tail's length. In the end however, it remains inconclusive whether the increase of the runlength by the KIF3B tail is achieved by tethering to the microtubule or another unknown mechanism, e.g. intra-motor binding.

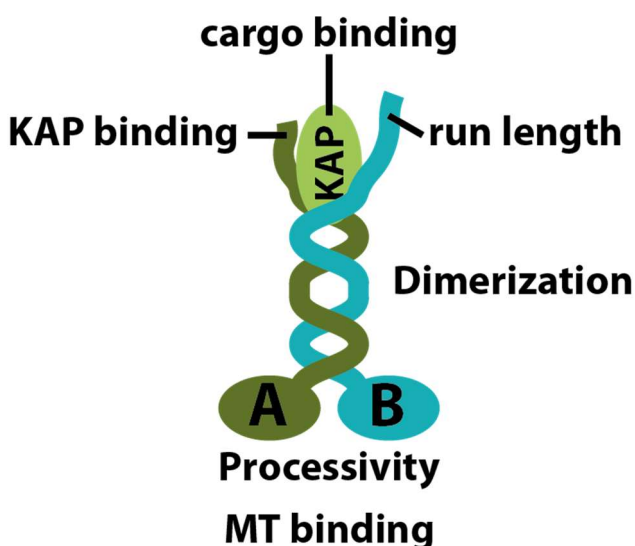


Figure 46: **Schematic depiction of the KIF3A/B/KAP motor and proposed functions of its domains.** The non-motor subunit KAP functions solely as a cargo-binder and is bound by the tail of the KIF3A motor subunit. The considerably longer tail of the KIF3B subunit is responsible for the long runlength of the motor. The head domains are responsible for binding and movement along the microtubule filaments, while the coiled-coiled stalk domain dimerizes the motor subunits.

Collectively, we have identified an example for the evolution of different tail structures within a motor, adapting the motor to the differentiated properties and functions of it. In the case of the Kinesin-1 motor, regulation appears to be achieved through competition between the tail domains binding to the cargo and on the other hand the tail domains binding to the head domains (Figure 4). However, in the case of the KIF3A/B/KAP, different tail domain structures offer a potential

explanation for the observed fact that this motor has differentiated, and not competing but rather synergetic functions and properties.

Also, as described above, we had shown that phosphorylation or mimicking phosphorylation through mutation does not influence the processivity of the heterodimer or heterotrimer in a manner that we could detect here (Figure 25). However, as with the KAP subunit described above, subtle changes that have significant influence *in vivo* could have stayed undetected in the bulk *in vitro* assays

9 Discussion

conducted in this thesis or simply haven't been tested for, e.g. change in behavior under force, as described for Kinesin-1 [101]. On the other hand, we discovered that dephosphorylation would indeed have an inhibitory effect on the motor (Figure 26, SI Movie 1+2), which we could narrow down to both head domains (Figure 29, SI Movie 4). However, whether this dephosphorylation influenced the ATPase activity, microtubule affinity or any other mechanism remains unknown.

Nevertheless, phosphorylation of the motor domain as means of influencing the motility of a molecular motor has been demonstrated many times in the past. For example, phosphorylation of three specific sites all over the head domains of Kinesin-5 have been shown to alter microtubule affinity, velocity and even the motor's directionality itself [102, 183]. The toolbox motor Kinesin-1 has also been proposed to be regulated by phosphorylation of the motor domains [101]. Here, a single serine is phosphorylated, resulting in a more stable autoinhibiting confirmation of the motor as well as a decrease in velocity under load. Curiously, this serine is located far from the microtubule- and ATP-binding sites and thus does not interfere with those main motor functions. The resulting, fine regulation of the motor could be enough to shift the tug-of-war between Kinesin-1 and dynein to dynein's favor in their respective transport system [101]. It is therefore reasonable to assume that the processivity of the amphibian KIF3A/B/KAP motor can also be finely regulated through phosphorylation as well, especially considering how many predicted phosphorylation sites are located within the head domains of both KIF3A and KIF3B (Figure S 5).

All in all, the KIF3A tail is responsible for the binding to the KAP subunit, while the KIF3B tail is necessary to increase the runlength of the motor. However, modification of the motor domains through dephosphorylation on the other hand renders the motor unprocessive. These findings are in good agreement with previously postulated models for the melanosome transport: All three motors of the melanosome transport system are constantly bound to the vesicles (KIF3A/B/KAP via its KAP subunit), and the directionality of the vesicle is governed by a coordinated bidirectional movement, regulated by the activity of each motor by external factors, like e.g. the state of phosphorylation (Figure 9) [109, 110, 113, 138-140, 184].

9 Discussion

On the one hand, whenever the activity of the protein kinase is high, melanosome transport is dominated by the plus-end directed transport of the KIF3A/B/KAP motor and the actin-based Myosin-Va motor (Figure 5). However, this dominance by KIF3A/B/KAP is also caused by the down regulation of the dynein activity, while the processivity of the heterotrimeric Kinesin-2 itself remains seemingly unchanged (Figure 8). This is in good agreement with our findings, showing no apparent effect of phosphorylation on the processivity of the KIF3A/B/KAP motor (Figure 25). Nevertheless, as phosphorylation of the head domains of Kinesin-1 have been shown to also not affect the general processivity of the motor domain, but rather lowering the Kinesin-1 velocity under load to a point where the opposing motor dynein wins the tug-of-war in their respective transport system [101] a similar, but positive effect on the stall force, that remained undetected in our set of experiments, could very well be possible for the KIF3A/B/KAP motor in the melanosome transport.

On the other hand, when the activity of the protein kinase is decreased, the dominance over the melanosome transport shifts towards the minus-end directed transport of the dynein motor, resulting in the aggregation of the melanosomes in the cell center (Figure 5) [117, 122]. This shift is seemingly induced by an increased runlength of the minus-end directed movement of the dynein motor, while, as it was generally assumed, the activity of the KIF3A/B/KAP motor remains unchanged yet again. Here, we could show for the first time that in fact, under these circumstances, processivity of the KIF3A/B/KAP motor domains are down regulated (Figure 26, SI Movie 1+2). This further amplifies the power shifting towards favoring the dynein motor's activity and thus increasing the runlength of the dynein driven runs (Figure 47). This curious change in behavior upon dephosphorylation, but not phosphorylation has also been shown for the actin-based Myosin-Va transport. Only during aggregation and decreased kinase activity is the behavior of the Melanophilin and in turn the Myosin-Va motor changed from its normal binding affinity towards the f-actin filaments to the microtubule filaments [105]. This change gives the dynein the necessary upper hand in the tug-of-war between the f-actin- and microtubule-based transport and supports the aggregation of the melanosomes in the cell center.

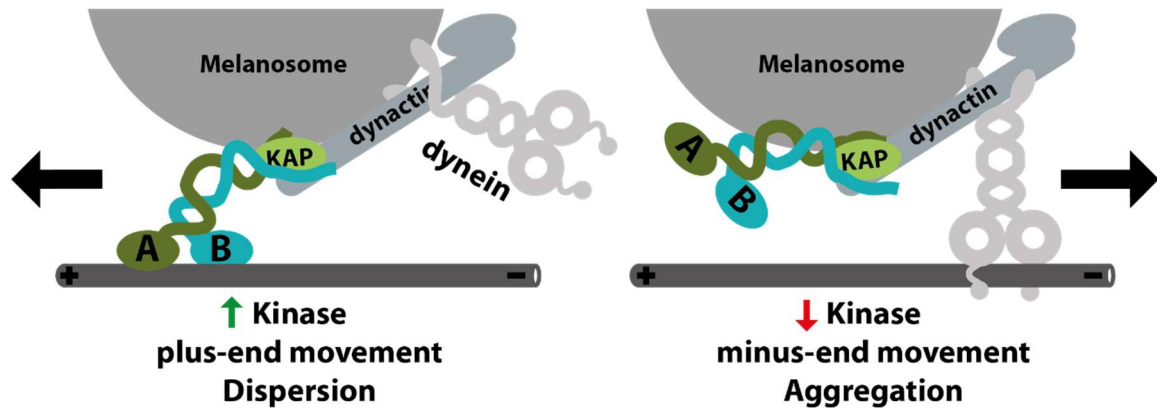


Figure 47: Graphic depiction of the proposed bidirectional microtubule-based transport of melanosomes in *X. laevis* driven by the plus-end directed KIF3A/B/KAP and minus-end directed dynein. During increased kinase activity (left), the movement is dominated by the plus-end directed KIF3A/B/KAP motor, while the dephosphorylation (right) of the KIF3A and KIF3B head domains leads to decreased processivity of these domains and in turn minus-end movement driven by the dynein motor. The binding of the KAP subunit by the KIF3A tail and the runlength-enhancing function of the KIF3B tail are however not affected by the activity of the protein kinase.

9.2. Linking KIF3A/B/KAP to other players of the melanosome transport system

The overall directionality of the melanosome transport is the result of a constant back and forth movement governed by the sum of finely coordinated activity of all three motors at the same time, rather than an unidirectional motion as in the case of the intraflagellar transport (IFT) [109, 118]. Determining the molecular regulation and mechanism of individual motors may therefore be insufficient to the understanding of the melanosome transport. Studying the direct interaction between two or more players is crucial and has been attempted several times before [109, 113, 115, 118, 138]. Following up on this, we attempted to couple the previously discussed KIF3A/B/KAP motor with the p150^{glued} subunit of the dynactin complex, for which it has previously been proposed that it binds to the KIF3A/B/KAP motor and supports its processivity [76, 97]. In a parallel approach, we attempted to artificially link the KIF3A/B and Myosin-Va/Melanophilin/Rab27a complexes, in order to investigate how the now known regulatory mechanisms of each individual motor would affect the collectivity of both motors [105, 106].

9.2.1. Direct binding of the dynein subunit p150^{glued} to KIF3A/B/KAP is more complex than anticipated

In 2015, Urnavicius *et al.* have determined the structure of the p150^{glued} subunit and have postulated that the coiled-coil domains CC1a and CC1b fold onto each other and thereby bury the Cap-Gly domain at the N-terminal end of the p150^{glued} folds in the intercoil domain (ICD), with Cap-Gly being responsible for the binding to the microtubule (Figure 7) [1]. The folded CC1 domain is assumed to be the binding site of the dynein motor and unfolds upon binding; a process shown in a very recent publication [185]. However, the ICD is supposedly the site which is responsible for binding to the KAP subunit of the KIF3A/B/KAP motor [76]. It has remained unknown so far whether this latter binding also triggers the opening of the CC1 coiled-coil domains and subsequently the release of the Cap-Gly domain.

Based on coiled-coil predictions and previous publications, we designed a full-length construct of the p150^{glued} and two constructs, one containing only the Cap-Gly and CC1a, and the other one containing only the Cap-Gly, CC1a, CC1b, as well as part of the Intercoil domain, respectively (Figure 31) [1]. *In vitro* phosphorylation assays with isotope-labeled ATP^{γ-32P} revealed that the ICD and/or CC1b can be phosphorylated (Figure 31). This now allows to investigate the hypothesis, by which it could indeed be phosphorylation that regulates KAP binding, followed by the opening of the coiled-coil domains (or else direct opening of the p150^{glued} subunit) which would in turn trigger binding to the microtubule filaments. As a first step, we confirmed that the Cap-Gly domain is indeed responsible for the binding to the microtubule, by showing binding of the truncated construct, containing only the Cap-Gly and CC1 domains, to the microtubule. However, using the full-length construct as the binding partner, it turned out to be impossible to trigger the opening of the coiled-coil domains and consequent binding to the microtubule or to the KIF3A/B/KAP motor (Figure 32 and Figure 33). Previously postulated binding of the p150^{glued} subunit to the KIF3A/B/KAP motor or to the microtubule could thus not be confirmed, and no influence of the p150^{glued} subunit on the processivity of the Kinesin motor could be found [76, 97].

Previous publications did show both binding to the KIF3A/B/KAP motor, and a positive influence on its processivity. But these experiments had either been carried out through immunoprecipitation from cell extracts with an unknown number of additional binding partners [76], or with the complete dynactin complex, consisting of numerous additional proteins, that were possibly conditional for obtaining these results [97]. The bottom-up reconstitution of the connection between the KIF3A/B/KAP motor and the dynactin complex is thus clearly more complicated than it had been assumed at the outset of this thesis.

9.2.2. Linking of KIF3A/B/KAP to Myosin-Va/Melanophilin/Rab27a via dsDNA handle

In a next project, we attempted to link the KIF3A/B/KAP motor with the well-studied Myosin-Va motor. The obvious complicated nature of direct inter-motor connections and general lack of known, direct links between these motors made it necessary to link them via an artificial dsDNA bridge (Figure 34). The dsDNA handle was functionalized with “anti-Halo” Iodoacetamide O4-ligands on either end, that could bind to Halo-tagged motor proteins. As a first step, we established that the dsDNA handle would successfully link two Halo-tagged KIF3A/B motors (Figure 35). However, we quite soon encountered problems caused by unspecific binding of the Melanophilin/Rab27a cargo units between themselves and to the KIF3A/B motor, which impeded further follow-up of these studies (Figure 36), as this ancillary binding of the Melanophilin/Rab27a complex prevented proper build-up of a link between the two motor complexes. Specific binding between one KIF3A/B complex and one Myosin-Va/Melanophilin/Rab27a complex without compromising any of the two motors functions were pre-conditions for this project, but this could not be achieved at this point. Both Rab27a and Melanophilin are known for their multitude of binding functions; e.g. Melanophilin simultaneously interconnects Rab27a with both the Myosin-Va motor and the actin or microtubule filaments [105, 186]. Similarly, Rab27a is known for its multitude of additional binding partners within the cell [187-189]. This affinity towards many other proteins with unknown effects on molecular regulation might be the reason for the unwanted binding to a.o. the KIF3A/B motor, as described above.

9.2.3. Photoisomeric Myosin-Va inhibitor AzoMyoVin-1 shows promising results

In support to the coupling project (7.3), we also attempted to implement a protocol for the photoisomeric AzoMyoVin-1, a compound that promises instant, reversible and specific inhibition of the Myosin-Va motor (Figure 37). This would allow for more precise observations of each players' influence on the processivity of the Myosin-Va-KIF3A/B complex at any given moment. This project was particularly tempting since much is already known about the behavior of the Myosin-Va/Melanophilin/Rab27a complex and its regulation by phosphorylation on a microtubule/f-actin cross-network [105, 106]. The ability to observe the linked KIF3A/B and Myosin-Va complexes on such a cross-network under different states of phosphorylation, while being able to readily and specifically inhibit the Myosin-Va motor, could give us valuable insight into the specific contribution of each of the two individual motors to the tug-of-war at microtubule/f-actin intersections.

First, we could quickly verify a specific inhibitory function of AzoMyoVin-1, i.e. that it did affect the Myosin-Va motor, but not the KIF3A/B motor, by which AzoMyoVin-1 became an important tool for our future research (Figure 39E). However, the desired switching from inhibitory to non-inhibitory state upon exposure to irradiation turned out to be more complex. Exposing approx. 1 nM of Myosin-Va motor complex to 2.5 μ M of AzoMyoVin-1 resulted in severe inhibition of the motor, as hoped for, while prior irradiation of the same mix with 360 nm laser light would significantly rescue the activity of the motor (Figure 39), suggesting that irradiation with 360 nm light switches the compounds mainly occupied state from the inhibiting trans-form to the inert cis-form. According to prior publications by the Thorn-Seshold group, who designed the AzoMyoVin-1 molecule, photoswitchable compounds shift from approx. 90% cis-isomer, when exposed to ultraviolet light, to 85% trans-isomer, when exposed to 500-530 nm light [172]. Assuming that those values would be applicable to the untested AzoMyoVin-1, about 10% of the compound would be inhibiting at all times and 15 % would never be inhibiting. This means that the motor to inhibitor ratio needs to be very finely adjusted to ensure reliable and significant results from a system that is already affected by a vast array of influencing factors. Our results show that a concentration of 2.5 μ M inhibitor would be too high for a

motor concentration of 1 nM, since the mix irradiated with natural light was well under 15% active, while the mix irradiated with ultraviolet light was far from 90% active, and therefore the concentration of the inhibitor needs to be adjusted further (Figure 39). These results establish that the AzoMyoVin-1 is specific to the Myosin-Va motor, and, in addition, show that reversible activation during experiments can be achieved, which promises to be a valuable tool to control Myosin-Va activity in future experiments.

9.3. The OSM-3 motor is autoinhibited by its random tail domains and activated through binding of DYF-1/OSM-6 to its tail domains

Autoinhibition is necessary to suppress futile ATPase activity when the motor is not currently bound to its cargo or not supposed to actively drive the transport. Autoinhibition is therefore a common feature of many motors and transport systems [2, 44, 46, 72, 79, 82]. In the state of autoinhibition of e.g. Kinesin-1, the central stalk domains bend at their helix breaker position and allow the C-terminal tail domains to bind to the N-terminal regions of the motor protein. Thereby, hydrolysis of ATP or e.g. the affinity to the filament track are suppressed [2, 44, 69, 72, 84, 85]. In 2006, Imanishi *et al.* published their findings on the OSM-3 motor, showing that this motor is, again, regulated by its tail domains and by the ability of the stalk domain to bend at its helix breaker position. At least they obtained indications pointing in that direction through deletion or mutation of the helix breaker position [72]. However, these findings do not conclusively show whether the binding of the tail domain to the head domains is indeed the mechanism behind this regulation as different mechanisms have been discovered that have been found to be responsible for autoinhibition of other motors, or at least contribute to it [44, 86, 190].

Work by Mohamed *et al.* [92] and by Cleetus *et al.* [93] revealed that the binding of subunits of the physiologically relevant IFT-B cargo protein complex, namely the subunits DYF-1 and OSM-6, release autoinhibition of OSM-3. These findings have given great insight into the regulation of this motor. Still, molecular evidence for

9 Discussion

direct binding of the tail domains to the head domains, or to the DYF-1/OSM-6 cargo is still missing here as well.

Based on the coiled-coil predictions of the OSM-3 sequence, we designed constructs of the head, stalk and tail domains (Figure 40) and tested their binding to one another. Through this approach, we could, for the first time, show that indeed the C-terminal tail domains bind directly to the head domains, substantiating further the previously discussed way of autoinhibition by tail-to-head binding (Figure 41,

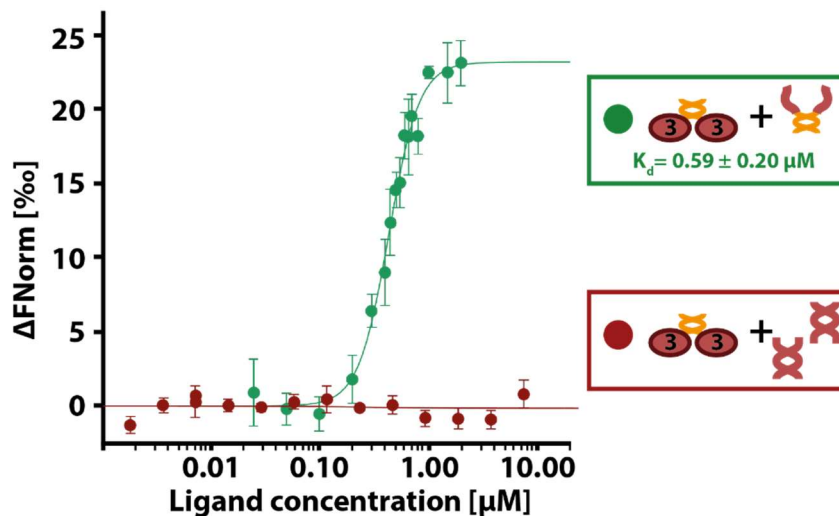


Figure 42, Figure 48 A). To conclusively show that the tail domains inhibit the motor by binding to the motor domains, we showed in an ATPase activity assay that by adding dimerized tail domains to dimerized head domains *in trans*, the enzymatic activity of the head domains is reduced by more than 50 % (Figure 43).

Especially the conducted micro-scale thermophoresis assay highlights the fact that the tail domains, and not the stalk domains, bind to the head domains (

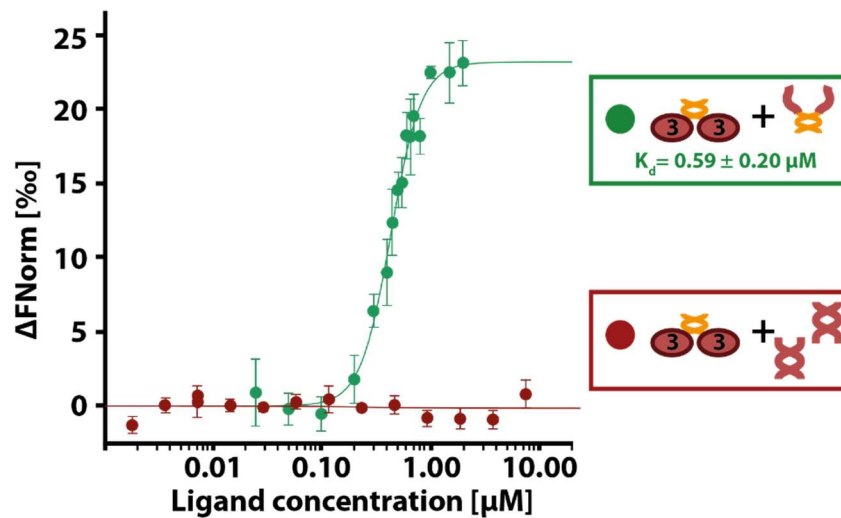


Figure 42). This strongly indicates that the tail domains are the only domains that directly regulate the activity of the heads, contrary to e.g. the KIF-17 motor, where both the tail as well as the stalk domains autoinhibit the motor [44]. Regarding the determined K_d value of $0.59 \pm 0.20 \mu\text{M}$ (

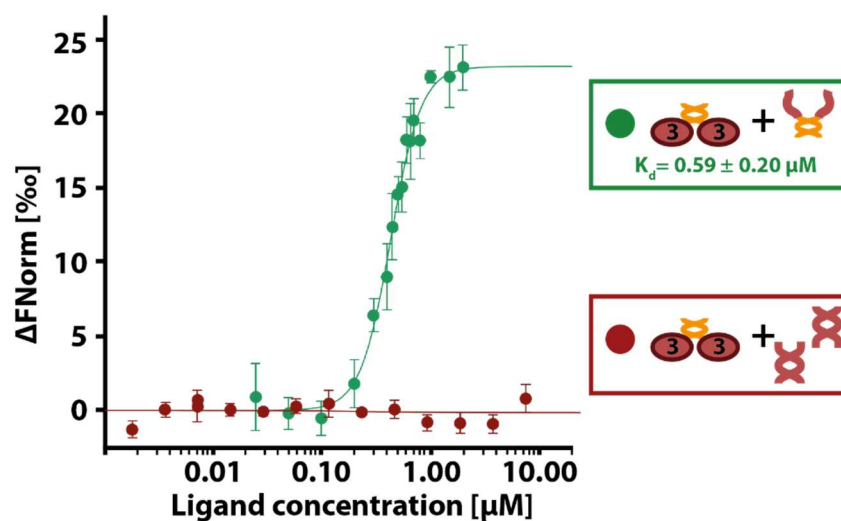


Figure 42), it is important to note that the MST method is only suited for comparing two simultaneously conducted assays, rather than for determining refined K_d values, as the indicated K_d value is highly dependent on the mode and settings used for each analysis [191]. In order to ensure future comparisons, it is therefore crucial that the setting for both, the experiment and the analysis, are indicated alongside any stated K_d value (5.2.10).

9 Discussion

Regarding the folding of the stalk domains, previous publications have shown that through replacement of the conserved glycine G444 in the stalk by a glutamic acid (OSM-3^{G444E}), the motor would be turned inherently active [72] (Figure 48 B). Imanishi *et al.* ascribed this effect to either the larger size and/or to the negative charge of the glutamic acid, which reduces the period which the motor spends predominantly in the folded i.e. inhibited conformation, and increases the duration of the period of the unfolded i.e. active state [72]. Coiled-coil predictions for OSM-3 show that the simultaneous deletion of the P428 and F442 positions causes the helix breaker to vanish, suggesting that the G444 position is indeed beyond the helix breaker position itself i.e. on the C-terminal part of the coiled-coil domain (Figure 44, Figure S 3). This suggests that the previously shown suppression of the folding by the glutamic acid mutant on the C-terminal part of the stalk is indeed caused by the interaction with the N-terminal part of the stalk through either steric hinderance or charge repulsion rather than a direct influence on the helix breaker hinge itself, e.g. making it impossible for the stalk to bend down completely. To test this theory, we designed, in addition to the glutamic acid mutant OSM-3^{G444E}, a glutamine mutant (OSM-3^{G444Q}), thereby mimicking the size but not the charge of the OSM-3^{G444E} mutant. Surprisingly, in an ATPase activity assay, the OSM-3^{G444Q} showed a remaining activity, which was however reduced by approx. 50 % as compared directly to the OSM-3^{G444E} construct. This suggests that both - steric hinderance and charge – contribute to the full shift towards the open conformation proposed for the OSM-3^{G444E} mutant (Figure 44, Figure 48 B, C).

We then turned our focus on the assumed release of this inhibition through binding to its cargo. Recently, Cleetus *et al.* were able to show that the addition of the IFT-B subunits DYF-1 and OSM-6 turned the autoinhibited wild-type motor fully active [93]. Similar to the previously conducted intra-motor binding assays in (8.2), we tested these two IFT-B subunits for binding to the different domains of the OSM-3 motor. We showed that the DYF-1/OSM-6 dimer binds to the C-terminal tail domains of the OSM-3 motor in the same manner as the OSM-3 head domains, suggesting a competitive binding of both the cargo and the head domains to the tail domains (Figure 45, Figure 48 D). To underpin this theory, we attempted a series of microscale thermophoresis (MST) assays, in which we added a titration of the head

domains and DYF-1/OSM-6 dimer to the tail domains to determine their relative K_d values (not shown). However, we were unable to conclusively show a binding curve because the necessary saturation plateau could not be reached without difficulties at higher concentrations. Thus, a comparatively lower K_d value for the binding of the DYF-1/OSM-6 dimer to the OSM-3 tail domains in comparison to the K_d value established for the binding between the OSM-3 tail and head domains could not be determined and the expected competitive binding could not be demonstrated. Nevertheless, these preliminary indications from the MST assay, the successful pull-down assays (Figure 45) and the findings from Cleetus *et al.* [93] strongly suggests in what manner the DYF-1/OSM-6 dimer releases the autoinhibition of the OSM-3 motor. Collectively, the mechanism behind regulation and release of autoinhibition of the OSM-3 motor on a molecular level could be demonstrated, confirming the tail-to-head binding postulated by Imanishi *et al.*, in analogy to the mechanism of the Kinesin-1 motor, although much is still unknown about the binding between the DYF-1/OSM-6 dimer and the OSM-3 motor [72, 84].

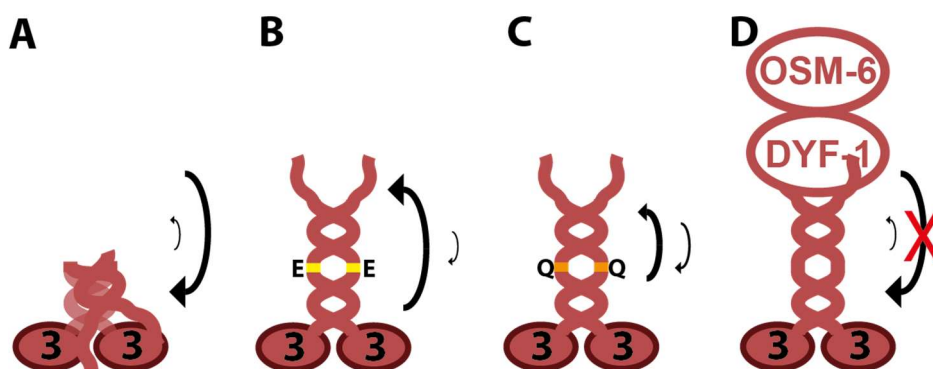


Figure 48: **Schematic depiction of the autoinhibition mechanism of OSM-3.** (A) OSM-3 wild-type motor is autoinhibited by the folding of the stalk domain and consequent binding of the tail domains to the head domains. (B) Mutating the G444 position near the helix breaker position in the stalk into a bigger and negatively charged glutamic acid results in suppression of the autoinhibition in the mutant motor OSM-3^{G444E} by shifting the folding equilibrium significantly to the open conformation (C) The significantly reduced suppression of the autoinhibition and in turn folding of the stalk of the OSM-3^{G444Q} mutant, where an equally longer but uncharged glutamine replaces the G444, shows that both, steric hinderance and charge repulsion are responsible for the fully achieved preference for the open conformation of the OSM-3^{G444E} mutant. (D) The physiologically relevant release of the autoinhibition is achieved by binding of the DYF-1/OSM-6 IFT subunits to the tails and consequent inability of the tails to bind to the head domains.

All in all, these determined features fit perfectly with the required function of the OSM-3 motor, as one of the anterograde intraflagellar motors. Inherently inactive, this motor is activated upon binding to the IFT train at the base of the cilia (in detail

the DYF-1/OSM-6 IFT-B subunits) and subsequently drives this transport until its disassembly at the tip of the cilia (Figure 49). A simple on/off switch upon cargo binding is all that is needed to regulate all desired functions of this motor *in vivo* [55]. However, it still remains so far unknown how the assembly and disassembly at the base and the tip of the cilium is regulated.

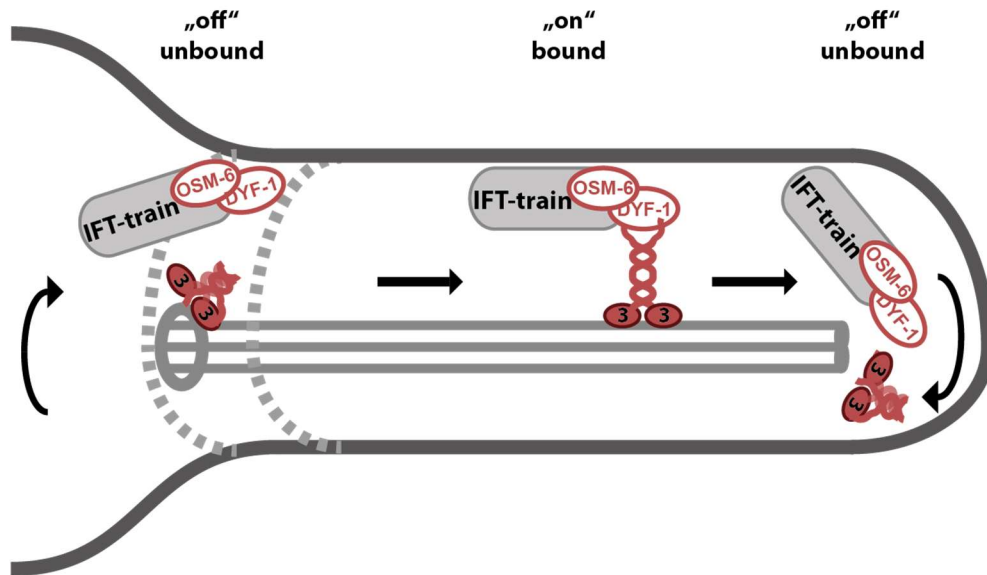


Figure 49: **Proposed model depicting how OSM-3 is inherently inactive unless it fulfills its function as the driving force of the anterograde transport in IFT.** The IFT subunits DYF-1/OSM-6 recruit the inactive OSM-3 motor by binding to its tail domains and in turn activating it. The IFT train is subsequently driven by the OSM-3 motor to the tip of the cilium, where the binding between the IFT train and the motor is severed, and OSM-3 is turned inactive again.

9.4. Summary and Outlook

In this thesis, we have determined both functions of the distinct tail domains of the KIF3A/B/KAP motor plus the regulatory effect of dephosphorylation of its head domains on the motor's processivity. In doing so, we were able to establish for the very first time a rather complete picture of the molecular regulation and mechanism of this motor. Still, many questions are left open.

For example, the mechanism behind the elongated runlength achieved by the tail domain of the KIF3B is still unknown. Intra-motor binding assays with constructs of each distinct domain of the motor, as performed with OSM-3 (8.2), and decoration

9 Discussion

assays with fluorescently labeled KIF3B tail domains on surface-attached microtubules could help to reveal, whether the KIF3B tail domains increase the runlength by binding to other domains within the KIF3A/B motor or by tethering the motor to the microtubule filaments.

Also, it remains unknown which exact position in the head domains get dephosphorylated, and in turn, which function is targeted that would be necessary for proper processivity. Mimicking dephosphorylation by mutating the different predicted phosphorylation sites in the head domains could shed light on both of these questions.

Other so far untested features, such as the motor's stall force, might possibly also be influenced by phosphorylation or dephosphorylation of either the tail or the head domains and these effects might have remained undetected in the assays conducted in this thesis. Additional assays, such as optical tweezer assays, for example, that would not bind to the necessary tail domains but rather e.g. the KAP subunit might reveal such features.

Finally, the next logical step of this bottom-up approach of reconstituting the KIF3A/B/KAP, and in turn the melanosome transport as a whole, would be to add more and more known participants to the now well-established KIF3A/B/KAP motor.

The addition of the p150^{glued} from the dynactin protein complex for example is one of these additions, as it has already been postulated that it is a direct binding partner to the KAP subunit [76]. Although we were unable to show any binding between these two at this point, we cannot exclude that they do either. Further experiments and additional approaches to clarify this will be therefore necessary. For example, designing constructs of each separate domain of the p150^{glued} to test for binding to the KAP subunit, as we have done in this thesis with the OSM-3 motor, might shed some light on the exact location of interaction between those two proteins. However, previous successful depictions of the p150^{glued}/KAP binding were done with the entire dynactin complex (p150^{glued} + another 22 proteins), suggesting that addition of one or more of those remaining 22 proteins to the p150^{glued}/KAP binding assay might be more successful than the binding assays with the truncated p150^{glued} and KAP alone.

9 Discussion

The equally well-established Myosin-Va/Melanophilin/Rab27a complex is another promising binding partner to the KIF3A/B/KAP motor to reconstitute the melanosome transport system further. Although we were able to link two different KIF3A/B motors through an artificial dsDNA handle, attempts to link this motor with Myosin-Va/Melanophilin/Rab27a failed due to the tendency of the Melanophilin/Rab27a subunits to unspecifically interact with the Kinesin-2 motor. Solving this ancillary aggregation seems to be the next step to this otherwise very auspicious project. Myosin-Va is known to be deployed at various locations in the cell and thus to be capable to bind to a number of different adaptor and scaffold proteins [192]. This might suggest that the Myosin-Va/Melanophilin/Rab27a complex is incomplete and lacks a possible fourth or more binding partners to both increase its stability and suppress its unspecific binding to other proteins. Whatever the case may be, we could show that the dsDNA handle works. Linking of the KIF3A/B/KAP motor with different motors, for example the dynein motor, could still be a viable option for future experiments.

Also, we successfully conducted preliminary experiments to establish a photo-switchable inhibitor of Myosin-Va, called AzoMyoVin-1, to add a valuable tool to the project observing the linked KIF3A/B and Myosin-Va motor complexes. However, these preliminary experiments showed that the very promising AzoMyoVin-1 project needs further work in order to be used without any compunction regarding e.g. the exact concentration used in future assays. Even if the a.m. artificial coupling of the KIF3A/B/KAP and Myosin-Va motor do not yield satisfactory results, the AzoMyoVin-1 may well be equally handy in *in vivo* experiments or e.g. in *in vitro* observations of purified melanosomes on reconstituted microtubule/actin cross-networks.

Regarding the OSM-3 motor from *C. elegans*, we showed that this motor is, in contrast to the KIF3A/B/KAP motor, indeed autoinhibited by the binding of its tail domains to the head domains. This autoinhibition can be released by binding of the IFT-B subunits DYF-1/OSM-6 to the tail domains, which in turn prevents the binding of the tail to the head domains. However, additional conformation of this competitive binding between the head domains and the IFT-B subunits to the tail domains through e.g. a comparative MST assay are still necessary. Also, it still needs to be

9 Discussion

determined how this assembly at the base and disassembly at the tip of the cilium is achieved. For example, it is still unknown how the OSM-3 motor is switched off at the tip of the cilium. It is possible that the motor is directly autoinhibited through e.g. dephosphorylation, but it could also be possible that its preference towards the OSM-6/DYF-1 subunits is switched to the preference towards yet unknown IFT-B subunits, that also bind to the OSM-3 motor but do not activate it during the transport back from the tip to the base. Assays as conducted in this thesis, but with the addition of other IFT-B subunits and/or e.g. phosphorylation could shed light on these questions.

We have also shown that the previously described OSM-3^{G444E} mutant is inherently active, which in this particular case is due to the size and charge of the introduced glutamic acid at the helix breaker position. This finding was based on comparative ATPase assays with the OSM-3^{G444Q} mutant, with introduced glutamine of similar size, but without the charge of the glutamic acid. This OSM-3^{G444Q} mutant, consequently, showed a significant reduction in activity in comparison to the OSM-3^{G444E} mutant. This hints towards a mechanism in which the respective mutations dissimilarly shift the balance from a folded and autoinhibited conformation towards an open and active state, instead of disabling the capability of the motor to fold at the helix breaker position altogether. Further assays, such as single molecule assays in a TIRF microscope or electron microscope (EM) could shed light on the folding of this motor and could help understand this crucial mechanism in more detail.

Finally, combining previously discussed findings, it would be particularly interesting to couple the OSM-3 homodimer with its partner in the intraflagellar transport, the KLP11/20/KAP heterotrimer, through the established dsDNA handle. The interplay between the OSM-3 and KLP11/20/KAP motor has been the focus of many research groups [147], and it has been proposed that the heterotrimeric KLP11/20/KAP functions as the loader at the base and consecutively navigates the IFT train through the structurally dense first zone of the cilium by so-called side-stepping on the filament tracks and thus avoiding any “roadblocks”. Subsequently, the OSM-3 motor, which is faster and does not do side-stepping, supposedly functions as the long-range transporter and gradually takes over the transport [193].

9 Discussion

Since it is possible to track individual head domains and every single resulting step at subpixel resolution using FIONA (Fluorescent Imaging using One Nanometer Accuracy) [65, 194], as described by Stepp *et al.* [195], one could determine in more detail how these two distinct motors influence each other in terms of velocity, but also regarding the proposed sidestepping of the KLP11/20/KAP motor. This might reveal more details about this coordinated transport.

10. Supplementary Information

10.1. SI Movies

SI Movie 1: Dephosphorylation inhibits processivity of the KIF3A/B/KAP motor protein. (Left panel) Full-length, fluorescently labelled KIF3A/B/KAP motors move processively after treatment with PKA. **(Right panel)** Full-length, fluorescently labelled KIF3A/B/KAP motors remain mostly stationary or show diffusion along the surface-fixed microtubule (not shown) after treatment with AP. Motors were labelled with Alexa-SNAP-647 and surface-fixed microtubule with Atto-488 (not shown).

SI Movie 2: Dephosphorylation inhibits processivity of the KIF3A/B motor protein. (Left panel) Full-length, fluorescently labelled KIF3A/B motors move processively after treatment with PKA. **(Right panel)** Full-length, fluorescently labelled KIF3A/B motors remain mostly stationary or showed diffusion along the surface-fixed microtubule after treatment with AP. Motors were labelled with Alexa-SNAP-647 and surface-fixed microtubule with Atto-488 (not shown).

SI Movie 3: Inhibition of the KIF3A/B motor is a direct effect of the treatment with the Antarctic Phosphatase enzyme. (First panel) Full-length, fluorescently labelled KIF3A/B motors remain mostly stationary or show diffusion along the surface-fixed microtubule (not shown) after treatment with AP. **(Second panel)** Full-length, fluorescently labelled KIF3A/B/KAP motors move processively after exposure to room temperature for 30 mins. **(Third panel)** Full-length, fluorescently labelled KIF3A/B/KAP motors move processively after exposure to AP enzyme without the required AP-buffer mix. **(Fourth panel)** Full-length, fluorescently labelled KIF3A/B/KAP motors move processively after exposure to the AP-buffer mix without the AP enzyme. **(Fifth panel)** Full-length, fluorescently labelled KIF3A/B/KAP motors move processively after exposure to PP2A phosphatase and respective buffer mix. Motors were labelled with Alexa-SNAP-647 and surface-fixed microtubule with Atto-488 (not shown).

SI Movie 4: The head-domains of KIF3A and KIF3B, as well as of OSM-3, but not of Kin-1 are affected by the Antarctic Phosphatase. (First panel) GFP-

tagged, dimerized head domains of KIF3A (KIF3AGCN4) show (upper panel) processivity after treatment with PKA and (lower panel) diffusive or stationary behavior after treatment with AP. **(Second panel)** GFP-tagged, dimerized head domains of KIF3B (KIF3BGCN4) show (upper panel) processivity after treatment with PKA and (lower panel) diffusive or stationary behavior after treatment with AP. **(Third panel)** GFP-tagged, dimerized head domains of OSM-3 (OSM3GCN4) show (upper panel) processivity after treatment with PKA and (lower panel) diffusive or stationary behavior after treatment with AP. **(Fourth panel)** GFP-tagged, dimerized head domains of Kin-1 (Kin1GCN4) show processivity after treatment with both (upper panel) PKA or (lower panel) AP.

SI Movie 5: KIF3A/B can bind the dsDNA handle. Full-length, fluorescently labelled KIF3A/B/KAP (**left panel**, 488, Alexa-SNAP-488) motors and bound dsDNA (**middle panel**, 633, Atto-633) show colocalized movement (**right panel**, merged) on unlabelled surface-fixed microtubule.

SI Movie 6: KIF3A/B can be linked via the dsDNA handle. Full-length, fluorescently labelled KIF3A/B/KAP (**first panel**, 488, Alexa-SNAP-488 and **second panel**, 555, Alexa-SNAP-555) motors are linked by dsDNA (**third panel**, 633, Atto-633) and show colocalized movement (**fourth panel**, merged) on unlabelled surface-fixed microtubule.

SI Movie 7: KIF3A/B motors need the dsDNA handle to show colocalized movement. Full-length, fluorescently labelled KIF3A/B/KAP (**first panel**, 488, Alexa-SNAP-488 and **second panel**, 555, Alexa-SNAP-555) motors do not show colocalized movement (**third panel**, merged) on unlabelled surface-fixed microtubule.

SI Movie 8: AzoMyoVin-1 specifically inhibits the Myosin-Va motor, just as MyoVin-1 does. Gliding assay with fluorescently labelled f-actin filaments (Atto-633) show loss of activity of the surface-fixed Myosin-Va motor after treatment with (**first panel**) MyoVin-1, as well as (**second panel**) AzoMyoVin-1. (**Third panel**) Treating the Myosin-Va motor with the same amount of DMSO as found in the AzoMyoVin-1 buffer show no effect to the motor's activity, when compared to (**fourth panel**) untreated motors. (**fifth panel**) Gliding assay with fluorescently

labelled microtubule (Atto-488) show activity of unlabelled, surface-fixed KIF3A/B motors after treatment with AzoMyoVin-1.

SI Movie 9: Exposure of UV-light to the AzoMyoVin-1 compound shows isomerization to the non-inhibiting form. (first panel) fluorescently labelled Myosin-Va/Melanophilin/Rab27a show processivity on surface-fixed unlabelled f-actin filaments. **(second panel)** Fluorescently labelled Myosin-Va/Melanophilin/Rab27a show no motility after treatment with 1 μ M of MyoVin-1. **(third panel)** Fluorescently labelled Myosin-Va/Melanophilin/Rab27a show the same inhibited motility after treatment with 2.5 μ M of AzoMyoVin-1 and exposure to natural light for 30 mins. **(third panel)** Fluorescently labelled Myosin-Va/Melanophilin/Rab27a show the significantly lowered number of processive motors after treatment with 2.5 μ M of AzoMyoVin-1 and exposure to natural light for 30 mins. **(fourth panel)** Treating the fluorescently labelled Myosin-Va/Melanophilin/Rab27a complex to again 2.5 μ M of AzoMyoVin-1, but exposing it to 360 nm light for 30 mins increases the number of processive motors noticeably. **(fifth panel)** Treating the fluorescently labelled Myosin-Va/Melanophilin/Rab27a complex with 50 μ M AzoMyoVin-1 and exposure to 360 nm light for 30 mins, shows the same complete inhibition of processivity as treatment with 1 μ M MyoVin-1 (second panel). All Motors were labelled with Alexa-SNAP-647.

10.2. Supplementary Figures

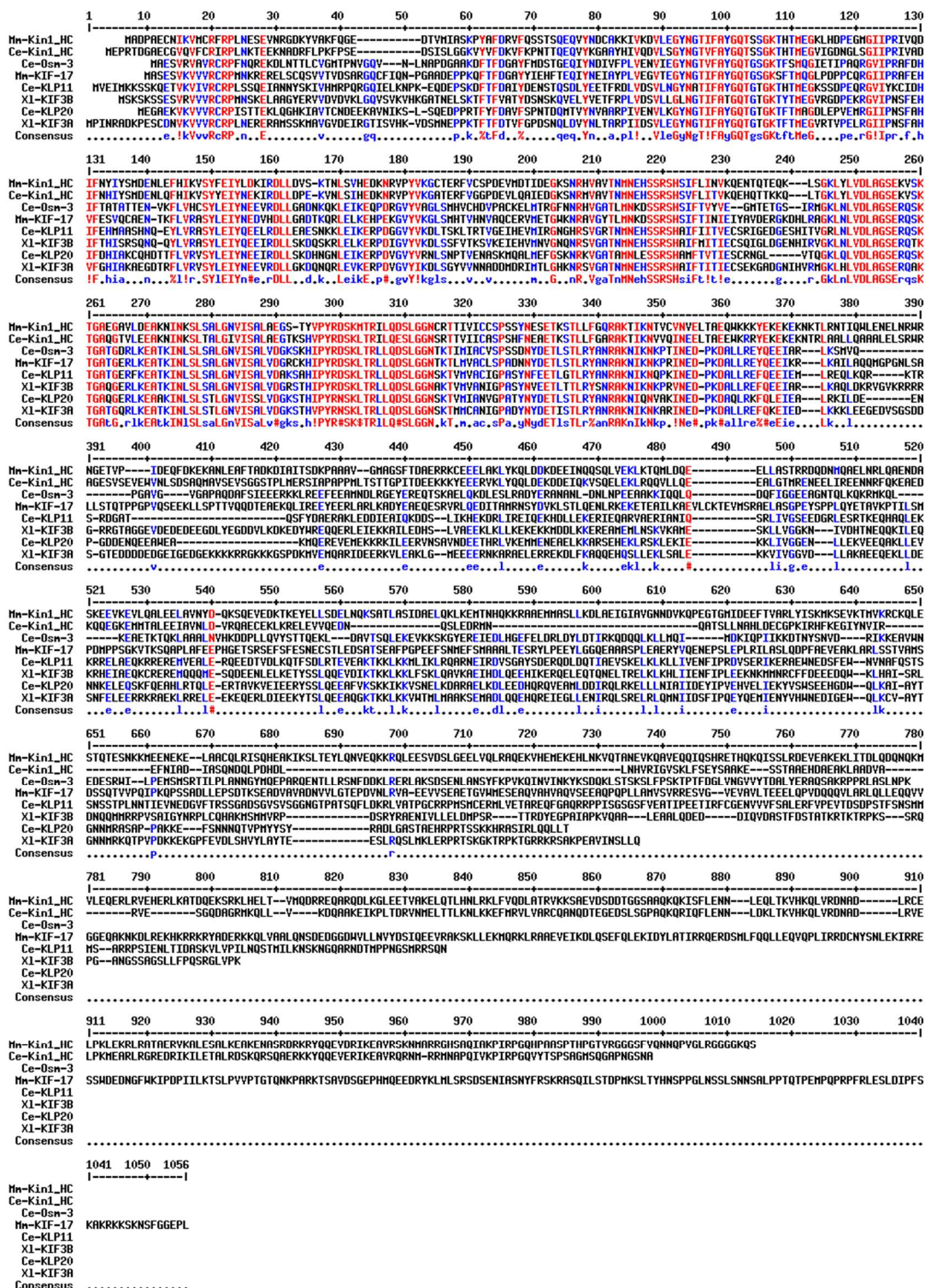


Figure S 1: Sequence alignments of full-length motors show conserved head domains and specific tail domains. (Mm) *M. musculus*, (Ce) *C. elegans*, (Xi) *X. laevis*, (HC) heavy chain, (red) >90% Consensus, (blue) >50% Consensus. [196]

10 Supplementary Information

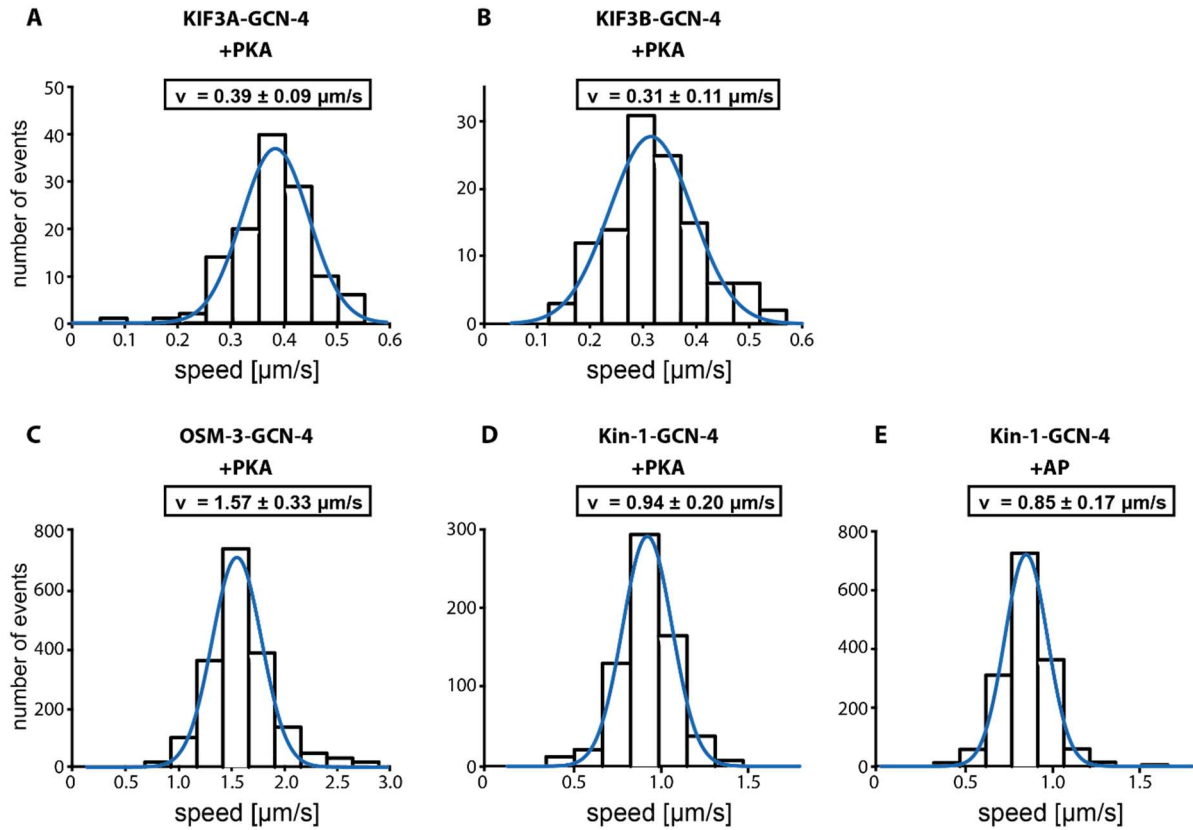


Figure S 2: Measured velocities of the processive head-domains of KIF3A, KIF3B, OSM-3, as well as Kin-1. The head domains of KIF3A, KIF3B, OSM-3 and Kin-1 were phosphorylated (+PKA) or dephosphorylated (+AP). Dephosphorylation turned the head domains of KIF3A, KIF3B and OSM-3 unprocessive. Velocities of the processive motor domains were measured. (A) KIF3A-GCN-4 + PKA, N = 123, (B) KIF3B-GCN-4 + PKA, N = 114, (C) OSM-3-GCN-4 + PKA, N = 1868, (D) Kin-1-GCN-4 + PKA, N = 675, (E) Kin-1-GCN-4 + AP, N = 1562. The velocity data was fit to a Gaussian (\pm width of distribution) distribution. Repeated two times.

10 Supplementary Information

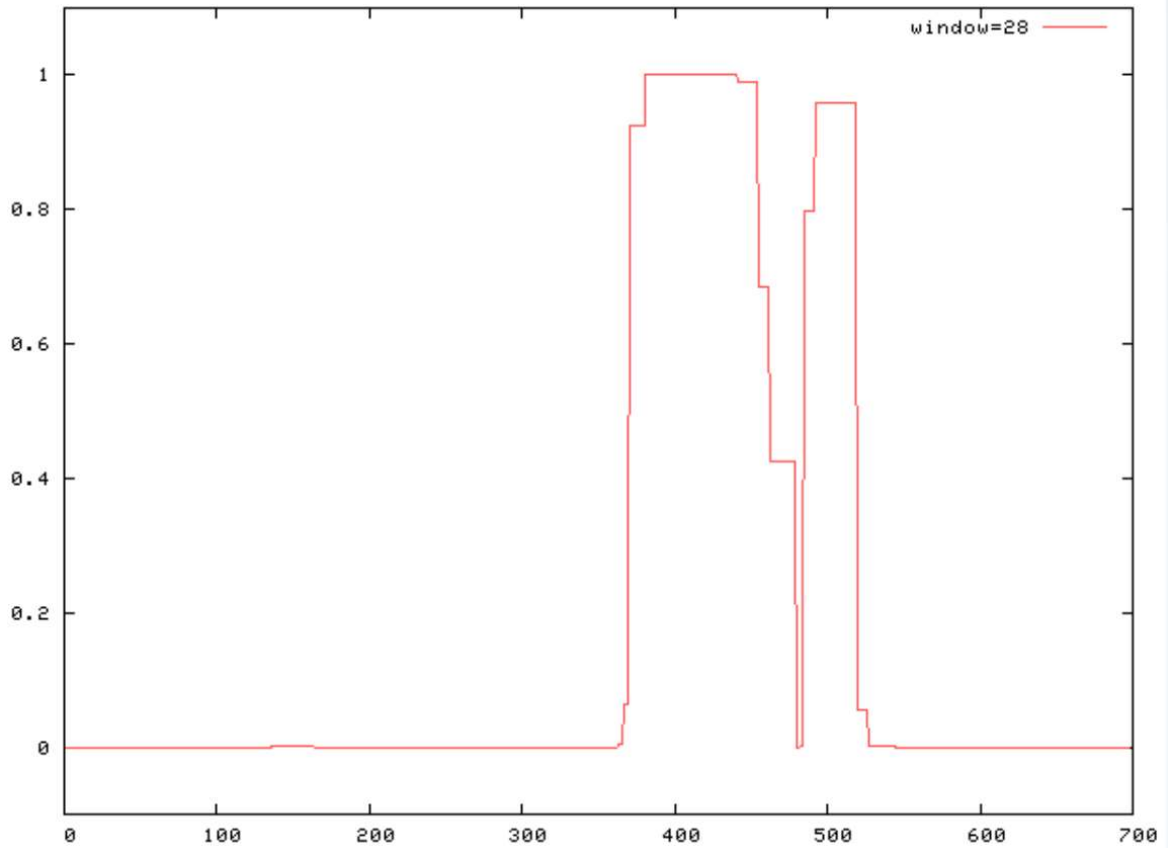


Figure S 3: The helix-breaker for OSM-3 is between position 428 and 442. Coil prediction for OSM-3 sequence missing P428 and F442 show no helix breaker position within the coiled-coiled stalk anymore [175]. Compare coil predictions for wild-type sequence Figure 40 A.

```

KIF3A-tail  FIPQEYQEMIEINYVHINEDIGEHQLKCYRYTGNNHRKQTPVPDKKEKGFPEVDLSHYVLYAYTEESLRQSLMKLERPRTSKGKTRPKTGRRKRSRKPPEAVINSLQ
KIF3B-tail  FIPLEEKRRKHMNRCCFFDEEEDQWKLHAI SRLDNQVMRRPVSRIIGYNRPLCQHRKMSHMYRPOSRYSRAENIVLLELDNMPSTRTRDYEGPRL-APKYQHALEHALQDEDDIQVDRSTFDSTATKRTKTRPK
Consensus  FIPqEeq#kie#r#chf#E#ed#WqLha!arldN#qrkrr#PYpaigenrP!cqdakhs#arp#er!Raenikler!rmpkrkTRdkeGra!aaKp#Rai#aalQ.....
KIF3A-tail
KIF3B-tail  SSRQPANGSSAGSLLFPQSRGLVPK
Consensus  .....

```

Figure S 4: Sequence alignment of the KIF3A and KIF3B random coil tail domains. Alignment of KIF3A and KIF3B sequences after the conserved FIP coiled-coil breaker (KIF3A-tail = KIF3A⁵⁹⁵⁻⁶⁹⁹ and KIF3B-tail = KIF3B⁵⁹⁰⁻⁷⁴⁴) shows no particularly conserved sequences, but a significant difference in length.

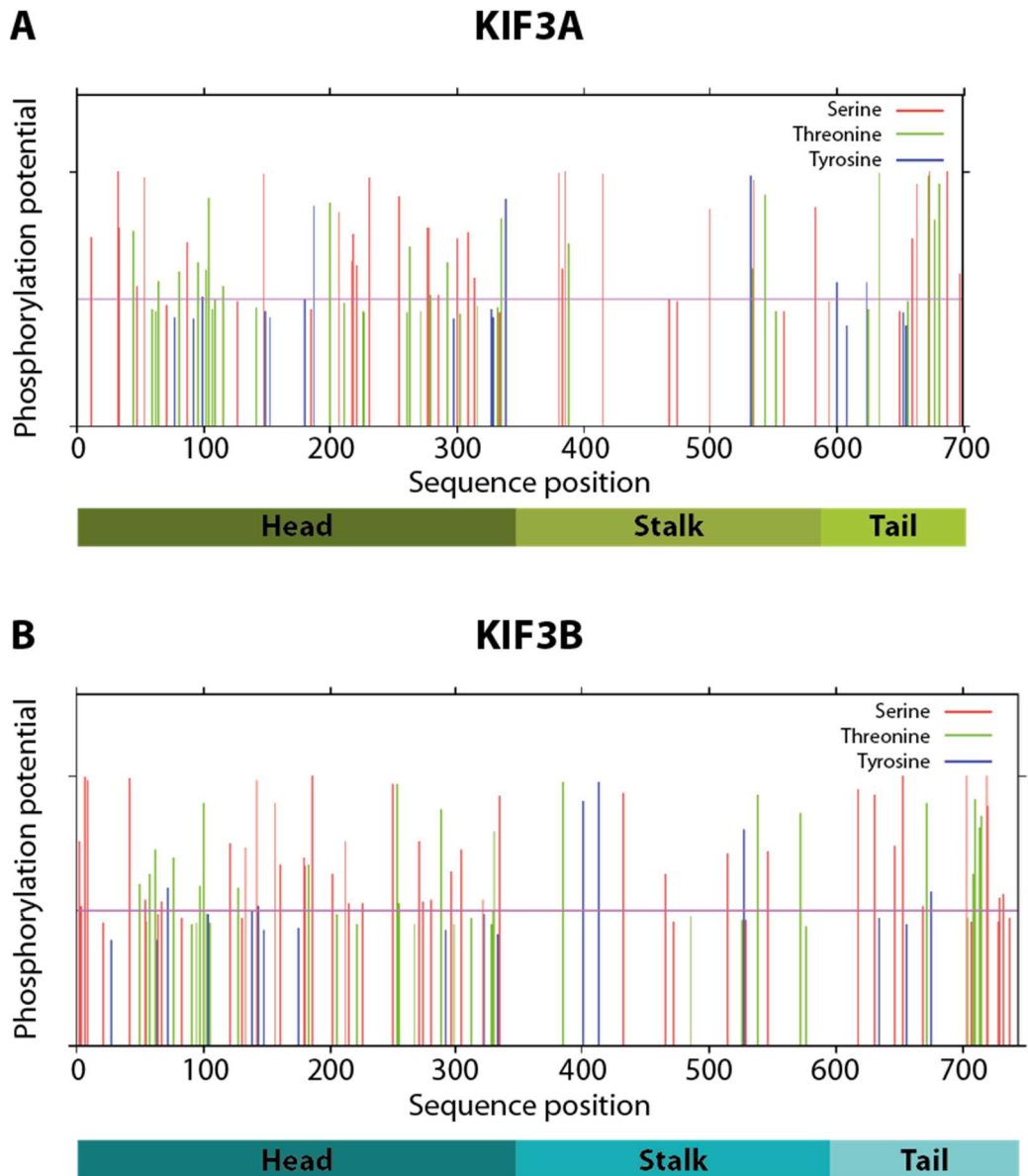


Figure S 5: **Predicted phosphorylation sites for full-length (A) KIF3A and (B) KIF3B show that the head domains of both subunits are likely target of phosphorylation.** Different domains of the respective motors are depicted underneath the Graph depicting predicted phosphorylation sites. Phosphorylation site predictions are taken from [171]

10.3. Abbreviations

a.m.	above mentioned
a.o.	amongst others
AP	Antartic phosphatase
ATP	Adenosine triphosphate
ATPase	Adenosine triphosphatase
bBSA	Biotinylated bovine serum albumin
BSA	Bovine serum albumin
<i>C. elegans</i>	<i>Caenorhabditis elegans</i>
cAMP	Cyclic adenosine monophosphate
C-terminal	Carboxy terminal
DMSO	Dimethyl sulfoxide
dsDNA	Double stranded DNA
<i>E. coli</i>	<i>Escherichia coli</i>
e.g.	exempli gratia, for example
EDTA	Ethylenediaminetetraacetic acid
EGTA	Ethylene-bis(oxyethylenitrilo)tetraacetic acid
f-actin	Filamentous actin
FBS	Fetal bovine serum
g-actin	Globular actin
GFP	Green fluorescent protein
GTPase	Guanosine triphosphatase
i.e.	id est, that is
IFT	Intraflagellar transport
KAc	Potassium acetate
krpm	Rounds per minute x1000
LB	Luria broth

10 Supplementary Information

Mlph	Melanophilin
MST	Microscale thermophoresis
MT	Microtubule
MyoVa	Myosin-Va
NAc	Sodium acetate
N-terminal	Amino terminal
OSM-3	Osmotic avoidance abnormal protein 3
PAGE	Polyacryl amide gel electrophoresis
PCR	Polymerase chain reaction
PIPES	Piperazine-1,4-bis(2-ethanesulfonic acid)
PKA	Protein kinase A
PP2A	protein phosphatase 2A
RT	room temperature
<i>S. frugiperda</i>	<i>Spodoptera frugiperda</i>
S.O.C.	Super optimal catabolite
SD	Standard deviation
SDS	Sodium dodecyl sulphate
TAE	Tris-acetate-EDTA
TEMED	N,N,N',N'-Tetramethylethylenediamine
TIRF	Total inner reflection fluorescence
<i>X. laevis</i>	<i>Xenopus Laevis</i> , African clawed frog
α-MSH	α -melanocyte-stimulating hormone

10.4. Sequences

Color-coded protein sequences of all constructs that are used in this study

X/KIF3A Flag

MPINRADKPESCDNVKVVVRCRPLNERERAMSSKMAVGVDEIRGTISVHKVDSMNEPPKTFTFDT
VFGPDSNQLDVYNLTARPIIDSVLEGYNGTIFAYGQTGTGKTFTMEGVRTVPELRGIIPNSFAHVFG
HIAKAEGDTRFLVRVSYLEIYNEEVRDLLGKDQNRLEVKERPVDVGVYIKDLSGYVVNNADDMDRI
MTLGHKNRSVGATNMNEHSSRSHAIFTITIECSEKGADGNIHVRMGKHLVLDLAGSERQAKTGAT
GQRLKEATKINLSLSTLGNVISALVDGKSTHVPYRNSKLTRLLQDSLGGNSKTMMCANIGPADYNY
DETISTLRYANRAKNIKNKARINEDPKDALLREFQKEIEDLKKKLEEGEDVSGSDDSGTEDDDDED

10 Supplementary Information

EAAQGKTKKLLKVVWTMLMAAKSEMADLQQEHQREIEGLLENIRQLSRELRLQMNIIDSFIPGGDYK
DDDDK

X/KIF3A GCN4 sfGFP Flag

MPINRADKPESCDNVKVVVRCRPLNERERAMSSKMAVGVDIEIRGTISVHKVDSMNEPPKTFTFDT
VFGPDSNQLDVYNLTARPIIDSVLENGTIFAYGQTGTGKFTMEGVRTVPELGIIPNSFAHVFG
HIAKAEGDTRFLVRVSYLEIYNNEVRDLLGKDQNRLEVKERPDVGVYIKDLSGYVNNADDMDRI
MTLGHNRSVSGATNMNEHSSRSHAIFTITIECSEKADGNIHV RMGKHLVLDLAGSERQAKTGAT
GQRLKEATKINLSLSTLGNVISALVDGKSTHVPYRNSKLTRLLQDSLGGNSKTMMCANIGPADYNY
DETISTLRYANRAKNIKARINEDPKDALLREFQKEI **GAPRMKQLEDKVEELLSKNYHLENEVARL**
KKLVGEGGSKGEELFTGVVPILVELDGDVNGHKFSVRGEGEGDATNGKLTCLKICTTGKLPVWP
TLVTTLTYGVCVFARYPDHMKQHDFFKSAMPEGYVQERTISFKDDGTYKTRAEVKFEGDTLVNRI
ELKGIDFKEDGNILGHKLEYNFNHNVYITADKQKNGIKANFKIRHNVEDGSVQLADHYQQNTPIGD
GPVLLPDNHVLTQSVLSKDPNEKRDHMLLEFVTAAGITHGMDELKGGDYKDDDDK

X/KIF3A(482-699) Flag

MGVDLLAKAEQEKLDESNEFEERRKRAEKLRRLEEEKEQERLDIEEKYTSLQEEAQGKTKKLL
KVWTMLMAAKSEMADLQQEHQREIEGLLENIRQLSRELRLQMNIIDSFIPQEQEMIENYVHWNE
IGEWQLKCVAYTGNMNRKQTPVPDKKEKGPFEVDLSHVYLAYTEESLRQSLMKLERPRTSKGKT
RPKTGRRKRSAPPEAVINSLLQGGDYKDDDDK

X/KIF3B His

MSKSKSSESVRVVRCRPMNSKELAAGYERVVDVDVVLGQVSVKVHKGATNELSKTFTFDIYDS
NSKQVELYDETFRPLVDSVLLGFNGTIFAYGQTGTGKTYTMEGVRGDPEKRGVIPNSFEHIFTHIS
RSQNQQYLVRASYLEIYQEEIRDLLSKDQSKRLELKERPDTGVYVKDLSSFVTKSVKEIEHVMNVG
NQNRVSGATNMNEHSSRSHAIFMITIECSQIGLDGENHIRVGLNLDLAGSERQTKTGAQGERLK
EATKINLSLSALGNVISALVDGRSTHIPPYRDSKLTRLLQDSLGGNAKTMVANIGPASYNVEETLTL
RYSNRAKNIKPRVNEPKDALLREFQEEIARLKAQLDKRVGVKRRRRRGRRTAGGEVDEDED
EEGDLYEGDDVLKDKEDYWREQQERLEIEKKAILEDHSLVAEEKLKLKEKEKMDLKKERAM
EMLNSKVKAMESKLLVGGKNIVDHTNEQQKILEQKRHEIAEQKCREREMQQMESQDEENLELK
ETYSSLQQEVDIKTKKLLKLFSLQAVKAEIHDLQEEHIKERQELETQNELTRELKHLIENFIPL
EEKNKMMNRCFFDEEEDQWKLHAISRLDNQQMMRRPVSAIGYNRPLCQHAKMSMMVRPDSRY
RAENIVLLELDMPSTRTRDYEGPAIAPKVQAALAEALQDEDDIQVDASTFDSTATKRTKTRPKSSR
QPGANGSSAGSLLFPQSRGLVPGGGHHHHHH

X/KIF3B Halo His

MSKSKSSESVRVVRCRPMNSKELAAGYERVVDVDVVLGQVSVKVHKGATNELSKTFTFDIYDS
NSKQVELYDETFRPLVDSVLLGFNGTIFAYGQTGTGKTYTMEGVRGDPEKRGVIPNSFEHIFTHIS
RSQNQQYLVRASYLEIYQEEIRDLLSKDQSKRLELKERPDTGVYVKDLSSFVTKSVKEIEHVMNVG
NQNRVSGATNMNEHSSRSHAIFMITIECSQIGLDGENHIRVGLNLDLAGSERQTKTGAQGERLK
EATKINLSLSALGNVISALVDGRSTHIPPYRDSKLTRLLQDSLGGNAKTMVANIGPASYNVEETLTL
RYSNRAKNIKPRVNEPKDALLREFQEEIARLKAQLDKRVGVKRRRRRGRRTAGGEVDEDED
EEGDLYEGDDVLKDKEDYWREQQERLEIEKKAILEDHSLVAEEKLKLKEKEKMDLKKERAM
EMLNSKVKAMESKLLVGGKNIVDHTNEQQKILEQKRHEIAEQKCREREMQQMESQDEENLELK
ETYSSLQQEVDIKTKKLLKLFSLQAVKAEIHDLQEEHIKERQELETQNELTRELKHLIENFIPL
EEKNKMMNRCFFDEEEDQWKLHAISRLDNQQMMRRPVSAIGYNRPLCQHAKMSMMVRPDSRY
RAENIVLLELDMPSTRTRDYEGPAIAPKVQAALAEALQDEDDIQVDASTFDSTATKRTKTRPKSSR
QPGANGSSAGSLLFPQSRGLVPGGG**MEIGTGFPDPHYVEVLGERMHYVDVGPDPVFLHG**
NPTSSYVWRNIIPHVAPTHRCIAPDLIGMGKSDKPDLYFFDDHVRFMDFIALGLEEVVLIHDW

10 Supplementary Information

GSALGFHWAKRNPVRVKGIAMFIRPIPTWDEWPEFARETFQAFRTTVDVGRKLIIDQNVFIEGTLP
MGVVRPLTEVEMDHYREPFLNPVDREPLWRFPNELPIAGEPANIVALVEEYMDWLHQSPVKLLF
WGTPGVLIPPAEAARLAKSLPNCKAVDIGPGLNLLQEDNPDIGSEIARWLSTLEISHHHHHH

X/KIF3B(1-592) His

MSKSKSSESVRVVVRCRPMNSKELAAGYERVVDVDVVLGQVSVKVKHGATNELSKTFTFDIYDS
NSKQVELYDETFRPLVDSVLLGFNGTIFAYGQTGTGKTYTMEGVVRGDPEKRGVIPNSFEHIFTHIS
RSQNQQYLVRASYLEIYQEEIRDLLSKDQSKRLELKERPDTGVYVKDLSSFVTKSVKEIEHVMNVG
NQNRSVGATNMNEHSSRSHAIFMITIECSQIGLDGENHIRVGKLNLDLAGSERQTKTGAQGERLK
EATKINLSLSALGNVISALVDGRSTHIPPYRDSKLTRLLQDSLGGNAKTMVANIGPASYNVEETLTL
RYSNRAKNIKPKRVNEDPKDALLREFQEEIARLKAQLDKRVGVKRRRRRGRRTAGGEVDEDED
EEGDLYEGDDVLKDKEDYWREQQERLEIEKKAILEDHSLVAEEKLKLKEKEKMMDDLKKERAM
EMLNSKVKAMESKLLVGGKNIVDHTNEQQKILEQKRHEIAEQKCREREMQQQMESQDEENLELK
ETYSSLQQEVDIKTKKLKLFKSLQAVKAEIHDLQEEHIKERQELETQNELTRELKHLIENFIPIG
GHHHHH

X/KIF3B(1-723) His

MSKSKSSESVRVVVRCRPMNSKELAAGYERVVDVDVVLGQVSVKVKHGATNELSKTFTFDIYDS
NSKQVELYDETFRPLVDSVLLGFNGTIFAYGQTGTGKTYTMEGVVRGDPEKRGVIPNSFEHIFTHIS
RSQNQQYLVRASYLEIYQEEIRDLLSKDQSKRLELKERPDTGVYVKDLSSFVTKSVKEIEHVMNVG
NQNRSVGATNMNEHSSRSHAIFMITIECSQIGLDGENHIRVGKLNLDLAGSERQTKTGAQGERLK
EATKINLSLSALGNVISALVDGRSTHIPPYRDSKLTRLLQDSLGGNAKTMVANIGPASYNVEETLTL
RYSNRAKNIKPKRVNEDPKDALLREFQEEIARLKAQLDKRVGVKRRRRRGRRTAGGEVDEDED
EEGDLYEGDDVLKDKEDYWREQQERLEIEKKAILEDHSLVAEEKLKLKEKEKMMDDLKKERAM
EMLNSKVKAMESKLLVGGKNIVDHTNEQQKILEQKRHEIAEQKCREREMQQQMESQDEENLELK
ETYSSLQQEVDIKTKKLKLFKSLQAVKAEIHDLQEEHIKERQELETQNELTRELKHLIENFIPL
EENKMMNRCFFDEEEDQWKLHAISRLDNQQMMRRPVSAIGYNRPLCQHAKMSMMVRPDSRY
RAENIVLLELDMPSTRTRDYEGPAIAPKVQAALQDEDDIQVDASTFDSTATKRTKTRPKSSR
QPGGHHHHH

X/KIF3B GCN4 sfGFP Flag

MSKSKSSESVRVVVRCRPMNSKELAAGYERVVDVDVVLGQVSVKVKHGATNELSKTFTFDIYDS
NSKQVELYDETFRPLVDSVLLGFNGTIFAYGQTGTGKTYTMEGVVRGDPEKRGVIPNSFEHIFTHIS
RSQNQQYLVRASYLEIYQEEIRDLLSKDQSKRLELKERPDTGVYVKDLSSFVTKSVKEIEHVMNVG
NQNRSVGATNMNEHSSRSHAIFMITIECSQIGLDGENHIRVGKLNLDLAGSERQTKTGAQGERLK
EATKINLSLSALGNVISALVDGRSTHIPPYRDSKLTRLLQDSLGGNAKTMVANIGPASYNVEETLTL
RYSNRAKNIKPKRVNEDPKDALLREFQEEI **GAPRMKQLEDKVEELLSKNYHLENEVARLKKLVGE**
GGSKGEELFTGVVPILVELDGDVNGHKFSVRGEGEGDATNGKLTLCFICTTGKLPVPWPTLVTTLT
YGVQCFARYPDHMKQHDFFKSAMPEGYVQERTISFKDDGTYKTRAEVVFEGDTLVNRIELKGIDF
KEDGNILGHKLEYNFNHNYYITADKQKNGIKANFKIRHNVEDGSVQLADHYQQNTPIGDGPVLLP
DNHYLSTQSVLSKDPNEKRDHMLLEFVTAAGITHGMDELYKGGDYKDDDDK

X/KIF3B(477-744) FLAG

MGKNIVDHTNEQQKILEQKRHEIAEQKCREREMQQQMESQDEENLELKETYSSLQQEVDIKTKKL
KKLFSKLQAVKAEIHDLQEEHIKERQELETQNELTRELKHLIENFIPL EENKMMNRCFFDEE
DQWKLHAISRLDNQQMMRRPVSAIGYNRPLCQHAKMSMMVRPDSRYRAENIVLLELDMPSTRTR
DYEGPAIAPKVQAALQDEDDIQVDASTFDSTATKRTKTRPKSSRQPGANGSSAGSLLFPQS
RGLVPKGGDYKDDDDK

X/KAP SNAP His

MQSEDARFLKRKVKKEGNIDVHPTEKALVVHYEVEATILGERGDTMLGERKECQKIIRLKSLNANTDI
 SSLARKVVDECKLIHPSKLAEEVEQLLYLQNRDGLPSKAEEKKEKMNKPRDPPPFEGMEIDEVA
 NINDMDEYIELLYENIADKVRGSALILQLARNPDNLEELLNETALGALARVLRDWDKQSVELATNII
 YIFFCFSSFSQFHGLITHYKIGALCMNIIDHELKRHDLWQEELSKKKRAVDDADNQNMMKKEYEKT
 YKKYQGLLVKQEQLLRVALYLLNLAEDTRTELKMRNKNIVHMLVKALDRDNFELLILVVSFLKLSI
 FLENKNDMAEMDIEKLSKLVPCHEHEDLLNISLRLLLNLSFDTGLRNKMVQVGLLPKLTVLLDNENY
 KQIVMCILYHISMDDRFSMFAITDCIPQLMKMLFESSEERVLELISFCINLAANKRNAQLICEGN
 GLKMLMKKALKFKDPLLMKIRNISQHDGQTKNLFIDYVVDLAAQITNDEEEEFVIECLGTLANLTIT
 DLDWELVLKEYKLVYKDKLKPGLAEDDLVLEVVIMIGTVSTDDSCAALLAKSGMIPALIELLNAQQ
 EDDEFVQCQIVVYFYQMVFHQATRDVIIKDTQAPAYLIDLMDKNAEIRKVCNTLDIAEYDEEWAK
 KIQSEKFRWHNSQWLEMVESRQLDENEQYLYGDEPIEPIYIHERDILERPDLYYSAEGLIPSDGVVS
 PDFNFHFHQNDLIGQHSFNTGMSSEDFGQGHAGMPGRPTTAYGYRPEDEPYYYGFGARGAPGG
 SGGSDKDCCEMKRITLDSPLGKLELSCCEQLHEIKLLGKGTSAADAVEVPAPA AVLGGPEPLMQA
 TAWLNAYFHQPEAIEEFVVPALHHPVFFQESFTRQVLWKLKVVKFGEVISYQQLAALAGNPAATA
 AVKTALSGNPVPIIPCHRVSSSGAVGGYEGGLAVKEWLLAHEGHRLGKPGGLGGHHHHHH

X/p150^{glued} Halo Flag

MSVEATGKPLKVGSRVEVIGKGYRGTVAAYVATLGFATGKWWGVILDDSKGKNDGTVQGRRYFTC
 EENHGIFVRQSQIQVIEDGADTTSPETPEPTASKGLKDKVMETPKSSKLPTRPSSSAASSGTASAS
 CGEISSSEPSTPAQTPLAAPIIPSPSSAITSPVAPLPGGPSKEEENLRAQVKDLEEKLETLMKRA
 EDKAKLKEMEKSLLQLEQVQEWKSKMQEQQADIQRQLKEAKKEAKEALEAKERYMEEMADTAD
 AIEMATLDKEMAEERAESLQQEVDTLKDVEEHKIDLEILKHEIEEKGS DGAASSYQVKQLEEQNA
 RLKEALVRMRDLSASEKQEHKVKQKMEKKNTELDTLRQQKEKLQEEASHMEKTIDELKEQVDA
 LGAEEMVETLAERNLDLEEKVRELRETVSDLEAINEMNDELQENARETELELREQLDMAGARVRE
 AEKRVEAAQETVADYQQTIKKYRDLTAHLQEVNSELRNQQEASVEKEQQSPPEMDFKIKFAETK
 AHAKAIEMELRKMEVTQANRHVSLTFSMPDSFLRHGGDHDCILVLLIPRLICKAELISKQAQEK
 ELSEVGEQKSGMRGAVGEQMSFAAGLVYSLTLLQATLHKYEQALDKCSVEVYKKGMLYPMSV
 HERSLDFLIELLHKDQLDET VNV EPLTKAIKYYQHLYSIHLADQAEECTMQLSDHIKFTQSALDCMG
 VEVSRLRAFLHAGQESSDFAILLKDLETSCSDIRQFCKIRRRMPGTEAAGIPAALGFGQQVCETLL
 DCRKYLKCVAVFQEVAAAGAQMIAPMGENEGLQALKLEDVAFKATEQIYGTGKSNPYECLRQSC
 SVVIATMNKMATAMQEGEYDAEKPQSKSPPPVEQRAALRAEITDAEGLGLKLEDRETVIKELKKS
 LKIKGEELSEANVRLSLEKLDASKEADDRVEKIQTKLEETQTVLKKKEKEFEETMDALQADIDQ
 LESEKAELRQRLNNQSKRTIEGLRGVPASGVASIVSGLAGGVSSGQSLINGS GPVQVKDSPLLLQ
 QIDALRLSMKHLKHENKLAHQIKTDLSSLPALHVPKLTLPKDRQKEEAMSGTLRYKTSQLLDAL
 QQMSANAKVVDITHKKAGNPAALQLEQTARLKSLSDTIDKLNEMVMKETVSQCPGANVPTDFATF
 PSTDFIKAKEEKEDTVYIGKVTLSQCPGQGIHKLVLTPPEQLHELHERLICGAPGGGSGGSMEIG
 TGFPPDPHYVEVLGERMHYVDVGPDRGTPVFLHGNPTSSYVWRNIIPHVAPTHRCIAPDLIGMG
 KSDKPDLGYFFDDHVRFMDFIAELGLEEVVLIHDWGSALGFHWAKRNPVVKGI AFMEFIRPIP
 TWDEWPEFARETFQAFRTTDVGRKLIIDQNVFIEGTLPMGVVRPLTEVEMDHYREPFLNPVDREP
 LWRFPNELPIAGEPANIVALVEEYMDWLHQSPVPKLLFWGTPGVLPVPPAEARLAKSLPNCKAVDI
 GPGLNLLQEDNPD LIGSEIARWLSTLEISGGDYKDDDDK

X/p150^{glued}(1-559) Halo Flag

MSVEATGKPLKVGSRVEVIGKGYRGTVAAYVATLGFATGKWWGVILDDSKGKNDGTVQGRRYFTC
 EENHGIFVRQSQIQVIEDGADTTSPETPEPTASKGLKDKVMETPKSSKLPTRPSSSAASSGTASAS
 CGEISSSEPSTPAQTPLAAPIIPSPSSAITSPVAPLPGGPSKEEENLRAQVKDLEEKLETLMKRA
 EDKAKLKEMEKSLLQLEQVQEWKSKMQEQQADIQRQLKEAKKEAKEALEAKERYMEEMADTAD
 AIEMATLDKEMAEERAESLQQEVDTLKDVEEHKIDLEILKHEIEEKGS DGAASSYQVKQLEEQNA
 RLKEALVRMRDLSASEKQEHKVKQKMEKKNTELDTLRQQKEKLQEEASHMEKTIDELKEQVDA
 LGAEEMVETLAERNLDLEEKVRELRETVSDLEAINEMNDELQENARETELELREQLDMAGARVRE

10 Supplementary Information

AEKRVEAAQETVADYQQTIKKYRDLTAHLQEVNSELRNQQEASVEKEQQPSPPEMDFKIKFAETK
AHAKAIEMELRKMVEVTQANRHVSLTFSMPDSFLRHGGGAPGGGSGGSMEIGTGFPDPHYVEV
LGERMHYVDVGPDRDGTPLVFLHGNPTSSYVWRNIIPHVAPTHRCIAPDLIGMGKSDKPDLYFFD
DHVRFMDAFIEALGLEEVVLIHDWGSALGFHWAKRNPERVKGIAFMFIRPIPTWDEWPEFARET
FQAFRTTDVGRKLIIDQNVFIEGTLPNGVVRPLTEVEMDHYREPFLNPVDREPLWRFPNELPIAGE
PANIVALVEEYMDWLHQSPVPKLLFWGTPGVLIPPAEAARLAKSLPNCKAVDIGPGLNLLQEDNPD
LIGSEIARWLSTLEISGGDYKDDDDK

X/p150^{glued}(1-311) Halo Flag

MSVEATGKPLKVGSRVEVIGKGYRGTVAIVGATLFATGKWWGVILDDSKGKNDGTVQGRRYFTC
EENHGIFVRQSQIQVIEDGADTTSPETPEPTASKGLKDKVMEETPKSSKLPTRPSSSAASSGTASAS
CGEISSSEPSTPAQTPLAAPIIPSPSSAITSPVAPLPGGPSKEEENLRAQVKDLEEKLETLMKRA
EDKAKLKEMEKSKLQLEQVQEWKSKMQEQQADIQRQLKEAKKEAKEALEAKERYMEEMADTAD
AIEMATLDKEMAEERAESLQQEVDTLKDKVEEHKIDLEILKHEIEEKGSDDGAPGGGSGGSMEIGT
GFPDPHYVEVLGERMHYVDVGPDRDGTPLVFLHGNPTSSYVWRNIIPHVAPTHRCIAPDLIGMGK
SDKPDLYFFDDHVRFMDAFIEALGLEEVVLIHDWGSALGFHWAKRNPERVKGIAFMFIRPIPT
WDEWPEFARETFQAFRTTDVGRKLIIDQNVFIEGTLPNGVVRPLTEVEMDHYREPFLNPVDREPL
WRFPNELPIAGEPANIVALVEEYMDWLHQSPVPKLLFWGTPGVLIPPAEAARLAKSLPNCKAVDIG
PGLNLLQEDNPDIGSEIARWLSTLEISGGDYKDDDDK

X/Rab27a^{Q78L} Halo His

MSDGDYDYLIKFLALGDSGVGKTSFLYQYTDGKFNSKFITTVGIDFREKRWVYRSNGPDGNTGRG
QRIHLQLWDTAGLERFRSLTFAFRDAMGFLLLFDLTSEQSFLNVRNWMSQLQVHAYCENPDIVL
CGNKSDLDDQRAVKEEEAKEFAEKYGIPIYFETSAANGTNVNKAVDTLLDLIMKRMERCVDKSWIP
QGVVQSNHGSSTEQLTEEKDKGKCGGAPGGGSGGSMEIGTGFPDPHYVEVLGERMHYVDV
GPRDGTPLVFLHGNPTSSYVWRNIIPHVAPTHRCIAPDLIGMGKSDKPDLYFFDDHVRFMDAFIE
ALGLEEVVLIHDWGSALGFHWAKRNPERVKGIAFMFIRPIPTWDEWPEFARETFQAFRTTDVG
RKLIIIDQNVFIEGTLPNGVVRPLTEVEMDHYREPFLNPVDREPLWRFPNELPIAGEPANIVALVEEY
MDWLHQSPVPKLLFWGTPGVLIPPAEAARLAKSLPNCKAVDIGPGLNLLQEDNPDIGSEIARWLS
TLEISGGHHHHHH

XtMelanophilin Flag

MGKKLDLSKLSSEEAHVVDVQRDINLRKIEEERIEDLKEKVEKESKRELLSNQSHLNETHCMH
CLQPFQFLINSKRQCKDCQFHVCKNCSRYNKKELGWVCDSCRVDRLVKVGSGLDWYYDHVRSRF
KRFGSAKVMRSLYMRHQSDARGASGLQNKVYSLPDINREYLRQARAGMFHDEDEDLIDSAEAQR
YNMMRKTTRKLSVHPYDFDMDSEYSTQSRQSMQLSPTLEQDVFKSF SERPSTGRDATSQKES
LIAEADLASMFFHILQEQQNAASPEQEFSTEVRILT VNSRRLSLENTRRPKLPFLTESQISNHFPDP
QLTRTRYLPKGSPLAPKGSQYSGDMDTSDDEEGAIPKVP PRRRRSRASSQENVHHS GGQISDLN
KRMSTIERMLNRLEERLSVNSDESTGPGVHTDADIEEETLKRKLGELASNISDKGGSSDEEKISKP
KSSHKEPQT TETQKVYMAAEKAYTLDKNLRDLEE HARQSGTTDSELSELEVSVASAIAQVQQTES
EVSDIESRIAALSAAGMTVSPVDKAKRKSSSRVFAPAISRSTEPFQESTPDMYSMSSPSDAKILAM
QQALRKKFNIDPDAIDL PVEKSALYRGS LTQRNPNGKNRKADRIFSKPIVNQRGGDYKDDDDK

Flag SNAP X/Myosin-Va

MDYKDDDDKGGDKDCEMKRTTLDSP LGKLELSGCEQGLHEIKLLGKGTSAADAVEVPAPAAVLG
GPEPLMQATAWLNAYFHQPEAIEEFPVPALHHPVFQQESFTRQVLWKLKVVKFGVISYQQLAA
LAGNPAATAAVKTALSGNPVPIIPCHRVS SSSGAVGGYEGGLAVKEWLLAHEGHRLGKPLGGA
PMENNLDFAYVTHARVWIPDPEEVWKS AEMLKDYKPGDTVLRRLLEEGTDLEYRLDAKTKELPPL
RNPDILVGENDLTALSYLHEPAVLHNLKVR FIDSKLIYTYCGIVLVAINPYEQLPIYGTDIINAYSGQN
MGDMDPHIFAVAE EAYKQMARDERNQSIIVSGESGAGKT VSAKYAMRYFATVSGSASETNVEEK

10 Supplementary Information

VLASNPIMESIGNAKTTRNDNSSRF GK YIEIGFDKRYRILGAHMRTYLLEKSRVVFQAE EERNYHIF
YQLCASASLPEFKMLRLGTANDFHYTKQGGSPVIDGVDDQKEMRNTRQACTLLGIGESYQMGIFR
ILAAIHLGNVEFKSRSDSCLIPPKHVPLTIFCDLMGV DYEEMSHWLCHRKLVTAAETYIKPISRLQ
ATNARDALAKHIYAFLFNWIVCHVNKALLSSTKQNSFIGVLDIYGFETFEINSFEQFCINYANEKLQQ
QFNLHVFKLEQEEYMKEQIPWTLIDFYDNQPCINLIEAKMGILDLLDEECKMPKGS DSTWAQKLYN
THLKKCALFEKPRLSNVAFIHKHFADKVEYQCDGFLEKNKDTVFEEQIKVLKASKFTLLTELFQDEER
ILSPTSSAPPSGR TLLSRTSLRSLKPKPDQTSKEHKKT VGHQFRNSLHLLMETLNATTPHYVRCVK
PNDFKYPFTFDSKRAVQQLRACGVLETIRISAAGFPSRWTYQE FFSRYRVLMKQKDVLSDWKQTC
RNVLEKLILDKDKYQFGKTKIFFRAGQVAYLEKIRADKL RMACIRIQKTIRGWLLRKKYL RMRKAAITI
QRYVRGBYQARCYAQFLRRTRAAIIIQKFQRMVVRQKYRHIQSFTLALQSYLRGYAARKRYQEILR
AHKATIIQKHVRGWLARV TYKRNL SAIVYLQCRYRRMMAKRELK KLIKIEARSVEHFKKNVGMENK
IMQLQCKVNDQNKDNKSLLERLTHLEVTYNADKDKLRNDVDRLRHFE EEAKNAANRMVSLQDELA
RLRKELLQTQTEKNNIKERAKEYQTETDRLVAELREQNALLKTEKEKLNLLIQEQARKMTEDMEKKI
IEETKQLELELNDERLRYQNLLEYSRLEERYDDLKDEMNTMSPPKPGHKRTDSTHSSNESEYTF
SSEITESEDFPYRNEEPADRKTPLDMSLFLKQKRVKELEQEKQLMQDDLDKKEEQIIRAKILEEAK
TPTRGTELEYESLKRQELESENK KLNELNELRKAITEKASPDAGPGGNVYHILLEQMTSVSEEL
DVRKEEVLILRSQ LVSQMEAI PHKDTMTDSMVLSEDVQKMKDKREIAQAYTGMKETNRNLPPDFQ
DLNEDGELWLVDGLKQANRVLESQ LQSQKAFENEVEALRGEIQALKEENNRQQQLLAQNLQL
PPEARIEASLQHEITRLTNENLFFEELYADEPMKYQSYRISLYRRIIDLMEQLEKQDKTVRKLKQKLK
VFAKKIGELEVGMENVSPGQIVDEPIRPVNIPRKEKDFQGMLEYKKEDELKLVKNLILELKP RQVA
VNLIPLPAYILFMCLRHADYLNDDQKVRSLTSTINGVKKILK KRGGDFETVSFWLSNTCRFLHCL
KQYSGEEGFMKHNSPRQNEHCLTNFDLAEYRQVLSDLAIQIYQQLVRVLENILQPMIVSGMLEHET
IQGVSGVKPTGLRKRTSSIADEGTYTLDSIVRQLNTFHSIMCQHGMPELIKQVVKQMFYIIGAVTL
NNLLL RKMCSWSKGMQIRYNVSQLEEWLRDKNLMNSSAKETLEPLIQAAQLLQVKKKTD EDAEA
ICSMCNALTTAQIVKVLNLYTPVNEFEERV LVSFIRNIQMRFRDRKDS PQLLMDAKHIFPVTFPFNP
SSLALETIQIPGSLGLGFLTRVGP

CeOSM-3 Flag

MAESVRVAVRCRPFNQREKDLNTTLCVGMTPNVGQVNLNAPDGA AKDFTFDGAYFMDSTGEQIY
NDIVFPLVENVIEGYNGTVFAYGQTGSGKTF SMQGIETIPAQRGVIPRAFDHIFTATATTENVKFLV
HCSYLEIYN EEEVRDLLGADNKQKLEIKEQPDRGVYVAGLSMHVCHDVPACKELMTRGFNNRHVG
ATLMNKDSSRSHSIFTVYVEGMTETGSIRMGKLNLDLAGSERQSKTGATGDRLKEATKINLSLSA
LGNVISALVDGKSKHIPYRDSKLTRLLQDSLGGNTKTIMIACVSPSSDNYDET LSTLRYANRAKNIK
NKPTINEDPKDALLREYQEEIARLKS MVQPGAVGVGAPAQDAFSIEEERK KLR EEFEEAMNDLRG
EYEREQTSKAELQKDLES LRADYERANANLDNLNPEEAAKKIQQLQDQFIGGEEAGNTQLKQKRM
KQLKEAETKTQKLAAALNVHKDDPLLQVYSTTQEKLDAVTSQLEKEVKKSKGYEREIEDLHGFEFL
DRLDYLD TIRKQDQQLKLLMQIMDKIQPIIKDNTNYSNVDRIKKEAVWNEDESRWILPEMSMRTIL
PLANNGYMQEPARQENTLLRSNFDDKLRERLAKSDSEN LANSYFKPVKQINVINKYKSDQKLSTS
KSLFSPKTPTFDGLVNGVVYTDALYERAQSAKRPPRLASLNP KGGDYKDDDDK

Flag SNAP CeOSM-3

MDYKDDDDKGGMDKDCMKRTTLDSP LGKLELSGCEQGLHEIKLLGKGTSAADAVEVPAPA AVL
GGPEPLMQATAWLNAYFHQPEAIEEFV PALHHPVFQQESFTRQVLWLLKVVKFGEVISYQQLA
ALAGNPAATAAVKTALSGNPVPIIPCHRVS SSGAVGGYEGGLAVKEWLLAHEGHRLGKPLGA
PGGGSGGSMAESVRVAVRCRPFNQREKDLNTTLCVGMTPNVGQVNLNAPDGA AKDFTFDGAYF
MDSTGEQIYNDIVFPLVENVIEGYNGTVFAYGQTGSGKTF SMQGIETIPAQRGVIPRAFDHIFTATA
TTENVKFLVHCSYLEIYN EEEVRDLLGADNKQKLEIKEQPDRGVYVAGLSMHVCHDVPACKELMTR
GFNNRHVGATLMNKDSSRSHSIFTVYVEGMTETGSIRMGKLNLDLAGSERQSKTGATGDRLKE
ATKINLSLSALGNVISALVDGKSKHIPYRDSKLTRLLQDSLGGNTKTIMIACVSPSSDNYDET LSTL
YANRAKNIK NKPTINEDPKDALLREYQEEIARLKS MVQPGAVGVGAPAQDAFSIEEERK KLR EEFEE
EAMNDLRGEYEREQTSKAELQKDLES LRADYERANANLDNLNPEEAAKKIQQLQDQFIGGEEAGN
TQLKQKRMKQLKEAETKTQKLAAALNVHKDDPLLQVYSTTQEKLDAVTSQLEKEVKKSKGYEREI
EDLHGFEFLDRLDYLD TIRKQDQQLKLLMQIMDKIQPIIKDNTNYSNVDRIKKEAVWNEDESRWILP

10 Supplementary Information

EMSMSRTILPLANNGYMQEPARQENTLLRSNFDDKLRERLAKSDSENLANSYFKPVKQINVINKYK
SDQKLSTSKSLFPSKTPTFDGLVNGVVYTDALYERAQSAKRPPRLASLNP

CeOSM-3(G444E) Flag

MAESVRVAVRCRPFNQREKDLNTTLCVGMTPNVGQVNLNAPDGAADFTFDGAYFMDSTGEQIY
NDIVFPLVENVIEGYNGTVFAYGQTGSGKTFMQGIETIPAQRGVIPRAFDHIFTATATTENVKFLV
HCSYLEIYNEEVRDLLGADNKQKLEIKEQPDRGVYVAGLSMHVCHDVPACKELMTRGFNRRHVG
ATLMNKDSSRSHSIFTVYVEGMTETGSIRMGKLNLDLAGSERQSKTGATGDRLKEATKINLSLSA
LGNVISALVDGKSKHIPYRDSKLTRLLQDSLGGNTKTIMIAVSPSSDNYDETLSTLRYANRAKNIK
NKPTINEDPKDALLREYQEEIARLKSMVQPGAVGVGAPAQDAFSIEEERKKLREEFEEAMNDLRG
EYEREQTSKAELQKDLESRLADYERANANLDNLNPEEAAKKIQQQLQDQFIEGEEAGNTQLKQKRM
KQLKEAETKTQKLAAALNVHKDDPLLQVYSTTQEKLDAVTSQLEKEVKKSKGYEREIEDLHGEFEL
DRLDYLDITIRKQDQQLKLLMQIMDKIQPIIKKDTNYSNVDRIKKEAVWNEDESRWILPEMSMSRTIL
PLANNGYMQEPARQENTLLRSNFDDKLRERLAKSDSENLANSYFKPVKQINVINKYKSDQKLST
KSLFPSKTPTFDGLVNGVVYTDALYERAQSAKRPPRLASLNP

CeOSM-3(G444Q) Flag

MAESVRVAVRCRPFNQREKDLNTTLCVGMTPNVGQVNLNAPDGAADFTFDGAYFMDSTGEQIY
NDIVFPLVENVIEGYNGTVFAYGQTGSGKTFMQGIETIPAQRGVIPRAFDHIFTATATTENVKFLV
HCSYLEIYNEEVRDLLGADNKQKLEIKEQPDRGVYVAGLSMHVCHDVPACKELMTRGFNRRHVG
ATLMNKDSSRSHSIFTVYVEGMTETGSIRMGKLNLDLAGSERQSKTGATGDRLKEATKINLSLSA
LGNVISALVDGKSKHIPYRDSKLTRLLQDSLGGNTKTIMIAVSPSSDNYDETLSTLRYANRAKNIK
NKPTINEDPKDALLREYQEEIARLKSMVQPGAVGVGAPAQDAFSIEEERKKLREEFEEAMNDLRG
EYEREQTSKAELQKDLESRLADYERANANLDNLNPEEAAKKIQQQLQDQFIQGEEAGNTQLKQKRM
KQLKEAETKTQKLAAALNVHKDDPLLQVYSTTQEKLDAVTSQLEKEVKKSKGYEREIEDLHGEFEL
DRLDYLDITIRKQDQQLKLLMQIMDKIQPIIKKDTNYSNVDRIKKEAVWNEDESRWILPEMSMSRTIL
PLANNGYMQEPARQENTLLRSNFDDKLRERLAKSDSENLANSYFKPVKQINVINKYKSDQKLST
KSLFPSKTPTFDGLVNGVVYTDALYERAQSAKRPPRLASLNP

CeOSM-3(1-349) Flag

MAESVRVAVRCRPFNQREKDLNTTLCVGMTPNVGQVNLNAPDGAADFTFDGAYFMDSTGEQIY
NDIVFPLVENVIEGYNGTVFAYGQTGSGKTFMQGIETIPAQRGVIPRAFDHIFTATATTENVKFLV
HCSYLEIYNEEVRDLLGADNKQKLEIKEQPDRGVYVAGLSMHVCHDVPACKELMTRGFNRRHVG
ATLMNKDSSRSHSIFTVYVEGMTETGSIRMGKLNLDLAGSERQSKTGATGDRLKEATKINLSLSA
LGNVISALVDGKSKHIPYRDSKLTRLLQDSLGGNTKTIMIAVSPSSDNYDETLSTLRYANRAKNIK
NKPTINEDPKDALLREYQEEIGGDYKDDDDK

CeOSM-3(1-349) GCN4 Flag

MAESVRVAVRCRPFNQREKDLNTTLCVGMTPNVGQVNLNAPDGAADFTFDGAYFMDSTGEQIY
NDIVFPLVENVIEGYNGTVFAYGQTGSGKTFMQGIETIPAQRGVIPRAFDHIFTATATTENVKFLV
HCSYLEIYNEEVRDLLGADNKQKLEIKEQPDRGVYVAGLSMHVCHDVPACKELMTRGFNRRHVG
ATLMNKDSSRSHSIFTVYVEGMTETGSIRMGKLNLDLAGSERQSKTGATGDRLKEATKINLSLSA
LGNVISALVDGKSKHIPYRDSKLTRLLQDSLGGNTKTIMIAVSPSSDNYDETLSTLRYANRAKNIK
NKPTINEDPKDALLREYQEEIGAPRMKQLEDKVEELLSKNYHLENEVARLKKLVGEGGDYKDDDD
K

CeOSM-3(1-349) GCN4 His

10 Supplementary Information

MAESVRVAVRCRPFNQREKDLNTTLCVGMTPNVGQVNLNAPDGAADFTFDGAYFMDSTGEQIY
NDIVFPLVENVIEGYNGTVFAYGQTGSGKTFMQGIETIPAQRGVIPRAFDHIFTATATTENVKFLV
HCSYLEIYNEEV RDLLGADNKQKLEIKEQPDRGVYVAGLSMHVCHDVPACKELMTRGFNRRHVG
ATLMNKDSSRSHSIFTVYVEGMTETGSIRMGKLNLDLAGSERQSKTGATGDRLKEATKINLSLSA
LGNVISALVDGKSKHIPYRDSKLRLLQDSLGGNTKTIMACVSPSSDNYDELSTLRYANRAKNIK
NKPTINEDPKDALLREYQEEI **GAPRMKQLEDKVEELLSKNYHLENEVARLKKLVGEGGHHHHHH**

Flag Halo CeOSM-3(350-444)

MDYKDDDDKGAPGGGSGGSMEIGTGFPDPHYVEVLGERMHYVDVGPRDGTVPVFLHGNPTSS
YVWRNIIPHVAPTHRCIAPDLIGMGKSDKPDLYFFDDHVRFMDFIEALGLEEVVLIHDWGSAL
GFHWAKRNPERVKGIAFMFIRPIPTWDEWPEFARETFQAFRTTDVGRKLIIDQNVFIEGTLPMGV
VRPLTEVEMDHYREPFLNPVDREPLWRFPNELPIAGEPANIVALVEEYMDWLHQSPVPKLLFWGT
PGVLIPPAEAARLAKSLPNCKAVDIGPGLNLLQEDNPDIGSEIARWLSTLEISGGARLKSVMQPGA
VGVGAPAQDAFSIEERKKLREEFEEAMNDLRGEYEREQTSKAELQKDLESLRADYERANANLDN
LNPEEAAKKIQQQLQDQFIG

His Halo CeOSM-3(350-444)

MHHHHHHGGAPGGGSGGSMEIGTGFPDPHYVEVLGERMHYVDVGPRDGTVPVFLHGNPTSSYV
WRNIIPHVAPTHRCIAPDLIGMGKSDKPDLYFFDDHVRFMDFIEALGLEEVVLIHDWGSALGF
HWAKRNPERVKGIAFMFIRPIPTWDEWPEFARETFQAFRTTDVGRKLIIDQNVFIEGTLPMGV
PLTEVEMDHYREPFLNPVDREPLWRFPNELPIAGEPANIVALVEEYMDWLHQSPVPKLLFWGT
VLIPPAEAARLAKSLPNCKAVDIGPGLNLLQEDNPDIGSEIARWLSTLEISGGARLKSVMQPGAVG
VGAPAQDAFSIEERKKLREEFEEAMNDLRGEYEREQTSKAELQKDLESLRADYERANANLDNLN
PEEAAKKIQQQLQDQFIG

Flag Halo CeOSM-3(445-552)

MDYKDDDDKGAPGGGSGGSMEIGTGFPDPHYVEVLGERMHYVDVGPRDGTVPVFLHGNPTSS
YVWRNIIPHVAPTHRCIAPDLIGMGKSDKPDLYFFDDHVRFMDFIEALGLEEVVLIHDWGSAL
GFHWAKRNPERVKGIAFMFIRPIPTWDEWPEFARETFQAFRTTDVGRKLIIDQNVFIEGTLPMGV
VRPLTEVEMDHYREPFLNPVDREPLWRFPNELPIAGEPANIVALVEEYMDWLHQSPVPKLLFWGT
PGVLIPPAEAARLAKSLPNCKAVDIGPGLNLLQEDNPDIGSEIARWLSTLEISGGGEEAGNTQLKQ
KRMKQLKEAETKTQKLAALNVHKDDPLLQVYSTTQEKLDAVTSQLEKEVKKSKGYEREIEDLHG
EFELDRLDYLDTIRKQDQQLKLLMQIMDKIQP

His Halo CeOSM-3(445-552)

MHHHHHHGGAPGGGSGGSMEIGTGFPDPHYVEVLGERMHYVDVGPRDGTVPVFLHGNPTSSYV
WRNIIPHVAPTHRCIAPDLIGMGKSDKPDLYFFDDHVRFMDFIEALGLEEVVLIHDWGSALGF
HWAKRNPERVKGIAFMFIRPIPTWDEWPEFARETFQAFRTTDVGRKLIIDQNVFIEGTLPMGV
PLTEVEMDHYREPFLNPVDREPLWRFPNELPIAGEPANIVALVEEYMDWLHQSPVPKLLFWGT
VLIPPAEAARLAKSLPNCKAVDIGPGLNLLQEDNPDIGSEIARWLSTLEISGGGEEAGNTQLKQKR
MKQLKEAETKTQKLAALNVHKDDPLLQVYSTTQEKLDAVTSQLEKEVKKSKGYEREIEDLHGFE
LDRLDYLDTIRKQDQQLKLLMQIMDKIQP

Flag Halo CeOSM-3(552-699) GCN4

MDYKDDDDKGAPGGGSGGSMEIGTGFPDPHYVEVLGERMHYVDVGPRDGTVPVFLHGNPTSS
YVWRNIIPHVAPTHRCIAPDLIGMGKSDKPDLYFFDDHVRFMDFIEALGLEEVVLIHDWGSAL

10 Supplementary Information

GFHWAKRNPERVKGIAFMFIRPIPTWDEWPEFARETFQAFRTTDVGRKLIIDQNVFIEGTLPMGV
VRPLTEVEMDHYREPFLNPVDREPLWRFPNELPIAGEPANIVALVEEYMDWLHQSPVPKLLFWGT
PGVLIPPAEAARLAKSLPNCKAVDIGPGLNLLQEDNPDIGSEIARWLSTLEISGGIIKKDTNYSNVD
RIKKEAVWNEDESRWILPEMSMSRTILPLANNGYMQEPARQENTLLRSNFDDKLRERLAKSDSEN
LANSYFKPVKQINVINKYKSDQKLSTSKSLFPSKTPTFDGLVNGVVYTDALYERAQSAKRPPRLAS
LNPKG **GAPRMKQLEDKVEELLSKNYHLENEVARLKKLVGE**

Flag Halo CeOSM-3(552-699) GCN4 His

MHHHHH **GAPGGGSGGSMEIGTGFPDPHYVEVLGERMHYVDVGRDGPVFLHGNPTSSYV**
WRNIIPHVAPTHRCIAPDLIGMGKSDKPDLYFFDDHVRFMDFIEALGLEEVVLIHDWGSALGF
HWAKRNPERVKGIAFMFIRPIPTWDEWPEFARETFQAFRTTDVGRKLIIDQNVFIEGTLPMGVVR
PLTEVEMDHYREPFLNPVDREPLWRFPNELPIAGEPANIVALVEEYMDWLHQSPVPKLLFWGTGP
VLIPPAEAARLAKSLPNCKAVDIGPGLNLLQEDNPDIGSEIARWLSTLEISGGIIKKDTNYSNVDRIK
KEAVWNEDESRWILPEMSMSRTILPLANNGYMQEPARQENTLLRSNFDDKLRERLAKSDSENLA
NSYFKPVKQINVINKYKSDQKLSTSKSLFPSKTPTFDGLVNGVVYTDALYERAQSAKRPPRLASLN
PKGG **GAPRMKQLEDKVEELLSKNYHLENEVARLKKLVGE**

CeDYF-1 Flag

MNAMLNKEGEFTSTIYTLIHEHKFNDAIRILQYQHERNPKNLAALSLLAYCYYYTQDFMNAADCYS
QLSYNFPQYSQYKLYHAQSLYNAFRPADALAVVSMIQDENLLNESVKLEAAIKYQEDDLVNCRILV
EQLPENDAAVIINTACIDYKEGNYEEALKKFNEATEFSGYQSGLAYSIALCHYRRGDYDSALKLISEII
NRGVKDHPEFNIGMVTEGIDVNFQNTQKLHESALIEAFNLKFAIYYRTKDFKAAKESLTDMPPRNE
HDADPITLHNLAINANSDFGDSSAKLQFLGINPFPQETFANLLFLYCKNDYFGLAADVLAENPSH
TFYCLNEYQFNLEALIYMPNPEESLKKLEKLEKECLDRLRKAIEIQIKKEQKTTDSDDSLEMRNL
IESYDDSLEMYLPVLMYAKYYWDKRDYQAVEKLFNSVDYCKEHTWKLNVHAHTIFMQEKKYKD
AAAFYEPIVHKKYDDGILEVPAMILANLVVCYIMTNQTDEAELIKAVENEEEAALMMKPNEKFFHN
SIISLVIGSLYCSKGNFEFGISR VVKALEPPEK KLGVDTWYYAKRCIVAAIELMAKNLLVMRDSVME
VIQFLTSCVPGRN IYTPDDLFEQAGESKVKCNVTYEARMIKAALLMVFN DGAP **DYKDDDDK**

CeOSM-6 Flag (CAA03975.1)

MPPFSDEKMTNRSIGRKVLIDQSKQQQISLISGFRGVARHLKSVLTVEINTEPINLNGLEDVRMLIIP
QPKTSFGTGEIEAIWKFVEEGGSLMILSGEGGERQSLNEMIAKYGITVNKDSVIRTVFLKYFDPKEA
LVANGVINRAIAVAACKNVSTEQKHNSQALSFIYPYGCTLDVNNRMSNVVLSSGSTSFPTSRPVAA
FHETKLNEMKKKGRVCVVGVSVMFHDTYIDKEENGKIFDTFVEFLVNGLELNTIDAAEPEINDYTNI
PDHIHMSQQIKVCMYEGELDQAISDFMKIMDTSLHSFNLKHWPM TIRLYEALNLSPPPLTLVEPQ
FELPMPFPQPAVFPPTFQELPMPPELFDLDEQFSSPEIQLSQLANRSEEDLIFFIEKAGEITGISA
ELTRSERTPKKIIELAVSKLMLFKRSMMDGELEVASAFDIGEHDAHHQSFNQGEEMDEQLFSDIDE
FDDL GAPGG **DYKDDDDK**

11. Literature

1. Urnavicius, L., et al., *The structure of the dynactin complex and its interaction with dynein*. Science, 2015. **347**(6229): p. 1441-1446.
2. Verhey, K.J. and J.W. Hammond, *Traffic control: regulation of kinesin motors*. Nature Reviews Molecular Cell Biology, 2009. **10**(11): p. 765-777.
3. Howard, J., *Mechanics of Motor Proteins and the Cytoskeleton* Sunderland. 2001.
4. Schliwa, M. and G. Woehlke, *Molecular motors*. Nature, 2003. **422**(6933): p. 759-65.
5. Endow, S.A., *Kinesin motors as molecular machines*. BioEssays, 2003. **25**(12): p. 1212-1219.
6. Gennerich, A. and R.D. Vale, *Walking the walk: how kinesin and dynein coordinate their steps*. Current opinion in cell biology, 2009. **21**(1): p. 59-67.
7. Svoboda, K., et al., *Direct observation of kinesin stepping by optical trapping interferometry*. Nature, 1993. **365**(6448): p. 721-727.
8. Wordeman, L., *How kinesin motor proteins drive mitotic spindle function: Lessons from molecular assays*. Semin Cell Dev Biol, 2010. **21**(3): p. 260-8.
9. Sharp, D.J., G.C. Rogers, and J.M. Scholey, *Microtubule motors in mitosis*. Nature, 2000. **407**(6800): p. 41-7.
10. Wasmeier, C., et al., *Melanosomes at a glance*. J Cell Sci, 2008. **121**(Pt 24): p. 3995-9.
11. Sheetz, M.P., *Motor and cargo interactions*. European Journal of Biochemistry, 1999. **262**(1): p. 19-25.
12. Rosenbaum, J.L. and G.B. Witman, *Intraflagellar transport*. Nature Reviews Molecular Cell Biology, 2002. **3**(11): p. 813-825.
13. Anvarian, Z., et al., *Cellular signalling by primary cilia in development, organ function and disease*. Nature Reviews Nephrology, 2019. **15**(4): p. 199-219.
14. Badano, J.L., et al., *The Ciliopathies: An Emerging Class of Human Genetic Disorders*. Annual Review of Genomics and Human Genetics, 2006. **7**(1): p. 125-148.
15. Nigg, E.A. and J.W. Raff, *Centrioles, Centrosomes, and Cilia in Health and Disease*. Cell, 2009. **139**(4): p. 663-678.
16. Pan, J., Q. Wang, and W.J. Snell, *Cilium-generated signaling and cilia-related disorders*. Laboratory Investigation, 2005. **85**(4): p. 452-463.
17. Scholey, J.M. and K.V. Anderson, *Intraflagellar Transport and Cilium-Based Signaling*. Cell, 2006. **125**(3): p. 439-442.
18. Chevalier-Larsen, E. and E.L. Holzbaur, *Axonal transport and neurodegenerative disease*. Biochim Biophys Acta, 2006. **1762**(11-12): p. 1094-108.
19. Bilsland, L.G., et al., *Deficits in axonal transport precede ALS symptoms in vivo*. Proc Natl Acad Sci U S A, 2010. **107**(47): p. 20523-8.
20. Morfini, G.A., et al., *Pathogenic huntingtin inhibits fast axonal transport by activating JNK3 and phosphorylating kinesin*. Nat Neurosci, 2009. **12**(7): p. 864-71.
21. Perlson, E., et al., *A switch in retrograde signaling from survival to stress in rapid-onset neurodegeneration*. J Neurosci, 2009. **29**(31): p. 9903-17.

22. Ström, A.L., et al., *Retrograde axonal transport and motor neuron disease*. J Neurochem, 2008. **106**(2): p. 495-505.
23. Alberts, B., *Molecular biology of the cell*. Sixth edition. ed. 2015, New York, NY: Garland Science, Taylor and Francis Group. 1 volume (various pagings).
24. Kayser, H., *Guidebook to the Cytoskeletal and Motor Proteins*. Herausgegeben von Th. Kreis und R. Vale. 276 Seiten, zahlr. Abb. und Tab. Oxford University Press. Oxford, New York, Tokyo 1993. Preis: 22,50 £. Food / Nahrung, 1994. **38**(3): p. 349-349.
25. Virtual eUniversity, I.W., *Anatomy Physiology - The Cellular Level of Organization*, in *E-Book 2 - The Cytoplasm and cellular Organelles - Chapter 5 The Cytoskeleton*. p. <https://iitway.com/mod/book/view.php?id=997&chapterid=3161>.
26. Rodionov, V.I. and G.G. Borisy, *Microtubule Treadmilling in Vivo*. Science, 1997. **275**(5297): p. 215.
27. Chalfie, M. and J.N. Thomson, *Organization of neuronal microtubules in the nematode Caenorhabditis elegans*. Journal of Cell Biology, 1979. **82**(1): p. 278-289.
28. Tilney, L.G., et al., *Microtubules: evidence for 13 protofilaments*. J Cell Biol, 1973. **59**(2 Pt 1): p. 267-75.
29. Porter, M.E. and W.S. Sale, *The 9 + 2 axoneme anchors multiple inner arm dyneins and a network of kinases and phosphatases that control motility*. The Journal of cell biology, 2000. **151**(5): p. F37-F42.
30. Vale, R.D., *The molecular motor toolbox for intracellular transport*. Cell, 2003. **112**(4): p. 467-80.
31. Wade, R.H. and A.A. Hyman, *Microtubule structure and dynamics*. Curr Opin Cell Biol, 1997. **9**(1): p. 12-7.
32. Woehlke, G., et al., *Microtubule Interaction Site of the Kinesin Motor*. Cell, 1997. **90**(2): p. 207-216.
33. Reisler, E. and E.H. Egelman, *Actin Structure and Function: What We Still Do Not Understand*. Journal of Biological Chemistry, 2007. **282**(50): p. 36133-36137.
34. Gunning, P.W., et al., *The evolution of compositionally and functionally distinct actin filaments*. Journal of Cell Science, 2015. **128**(11): p. 2009-2019.
35. Reisler, E., *Actin molecular structure and function*. Current Opinion in Cell Biology, 1993. **5**(1): p. 41-47.
36. Herrmann, H., et al., *Intermediate filaments: from cell architecture to nanomechanics*. Nature Reviews Molecular Cell Biology, 2007. **8**(7): p. 562-573.
37. Helfand, B.T., L. Chang, and R.D. Goldman, *Intermediate filaments are dynamic and motile elements of cellular architecture*. J Cell Sci, 2004. **117**(Pt 2): p. 133-41.
38. Bott, C.J. and B. Winckler, *Intermediate filaments in developing neurons: Beyond structure*. Cytoskeleton (Hoboken), 2020. **77**(3-4): p. 110-128.
39. Thompson, R.F. and G.M. Langford, *Myosin superfamily evolutionary history*. The Anatomical Record, 2002. **268**(3): p. 276-289.
40. Miki, H., Y. Okada, and N. Hirokawa, *Analysis of the kinesin superfamily: insights into structure and function*. Trends in Cell Biology, 2005. **15**(9): p. 467-476.

41. Lawrence , C.J., et al., *A standardized kinesin nomenclature*. Journal of Cell Biology, 2004. **167**(1): p. 19-22.
42. Mallik, R. and S.P. Gross, *Molecular Motors: Strategies to Get Along*. Current Biology, 2004. **14**(22): p. R971-R982.
43. Karcher, R.L., S.W. Deacon, and V.I. Gelfand, *Motor-cargo interactions: the key to transport specificity*. Trends Cell Biol, 2002. **12**(1): p. 21-7.
44. Hammond, J.W., et al., *Autoinhibition of the kinesin-2 motor KIF17 via dual intramolecular mechanisms*. J Cell Biol, 2010. **189**(6): p. 1013-25.
45. Cole, D., et al., *Novel heterotrimeric kinesin-related protein purified from sea urchin eggs*. Nature, 1993. **366**: p. 268-70.
46. Brunnbauer, M., et al., *Regulation of a heterodimeric kinesin-2 through an unprocessive motor domain that is turned processive by its partner*. Proc Natl Acad Sci U S A, 2010. **107**(23): p. 10460-5.
47. Schroeder, H.W., 3rd, et al., *Force-dependent detachment of kinesin-2 biases track switching at cytoskeletal filament intersections*. Biophys J, 2012. **103**(1): p. 48-58.
48. Muthukrishnan, G., et al., *The processivity of kinesin-2 motors suggests diminished front-head gating*. Curr Biol, 2009. **19**(5): p. 442-7.
49. Milic, B., et al., *Intraflagellar transport velocity is governed by the number of active KIF17 and KIF3AB motors and their motility properties under load*. Proc Natl Acad Sci U S A, 2017. **114**(33): p. E6830-e6838.
50. Andreasson, J.O., et al., *The Mechanochemical Cycle of Mammalian Kinesin-2 KIF3A/B under Load*. Curr Biol, 2015. **25**(9): p. 1166-75.
51. Guzik-Lendrum, S., et al., *Kinesin-2 KIF3AC and KIF3AB Can Drive Long-Range Transport along Microtubules*. Biophys J, 2015. **109**(7): p. 1472-82.
52. Mueller, J., et al., *The FLA3 KAP subunit is required for localization of kinesin-2 to the site of flagellar assembly and processive anterograde intraflagellar transport*. Mol Biol Cell, 2005. **16**(3): p. 1341-54.
53. Scholey, J.M., *Kinesin-2: a family of heterotrimeric and homodimeric motors with diverse intracellular transport functions*. Annu Rev Cell Dev Biol, 2013. **29**: p. 443-69.
54. Mitchell, D.R., *The evolution of eukaryotic cilia and flagella as motile and sensory organelles*. Adv Exp Med Biol, 2007. **607**: p. 130-40.
55. Scholey, J.M., *Intraflagellar transport*. Annu Rev Cell Dev Biol, 2003. **19**: p. 423-43.
56. Xie, C., et al., *Optimal sidestepping of intraflagellar transport kinesins regulates structure and function of sensory cilia*. Embo j, 2020. **39**(12): p. e103955.
57. Brunnbauer, M., et al., *Torque generation of kinesin motors is governed by the stability of the neck domain*. Mol Cell, 2012. **46**(2): p. 147-58.
58. De Marco, V., et al., *Dimerization properties of a Xenopus laevis kinesin-II carboxy-terminal stalk fragment*. EMBO Rep, 2003. **4**(7): p. 717-22.
59. Cole, D.G., et al., *Isolation of a sea urchin egg kinesin-related protein using peptide antibodies*. Journal of Cell Science, 1992. **101**(2): p. 291-301.
60. Cole, D.G., *Kinesin-II, the heteromeric kinesin*. Cellular and Molecular Life Sciences CMLS, 1999. **56**(3): p. 217-226.
61. Hancock, W.O. and J. Howard, *Kinesin's processivity results from mechanical and chemical coordination between the ATP hydrolysis cycles of*

- the two motor domains*. Proceedings of the National Academy of Sciences, 1999. **96**(23): p. 13147-13152.
62. Lakamper, S. and E. Meyhofer, *The E-hook of tubulin interacts with kinesin's head to increase processivity and speed*. Biophys J, 2005. **89**(5): p. 3223-34.
 63. Vale, R.D. and R.J. Fletterick, *The design plan of kinesin motors*. Annu Rev Cell Dev Biol, 1997. **13**: p. 745-77.
 64. Woehlke, G. and M. Schliwa, *Walking on two heads: the many talents of kinesin*. Nat Rev Mol Cell Biol, 2000. **1**(1): p. 50-8.
 65. Yildiz, A., et al., *Kinesin Walks Hand-Over-Hand*. Science, 2004. **303**(5658): p. 676-678.
 66. Rashid, D.J., K.P. Wedaman, and J.M. Scholey, *Heterodimerization of the two motor subunits of the heterotrimeric kinesin, KRP85/95*. J Mol Biol, 1995. **252**(2): p. 157-62.
 67. Vukajlovic, M., et al., *How kinesin-2 forms a stalk*. Molecular biology of the cell, 2011. **22**(22): p. 4279-4287.
 68. Friedman, D.S. and R.D. Vale, *Single-molecule analysis of kinesin motility reveals regulation by the cargo-binding tail domain*. Nature Cell Biology, 1999. **1**(5): p. 293-297.
 69. Coy, D.L., et al., *Kinesin's tail domain is an inhibitory regulator of the motor domain*. Nature Cell Biology, 1999. **1**(5): p. 288-292.
 70. Hackney, D.D., J.D. Levitt, and J. Suhan, *Kinesin undergoes a 9 S to 6 S conformational transition*. J Biol Chem, 1992. **267**(12): p. 8696-701.
 71. Yonekura, H., et al., *Mechanism of tail-mediated inhibition of kinesin activities studied using synthetic peptides*. Biochem Biophys Res Commun, 2006. **343**(2): p. 420-7.
 72. Imanishi, M., et al., *Autoinhibition regulates the motility of the C. elegans intraflagellar transport motor OSM-3*. The Journal of cell biology, 2006. **174**(7): p. 931-937.
 73. Wedaman, K.P., et al., *Sequence and submolecular localization of the 115-kD accessory subunit of the heterotrimeric kinesin-II (KRP85/95) complex*. Journal of Cell Biology, 1996. **132**(3): p. 371-380.
 74. Gindhart, J.G., Jr. and L.S. Goldstein, *Armadillo repeats in the SpKAP115 subunit of kinesin-II*. Trends Cell Biol, 1996. **6**(11): p. 415-6.
 75. Peifer, M., S. Berg, and A.B. Reynolds, *A repeating amino acid motif shared by proteins with diverse cellular roles*. Cell, 1994. **76**(5): p. 789-91.
 76. Deacon, S.W., et al., *Dynactin is required for bidirectional organelle transport*. J Cell Biol, 2003. **160**(3): p. 297-301.
 77. Doodhi, H., et al., *KAP, the Accessory Subunit of Kinesin-2, Binds the Predicted Coiled-Coil Stalk of the Motor Subunits*. Biochemistry, 2009. **48**(10): p. 2248-2260.
 78. Doodhi, H., et al., *Biochemical and Molecular Dynamic Simulation Analysis of a Weak Coiled Coil Association between Kinesin-II Stalks*. PLOS ONE, 2012. **7**(9): p. e45981.
 79. Sonar, P., et al., *Kinesin-2 from C. reinhardtii Is an Atypically Fast and Autoinhibited Motor that Is Activated by Heterotrimerization for Intraflagellar Transport*. Curr Biol, 2020. **30**(6): p. 1160-1166.e5.

80. Hirokawa, N., et al., *Submolecular domains of bovine brain kinesin identified by electron microscopy and monoclonal antibody decoration*. Cell, 1989. **56**(5): p. 867-78.
81. Adio, S., et al., *Review: regulation mechanisms of Kinesin-1*. J Muscle Res Cell Motil, 2006. **27**(2): p. 153-60.
82. Wong, Y.L., et al., *The Kinesin-1 tail conformationally restricts the nucleotide pocket*. Biophysical journal, 2009. **96**(7): p. 2799-2807.
83. Dietrich, K.A., et al., *The kinesin-1 motor protein is regulated by a direct interaction of its head and tail*. Proc Natl Acad Sci U S A, 2008. **105**(26): p. 8938-43.
84. Kaan, H.Y.K., D.D. Hackney, and F. Kozielski, *The Structure of the Kinesin-1 Motor-Tail Complex Reveals the Mechanism of Autoinhibition*. Science, 2011. **333**(6044): p. 883-885.
85. Hackney, D.D., N. Baek, and A.C. Snyder, *Half-site inhibition of dimeric kinesin head domains by monomeric tail domains*. Biochemistry, 2009. **48**(15): p. 3448-56.
86. Hammond, J.W., et al., *Mammalian Kinesin-3 Motors Are Dimeric In Vivo and Move by Processive Motility upon Release of Autoinhibition*. PLOS Biology, 2009. **7**(3): p. e1000072.
87. Al-Bassam, J., et al., *Distinct conformations of the kinesin Unc104 neck regulate a monomer to dimer motor transition*. The Journal of cell biology, 2003. **163**(4): p. 743-753.
88. Yamada, K.H., T. Hanada, and A.H. Chishti, *The effector domain of human Dlg tumor suppressor acts as a switch that relieves autoinhibition of kinesin-3 motor GAKIN/KIF13B*. Biochemistry, 2007. **46**(35): p. 10039-45.
89. Siddiqui, N. and A. Straube, *Intracellular cargo transport by kinesin-3 motors*. Biochemistry (Moscow), 2017. **82**(7): p. 803-815.
90. Blasius, T.L., et al., *Two binding partners cooperate to activate the molecular motor Kinesin-1*. J Cell Biol, 2007. **176**(1): p. 11-7.
91. Tafoya, S. and C. Bustamante, *Molecular switch-like regulation in motor proteins*. Philosophical transactions of the Royal Society of London. Series B, Biological sciences, 2018. **373**(1749): p. 20170181.
92. Mohamed, M.A.A., W.L. Stepp, and Z. Okten, *Reconstitution reveals motor activation for intraflagellar transport*. Nature, 2018. **557**(7705): p. 387-391.
93. Cleetus, A., G. Merck, and Z. Ökten, *Retracing the evolution of kinesin-2 deployment from mouse to worm*. bioRxiv, 2020: p. 2020.08.17.254268.
94. Lindsay, A.J., et al., *Identification and characterization of multiple novel Rab-myosin Va interactions*. Mol Biol Cell, 2013. **24**(21): p. 3420-34.
95. Rojo Pulido, I., et al., *Myosin Va acts in concert with Rab27a and MyRIP to regulate acute von-Willebrand factor release from endothelial cells*. Traffic, 2011. **12**(10): p. 1371-82.
96. Robinson, C.L., et al., *The adaptor protein melanophilin regulates dynamic myosin-Va: cargo interaction and dendrite development in melanocytes*. Mol Biol Cell, 2019. **30**(6): p. 742-752.
97. Berezuk, M.A. and T.A. Schroer, *Dynactin enhances the processivity of kinesin-2*. Traffic, 2007. **8**(2): p. 124-9.
98. Ross, J.L., et al., *Kinesin and dynein-dynactin at intersecting microtubules: motor density affects dynein function*. Biophys J, 2008. **94**(8): p. 3115-25.

99. Sarpal, R., et al., *Drosophila KAP interacts with the kinesin II motor subunit KLP64D to assemble chordotonal sensory cilia, but not sperm tails*. *Curr Biol*, 2003. **13**(19): p. 1687-96.
100. Yamazaki, H., et al., *Cloning and characterization of KAP3: a novel kinesin superfamily-associated protein of KIF3A/3B*. *Proc Natl Acad Sci U S A*, 1996. **93**(16): p. 8443-8.
101. DeBerg, H.A., et al., *Motor domain phosphorylation modulates kinesin-1 transport*. *J Biol Chem*, 2013. **288**(45): p. 32612-21.
102. Shapira, O. and L. Gheber, *Motile properties of the bi-directional kinesin-5 Cin8 are affected by phosphorylation in its motor domain*. *Scientific reports*, 2016. **6**: p. 25597-25597.
103. Espeut, J., et al., *Phosphorylation relieves autoinhibition of the kinetochore motor Cenp-E*. *Mol Cell*, 2008. **29**(5): p. 637-43.
104. Liang, Y., et al., *FLA8/KIF3B phosphorylation regulates kinesin-II interaction with IFT-B to control IFT entry and turnaround*. *Dev Cell*, 2014. **30**(5): p. 585-97.
105. Oberhofer, A., et al., *Myosin Va's adaptor protein melanophilin enforces track selection on the microtubule and actin networks in vitro*. *Proc Natl Acad Sci U S A*, 2017. **114**(24): p. E4714-e4723.
106. Oberhofer, A., et al., *Molecular underpinnings of cytoskeletal cross-talk*. *Proc Natl Acad Sci U S A*, 2020. **117**(8): p. 3944-3952.
107. Cai, D., et al., *Single molecule imaging reveals differences in microtubule track selection between Kinesin motors*. *PLoS Biol*, 2009. **7**(10): p. e1000216.
108. Gross, S.P., *Dynactin: coordinating motors with opposite inclinations*. *Curr Biol*, 2003. **13**(8): p. R320-2.
109. Welte, M.A., *Bidirectional transport along microtubules*. *Curr Biol*, 2004. **14**(13): p. R525-37.
110. Gross, S.P., *Hither and yon: a review of bi-directional microtubule-based transport*. *Phys Biol*, 2004. **1**(1-2): p. R1-11.
111. Welte, M.A., *Fat on the move: intracellular motion of lipid droplets*. *Biochem Soc Trans*, 2009. **37**(Pt 5): p. 991-6.
112. Maeder, C.I., K. Shen, and C.C. Hoogenraad, *Axon and dendritic trafficking*. *Curr Opin Neurobiol*, 2014. **27**: p. 165-70.
113. Hancock, W.O., *Bidirectional cargo transport: moving beyond tug of war*. *Nature Reviews Molecular Cell Biology*, 2014. **15**(9): p. 615-628.
114. Osunbayo, O., et al., *Cargo transport at microtubule crossings: evidence for prolonged tug-of-war between kinesin motors*. *Biophysical journal*, 2015. **108**(6): p. 1480-1483.
115. Bryantseva, S.A. and O.N. Zhapparova, *Bidirectional transport of organelles: unity and struggle of opposing motors*. *Cell Biol Int*, 2012. **36**(1): p. 1-6.
116. Kozminski, K.G., et al., *A motility in the eukaryotic flagellum unrelated to flagellar beating*. *Proceedings of the National Academy of Sciences of the United States of America*, 1993. **90**(12): p. 5519-5523.
117. Aspengren, S., et al., *New insights into melanosome transport in vertebrate pigment cells*. *Int Rev Cell Mol Biol*, 2009. **272**: p. 245-302.
118. Gross, S.P., et al., *Interactions and regulation of molecular motors in Xenopus melanophores*. *J Cell Biol*, 2002. **156**(5): p. 855-65.

119. Mackintosh, J.A., *The antimicrobial properties of melanocytes, melanosomes and melanin and the evolution of black skin*. J Theor Biol, 2001. **211**(2): p. 101-13.
120. Daniolos, A., A.B. Lerner, and M.R. Lerner, *Action of light on frog pigment cells in culture*. Pigment Cell Res, 1990. **3**(1): p. 38-43.
121. Reilein, A.R., et al., *Regulation of organelle movement in melanophores by protein kinase A (PKA), protein kinase C (PKC), and protein phosphatase 2A (PP2A)*. J Cell Biol, 1998. **142**(3): p. 803-13.
122. Alexandra A. Nascimento, a. Joseph T. Roland, and V.I. Gelfand, *Pigment Cells: A Model for the Study of Organelle Transport*. Annual Review of Cell and Developmental Biology, 2003. **19**(1): p. 469-491.
123. Gundersen, G.G. and T.A. Cook, *Microtubules and signal transduction*. Curr Opin Cell Biol, 1999. **11**(1): p. 81-94.
124. Pollard, T.D. and G.G. Borisy, *Cellular motility driven by assembly and disassembly of actin filaments*. Cell, 2003. **112**(4): p. 453-65.
125. Park, M., et al., *Rab32 regulates melanosome transport in Xenopus melanophores by protein kinase a recruitment*. Curr Biol, 2007. **17**(23): p. 2030-4.
126. Kashina, A.S., et al., *Protein kinase A, which regulates intracellular transport, forms complexes with molecular motors on organelles*. Curr Biol, 2004. **14**(20): p. 1877-81.
127. Oberhofer, A., *Mechanistic dissection of myosin Va-based melanosome transport in vitro*, in *Faculty of Biology*. 2017, Ludwig-Maximilian Universität: Munich.
128. Roman, v., *Studying Kinesin-2 Regulation and Coordination in vitro*, in *Fakultät der Biologie*. 2016, Ludwid-Maximilian Universität München.
129. Rogers, S.L. and V.I. Gelfand, *Myosin cooperates with microtubule motors during organelle transport in melanophores*. Curr Biol, 1998. **8**(3): p. 161-4.
130. Wu, X., et al., *Rab27a is an essential component of melanosome receptor for myosin Va*. Mol Biol Cell, 2002. **13**(5): p. 1735-49.
131. Fukuda, M., T.S. Kuroda, and K. Mikoshiba, *Slac2-a/melanophilin, the missing link between Rab27 and myosin Va: implications of a tripartite protein complex for melanosome transport*. J Biol Chem, 2002. **277**(14): p. 12432-6.
132. Nilsson, H. and M. Wallin, *Evidence for several roles of dynein in pigment transport in melanophores*. Cell Motil Cytoskeleton, 1997. **38**(4): p. 397-409.
133. Canty, J.T. and A. Yildiz, *Activation and Regulation of Cytoplasmic Dynein*. Trends in Biochemical Sciences, 2020. **45**(5): p. 440-453.
134. Schroer, T.A., *Dynactin*. Annu Rev Cell Dev Biol, 2004. **20**: p. 759-79.
135. Vaughan, P.S., et al., *A role for regulated binding of p150(Glued) to microtubule plus ends in organelle transport*. J Cell Biol, 2002. **158**(2): p. 305-19.
136. Zhapparova, O.N., et al., *Dynactin subunit p150Glued isoforms notable for differential interaction with microtubules*. Traffic, 2009. **10**(11): p. 1635-46.
137. Fu, M.-m. and E.L.F. Holzbaur, *Integrated regulation of motor-driven organelle transport by scaffolding proteins*. Trends in Cell Biology, 2014. **24**(10): p. 564-574.

138. Blehm, B.H. and P.R. Selvin, *Single-molecule fluorescence and in vivo optical traps: how multiple dyneins and kinesins interact*. Chem Rev, 2014. **114**(6): p. 3335-52.
139. Jolly, A.L. and V.I. Gelfand, *Bidirectional intracellular transport: utility and mechanism*. Biochem Soc Trans, 2011. **39**(5): p. 1126-30.
140. Barlan, K., M.J. Rossow, and V.I. Gelfand, *The journey of the organelle: teamwork and regulation in intracellular transport*. Curr Opin Cell Biol, 2013. **25**(4): p. 483-8.
141. Lipowsky, R. and S. Klumpp, *'Life is motion': multiscale motility of molecular motors*. Physica A: Statistical Mechanics and its Applications, 2005. **352**(1): p. 53-112.
142. Zaliapin, I., et al., *Multiscale trend analysis of microtubule transport in melanophores*. Biophys J, 2005. **88**(6): p. 4008-16.
143. Sui, H. and K.H. Downing, *Molecular architecture of axonemal microtubule doublets revealed by cryo-electron tomography*. Nature, 2006. **442**(7101): p. 475-8.
144. Cole, D.G., et al., *Chlamydomonas kinesin-II-dependent intraflagellar transport (IFT): IFT particles contain proteins required for ciliary assembly in Caenorhabditis elegans sensory neurons*. J Cell Biol, 1998. **141**(4): p. 993-1008.
145. Piperno, G., et al., *Distinct mutants of retrograde intraflagellar transport (IFT) share similar morphological and molecular defects*. The Journal of cell biology, 1998. **143**(6): p. 1591-1601.
146. Taschner, M., et al., *Intraflagellar transport proteins 172, 80, 57, 54, 38, and 20 form a stable tubulin-binding IFT-B2 complex*. Embo j, 2016. **35**(7): p. 773-90.
147. Prevo, B., J.M. Scholey, and E.J.G. Peterman, *Intraflagellar transport: mechanisms of motor action, cooperation, and cargo delivery*. Febs j, 2017. **284**(18): p. 2905-2931.
148. Taschner, M. and E. Lorentzen, *The Intraflagellar Transport Machinery*. Cold Spring Harb Perspect Biol, 2016. **8**(10).
149. Snow, J.J., et al., *Two anterograde intraflagellar transport motors cooperate to build sensory cilia on C. elegans neurons*. Nature Cell Biology, 2004. **6**(11): p. 1109-1113.
150. Ou, G., et al., *Functional coordination of intraflagellar transport motors*. Nature, 2005. **436**(7050): p. 583-587.
151. Pan, X., et al., *Mechanism of transport of IFT particles in C. elegans cilia by the concerted action of kinesin-II and OSM-3 motors*. The Journal of cell biology, 2006. **174**(7): p. 1035-1045.
152. Rogers, S.L., et al., *Regulated bidirectional motility of melanophore pigment granules along microtubules *in vitro**. Proceedings of the National Academy of Sciences, 1997. **94**(8): p. 3720-3725.
153. Green, M.R. and J. Sambrook, *Molecular Cloning: A Laboratory Manual*. 2012: Cold Spring Harbor Laboratory Press.
154. Luckow, V.A., et al., *Efficient generation of infectious recombinant baculoviruses by site-specific transposon-mediated insertion of foreign genes into a baculovirus genome propagated in Escherichia coli*. Journal of virology, 1993. **67**(8): p. 4566-4579.

155. Wang, F., et al., *Effect of ADP and ionic strength on the kinetic and motile properties of recombinant mouse myosin V*. J Biol Chem, 2000. **275**(6): p. 4329-35.
156. Spudich, J.A. and S. Watt, *The regulation of rabbit skeletal muscle contraction. I. Biochemical studies of the interaction of the tropomyosin-troponin complex with actin and the proteolytic fragments of myosin*. J Biol Chem, 1971. **246**(15): p. 4866-71.
157. Mandelkow, E.M., M. Herrmann, and U. Ruhl, *Tubulin domains probed by limited proteolysis and subunit-specific antibodies*. J Mol Biol, 1985. **185**(2): p. 311-27.
158. Carter, N.J. and R.A. Cross, *Mechanics of the kinesin step*. Nature, 2005. **435**(7040): p. 308-12.
159. Takaki, R., et al., *How kinesin waits for ATP affects the nucleotide and load dependence of the stepping kinetics*. Proc Natl Acad Sci U S A, 2019. **116**(46): p. 23091-23099.
160. Haid, E., P. Lehmann, and J. Ziegenhorn, *Molar absorptivities of beta-NADH and beta-NAD at 260 nm*. Clin Chem, 1975. **21**(7): p. 884-7.
161. Jerabek-Willemsen, M., et al., *MicroScale Thermophoresis: Interaction analysis and beyond*. Journal of Molecular Structure, 2014. **1077**: p. 101-113.
162. Ludwig, C., et al., *Diffusion zwischen ungleich erwärmten Orten gleich zusammengesetzter Lösung*. 1856, Wien: Aus der K.K. Hof- und Staatsdruckerei, in Commission bei W. Braumüller, Buchhändler des K.K. Hofes und der K. Akademie der Wissenschaften.
163. Duhr, S. and D. Braun, *Thermophoretic Depletion Follows Boltzmann Distribution*. Physical Review Letters, 2006. **96**(16): p. 168301.
164. Duhr, S. and D. Braun, *Why molecules move along a temperature gradient*. Proceedings of the National Academy of Sciences, 2006. **103**(52): p. 19678-19682.
165. *Molecular Interaction Studies Using Microscale Thermophoresis*. ASSAY and Drug Development Technologies, 2011. **9**(4): p. 342-353.
166. De Groot, S.R. and P. Mazur, *Non-equilibrium thermodynamics*. 2013: Courier Corporation.
167. Tuma MC, Z.A., Le Bot N, Vernos I, Gelfand V, *Heterotrimeric kinesin II is the microtubule motor protein responsible for pigment dispersion in Xenopus melanophores*. The Journal of Cell Biology, 1998. **143**(6): p. 1547-1558.
168. Vukajlovic, M., *Regulation of the subunit assembly and the catalytic activity in heteromeric kinesin-2 from Caenorhabditis elegans*, in Faculty of Biology. 2012, Ludwig-Maximilian Universität: Munich.
169. Ben-Shimon, A. and M.Y. Niv, *Deciphering the Arginine-Binding Preferences at the Substrate-Binding Groove of Ser/Thr Kinases by Computational Surface Mapping*. PLOS Computational Biology, 2011. **7**(11): p. e1002288.
170. Ubersax, J.A. and J.E. Ferrell Jr, *Mechanisms of specificity in protein phosphorylation*. Nature Reviews Molecular Cell Biology, 2007. **8**(7): p. 530-541.
171. Blom, N., et al., *Prediction of post-translational glycosylation and phosphorylation of proteins from the amino acid sequence*. PROTEOMICS, 2004. **4**(6): p. 1633-1649.

172. Borowiak, M., et al., *Photoswitchable Inhibitors of Microtubule Dynamics Optically Control Mitosis and Cell Death*. Cell, 2015. **162**(2): p. 403-411.
173. Avidor-Reiss, T. and M.R. Leroux, *Shared and Distinct Mechanisms of Compartmentalized and Cytosolic Ciliogenesis*. Current biology : CB, 2015. **25**(23): p. R1143-R1150.
174. Pedersen, L.B. and J.L. Rosenbaum, *Chapter Two Intraflagellar Transport (IFT): Role in Ciliary Assembly, Resorption and Signalling*, in *Current Topics in Developmental Biology*. 2008, Academic Press. p. 23-61.
175. Lupas, A., M. Van Dyke, and J. Stock, *Predicting coiled coils from protein sequences*. Science, 1991. **252**(5009): p. 1162-1164.
176. Sato-Yoshitake, R., et al., *The phosphorylation of kinesin regulates its binding to synaptic vesicles*. J Biol Chem, 1992. **267**(33): p. 23930-6.
177. Hollenbeck, P.J., *Phosphorylation of neuronal kinesin heavy and light chains in vivo*. J Neurochem, 1993. **60**(6): p. 2265-75.
178. Morfini, G., et al., *Glycogen synthase kinase 3 phosphorylates kinesin light chains and negatively regulates kinesin-based motility*. Embo j, 2002. **21**(3): p. 281-93.
179. Tajjelyato, N., et al., *E-hooks provide guidance and a soft landing for the microtubule binding domain of dynein*. Sci Rep, 2018. **8**(1): p. 13266.
180. Seidel, C., N. Zekert, and R. Fischer, *The Aspergillus nidulans kinesin-3 tail is necessary and sufficient to recognize modified microtubules*. PLoS One, 2012. **7**(2): p. e30976.
181. Acharya, B.R., C. Espenel, and G. Kreitzer, *Direct regulation of microtubule dynamics by KIF17 motor and tail domains*. J Biol Chem, 2013. **288**(45): p. 32302-13.
182. Seeger, M.A. and S.E. Rice, *Microtubule-associated protein-like binding of the kinesin-1 tail to microtubules*. J Biol Chem, 2010. **285**(11): p. 8155-62.
183. Singh, S.K., et al., *Bidirectional motility of kinesin-5 motor proteins: structural determinants, cumulative functions and physiological roles*. Cellular and Molecular Life Sciences, 2018. **75**(10): p. 1757-1771.
184. Hendricks, A.G., et al., *Motor coordination via a tug-of-war mechanism drives bidirectional vesicle transport*. Curr Biol, 2010. **20**(8): p. 697-702.
185. Saito, K., et al., *Conformational diversity of dynactin sidearm and domain organization of its subunit p150*. Mol Biol Cell, 2020. **31**(12): p. 1218-1231.
186. Strom, M., et al., *A family of Rab27-binding proteins. Melanophilin links Rab27a and myosin Va function in melanosome transport*. J Biol Chem, 2002. **277**(28): p. 25423-30.
187. Kuroda, T.S., et al., *The Slp homology domain of synaptotagmin-like proteins 1-4 and Slac2 functions as a novel Rab27A binding domain*. J Biol Chem, 2002. **277**(11): p. 9212-8.
188. Chavas, L.M., et al., *Elucidation of Rab27 recruitment by its effectors: structure of Rab27a bound to Exophilin4/Slp2-a*. Structure, 2008. **16**(10): p. 1468-77.
189. Kuroda, T.S., et al., *Synaptotagmin-like protein 5: a novel Rab27A effector with C-terminal tandem C2 domains*. Biochem Biophys Res Commun, 2002. **293**(3): p. 899-906.

11 Literature

190. Cai, D., et al., *Kinesin-1 structural organization and conformational changes revealed by FRET stoichiometry in live cells*. J Cell Biol, 2007. **176**(1): p. 51-63.
191. Scheuermann, T.H., et al., *On the acquisition and analysis of microscale thermophoresis data*. Anal Biochem, 2016. **496**: p. 79-93.
192. Alzahofi, N., et al., *Rab27a co-ordinates actin-dependent transport by controlling organelle-associated motors and track assembly proteins*. Nat Commun, 2020. **11**(1): p. 3495.
193. Prevo, B., et al., *Functional differentiation of cooperating kinesin-2 motors orchestrates cargo import and transport in C. elegans cilia*. Nat Cell Biol, 2015. **17**(12): p. 1536-45.
194. Yildiz, A. and P.R. Selvin, *Fluorescence imaging with one nanometer accuracy: application to molecular motors*. Acc Chem Res, 2005. **38**(7): p. 574-82.
195. Stepp, W.L., et al., *Kinesin-2 motors adapt their stepping behavior for processive transport on axonemes and microtubules*. EMBO Rep, 2017. **18**(11): p. 1947-1956.
196. Corpet, F., *Multiple sequence alignment with hierarchical clustering*. Nucleic acids research, 1988. **16**(22): p. 10881-10890.

12. Acknowledgements

First, I want to thank Dr. Zeynep Ökten for financing my position and work, patiently supervising my whole PhD project and the mixture of freedom and guidance she provides in her lab.

Next, I want to thank the life and soul of the lab, our TA Thi-Hieu. Without her selfless attitude to always help wherever she can, organization of the lab, as well as knowledge of where stuff is, this whole project would have been considerably more tedious. This, of course, also applies to Gabi Chmel, Karin Vogt, Monika Rusp and Rudi Lehrhuber from upstairs.

I also want to thank all the members of the Ökten group for creating such an enjoyable working environment in our little biology/biochemical bastion within the physics department. That includes special thanks to Dr. Angela Oberhofer for her help with the Myosin-Va project, Augustine Cleetus for his cooperation during the OSM-3 project, Mohamed Antar Mohamed for his support and countless super-smart discussions in and outside of the lab, Dr. Punam Sonar for the fun times we had purifying tubulin and her cooperation in the dsDNA handle project, and Dr. Willi Stepp for his help in analyzing my data with his MatLab routines and general help in all matters from the physics, microscope and IT world. Furthermore, I would like to thank our former members, Dr. Katharina v. Roman and Dr. Sülo Kösem, for their introduction to the project, the methods and the lab in general. Thanks also to all the other E22/27 members for the constructive feedback on my status reports and creating a welcoming and helping atmosphere upstairs, first and foremost Dr. Günther Woehlke.

I would also like to thank Dr. Maximilian Biebl and Dr. Florian Schopf for their management of the Isotope Lab, as well as Dr. Katharina Huell and Dr. Oliver Thorn-Seshold for giving me the opportunity to work on their remarkable AzoMyoVin-1 compound.

Finally, I want to express my gratitude to my family and friends for their endless support and for not always asking when I will be done. Especially my father for his input and support and of course my fiancée Charlotte Damm for her unconditional and endless patience. Without her, all of this would not have been possible.